NOVEL METHODS FOR FATIGUE DATA EDITING FOR HORIZONTAL AXIS WIND TURBINE BLADES

PANU PRATUMNOPHARAT

PhD

2012

NOVEL METHODS FOR FATIGUE DATA EDITING FOR HORIZONTAL AXIS WIND TURBINE BLADES

PANU PRATUMNOPHARAT

A thesis submitted in partial fulfilment
of the requirements of the
University of Northumbria at Newcastle
for the degree of Doctor of Philosophy
in Mechanical Engineering

Research undertaken in the
School of Computing, Engineering and
Information Sciences

August 2012

Abstract

Wind turbine blades are the most critical components of wind turbines. Full-scale blade fatigue testing is required to verify that the blades possess the strength and service life specified in the design. Unfortunately, the test must be run for a long time period. This problem led the blade testing laboratories to accelerate fatigue testing time. To achieve the objective, this thesis proposes two novel methods called STFT- and WT-based fatigue damage part extracting methods which are based on short-time Fourier transform (STFT) and wavelet transform (WT), respectively. For WT, different wavelet functions which are Morl, Meyr, Dmey, Mexh and DB30 are studied.

An aerodynamic computer code, HAWTsimulator, based on blade element momentum theory has been developed. This code is used to generate the sets of aerodynamic loads acting along the span of a 'SERI-8 wind turbine blade' in the range of wind speed from cut-in to cut-out. SERI-8 blades are installed on 65 kW wind turbines. Each set of aerodynamic loads is applied on the finite element model of the SERI-8 blade in structural software (ANSYS) to generate a plot of von Mises stress at the critical point on the blade versus wind speed. By relating this relationship to the wind speed data, the stress-time history at the critical point on the SERI-8 blade can be generated. It has the same sampling rate and length as the wind speed data.

A concept of applying accumulative power spectral density (AccPSD) distribution with time to identify fatigue damage events contained in the stress-time history has been introduced in this thesis. For STFT, AccPSD is the sum of power spectral density (PSD) of each frequency band at each time interval in the spectrogram. For WT, AccPSD is the sum of PSD of wavelet coefficients of each scale at each time interval in the scalogram. It has been found that the locations of AccPSD spikes imply where the fatigue damage events are. Based on an appropriate AccPSD level called a cutoff level, the fatigue damage events can be identified at time location of the stress-time history.

A fatigue computer code, HAWTfatigue, based on stress-life approach and Miner's linear cumulative damage rule has been developed. Basically, the code is used for evaluating the fatigue damage and service lifetime of horizontal axis wind turbine blade. In addition, the author has implemented STFT- and WT-based fatigue damage part extracting methods into the code. Fatigue damage parts are extracted from the stress-time history and they are

concatenated to form the edited stress-time history. The effectiveness of STFT- and WT-based algorithms is performed by comparing the reduction in length and the difference in fatigue damage per repetition of the edited stress-time histories generated by STFT and WT to those of the edited stress-time history generated by an existing method, Time Correlated Fatigue Damage (TCFD) used by commercial software.

The findings of this research project are as follows:

1. The comparison of the reduction in length of the edited stress-time histories generated by TCFD, STFT and WT indicates that WT with the Mexh wavelet has the maximum reduction of 20.77% in length with respect to the original length, followed by Meyr (20.24%), Dmey (19.70%), Morl (19.66%), DB30 (19.19%), STFT (15.38%), and TCFD (10.18%), respectively.

2. The comparison of the retained fatigue damage per repetition in the edited stress-time histories generated by TCFD, STFT and WT indicates that TCFD has the retained fatigue damage per repetition less than the original fatigue damage per repetition by 0.076%, followed by Mexh (0.068%), DB30 (0.063%), STFT (0.045%), Meyr (0.032%), Dmey (0.014%), and Morl (0.013%), respectively.

3. Both comparison of reduction in length and comparison in the retained fatigue damage per repetition of the edited stress-time histories suggest that WT is the best method for extracting fatigue damage parts from the given stress-time history. It has also been indicated that not only do STFT and WT improve accuracy of fatigue damage per repetition retained in the edited stress-time histories, but also they provide the length of the edited stress-time histories shorter than TCFD does. Thus, STFT and WT are useful methods for performing accelerated fatigue tests.

4. It has been found that STFT is controlled by two main factors which are window size and cutoff level. Also, WT is controlled by three main factors which are wavelet decomposition level, cutoff level and wavelet type.

To conclude, the edited stress-time history can be used by blade testing laboratories to accelerate fatigue testing time. STFT- and WT-based fatigue damage part extracting methods proposed in this thesis are suggested as alternative methods in accelerating fatigue testing time, especially for the field of wind turbine engineering.

List of Contents

List of Contents (continued)

Page

List of Contents (continued)

Page

List of Contents (continued)

Page

List of Tables

List of Tables (continued)

List of Tables (continued)

List of Figures

List of Figures (continued)

List of Figures (continued)

List of Figures (continued)

Nomenclature

a	Axial induction factor, scale parameter
a'	Tangential induction factor
a_c	Critical value of an induction factor
A_{disc}	Actuator disc area
B	The number of blades
b'	Translation parameter
c	Chord length, scale factor
C_D	Drag coefficient
C_L	Lift coefficient
$C_{M_{1/4}}$	Pitching moment coefficient
C_Q	Torque coefficient
C_T	Thrust coefficient
D	Drag force, fatigue damage per repetition
dA_e	Differential area of the blade element
$d\dot{m}_{\text{FW}}$	Differential mass flow rate at far wake station
$d\dot{m}_w$	Differential mass flow rate at upstream station
E	Wind shear exponent, Young's modulus
F	Overall loss factor
f	Frequency of cycle
f_0	Cyclic frequency
f_s	Sampling rate
F_{aero}	Aerodynamic force
F_{hub}	Hub loss factor
F_r	Radial force
F_t	Tangential force
F_{tip}	Tip loss factor
F_X	Flapwise force
F_Y	Edgewise force
$G(f_n)$	Power spectrum

Nomenclature (continued)

H_0	Hub height
H_L	Local height
k	Shape factor
L	Lift force
m	Total number of rainflow cycles counted
$\dot{m}$	Mass flow rate
M	Total number of repetitions
$M_{1/4}$	Pitching moment in local coordinate
M_Z	Pitching moment in global coordinate
n	Number of stress cycles, number of discrete points
N	Number of cycles to failure
n_{sector}	The number of circumferential sectors
n_{segment}	Total number of the blade elements
P	Rotor power
P_{avg}	Average power of the wind turbine
Q	Rotor torque
R	Rotor radius, stress ratio, Rayleigh probability distribution function
r	Radius at blade element
r_{hub}	Hub radius
S	Stress
$S(f_n)$	Power spectral density
S_0	Static strength in the first fatigue cycle (at 10^0 cycles)
S_a	Alternating stress
S_e	Fully reversed fatigue strength or the alternating stress at $R = -1$
S_m	Mean stress
$S_{\max}$	Maximum stress
$S_{\min}$	Minimum stress
S_{ut}	Ultimate strength of the material
T	Rotor thrust, period, service lifetime

Nomenclature (continued)

T_n	Thrust force perpendicular to the cone surface
t_{history}	Duration of the stress-time history
$\overline{V}$	Site average wind velocity duration of the stress-time history
$V_{\text{cut}-\text{in}}$	Cut in wind velocity
$V_{\text{cut}-\text{out}}$	Cut out wind velocity
V_{disc}	Wind velocity at actuator disc
V_{FW}	Far wake velocity
V_L	Wind speed at a height
V_{rel}	Relative flow velocity
V_w	Upwind speed
W_ψ	Wavelet coefficient
X	Amplitude
$\bar{x}$	Mean value of an array x
x_{rms}	Root-mean-square value of an array x
α	Angle of attack
β	Pretwist angle
δ	Coning angle
Δf	Frequency interval
$\Delta\theta$	Width of an annular sector
ΔS	Stress range
ϕ	Pitch angle
Γ	Gamma function
φ	Incoming flow angle
λ	Tip speed ratio
λ_L	Local speed ratio
λ_r	Local speed ratio
θ	Azimuth angle, phase angle
ρ	Air density

Nomenclature (continued)

σ	Solidity ratio, standard deviation
ω	Angular velocity imparted to the slip-stream flow
Ω	Blade angular velocity
ψ	Wavelet function

AccPSD	Accumulative power spectral density
BEM	Blade element momentum theory
BET	Blade element theory
CA	Constant amplitude fatigue loading
CDF	Cumulative distribution function
DB30	The 30^{th} order Daubechies wavelet
Dmey	Discrete Meyer wavelet
FFT	Fast Fourier transform
FW	Far wake
HAWT	Horizontal axis wind turbine
Kurt	Kurtosis
Mexh	Mexican hat wavelet
Meyr	Meyer wavelet
Morl	Morlet wavelet
MT	Momentum theory
NREL	National Renewable Energy Laboratory
PDF	Probability density function
PSD	Power spectral density
PV	Peak-valley
RFC	Rainflow cycle
Re	Reynolds number
rms	Root-mean-square
SERI	Solar Energy Research Institute
SNL	Sandia National Laboratories
STFT	Short-time Fourier transform
TCFD	Time correlated fatigue damage
VA	Variable amplitude fatigue loading
WT	Wavelet transform

Acknowledgements

I would like to especially thank my principal supervisor, Dr. Pak Sing Leung, for his useful guidance and firm support. He has encouraged me to move forward confidently in my research work and made my life at Mechanical Engineering Division, University of Northumbria at Newcastle, a positive learning experience. I would like to thank my second supervisor, Dr. Alireza Maheri, for guiding me the implementation of an aerodynamic code. I would like to also thank my third supervisor, Dr. Richard Court, for his valuable advice on several issues.

I am grateful in particular to Dr. Tim Camp for wind speed data that was very useful in my research work. Grateful acknowledgement is due to Royal Thai Government for scholarship subsidization.

Finally, I would like to express profound gratitude to my parents and sisters for their lovely support.

Declaration

I declare that the work contained in the thesis has not been submitted for any other award and that it is all my own work. I also confirm that this work fully acknowledges opinions, ideas and contributions from the work of others. The work was done at the School of Computing, Engineering and Information Sciences.

Name: Panu Pratumnopharat

Signature:

Date: 28/08/2012

Chapter 1

Introduction

1.1 Background and Research Overview

Modern wind turbines are fatigue critical machines [1] used to generate electricity from the wind. These rotating machines are subject to combination of several loadings that are highly irregular in nature. Generally, wind turbine blade is considered as the most important part of the wind turbine [2]. The problem of interest is that wind turbine blades failed at unexpectedly high rates. The major cause of this failure is due to fatigue of the blade materials [3-6]. The word *fatigue* is an engineering terminology for damage of materials under the action of repeated loads. British Standards Institution [7] defined the definition of fatigue as "*the process of initiation and propagation of cracks through a structural part due to action of fluctuating stress.*" The unexpectedly high rate of the blade failure led the designers and researchers to develop fatigue analysis capabilities to prevent breakage of the blade. After finalising the aerodynamic design of any new blades, full-scale blade fatigue testing is required to verify that the blades possess the strength and service life specified in the design. Fatigue lifetime of the blades over 20 years is one of the structural design requirements specified by IEC 61400-1 standard [8].

Wind turbine blades have been manufactured from wood, metals and composites. Wood has high ratio of strength to weight, good stiffness and good resilience but it has the inherent problems about moisture stability and joining efficiency. These problems led designers to examine other materials. Steel, a strong hard metal, has become a popular material because it can be manufactured with a high reliability and it yields a low cost of the blades. However, steel blades are so relatively heavy that their applications in commercial wind turbines are limited. Later, aluminum, a lightweight metal, has been used instead of steel. Composites have become widespread for use as a blade material. They have several advantages such as high strength to weight ratio, light weight, good stiffness, corrosion resistance, etc. At present, modern wind turbine blades are commonly made from composite materials.

As mentioned above, wind turbine blade is the most important part of the wind turbine. The design of wind turbine blades is dictated by fatigue considerations. Fatigue

phenomena of the blade are relevant to several factors such as long and flexible blades, resonant vibration, randomness of the wind, different operating conditions and lack of maintenance during service lifetime [9]. Wind turbine blades are expected to work over 20 years. Most researches on fatigue evaluate the fatigue damage of the wind turbine blades by using the strain history in accordance with the concept of linear damage proposed by Palmgren [10] and Miner [11-12]. The strain history is obtained by digital sampling of strain gauges measuring the strain at a specified point in the root region of the blade. Fatigue life prediction can be done with and without neglecting the effect of load sequence. Sequence effects may have negative effect on fatigue life compared to predictions where they are not considered [13]. The linear accumulative damage and fracture mechanics are two approaches for analysing the fatigue damage of the wind turbine blades. Details of load spectra and fatigue characteristics of the blade materials are required. Linear accumulative damage is one of the simplest approaches. If the stress cycle remains constant throughout a fatigue lifetime, the fraction of that lifetime consumed on every cycle is constant and equal to the reciprocal value of the fatigue lifetime. The failure occurs when the total damage value is equal to unity. The fatigue characteristics of the blade materials can be illustrated by a Goodman's diagram. A number of cycles to failure are plotted along the lines of constant stress ratio which is a function of mean stress and stress range [14]. The difficulty in predicting fatigue damage is due to an insufficient knowledge of the dynamic behaviour of wind turbines. Moreover, S - N curve (where S is the maximum cyclic stress and N is the number of cycles to failure) is encumbered with uncertainty due to a limited number of test specimens as well as variability from one specimen to another [15].

Fatigue testing must be carried out at some stage in the development of a wind turbine blade to gain confidence in its ultimate service performance and on legal requirement. Full-scale blade fatigue testing is evaluated when the desire to reduce production costs must be balanced with the necessity to avoid expensive service failures. At present, there are many full-scale blade fatigue testing laboratories as follows:

1. NREL - National Renewable Energy Laboratory (United States)
2. WMC and ECN - Wind Turbine Materials and Constructions (Netherland), and Energy Research Centre of the Netherlands
3. RISØ National Laboratories (Denmark) and Blaest which is a spin-out of RISØ
4. NaREC - National Renewable Energy Centre (United Kingdom)

5. CRES - Centre for Renewable Energy Sources (Greece)
6. CENER - Centro Nacional de Energías Renovables (Spain)
7. Private Labs - LM Glasfibers (www.lmglasfiber.com), Vestas (www.vestas.com), MHI (www.mpshq.com), other manufacturers

Full-scale blade fatigue testing is an essential part of verifying the design of any new wind turbine blades. Wind turbine blades are subject to the complicated loads throughout their operating life. It is not possible to exactly apply the complicated loads in any accelerated laboratories [4]. Also, durability requires knowledge of service loads to be used for the component testing in the laboratory [16-17]. The laboratory based accelerated testing needs to expose the component with the equivalent test loading which its length is shorter than the length of the target loading whilst it has approximately the same damage potential. Techniques used to accelerate laboratory fatigue testing [18] are increasing the frequency of the cyclic loading, increasing the load level and removing small amplitude cycles from the time history. Testing time and cost can become too expensive if the service load is not edited before testing.

In the field of wind turbines, there are two methods [19] used to accelerate fatigue test of large wind turbine blades. Two methods are either resonant testing or forced actuation. Resonant testing can be achieved in at least two known ways, e.g. the NREL/NaREC/CENER way of using a moving mass on the blade, which is powered by hydraulics or the eccentric rotating mass method – and possibly other ways. Recently, a novel procedure for conducting wind turbine blade fatigue testing has been presented [20-21]. It features simultaneous loading in two orthogonal directions, which are flapwise and edgewise, and it uses the blade natural frequencies to force cyclic fatigue loads. The forced actuation method can use hydraulic actuators which are mounted onto a fixed part of the test lab and then push/pull the blade. Of the two methods flexing the blade using hydraulic actuators will simulate the fatigue loading more realistically [19]. The realism of the test is determined by how well the blade bending moment distribution matches that observed in-service – this is more a matter of how many loading points there are, rather than whether hydraulic actuators are used. According to technical specification [2], testing time can be reduced either by increasing the load magnitudes, increasing the frequency of load application or both. Increasing loading frequency is only possible in forced actuation tests. In resonant tests, it is not really possible to alter the resonant frequency, since this is a property of the structure.

1.2 What is the Problem of Interest?

At present, it is found in the wind turbine community that the racetrack method [22-23] is the only one method existing used in editing fatigue loading. The racetrack method is used to produce a condensed history in which essential peaks and valleys are listed in their original sequence. By removing small amplitude cycles from the time history, this method is useful for condensing histories to those few events, perhaps the 10 percent of events that do most of the damage [24-26]. Unfortunately, the racetrack method does not shorten the length of the fatigue loading. So, it does not serve the purpose of accelerating the testing time. The need to reduce testing time and energy cost whilst simultaneously retaining the high amplitude cycles that produce the fatigue damage is of interest to investigate the issue of fatigue loading compression.

The author reviews the techniques of fatigue data editing. For all editing techniques reviewed in Chapter 5, different variable loadings are used for different techniques. There seems to be no generally agreed rules that clarify which method is the best, or what amplitude should be chosen for load omission. Practically, any fatigue data editing techniques must reduce the testing period and be technically valid.

As mentioned, the racetrack method can remove small cycles from the time history but it does not shorten the time history; say, the edited loading has the same time length as the original loading. This is the problem that motivated the author to take an interest in fatigue data editing by removing small amplitude cycles. Such a method is defined as a method for omitting the small amplitude cycles which provide a minimal contribution to the overall fatigue damage. Also, it retains the high amplitude cycles which are the most damaging sections [18]. In the wind turbine application, this concept is still not proposed to accelerate fatigue testing time. Such a method to summarise variable loadings measured on the wind turbine blade whilst preserving the load sequences is the subject matter of this thesis.

1.3 What does the Author Want to Do?

In this research project, the author wants to develop two novel methods in extracting fatigue damage parts from the stress-time history of HAWT blades and to study the effectiveness of the methods proposed. Two novel methods are based on short time Fourier transform (STFT) and wavelet transform (WT). The STFT- and WT-based fatigue damage extracting methods are designed to identify and to extract fatigue damaging parts

from the stress-time history of HAWT blades. The extracted damage parts are concatenated to form the edited stress-time history with shorter time length whilst its retained fatigue damage per repetition and signal statistical parameters are equivalent to those of the original stress-time history.

The research described in this thesis is motivated by the author's belief that STFT and WT are the suitable methods for use in fatigue damage part extracting. Since the stress-time history normally exhibits non-stationary signal behaviour, STFT (time-frequency analysis) and WT (time-scale analysis) would be expected to be a natural choice of analysis method. With these methods, the fatigue damage events in the stress-time history can be identified by the accumulative power spectral density (AccPSD) level. Furthermore, literature review suggests that there is no fatigue damage part extracting method used the STFT and WT for identifying and extracting fatigue damage parts from the stress-time history of HAWT blades.

1.4 Organisation of Thesis

This thesis is organised in eight chapters as follows:

Chapter 1

This chapter introduces the background of the fatigue damage problem to be studied, methodologies used in this study, background and research overview, what the problem of interest is, what the author wants to do, organisation of thesis, research objectives, and original contributions to knowledge, respectively.

Chapter 2

This chapter deals with the derivation of a set of equations based on blade element momentum theory. All derived equations are used to implement an aerodynamic computer code, HAWTsimulator.

Chapter 3

This chapter deals with the implementation of the aerodynamic computer code, HAWTsimulator. The software is mainly used to generate the sets of aerodynamic loads acting along the blade span at wind speed ranging from cut-in to cut-out.

Chapter 4

This chapter mentions to stress-life approach, Miner's cumulative damage rule and the rainflow cycle counting method. They are implemented to a fatigue computer code, HAWTfatigue. This computer code is used to evaluate the fatigue damage and service lifetime of HAWT blades.

Chapter 5

This chapter reviews the available fatigue signal editing techniques. Signal analyses, which are Fourier transform, short-time Fourier transform (STFT) and wavelet transform (WT), are mentioned. Also, two Matlab toolboxes are mentioned in this chapter. Signal processing toolbox is used to analyse short-time Fourier transform (STFT) of the stress-time history and wavelet toolbox is used to analyse wavelet transform (WT). In the last section, how to generate a plot of accumulative power spectral density (AccPSD) distribution is introduced. The application of this plot will be discussed in Chapter 6.

Chapter 6

This chapter introduces a concept of applying accumulative power spectral density (AccPSD) to identify fatigue damage events contained in the stress-time history. Algorithm in extracting fatigue damage parts is also discussed in this chapter. This algorithm is implemented in a fatigue computer code, HAWTfatigue. Modules of HAWTfatigue and step-by-step in evaluating the fatigue damage and service lifetime of HAWT blades are described. The last section describes the processes in extracting fatigue damage parts by using STFT- and WT-based fatigue damage part extracting methods.

Chapter 7

This chapter reports, compares and discusses the results generated by the existing method, TCFD (time correlated fatigue damage), STFT and WT with the Morl, Meyr, Dmey, Mexh and DB30 wavelets. Also, the efficiencies of STFT- and WT-based fatigue damage part extracting methods are compared to that of TCFD.

Chapter 8

This chapter deals with summary of research project.

Chapter 9

This chapter deals with conclusions and suggestions for future research, respectively.

1.5 Research Objectives

Based on the related background and research overview, the main objective of the Ph.D. research project is to develop two novel fatigue damage part extracting methods involving STFT and WT. In order to achieve this objective, nine secondary objectives have to be accomplished:

1. Perform a literature review to find the recent developments of blade element momentum theory;
2. Develop an aerodynamic code, HAWTsimulator, which will be used to generate sets of aerodynamic loads acting along the blade span at wind speed ranging from cut-in to cut-out;
3. Validate the accuracy of the aerodynamic code by means of the existing results;
4. Develop a fatigue computer code, HAWTfatigue, which will be used to evaluate fatigue damage and service lifetime of HAWT blades;
5. Perform a literature review to find the available fatigue data editing techniques in various domains;
6. Edit stress-time history by using the existing method, TCFD in commercial software. The results generated by TCFD will be the baseline results to be compared by the results generated by the novel methods;
7. Develop a novel STFT-based fatigue damage part extracting method which will be able to identify and extract the fatigue damage parts from the original stress-time history;
8. Develop a novel WT-based fatigue damage part extracting method which will be able to identify and extract the fatigue damage parts from the original stress-time history;
9. Validate and evaluate the effectiveness of the novel methods in shortening the length of the stress-time history and retaining the fatigue damage per repetition.

Some of the questions which the research sought to answer are the following:

1. What is the best method among TCFD, STFT and WT for extracting fatigue damage parts from the given stress-time history under the purpose of accelerated fatigue test?
2. Among WT with the Morl, Meyr, Dmey, Mexh and DB30 wavelets, which one is the best one for extracting fatigue damage parts from the given stress-time history under the purpose of accelerated fatigue test?
3. Can STFT-based algorithm be developed to improve the accuracy of fatigue damage part extracting method with respect to TCFD, an existing method?

4. Can WT-based algorithm be developed to improve the accuracy of fatigue damage part extracting method with respect to TCFD, an existing method?
5. What are the main factors that influence the novel fatigue damage part extracting methods?
6. Are the edited stress-time histories generated by the novel methods suitable for accelerated fatigue testing of horizontal axis wind turbine blades?

These research questions have been answered in Chapter 8, Section 8.2. The findings of this research are expected to improve the effectiveness of STFT- and WT-based fatigue damage part extracting methods. The author hopes that this thesis clarifies some of the above listed research questions. Also, the author hopes that this thesis accurately describes the STFT- and WT-based fatigue damage part extracting methods.

1.6 Original Contributions to Knowledge

The thesis represents two original contributions to knowledge as follows:

1. Introducing a concept of applying a plot of accumulative power spectral density (AccPSD) distribution generated by either STFT or WT along with a cutoff level to identify fatigue damage events contained in the stress-time history of HAWT blades.

2. Proposing two novel methods which are STFT- and WT-based fatigue damage part extracting methods. Both methods are used for extracting the fatigue damage parts from the stress-time history of HAWT blades. They have a significant effect in improving the effectiveness of fatigue damage part extraction. Its significance is more noticeable in the fatigue damage analysis.

Chapter 2

Derivation of Aerodynamic Model

2.1 Introduction

In predicting performance of wind turbines, the blade element momentum (BEM) theory is still commonly used by wind turbine designers and researchers. Despite the fact that more sophisticated approaches are available, the BEM theory has significant advantages in computational speed [27-28] and ease of implementation. Historically, Glauert [29] originated the basic concepts of aerodynamic analysis of airscrew propellers and windmills. In 1974, Wilson *et al*. [30-31] extended Glauert's work for application to wind turbines and presented a step by step procedure for calculating performance characteristics of wind turbines. The BEM theory is based on one-dimensional momentum theory and two-dimensional blade element theory and then iterative solutions are obtained for the axial and tangential induction factors. The first assumption of the BEM theory is that there is no aerodynamic interaction between adjacent blade elements. This assumption is realistic if and only if the circulation distribution over the rotor disc is relatively uniform. The second assumption is that the flow is assumed to be two-dimensional, i.e. radial component of the flow passing through the rotor disc is neglected. Thus, the lift and drag coefficients from wind tunnel test can be used to predict the aerodynamic forces exerted by the wind on each blade element. It is indicated that the accuracy of the BEM codes is dependent on (or sensitive to) two-dimensional wind tunnel test that are normally known to over-predict thrust and under-predict peak torque [32-33]. The limitations, which lead to inaccurately predicted results, might be divided into two categories. Primary limitations are the effect of wind shear, the effect of tower shadow, the effect of discrete number of blades and so forth. Secondary limitations are the effect of dynamic stall, the effect of blade rotating, the geometric effects of coned shape and yawed rotors. In addition, the BEM theory does not include the effects of three-dimensional flow velocities induced on the blade by the shed tip vortex or radial components of flow induced by angular acceleration due to the rotation of the blade [33-34]. In order to take the three-dimensional representation into account, the wind tunnel experimental measurements must be modified by including the radial flow along the blades. At present, several researchers attempt to improve the accuracy of the BEM computation which the secondary limitations remain a highly active area of research in wind turbine aerodynamics. In spite of these limitations,

the BEM theory is considered to be an effective tool during the design process to get good first order predictions of wind turbine performance under a wide range of operating conditions and it can easily be implemented for the comparative studies. Furthermore, the BEM code does not require large calculation resources, works with a very short calculation time and gives reliable results.

In recent years, researchers have optimised and modified the BEM calculation to provide more accurate results. For the numerical stability, the most difficult issues are the correction of lift and drag coefficients in order to consider the radial flow along the blades and the determination of axial and tangential induction factors. There are some differences among several BEM codes because several strategies are used to solve the non-linear equations involved in this methodology. In addition, many corrections, such as tip and hub loss correction factors, windmill brake state models, etc., are proposed to increase accuracy of prediction.

At present, the windmill brake state model is still important because it can affect to the accuracy of wind turbine performance predicted the BEM calculation. Referring to Stoddard's work in 1977 [35], the correlation between the behaviour of wind turbine rotors and the known experimental data for helicopters reported by Glauert in 1926 [36] is studied. Stoddard reported that thrust coefficient predicted by momentum theory deviated dramatically from the Glauert's experimental data when the value of axial induction factor is greater than 0.5. Unfortunately, the Glauert's experimental data are given only the condition of without tip loss effect. In fact, the tip loss effect must be applied to the thrust coefficient relation to make more realistic of prediction. Owing to lack of the experimental data with tip loss effect, several researchers have proposed windmill brake state models to improve the accuracy of the prediction.

The advent of digital computer in the past makes the task of predicting performance characteristics of wind turbines quite easy. The basic concept of aerodynamic analysis is based on Glauert's airscrew theory [29]. The airscrew theory followed two independent lines of thought, which may conveniently be called the *momentum* theory and the *blade element* theory. Momentum theory refers to an analysis of thrust and torque by applying the conservation of the linear and angular momentum to an annulus control volume [37]. Blade element theory refers to an analysis of aerodynamic forces at a section of the blade as a function of blade geometry. Then, the results from both theories are combined into

what is known as *blade element momentum* theory. From 1974 to 1976, Wilson *et al.* [30-31] extended Glauert's airscrew theory by including the induced axial and tangential velocities into the analysis, implementing the first aerodynamic computer programme named PROP, and publishing the state of the art of performance prediction methods for application to wind turbines. Later, from 1981 to 1983, Hibbs and Radkey [38] made improvements to wind turbine analysis computer code, PROP, developed by Wilson *et al*. At present, several aerodynamic computer codes based on BEM theory are commonly used by wind turbine designers, researchers, and industries.

2.2 Kinematics of Blade Rotor

Figure 2.2-1 shows the turbine with the blades coned at an angle of δ. The length of each blade is R. Because the blade is coned, the radius of the projected swept rotor disc is $R\cos\delta$, giving a projected swept area of $\pi R^2\cos^2\delta$. It is the area to which the turbine thrust, torque and power coefficients are normalised. A blade element has a radius r and a width dr. Thus, the area of the element is cdr where c is the chord of the blade at the element. The projected area is $cdr\cos\delta$. The projected width of the swept annulus is $dr\cos\delta$, giving a swept area of $2\pi rdr\cos^2\delta$. The solidity ratio, σ, of the annulus is equal to the ratio of the area of the blades to the swept area. For an annulus this is

$$\sigma = \frac{Bc}{2\pi r\cos\delta} \tag{2.2-1}$$

where B is the number of blades.

The tip speed ratio of the turbine, λ, is defined as the ratio of the speed of the turbine blade tip to the upwind speed, V_w, thus

$$\lambda = \frac{\Omega R\cos\delta}{V_w} \tag{2.2-2}$$

where Ω is the blade angular velocity.

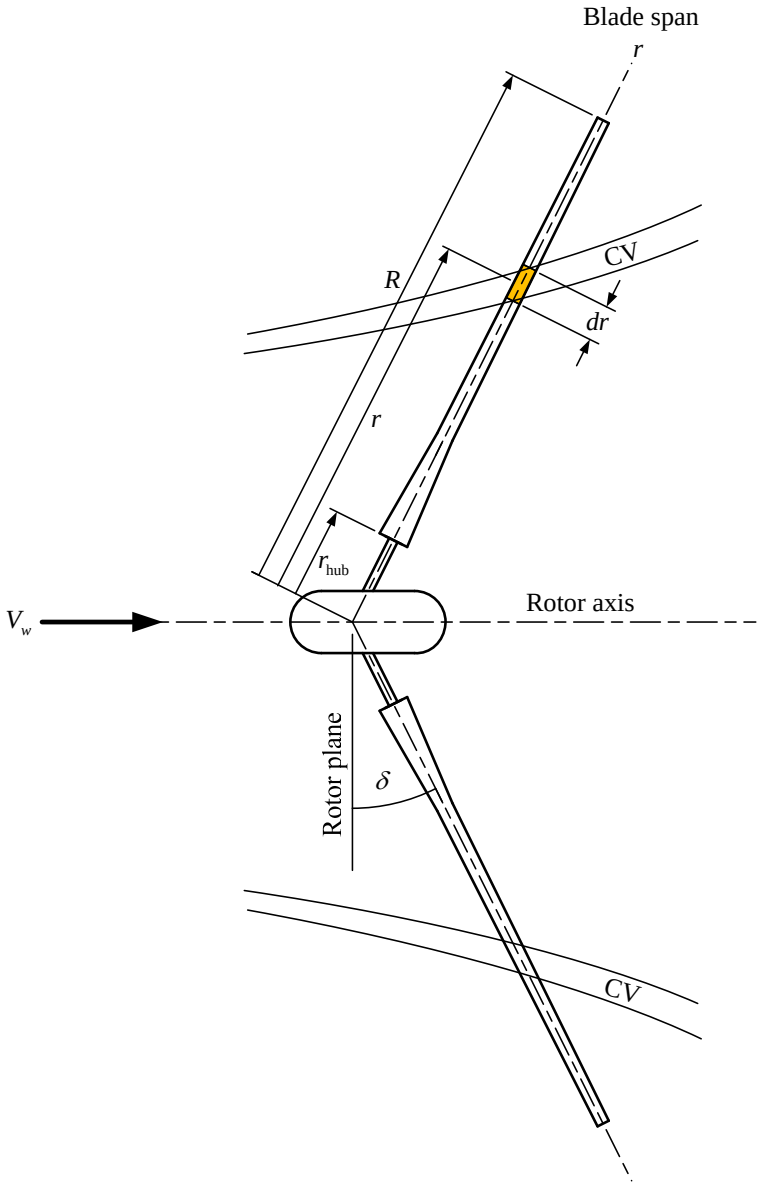

Figure 2.2-1. Rotor geometry

Similarly, the local speed ratio is defined as the ratio of the speed of the turbine blade at a radius r to the upwind speed, V_w, thus

$$\lambda_r = \frac{\Omega r \cos\delta}{V_w} \tag{2.2-3}$$

Equating Equations 2.2-2 and 2.2-3 gives an interesting relation.

$$\lambda_r = \lambda \frac{r}{R} \tag{2.2-4}$$

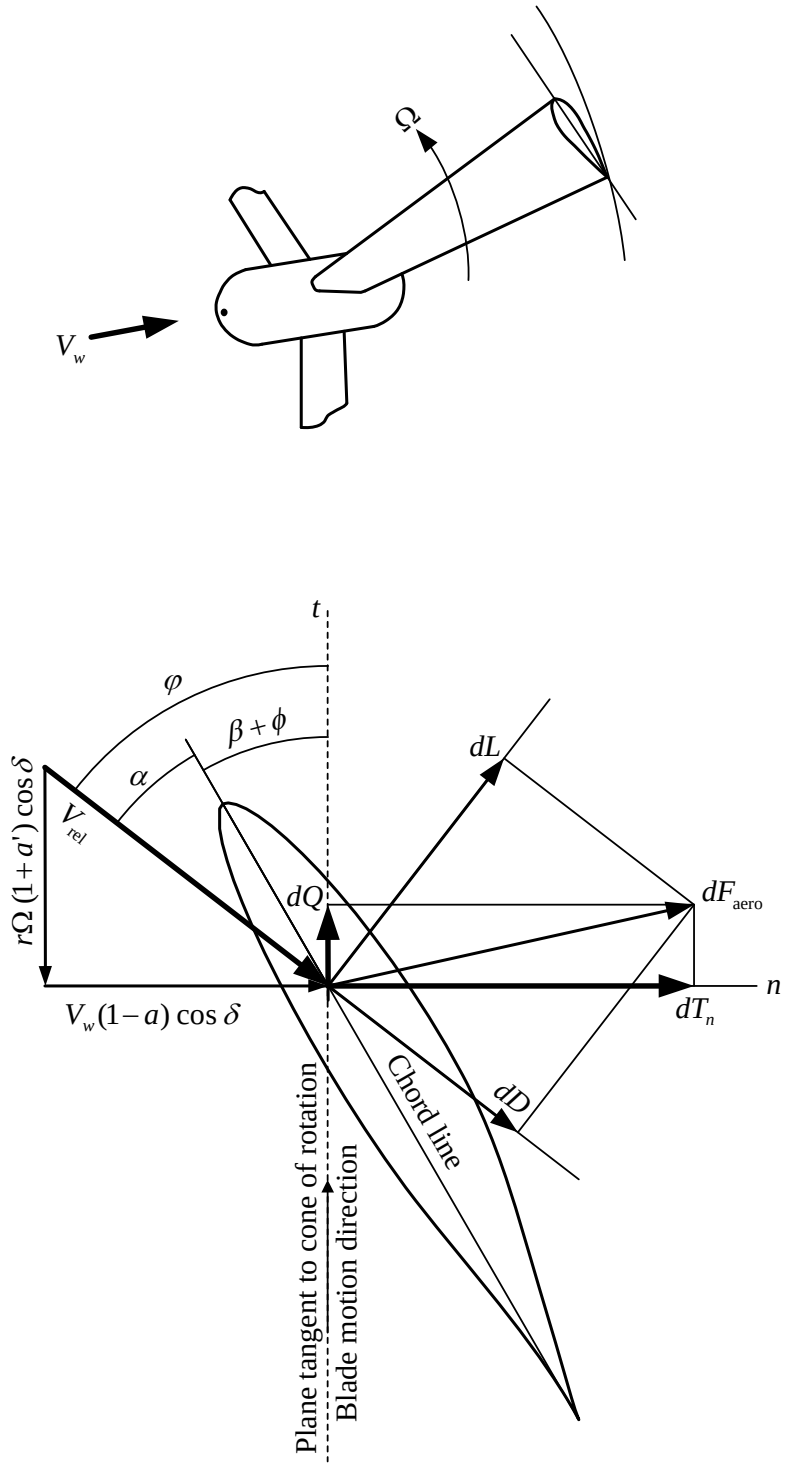

Figure 2.2-2. Velocity and force on a blade element

Considering Figure 2.2-2, an angle of attack, α, can be expressed as

$$\alpha = \varphi - \beta - \phi \tag{2.2-5}$$

where φ, β, and ϕ are incoming flow angle, pretwist angle, and pitch angle, respectively. dL, dD, dF_{aero}, dT_n, and dQ are lift force, drag force, resultant aerodynamic force, thrust force perpendicular to the cone surface, and torque at a blade element, respectively. Also, Figure 2.2-2 shows the velocity polygon and force polygon as seen by a blade element at radius r. The relative flow velocity in Figure 2.2-2 can either be expressed in the form

$$V_{\text{rel}} = \sqrt{[V_w(1-a)\cos\delta]^2 + [r\Omega(1+a')\cos\delta]^2} \tag{2.2-6}$$

or in the form

$$V_{\text{rel}} = V_w \frac{(1-a)\cos\delta}{\sin\varphi} \tag{2.2-7}$$

where a, a', and φ are axial induction factor, tangential induction factor, and incoming flow angle, respectively.

$$\varphi = \tan^{-1}\frac{V_w(1-a)\cos\delta}{r\Omega(1+a')\cos\delta} = \tan^{-1}\frac{(1-a)\cos\delta}{\lambda_r(1+a')} \tag{2.2-8}$$

Next section deals with the equations for the forces on the blade and the change of momentum of the wind flowing through the annulus. There are two sets of equations to be considered, one for the axial forces and linear momentum, and another for the tangential forces and angular momentum.

2.3 Momentum Theory

To analyse horizontal axis wind turbines, momentum analysis is applied to an annular control volume to find thrust and torque at the wind turbine blade. Thrust is obtained from a momentum analysis and torque is also obtained from an angular momentum analysis. To apply the principle of one-dimensional momentum, the wind turbine rotor is represented by a uniform actuator disc which causes a difference of pressure in wind flowing across the

rotor as shown in Figure 2.3-1. There are three basic assumptions as follows: (1) axisymmetric flow; (2) incompressible, steady flow; and (3) frictionless flow.

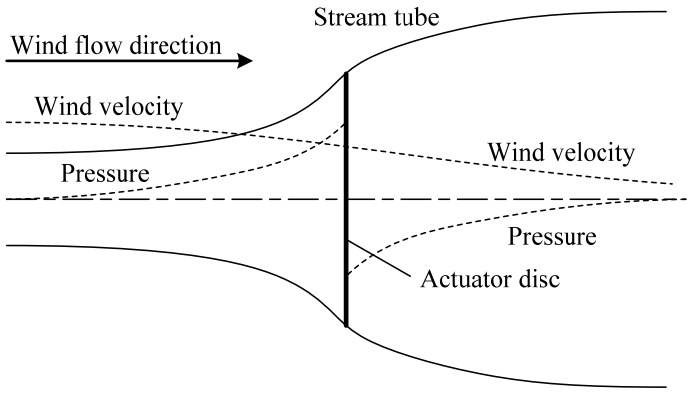

Figure 2.3-1. Wind velocity and pressure variations [39]

2.3.1 Linear Momentum Analysis

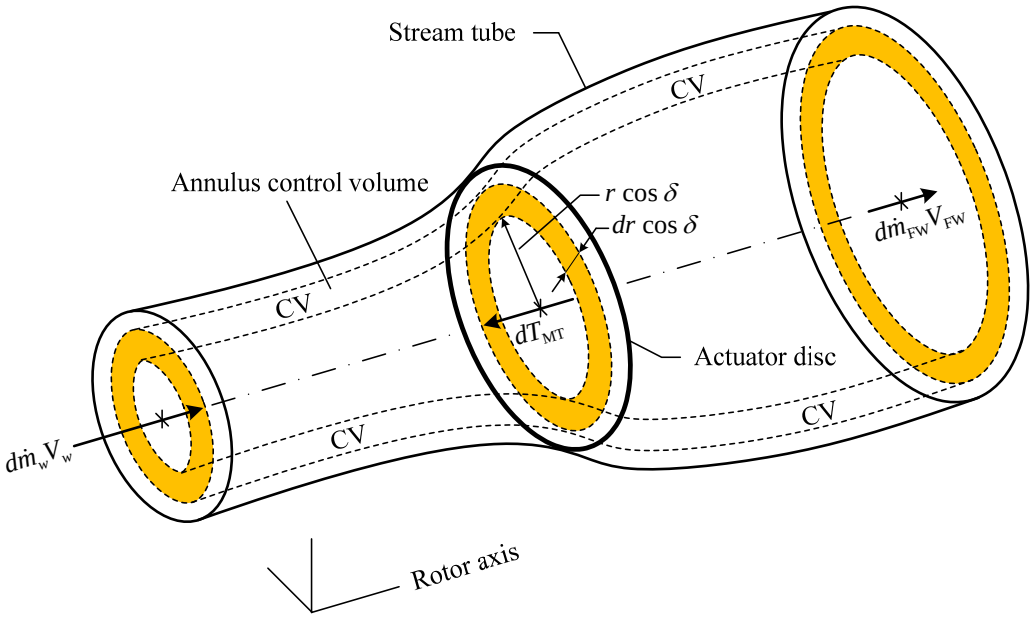

Figure 2.3-2. Stream tube and annulus control volume

The principle of linear momentum is applied to an annulus control volume enclosed by a stream tube with one inlet and one outlet as shown in Figure 2.3-2. There is only flow across both ends of the differential annulus control volume.

Applying linear momentum principle to the differential annulus control volume gives

$$dT_{\mathrm{MT}} = d\dot{m}_w V_w - d\dot{m}_{\mathrm{FW}} V_{\mathrm{FW}} \tag{2.3-1}$$

where dT_{MT}, V_w, V_{FW}, $d\dot{m}_w$, and $d\dot{m}_{\mathrm{FW}}$ are the differential rotor thrust derived from momentum theory, upstream wind velocity, far wake velocity, differential mass flow rate at upstream station, and differential mass flow rate at far wake stations, respectively.

Since the flow is incompressible, the mass flow rate is a constant, i.e.

$$d\dot{m}_w = d\dot{m}_{\mathrm{FW}} = d\dot{m} \tag{2.3-2}$$

and the volume flow rate may be expressed as

$$\frac{d\dot{m}}{\rho} = V_{\mathrm{disc}}\, dA_{\mathrm{disc}} = V_w (1-a)\, 2\pi r \cos\delta\, dr \cos\delta \tag{2.3-3}$$

where δ is a coning angle of the blade measured from the rotor plane and ρ is air density. Substituting Equation 2.3-3 into Equation 2.3-1 gives

$$dT_{\mathrm{MT}} = \rho V_w (1-a)(V_w - V_{\mathrm{FW}})\, 2\pi r\, dr \cos^2\delta \tag{2.3-4}$$

Since $V_{\mathrm{FW}} = V_w(1-2a)$, then Equation 2.3-4 becomes

$$dT_{\mathrm{MT}} = 4\pi r \rho V_w^2\, a(1-a)\, dr \cos^2\delta \tag{2.3-5}$$

By definition, thrust coefficient is defined as

$$\text{Thrust coefficient, } C_T = \frac{\text{Thrust}}{\text{Aerodynamic force}} = \frac{4\pi r \rho V_w^2\, a(1-a)\, dr \cos^2\delta}{\frac{1}{2}\rho V_w^2\, 2\pi r\, dr \cos^2\delta}$$

$$C_{T_{\mathrm{MT}}} = 4a(1-a) \tag{2.3-6}$$

2.3.2 Angular Momentum Analysis

Before applying the principle of the angular momentum to an overall annulus control volume shown in Figure 2.3-4, a relation between the rotational velocity in far wake and circumferential velocity at the actuator disc must be known first. Thus, the conservation of angular momentum is applied to the annulus control volume shown in Figure 2.3-3. The conservation of angular momentum yields

$$[(r\cos\delta)^2\omega]_{\mathrm{FW}} = [(r\cos\delta)^2\omega]_{\mathrm{disc}} \tag{2.3-7}$$

where ω is the angular velocity imparted to the slip-stream flow and it is derived from the definition of an tangential induction factor [29].

$$\text{Tangential induction factor, } a' = \frac{\text{Angular velocity of the wind at the rotor}}{\text{Twice the angular velocity of the rotor}} = \frac{\omega}{2\Omega} \tag{2.3-8}$$

Substituting $\omega = 2\Omega a'$ into the right hand side of Equation (2.3-7) gives

$$[(r\cos\delta)^2\omega]_{\mathrm{FW}} = 2r^2\Omega a'\cos^2\delta \tag{2.3-9}$$

Now, the angular momentum principle can be applied to an entire annulus control volume shown in Figure 2.3-4, which yields

$$dQ_{\mathrm{MT}} = d\dot{m}\left([(r\cos\delta)^2\omega]_{\mathrm{FW}} - [(r\cos\delta)^2\omega]_{w}\right) \tag{2.3-10}$$

where dQ_{MT} is the differential rotor torque derived by momentum theory. Since the upstream wind is under a uniform flow, the term $[(r\cos\delta)^2\omega]_{w}$ in the right hand side of Equation 2.3-10 must be vanished. Thus, Equation 2.3-10 becomes

$$dQ_{\mathrm{MT}} = d\dot{m}[(r\cos\delta)^2\omega]_{\mathrm{FW}} \tag{2.3-11}$$

Substituting Equations 2.3-3 and 2.3-9 into Equation 2.3-11 yields an equation of the rotor torque.

$$dQ_{\mathrm{MT}} = 4\pi r^3\rho V_w(1-a)a'\Omega\,dr\cos^4\delta \tag{2.3-12}$$

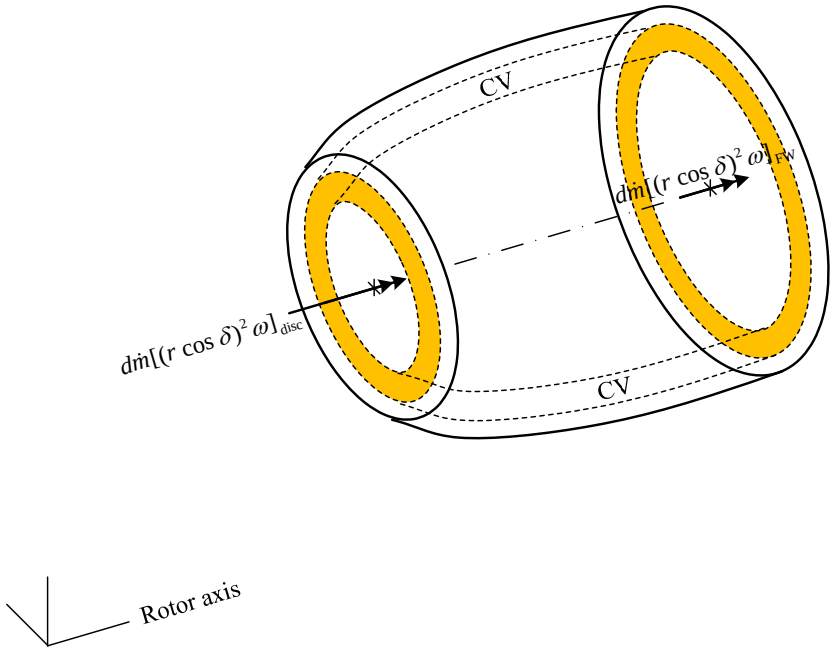

Figure 2.3-3. Annular control volume enclosed by an actuator disc and outlet

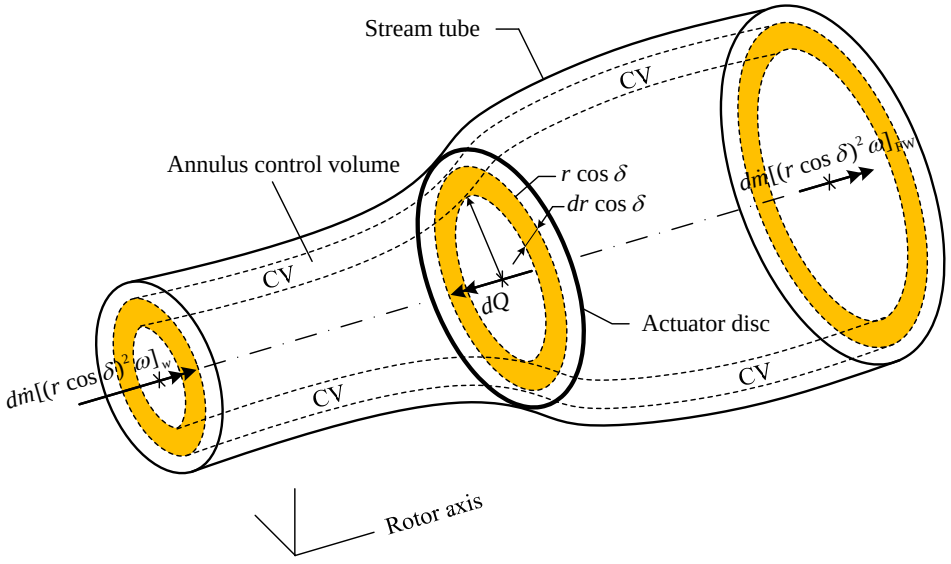

Figure 2.3-4. Annulus control volume for angular momentum analysis

By definition, torque coefficient is defined as

$$\text{Torque coefficient, } C_Q = \frac{\text{Rotor torque}}{\text{Aerodynamic torque}} = \frac{4\pi r^3 \rho V_w (1-a) a' \Omega dr \cos^4 \delta}{\frac{1}{2}\rho V_w^2 2\pi r\, dr \cos^2 \delta\, r \cos \delta}$$

which is

$$C_{Q_{\text{MT}}} = 4\lambda_r a'(1-a)\cos\delta \tag{2.3-13}$$

2.4 Overall Loss Correction Factor

Momentum theory treats the wind turbine rotor as an actuator disc, which represents an infinite number of blades with zero chord length, and the flow crossing each annulus is uniform. Consequently, the aerodynamic losses caused by vortices shed from the tips of finite blades are not taken into account in the analysis. In fact, the wind turbine rotor has a finite number of blades with finite tip chord and each blade sheds a discrete vortex near the tip. Vortex causes several effects to the turbine rotor such as the flow is not uniform, axial and tangential induction factors increase near the tip, the angle of attack at each section decreases, and lift force decreases resulting in torque decreases, etc. To correct these effects, an overall loss correction factor, F, is required to apply on the induced velocity or disc velocity [31,38,40].

$$F = F_{\text{tip}} F_{\text{hub}} \tag{2.4-1}$$

F_{tip} is a tip loss correction factor which is unity at inboard parts of the blade and takes smaller values near the tip of the blade. F_{hub} is a hub loss correction factor which is unity at outboard parts of the blade and takes smaller values near the hub of the blade.

In order to simulate a real wind turbine with a finite number of blades, Wilson *et al*. [31] recommended applying tip loss effect, which was proposed by Prandtl [29], to the momentum theory.

The expression of Prandtl's tip loss correction factor is

$$F_{\text{tip}}^{\text{Prandtl}} = \begin{cases} \frac{2}{\pi}\cos^{-1}(e^{-f_{\text{tip}}}), & \left| f_{\text{tip}} \right| \le 7 \\ 1, & \left| f_{\text{tip}} \right| > 7 \end{cases} \tag{2.4-2}$$

where

$$f_{\text{tip}} = \frac{B(R-r)}{2r\sin\varphi} \tag{2.4-3}$$

and the expression of the hub loss correction factor is [31,38]

$$F_{\text{hub}} = \begin{cases} \frac{2}{\pi}\cos^{-1}(e^{-f_{\text{hub}}}), & \left| f_{\text{hub}} \right| \le 7 \\ 1, & \left| f_{\text{hub}} \right| > 7 \end{cases} \tag{2.4-4}$$

where

$$f_{\text{hub}} = \frac{B(r-r_{\text{hub}})}{2r_{\text{hub}}\sin\varphi} \tag{2.4-5}$$

In 2002, Xu and Sankar [34] proposed an improvement to Prandtl's tip loss correction factor. Xu's tip loss correction factor has two expressions given by either pre-stalled or post-stalled conditions.

Pre-stalled condition $(\alpha < \alpha_{\text{stall}})$

$$F_{\text{tip}}^{\text{Xu}} = \begin{cases} 1 - \frac{r}{R}\frac{1 - F_{\text{tip}}^{\text{Prandtl}}\big|_{r/R=0.7}}{0.7}, & r/R < 0.7 \\ \frac{\left(F_{\text{tip}}^{\text{Prandtl}}\right)^{0.85} + 0.5}{2}, & 0.7 \le r/R \le 1 \end{cases} \tag{2.4-6}$$

where $F_{\text{tip}}^{\text{Prandtl}}$ can be directly calculated from Equation 2.4-2 and $F_{\text{tip}}^{\text{Prandtl}}\big|_{r/R=0.7}$ can be calculated by replacing r's in the denominator of the Equation 2.4-3 with $0.7R$, i.e.

$$f_{\text{tip}}\big|_{r/R=0.7} = \frac{0.3B}{1.4\sin\varphi} \tag{2.4-7}$$

Post-stalled condition $(\alpha \geq \alpha_{\text{stall}})$

$$F_{\text{tip}}^{\text{Xu}} = \begin{cases} 1, & r/R < 0.8 \\ 0.8, & 0.8 \leq r/R \leq 1 \end{cases} \tag{2.4-8}$$

In 2005, Shen *et al*. [41] proposed an improvement to Prandtl's tip loss model. Shen's tip loss correction factor gives the change in loading near the tip when two-dimensional airfoil data are applied.

$$F_{\text{tip}}^{\text{Shen}} = \frac{2}{\pi} \cos^{-1}(e^{-g f_{\text{tip}}}) \tag{2.4-9}$$

and

$$g = e^{-0.125(B\lambda - 21)} + 0.1 \tag{2.4-10}$$

where f_{tip} and λ are calculated from Equations 2.4-3 and 2.2-2, respectively.

2.5 Blade Element Theory

The key of this theory is that the rotor blade is divided into a number of elements or strips along the blade span as shown in Figure 2.5-1. Whilst the blade is rotating, each element sweeps and forms an annulus shape. The aerodynamic forces on the blades can be expressed as a function of lift coefficient, drag coefficient and angle of attack. Basically, this theory is based on the following assumptions: (1) there is no aerodynamic interaction between elements; and (2) the forces on the blades are determined solely by the lift and drag characteristics of the airfoil shape of the blades.

Consider Figure 2.5-2(*b*), the flow passing through a typical airfoil at radius r is assumed to be two-dimensional flow (neglected the differential radial force, dF_r, on the blade). Thus, the differential thrust on an element can be easily determined by summing forces in the direction of the rotor axis.

$$dT = dT_n \cos\delta \tag{2.5-1}$$

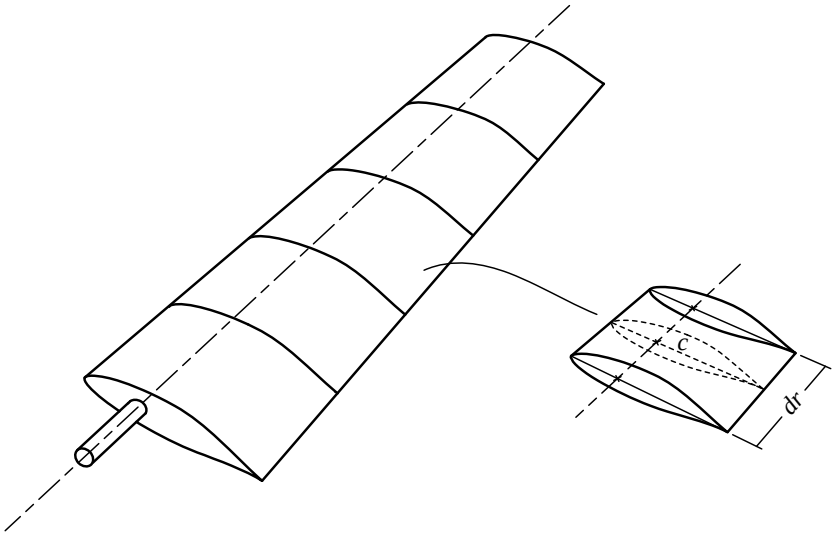

Figure 2.5-1. Schematic of blade elements

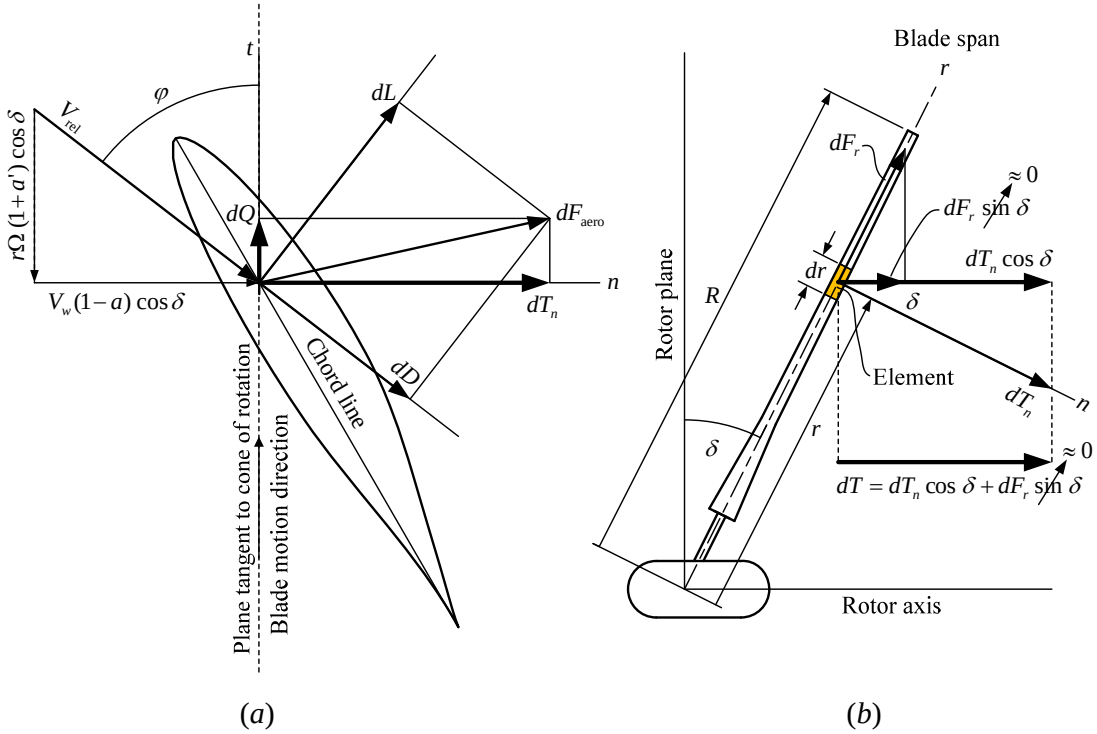

Figure 2.5-2. Force analysis at a typical blade element

By means of the rotation of axes shown in Figure 2.5-2(*a*), thrust can be expressed in terms of the differential lift and drag forces.

$$dT = (dL \cos \varphi + dD \sin \varphi) \cos \delta \tag{2.5-2}$$

By definition, lift coefficient [37] is

$$C_L = \frac{\text{Lift force}}{\text{Dynamic force}} = \frac{dL}{\frac{1}{2}\rho V_{\text{rel}}^2 \, dA_e} \tag{2.5-3}$$

and drag coefficient [37] is

$$C_D = \frac{\text{Drag force}}{\text{Dynamic force}} = \frac{dD}{\frac{1}{2}\rho V_{\text{rel}}^2 \, dA_e} \tag{2.5-4}$$

where dL and dD are the differential lift and drag forces acting on a blade element.

Considering Figure 2.5-2(*a*), the relative wind velocity in n-t plane can be expressed as

$$V_{\text{rel}} = \sqrt{[V_w(1-a)\cos\delta]^2 + [r\Omega(1+a')\cos\delta]^2} \tag{2.5-5}$$

where V_{rel} is relative velocity in the n-t plane and dA_e is the differential area of the blade element calculated by

$$dA_e = c\,dr \tag{2.5-6}$$

Substituting Equations 2.5-3 and 2.5-4 into Equation 2.5-2 yields an equation of the thrust acting on the blade element.

$$dT = \frac{1}{2}\rho c V_{\text{rel}}^2 (C_L \cos \varphi + C_D \sin \varphi)\, dr \cos \delta \tag{2.5-7}$$

For a wind turbine with B blades, Equation 2.5-7 becomes

$$dT_{\text{BET}} = \frac{1}{2}\rho BcV_{\text{rel}}^2 (C_L \cos\varphi + C_D \sin\varphi)\, dr \cos\delta \tag{2.5-8}$$

Similar to Equation 2.3-6, the thrust coefficient is

$$C_{T_{\text{BET}}} = \frac{\sigma \cos^2\delta\,(1-a)^2 (C_L \cos\varphi + C_D \sin\varphi)}{\sin^2\varphi} \tag{2.5-9}$$

The differential torque can be determined by taking moment of the differential tangential force, dF_t, about the Y- axis, i.e.

$$dQ_{\text{BET}} = \frac{1}{2}\rho BcV_{\text{rel}}^2 (C_L \sin\varphi - C_D \cos\varphi)\, r \cos\delta\, dr \tag{2.5-10}$$

Similar to Equation 2.3-13, the torque coefficient is

$$C_{Q_{\text{BET}}} = \frac{\sigma \cos\delta\,(1-a)^2 (C_L \sin\varphi - C_D \cos\varphi)}{\sin^2\varphi} \tag{2.5-11}$$

2.6 Blade Element Momentum Theory

Utilising both momentum theory and blade element theory, a set of equations can be developed to determine the performance of a wind turbine. By equating Equation 2.3-5 multiplied by an overall loss correction factor to Equation 2.5-8

$$\underbrace{\left(dT_{\text{MT}}\right)}_{\text{Equation 2.3-5}} F = \underbrace{dT_{\text{BET}}}_{\text{Equation 2.5-8}}$$

i.e.

$$[4\pi r\rho V_w^2\, a(1-a)\, dr \cos^2\delta]F = \frac{1}{2}\rho BcV_{\text{rel}}^2 (C_L \cos\varphi + C_D \sin\varphi)\, dr \cos\delta \tag{2.6-1}$$

the axial induction factor [42-44] can be derived by substituting Equation 2.2-7 into the right hand side of Equation 2.6-1.

$$a = \frac{1}{\dfrac{4F\sin^2\varphi}{\sigma\cos^2\delta\,(C_L\cos\varphi + C_D\sin\varphi)} + 1} \tag{2.6-2}$$

Remark: Referring to Glauert's experimental result [36], Equation 2.6-2 is only valid for a region of $0 \le a \le 0.4$. For $a > 0.4$, windmill brake model is needed (see details in Section 2.9).

Similarly, the tangential induction factor [42-44] is derived by equating Equation 2.3-12, the differential torque derived from momentum theory with overall loss correction factor, to Equation 2.5-10 derived from blade element theory.

$$\underbrace{\left(dQ_{\mathrm{MT}}\right)}_{\text{Equation 2.3-12}} F = \underbrace{dQ_{\mathrm{BET}}}_{\text{Equation 2.5-10}}$$

i.e.

$$[4\pi r^3 \rho V_w (1-a)\, a' \Omega\, dr \cos^4\delta] F = \frac{1}{2}\rho B c V_{\mathrm{rel}}^2 (C_L\sin\varphi - C_D\cos\varphi)\, r\cos\delta\, dr \tag{2.6-3}$$

Substituting the term $(1-a)$ in the left hand side of Equation 2.6-3 with the relation from Equation 2.2-8 and substituting the term V_{rel} in the right hand side of Equation 2.6-3 with the relation from Equation 2.2-7 yields the tangential induction factor.

$$a' = \frac{1}{\dfrac{4F\sin\varphi\cos\varphi}{\sigma(C_L\sin\varphi - C_D\cos\varphi)} - 1} \tag{2.6-4}$$

Referring to Stoddard's work in 1977 [35], he correlated the behaviour of wind turbine rotors with known experimental data for helicopters reported by Glauert in 1926 [35] and showed that thrust coefficient predicted by momentum theory deviated dramatically from the Glauert's experimental data when the value of axial induction factor is greater than 0.5. To solve this problem, windmill brake state model will be used when the value of axial

induction factor goes beyond 0.4. Also, six-different windmill brake state models will be compared in this research project. They are Glauert's characteristic equation [45-47], classical momentum brake state model [29-31,38,48], advanced brake state model [38,40,49-50], Wilson and Walker model [47,51], modified advanced brake state model [49-50] and Shen's correction [41].

The equations for a and a' must be solved in an iterative manner. The procedure used is:

1. Define the geometry of the turbine by specifying blade chord (c), pretwist (β), coning angle (δ), pitch angle (ϕ) and two-dimensional airfoil section characteristics (α, C_L, C_D).
2. Calculate azimuth angle, θ (Equation 2.7-1), if wind shear effect is included.
3. Calculate solidity ratio, σ (Equation 2.2-1).
4. Calculate wind speed at a height, V_L (Equation 2.7-7), if wind shear effect is included.
5. Calculate local speed ratio, λ_r (Equation 2.2-3). If wind shear effect is included, local speed ratio is represented by λ_L (Equation 2.7-8).
6. Assume initial values for $a = a_1$ and $a' = a'_1$ (zero is an acceptable initial assumption) for a given station.
7. Calculate incoming flow angle, φ (Equation 2.2-8).
8. Calculate angle of attack, $\alpha = \varphi - \beta - \phi$ (Equation 2.2-5).
9. Find C_L and C_D at the corresponding angle of attack found in step 8 by interpolation.
10. Determine a_2 and a'_2 from one of the windmill brake state models listed in Table 2.9-1 [52].
11. Compare a_2 to a_1 and a'_2 to a'_1. If both differences are within a certain preset magnitude, stop and go to the next blade element; otherwise iterate as described in step 12.
12. Find a new estimate for a and a', and go back to step 7. There are two methods for finding the new estimate for a and a'. The first one uses Equations 2.6-2 and 2.6-4. Another one uses the average values calculated from the values found in step 10 with those used at the start of the iteration, i.e.

$$a = \frac{a_1 + a_2}{2} \tag{2.6-5}$$

$$a' = \frac{a'_1 + a'_2}{2} \tag{2.6-6}$$

In practice, Hibbs and Radkey discussed that neither of these methods is unconditionally convergent. However, it has been found that if the assumed values for a and a' are incremented by small amounts toward the values found in step 10, with the increment being decreased whenever the direction of incrementation is reversed, then the method will converge [38].

After determining a and a' at each blade element, the values for the differential thrust, dT, and the differential torque, dQ, can be evaluated, and the differential power is also calculated from

$$dP = \Omega \, dQ \tag{2.6-7}$$

Therefore, the rotor thrust, torque and power are

$$T = \sum dT \tag{2.6-8}$$

$$Q = \sum dQ \tag{2.6-9}$$

$$P = Q\Omega \tag{2.6-10}$$

Finally, thrust, torque and power coefficients can be calculated by theirs definition as follows:

$$\text{Thrust coefficient} = \frac{\text{Thrust}}{\text{Aerodynamic force}} = \frac{\text{Thrust}}{\frac{1}{2}\rho V_w^2 \pi (R\cos\delta)^2} \tag{2.6-11}$$

$$\text{Torque coefficient} = \frac{\text{Rotor torque}}{\text{Aerodynamic torque}} = \frac{\text{Rotor torque}}{\frac{1}{2}\rho V_w^2 \pi (R\cos\delta)^2 (R\cos\delta)} \tag{2.6-12}$$

$$\text{Power coefficient} = \frac{\text{Rotor power}}{\text{Aerodynamic power}} = \frac{\text{Rotor power}}{\frac{1}{2}\rho V_w^3 \pi (R\cos\delta)^2} \tag{2.6-13}$$

The average power of the wind turbine is defined as [37]

$$P_{\text{avg}} = \int_{V=V_{\text{cut-in}}}^{V=V_{\text{cut-out}}} PR(V)\, dV \tag{2.6-14}$$

where P_{avg}, P, $V_{\text{cut-in}}$, and $V_{\text{cut-out}}$ are average power of the wind turbine, turbine power, cut-in wind velocity, and cut-out wind velocity, respectively. $R(V)$ is Rayleigh probability distribution function given by

$$R(V) = \frac{\pi}{2}\left(\frac{V}{\overline{V}^2}\right) e^{-\frac{\pi}{4}\left(\frac{V}{\overline{V}^2}\right)^2} \tag{2.6-15}$$

where $\overline{V}$ stands for the site average wind velocity.

2.7 Wind Shear Effect

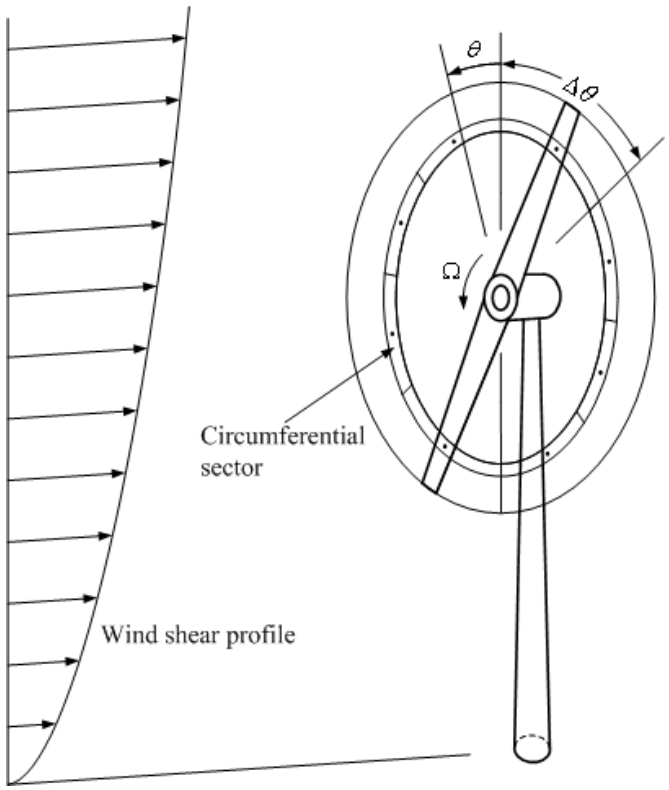

Figure 2.7-1. Analysis points for wind shear model

In Sections 2.3 to 2.6, the relative wind was assumed to be uniform and parallel and to be perpendicular to the rotor plane. In fact, real flows will not be uniform, steady and unidirectional. Wind shear from the atmospheric boundary layer can cause changes in the performance of the blade element whilst it is moving around its path, as well as changes in the average performance [30]. However, Hibbs and Radkey [38] reported that 17% wind speed change across the rotor, which has a rotor diameter equal to hub height for a wind profile exponent of 0.167, causes a small change in the magnitude of the wind shear, so the total performance would be expected to change by a very small amount. Hibbs and Radkey also showed that the final form of the equations for axial induction factor, tangential induction factor, thrust coefficient, torque coefficient and power coefficient are the same as discussed in Section 2.6. The analysis had been done by equating the blade forces to the momentum changes in the annulus, and also the analysis had been carried out over several different circumferential sectors about the annulus with the azimuth angle or circumferential angle, θ, measured from vertical axis.

$$\theta = \frac{180^\circ n_i - 90^\circ}{n_{\text{sector}}}, \quad n_i = 1, 2, \ldots, n_{\text{sector}} \tag{2.7-1}$$

where n_{sector} is the number of circumferential sectors. In Figure 2.7-1, the width of the annular sector is

$$\Delta\theta = \frac{2\pi}{n_{\text{sector}}} \tag{2.7-2}$$

The differential thrust on an annulus is

$$dT_{\text{BET}} = \frac{1}{2}\rho \frac{B\Delta\theta}{2\pi} c V_{\text{rel}}^2 (C_L \cos\varphi + C_D \sin\varphi)\, dr \cos\delta \tag{2.7-3}$$

where $B\Delta\theta/(2\pi)$ is the number of blades appearing in that particular circumferential sector.

The change in flow momentum expressed in terms of the thrust coefficient is

$$dT_{\text{MT}} = C_T \frac{1}{2}\rho V_w^2 2\pi r \frac{\Delta\theta}{2\pi} dr \cos^2\delta \tag{2.7-4}$$

Hibbs and Radkey gave a notice that these two equations are exactly the same as discussed in Section 2.6, except for a $\Delta\theta/(2\pi)$ term in both components. This term can be cancelled when the components are equated. Thus, the final form of the equations for axial induction factor, tangential induction factor, thrust coefficient, torque coefficient and power coefficient will be the same as before. All these equations will be normalised to the local velocity, i.e., the flow speed as seen by the sector. The formula for local wind speed as a function of height is

$$V_L = V_w \left(\frac{H_L}{H_0} \right)^E \tag{2.7-5}$$

where V_w, V_L, H_0, H_L, and E are wind speed at the hub height, the local wind speed, hub height, local height, and wind shear exponent, respectively. H_0 is normalised to the rotor radius. The position of any sector is specified by its radius and its azimuth angle measured from vertical axis. The height at this point is

$$H_L = H_0 + r\cos\theta \tag{2.7-6}$$

and the local wind speed is

$$V_L = V_w \left[1 + \frac{r}{H_0}\cos\theta \right]^E \tag{2.7-7}$$

At this point, it is convenient to introduce the local tip speed ratio based on the local upstream velocity, V_L, for an annulus segment with blade element at height H_L. It is defined as

$$\lambda_L = \frac{\Omega R\cos\delta}{V_L} \tag{2.7-8}$$

Equations 2.2-2 and 2.7-8 give an interesting relation.

$$\lambda_L = \lambda \frac{V_w}{V_L} \tag{2.7-9}$$

By summing the differential thrust, torque and power of each annular and circumferential sector, the averaged values for the entire rotor are obtained.

$$T = \sum \frac{dT}{n_{\text{sector}}} \tag{2.7-10}$$

$$Q = \sum \frac{dQ}{n_{\text{sector}}} \tag{2.7-11}$$

$$P = \sum \frac{dP}{n_{\text{sector}}} \tag{2.7-12}$$

Hibbs and Radkey recommended that it is only necessary to find the performance over half the circle; the other half will be the same. The station taken for each sector is circumferentially midway between the sides of the sector as shown in Figure 2.7-1. In practice, Hibbs and Radkey reported that three to four sections per half annulus give results of sufficient accuracy because there is no variation in the average values if more sections are taken.

2.8 Edgewise and Flapwise Forces and a Pitching Moment

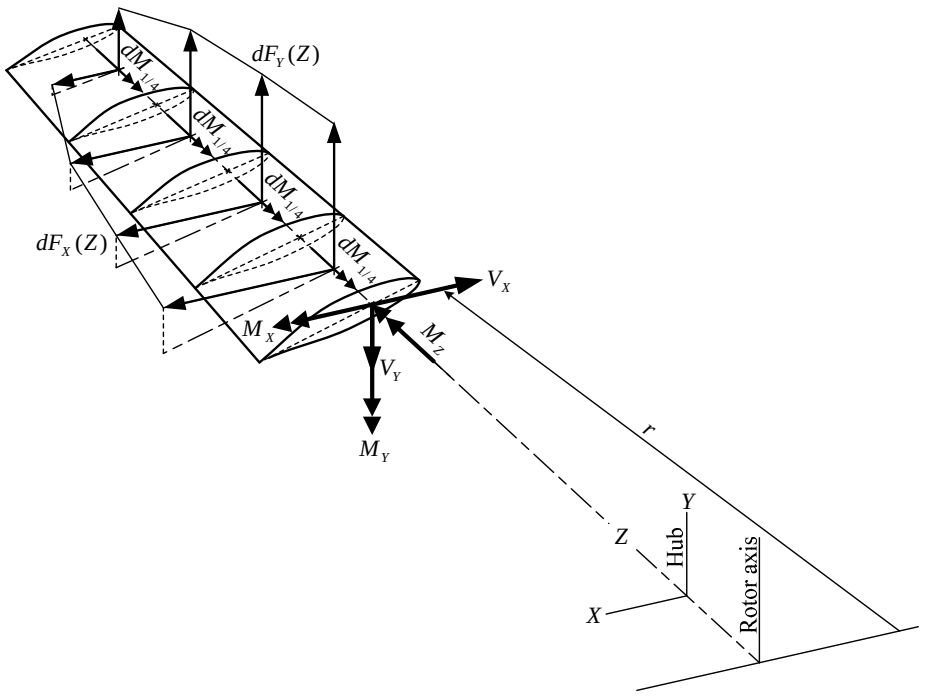

Figure 2.8-1. External loads in a global coordinate of a blade

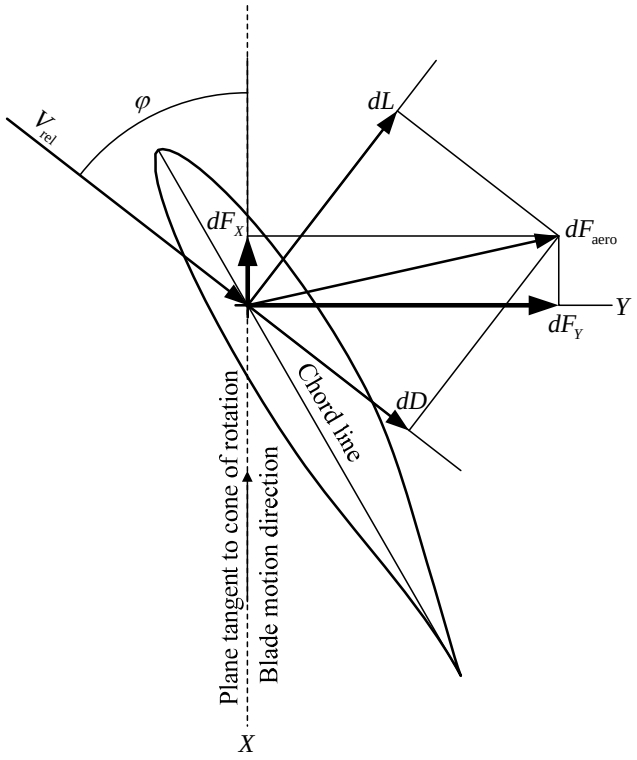

Figure 2.8-2. Aerodynamic forces at a typical element of the blade

This section deals with edgewise force, flapwise force and pitching moment typically shown in Figure 2.8-1. These loads are used by ANSYS structural software for stress analysis in Section 6.4.2. In addition, centrifugal and gravitational loads are included in stress analysis by using ANSYS commands. Knowing lift force, drag force, and pitching moment at each station along the blade span, the desired loads can be determined in a global coordinate of the blade.

In Figure 2.8-2, lift force at each station is

$$dL = \frac{1}{2}\rho c dr V_{\text{rel}}^2 C_L \tag{2.8-1}$$

drag force at each station is

$$dD = \frac{1}{2}\rho c dr V_{\text{rel}}^2 C_D \tag{2.8-2}$$

Therefore,

$$dF_{\text{aero}} = \sqrt{(dL)^2 + (dD)^2} \tag{2.8-3}$$

and pitching moment at each station is

$$dM_{1/4} = \frac{1}{2}\rho c^2 dr V_{\text{rel}}^2 C_{M_{1/4}} \tag{2.8-4}$$

By the principle of axes rotation, edgewise and flapwise forces at a typical blade element can be derived.

Edgewise force:

$$dF_X = -dL \sin\varphi + dD \cos\varphi \tag{2.8-5}$$

Flapwise force:

$$dF_Y = dL \cos\varphi + dD \sin\varphi \tag{2.8-6}$$

Pitching moment:

$$dM_Z = dM_{1/4} \tag{2.8-7}$$

2.9 Windmill Brake State Models

Sections 2.2 to 2.6 deal with basic necessary equations based on BEM theory. All relevant equations are used to implement the HAWTsimulator, an aerodynamic code used in this research project. The results predicted by this computer code are validated against the results predicted by WT_Perf [49] (see details in Chapter 3). In recent years, researchers have modified the BEM calculation to provide more accurate results. In this research project, six different windmill brake state models are included to the HAWTsimulator to improve the efficiency in calculation.

The windmill brake state model is important because it can affect the accuracy of predicted performance. The BEM calculation often calculates the value of thrust coefficient in this state of operation. In 1977, Stoddard [35] showed that thrust coefficient, $C_T = 4a(1-a)$,

predicted by momentum theory deviated dramatically from the Glauert's experimental data when the value of axial induction factor is greater than 0.5. Unfortunately, the Glauert's experimental data are given only for the condition without the tip loss effect which must be applied to the thrust coefficient relation to make more realistic of prediction. In 1983, Hibbs and Radkey [38] reported a quadratic equation used to fit some experimental data of rotors operating in the turbulent wake state. They quoted that this quadratic closely approximates *Glauert's empirical formula* so it might be called *quadratic approximation*.

$$C_T = 0.889 - 0.444a + 1.556a^2 \tag{2.9-1}$$

Another form of Equation 2.9-1 was reported by Buhl, Jr. [53].

$$C_T = 0.889 - \frac{0.0203 - (a - 0.143)^2}{0.6427} \tag{2.9-2}$$

This quadratic gives the same value as momentum theory when a is 0.4, as well as the same slope of the curve, and yields $C_T = 2$ at $a = 1$ (see Figure 2.9-1). However, the overall loss correction factor, F, is not taken into account. In BEM calculation, a numerical problem (gap) occurs when the overall loss correction factor is applied to the thrust equation obtained from the momentum theory, i.e.

$$C_T = 4aF(1 - a) \tag{2.9-3}$$

Plotting Equation 2.9-3 shows a gap between the momentum theory curve and quadratic curve as shown in Figure 2.9-1. This gap causes a discontinuity when a computer programme is used to iterate for the new induction factor, a_2.

Hibbs and Radkey attempted to correct the gap problem by replacing a with aF.

$$C_T = 0.889 - 0.444aF + 1.556a^2F^2 \tag{2.9-4}$$

Unfortunately, this modification just lowers the entire parabolic curve, but cannot completely eliminate the discontinuity as shown in Figure 2.9-1.

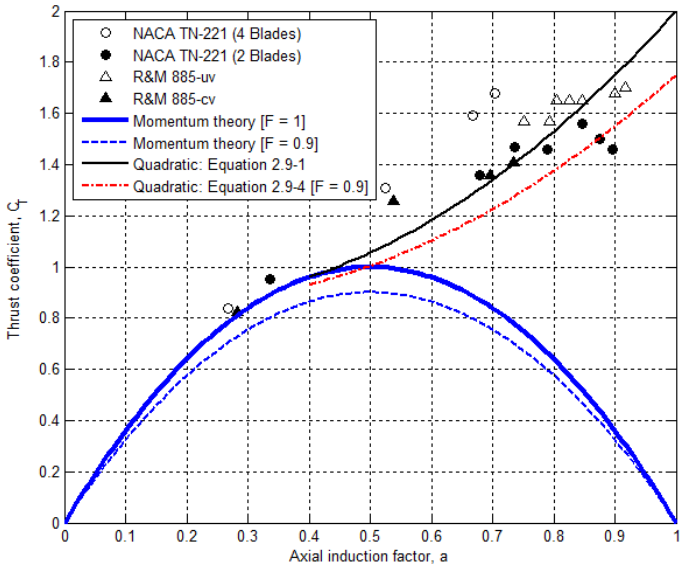

Figure 2.9-1. Discontinuity (gap) problem (Experimental data are digitised from [31])

Owing to lacking of experimental data with tip loss effect, several researchers proposed different empirical equations to correct discontinuity and to improve the accuracy of the prediction. At present, there are six windmill brake state models (see Table 2.9-1) which can be used for correcting the gap problem. They are Glauert's characteristic equation, classical momentum brake state model, advanced brake state model, Wilson and Walker model, modified advanced brake state model and Shen's correction.

2.9.1 Glauert's Characteristic Equation

$$C_T = 4aF\left(1-\frac{1}{4}(5-3a)a\right) \tag{2.9-5}$$

This windmill brake state model is reported by Bak *et al*. [45], Mejia *et al*. [46] and Hansen [47]. Glauert's characteristic equation is expressed in cubic form.

2.9.2 Classical Momentum Brake State Model

$$C_T = aF(1-aF) = \frac{\sigma\cos^2\delta}{4\sin^2\varphi}(C_L\cos\varphi + C_D\sin\varphi)(1-a)^2 \tag{2.9-6}$$

In 1974, Wilson and Lissaman reviewed the aerodynamics of various types of wind power machines and published paper titled "Applied Aerodynamics of Wind Power

Machines" [30]. Wilson and Lissaman developed an AeroVironment wind turbine analysis computer code named PROP and the "Wilson model" was used as a windmill brake state model. This model did not permit the thrust coefficient to exceed 1.0. Later, in 1976, Wilson, Lissaman and Walker [31] reported the state of the art of performance prediction methods for both horizontal and vertical wind turbines and suggested using Wilson model to predict the wind turbine performance. From 1981 to 1983, Hibbs and Radkey [38] updated the PROP code, developed by Wilson and Lissaman, for NASA Lewis Research Center. In the code, the Wilson model was called the "classical momentum brake state model". At present, the Wilson model is still implemented in several computer codes, e.g. WT_Perf developed by Buhl, Jr. [49]. In WT_Perf code, Wilson model is called "classical brake model". To avoid confusing the model name, in this thesis, Wilson model will be called "classical momentum brake state model".

2.9.3 Advanced Brake State Model

In 1983, Hibbs and Radkey modified Glauert's empirical formula for use with wind turbines and implemented this modification in the PROP code [38]. A quadratic described by Equation 2.9-4 was decided to approximate the relationship between a and C_T. Unfortunately, this modification just lowers the entire parabolic curve as shown in Figure 2.9-1. It cannot completely eliminate the discontinuity (gab problem). Later, in 1997, Buhl, Jr. [39] simplified the calculation of the advanced brake state model in WT_Perf code by replacing the quadratic, Equation 2.9-4, with a simple parabola.

$$C_T = B_2 a^2 + B_1 a + B_0 \tag{2.9-7}$$

where

$$\begin{aligned} B_2 &= 1/0.18 - 4F \\ B_1 &= 0.8(F - B_2) \\ B_0 &= 2 - B_1 - B_2 \end{aligned} \tag{2.9-8}$$

In 2005, Buhl, Jr. [53] published this simplification in another form

$$C_T = \frac{8}{9} + \left(4F - \frac{40}{9}\right)a + \left(\frac{50}{9} - 4F\right)a^2 \tag{2.9-9}$$

This relation is used when $a > 0.4$.

At present, advanced brake state model simplified by Buhl, Jr. is also implemented in AeroDyn code [40].

2.9.4 Wilson and Walker Model

$$C_T = \begin{cases} 4aF(1-a), & a \le (a_c = 0.2) \\ 4F(a_c^2 + (1-2a_c)a), & a > (a_c = 0.2) \end{cases} \quad (2.9\text{-}10)$$

In 1998, Wilson referred to a set of the local thrust coefficients shown by Wilson and Walker published in 1984 and reported this set of equations in David A. Spera's book [51]. Wilson quoted that a set of thrust coefficient equations agrees well with vortex theory calculations and produces good results between the calculated and measured performance and loads. At present, this model is also reported in Hansen's book published in 2008 [47].

2.9.5 Modified Advanced Brake State Model

In 1998, Buhl, Jr. [49] modified the use of the quadratic, Equation 2.9-1, implemented in WT_Perf code so that the coefficients of the quadratic are a function of the losses.

$$C_T = 0.889F - 0.444aF + 1.556a^2F^2 \quad (2.9\text{-}11)$$

This modification can completely solve the gap problem. Buhl, Jr. did not name this modification, so it might be called "modified advanced brake state model". Also, Buhl, Jr. changed equation of thrust coefficient for $C_T \le 0.4$ from $C_T = 4aF(1-aF)$ to $C_T = 4aF(1-a)$. In the same year, Pierce and Buhl, Jr. changed the induction factor calculations in AeroDyn [50] to mimic that of WT_Perf.

2.9.6 Shen's Correction

$$C_T = \begin{cases} 4aF(1-aF), & a \le (a_c = 1/3) \\ 4[a_c^2F^2 + (1-2a_cF)aF], & a > (a_c = 1/3) \end{cases} \quad (2.9\text{-}12)$$

In 2005, Shen *et al*. [41] proposed a new tip loss correction model to predict the physical behaviour in the proximity of the tip. In this work, Shen *et al*. replaced the local thrust coefficient by a linear relation when the value of axial induction factor becomes greater than a critical value.

Table 2.9-1. Wind mill brake state models [52]

Parameters	Glauert's Characteristic equation [45-47]	Classical momentum brake state model [30-31,38,49]	Advanced brake state model [38,49-50,53]	Wilson and Walker model [47,51]	Modified advanced brake state model [38,49-50]	Shen's correction [41]
Thrust coefficient	$C_T = \begin{cases} 4aF(1-a) \text{ or } S_w(1-a)^2 & a \le (a_c = 1/3) \\ 4aF(1-\frac{1}{4}(5-3a)a) & a > (a_c = 1/3) \end{cases}$	$C_T = aF(1-aF) = S_w(1-a)^2$	$C_T = \begin{cases} 4aF(1-a) \text{ or } S_w & a \le (a_c = 0.4) \\ \frac{8}{9} + \left(4F - \frac{40}{9}\right)a + \left(\frac{50}{9} - 4F\right)a^2 & a > (a_c = 0.4) \end{cases}$	$C_T = \begin{cases} 4aF(1-a) \text{ or } S_w(1-a)^2 & a \le (a_c = 0.2) \\ 4F[a_c^2 + (1-2a_c)a] & a > (a_c = 0.2) \end{cases}$	$C_T = \begin{cases} 4aF(1-a) \text{ or } S_w(1-a)^2 & a < (a_c = 0.4) \\ F(0.889 - 0.444a + 1.556a^2) & a \ge (a_c = 0.4) \end{cases}$	$C_T = \begin{cases} 4aF(1-a) \text{ or } S_w(1-a)^2 & a \le (a_c = 1/3) \\ 4[a_c^2F^2 + (1-2a_cF)aF] & a > (a_c = 1/3) \end{cases}$
Axial induction factor	$a = \begin{cases} \frac{1-\sqrt{1-C_T/F}}{2} & C_T \le 0.889F \\ Y - \frac{11}{81Y^2} + \frac{5}{9} & C_T > 0.889F \end{cases}$	$a = \frac{2S_w + F - \sqrt{F^2 + 4S_wF(1-F)}}{2(S_w + F^2)}$	$a = \begin{cases} \frac{1}{\frac{4F\sin^2\varphi}{\sigma(C_L\cos\varphi + C_D\sin\varphi)} + 1} & C_T \le 0.96F \\ \frac{18F - 20 - 3\sqrt{C_T(50-36F) + 12F(3F-4)}}{36F - 50} & C_T > 0.96F \end{cases}$	$a = \begin{cases} \frac{1-\sqrt{1-\frac{C_T}{F}}}{2} & C_T \le 0.64F \\ \frac{C_T - 4Fa_c^2}{4F(1-2a_c)} & C_T > 0.64F \end{cases}$	$a = \begin{cases} \frac{1-\sqrt{1-\frac{C_T}{F}}}{2} & C_T < 0.96F \\ 0.1432 + \sqrt{-0.55106 + 0.6427\frac{C_T}{F}} & C_T \ge 0.96F \end{cases}$	$a = \begin{cases} \frac{1-\sqrt{1-C_T}}{2F} & C_T \le 0.889 \\ \frac{2 + Y_1 - \sqrt{4Y_1(1-F) + Y_1^2}}{2(1+FY_1)} & C_T > 0.889 \end{cases}$
Tangential induction factor	$a' = \frac{1}{\frac{4F\sin\varphi\cos\varphi}{\sigma(C_L\sin\varphi - C_D\cos\varphi)} - 1}$	$a' = \frac{1}{\frac{8F\sin\varphi\cos\varphi}{\sigma(C_L\sin\varphi - C_D\cos\varphi)} - 1}$	$a' = \frac{1}{\frac{4F\sin\varphi\cos\varphi}{\sigma(C_L\sin\varphi - C_D\cos\varphi)} - 1}$	$a' = \frac{1}{\frac{4F\sin\varphi\cos\varphi}{\sigma(C_L\sin\varphi - C_D\cos\varphi)} - 1}$	$a' = \begin{cases} 0 & 1 + a'' < 0 \\ \frac{\sqrt{1+a''} - 1}{2} & 1 + a'' \ge 0 \end{cases}$	$a' = \frac{1}{\frac{(1-aF)Y_2}{1-a} - 1}$
Solidity ratio	$\sigma = \frac{Bc}{2\pi r\cos\delta}$	$\sigma = \frac{Bc}{\pi r\cos\delta}$	$\sigma = \frac{Bc}{2\pi r\cos\delta}$	$\sigma = \frac{Bc}{2\pi r\cos\delta}$	$\sigma = \frac{Bc}{2\pi r\cos\delta}$	$\sigma = \frac{Bc}{2\pi r\cos\delta}$
Constants	$S_w = \frac{\sigma\cos^2\delta}{\sin^2\varphi}(C_L\cos\varphi + C_D\sin\varphi)$ $Y = \left[\sqrt{\frac{1}{36}\left(\frac{C_T}{F}\right)^2 - \frac{145}{2187}\frac{C_T}{F} + \frac{92}{2187}} + \frac{C_T}{6F} - \frac{145}{729}\right]^{1/3}$	$S_w = \frac{\sigma\cos^2\delta}{8\sin^2\varphi}(C_L\cos\varphi + C_D\sin\varphi)$	$S_w = \frac{\sigma\cos^2\delta}{\sin^2\varphi}(C_L\cos\varphi + C_D\sin\varphi)$	$S_w = \frac{\sigma\cos^2\delta}{\sin^2\varphi}(C_L\cos\varphi + C_D\sin\varphi)$	$S_w = \frac{\sigma\cos^2\delta}{\sin^2\varphi}(C_L\cos\varphi + C_D\sin\varphi)$ $a'' = \frac{4aF(1-a)}{\lambda_r^2}$ $\lambda_r = \frac{\Omega r\cos\delta}{V_w}$	$S_w = \frac{\sigma\cos^2\delta}{\sin^2\varphi}(C_L\cos\varphi + C_D\sin\varphi)$ $Y_1 = \frac{4F\sin^2\varphi}{\sigma F_1(C_L\cos\varphi + C_D\sin\varphi)}$ $Y_2 = \frac{4F\sin\varphi\cos\varphi}{\sigma F_1(C_L\sin\varphi - C_D\cos\varphi)}$ $F_1 = \frac{2}{\pi}\cos^{-1}\left[\exp\left(-g\frac{B(R-r)}{2r\sin\varphi}\right)\right]$ $g = \exp[-0.125(B\lambda_r - 21)] + 0.1$ F is calculated from Equation 2.4-2.

2.10 Estimation of the Lift, Drag and Pitching Moment Coefficients

In BEM calculations, the airfoil sections are represented by tables of lift, drag and pitching moment coefficients as a function of angle of attack and Reynolds number. With these tables, the aerodynamic coefficients at a particular angle of attack are determined by interpolation. Frequently, the BEM calculation simulates conditions in which the angle of attack is beyond the normal range of an airfoil whilst the aerodynamic tables are often available in a limited range. In order to generate coefficients over this range, a set of Viterna's empirical equations [54-57] will be used to expand the limited aerodynamic table to cover the entire range of $\pm 180^{\circ}$.

2.11 Summary

This chapter mainly deals with the derivation of a set of BEM equations. In principle, the BEM theory is based on Glauert's airscrew theory which relates thrust and torque obtained from momentum theory to those obtained from blade element theory. Consequently, the axial and tangential induction factors are determined. For the comparative purpose, the BEM theory is commonly used to predict the wind turbine performance because of two advantages, i.e. the computational speed and ease of implementation. The BEM theory is considered to be an effective tool during the design process to get good first order prediction of wind turbine performance under a wide range of operating conditions.

Section 2.2 introduced the kinematic parameters and their definitions appearing in the aerodynamic model. The concept and assumptions in applying the linear and angular momentum principles to an annulus control volume enclosed by a stream tube is mentioned in Section 2.3. In theory, the wind turbine rotor is assumed to be an actuator disc which represents an infinite number of blades with zero chord length. Furthermore, the flow crossing each annulus is assumed as uniform. But, in fact, the wind turbine rotor has a finite number of blades with finite tip chord and each blade sheds a discrete vortex near the tip. Consequently, the aerodynamic losses caused by vortices shed from the tips of finite blades are not taken into account. To include this effect, an overall loss correction factor, detailed in Section 2.4, needs to be applied to thrust and torque equations. Section 2.5 deals with the concept and assumptions of blade element theory. Combining thrust equations obtained from momentum and blade element theories, an axial induction factor can be determined. Similarly, a tangential induction factor can be determined by combining torque equations obtained from each theory. Both axial and tangential

induction factors were mentioned in Section 2.6. These factors are results of the BEM theory. Knowing the values of axial and tangential induction factors, the rotor thrust, torque and power can easily be determined. Also, Section 2.6 summarised the step by step of the BEM calculation process implemented in HAWTsimulator, an aerodynamic code used in this research project. The implementation of HAWTsimulator will be mentioned in Chapter 3. To make the code more realistic in prediction, the wind shear effect is introduced in Section 2.7. Section 2.8 listed a set of equations in calculating flapwise force, edgewise force and pitching moment. These loads will be used for stress analysis discussed in Section 6.4.2. Section 2.9 mentioned to windmill brake state models. In Section 2.9.10, estimation of lift, drag and pitching moment coefficients are mentioned.

In summary, this chapter deals with the derivation of a set of BEM equations. All equations appeared in each section are implemented in HAWTsimulator. This code is used to generate the sets of aerodynamic loads acting along the blade span in a range of wind speed from cut-in to cut-out. These sets of aerodynamic loads will be used when stress analysis in ANSYS structural software is performed. By using ANSYS commands, centrifugal and gravitational loads are also included in stress analysis.

The outcome of this chapter is a journal paper [52]. This paper is relevant to the windmill brake state models mentioned in Section 2.9.

Chapter 3

Implementation of Aerodynamic Computer Code

3.1 Introduction

This chapter deals with an aerodynamic computer code for predicting the performance of HAWTs, called HAWTsimulator [52]. The computer code is developed by the author at University of Northumbria at Newcastle. It is designed to be run in a Matlab environment. The main objective of this implementation is to generate a set of aerodynamic loads acting along the blade span. The desired loads will be linked to ANSYS structural software to analyse stress in Section 6.4.2. Basically, HAWTsimulator is based on BEM theory derived in Chapter 2. BEM theory breaks the blade into small elements along the radius of the rotor plane; calculates the performance information for each element; then sums individual components such as power, torque, thrust, drag, etc. for total performance information of the entire rotor. BEM theory uses several equations in an iteration process to calculate performance. HAWTsimulator is improved the efficiency of prediction by adding up-to-date subroutines which are tip and hub loss correction factors (see Section 2.4) and windmill brake state models (see Section 2.9).

Under the same simulation conditions, the power curves generated by HAWTsimulator are validated against the power curve generated by WT_Perf [49], a wind turbine performance evaluation software. WT_Perf uses BEM theory to predict the performance of wind turbine rotor. This software is a descendent of the PROP code originally developed by Oregon State University decades ago [58]. It is written in Fortran 95 by Marshall L. Buhl, Jr. from National Renewable Energy Laboratory (NREL). The software is designed to be run in a DOS environment and it has been certified by NREL to be accurate through experimental testing (www.NREL.org).

In this research project, a set of aerodynamic loads, which are flapwise and edgewise forces and a pitching moment, must be linked to ANSYS structural software for stress analysis in Section 6.4.2. Unfortunately, WT_Perf cannot generate the desired loads. In addition, these loads are required to be acted in a global coordinate system of the blade. Thus, it is necessary to implement HAWTsimulator which is suitable for this objective. In

the next sections, implementation and validation of HAWTsimulator and generation of aerodynamic loads will be discussed.

3.2 Implementation of HAWTsimulator

HAWTsimulator uses the Graphic User Interface (GUI) shown in Figure 3.2-1 to get simulation conditions and to display results. Blade topology and aerodynamic tables of each airfoil are input from data files. Considering Block 1 in Figure 3.2-1, the simulation conditions are number of blades (B), rotor radius (R), hub radius (r_{hub}), pitch angle (ϕ), conning angle (δ), rotor speed (Ω), number of segments and maximum number of loop of iteration. Also, tip and hub loss correction factors mentioned in Section 2.4 can be applied here. Block 2 is relevant to cut-in and cut-out wind speeds, site average wind speed, air density, hub height and wind shear exponent. Block 3 deals with windmill brake state models (see Section 2.9) to be used in the simulation. They are Glauert's characteristic equation, classical momentum brake state model, advanced brake state model, Wilson and Walker model, modified advanced brake state model and Shen's correction. Tip and hub loss correction factors can be selected in Blocks 4 and 5. Block 6 shows a list of simulated results to be selected for displaying in Block 7. Finally, all results are saved to files in both Excel and TXT formats. A set of aerodynamic loads to be used by ANSYS structural software is saved in latter format. Next, how HAWTsimulator works is discussed.

Considering the flowchart in Figure 3.2-3, the calculation process of HAWTsimulator consists of three main loops: wind speed; segment; and circumferential loops. The latter is an optional loop for including wind shear effects in the simulation. At the beginning, all input parameters are loaded into the code and then three-dimensional figures of the blade are displayed as typically shown in Figure 3.2-2.

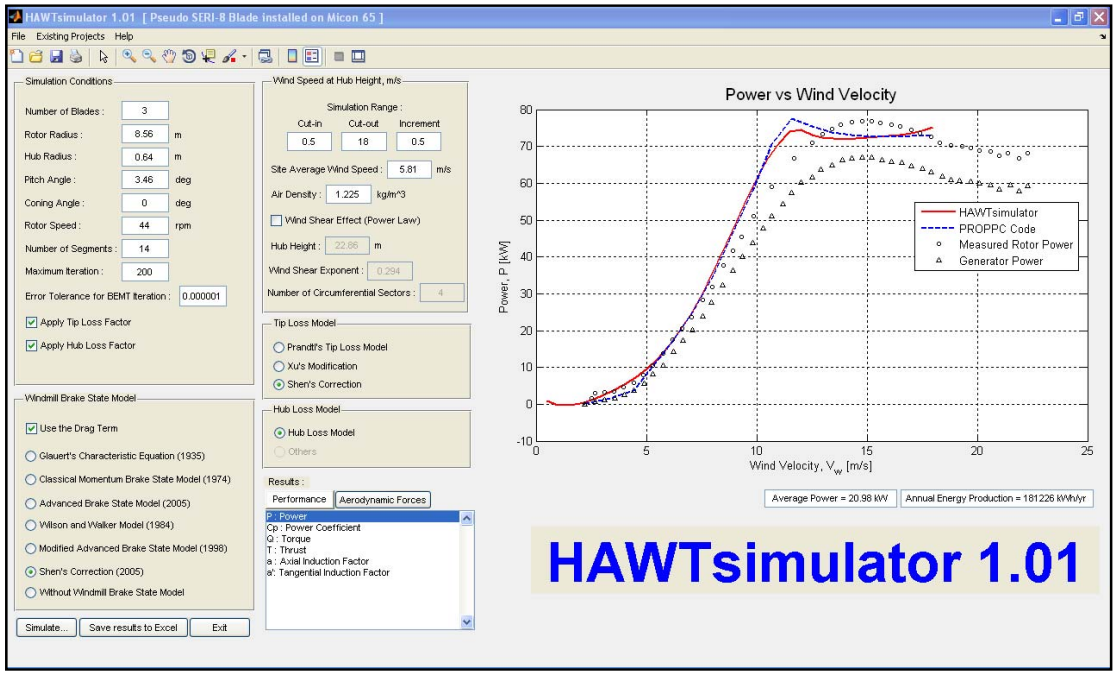

Figure 3.2-1. GUI of HAWTsimulator

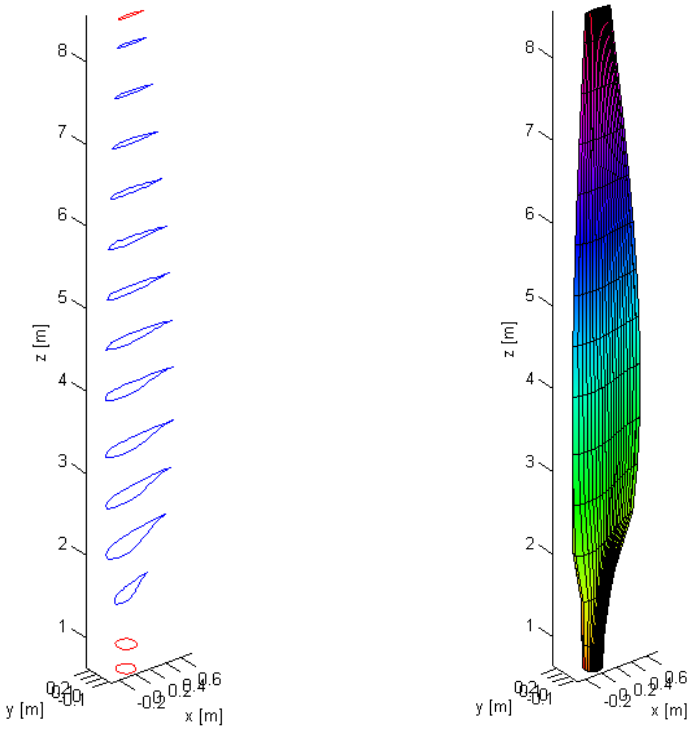

(*a*) (*b*)

Figure 3.2-2. Typical three-dimensional figures generated by HAWTsimulator (*a*) airfoil distribution (*b*) 15-blade stations and 14-blade elements

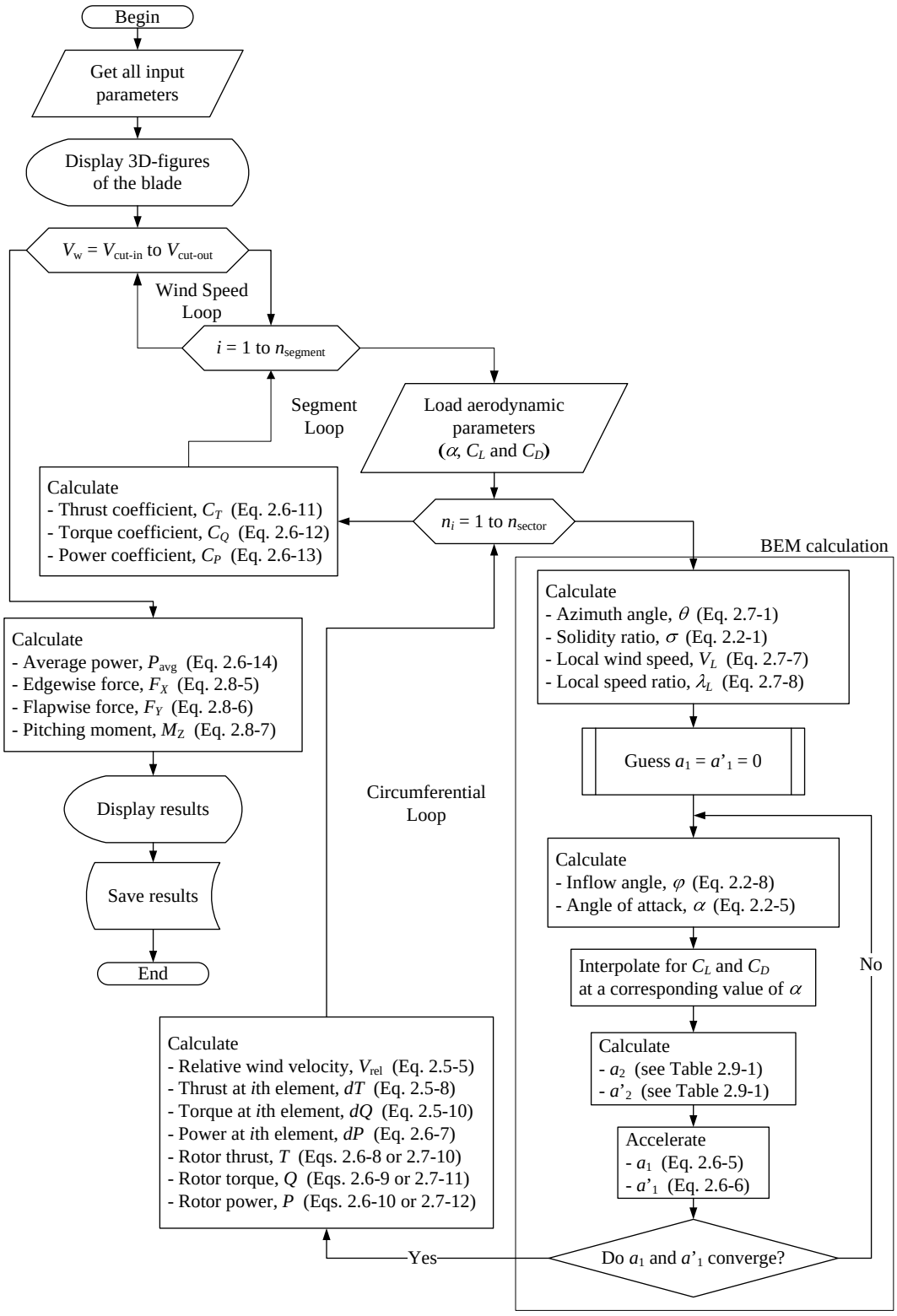

Figure 3.2-3. Flowchart of HAWTsimulator

The first loop is a wind speed loop which varies wind speed from cut-in speed to cut-out speed with a given increment.

The second loop is a segment loop which varies radius, r, from the middle of the first element near the hub to the middle of the final element near the tip as typically shown in Figure 3.2-4. The width of each blade element is defined by

$$dr_i = 2(r_i - r_{i-1}), \quad i = 1, 2, 3, \ldots, n_{\text{segment}} \tag{3.2-1}$$

where n_{segment} is total number of the blade elements and r_0 is the hub radius. In this loop, an aerodynamic table, listing α, C_L, and C_D of the airfoil at the *i*th blade element, is loaded into the code.

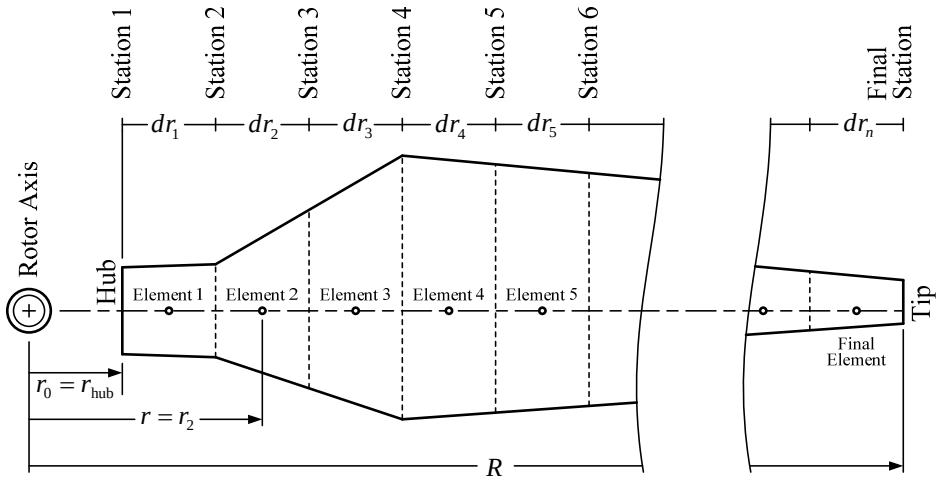

Figure 3.2-4. How to vary r in the segment loop

The third loop is a circumferential loop. This loop is optional for including wind shear effect detailed in Section 2.7. In the calculation process, the number of circumferential sectors is specified via GUI, Block 4. The computer sums the differential thrust, torque and power of each annular and circumferential sector typically shown in Figure 3.2-5 and then calculates the averaged values for the entire rotor.

Finally, BEM calculation, discussed in Sections 2.6 and 2.7, is performed in the segment loop with or without circumferential loop.

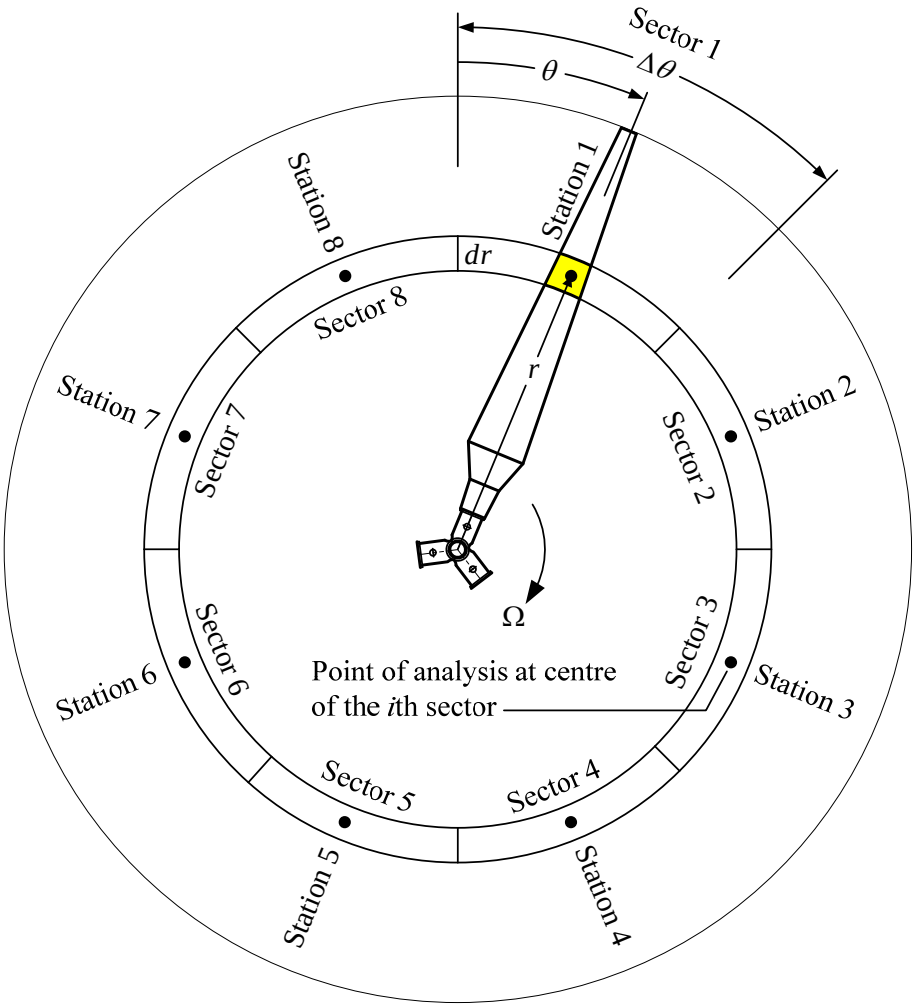

Figure 3.2-5. How to vary sector of each annulus in circumferential loop

3.3 Validation of HAWTsimulator

The results generated by HAWTsimulator are validated against those generated by WT_Perf [49]. The wind turbine model used in the validation is AWT-27CR2 wind turbine detailed in Table B1. For the validation purpose, all parameters listed in Table B1 are specified to the code via GUI as shown in Figure 3.3-1. After finished running the code, rotor power, rotor torque, thrust, power coefficient and maximum flap bending moment at the hub are compared to those generated by WT_Perf as shown in Figures 3.3-2 to 3.3-6. The validations indicate that all parameters are exactly the same as those generated by WT_Perf. This comparison indicates that HAWTsimulator is valid. In the next section, the aerodynamic simulation of a wind turbine model used in this research project will be discussed. Also, the desired loads to be used by ANSYS structural software will be reported.

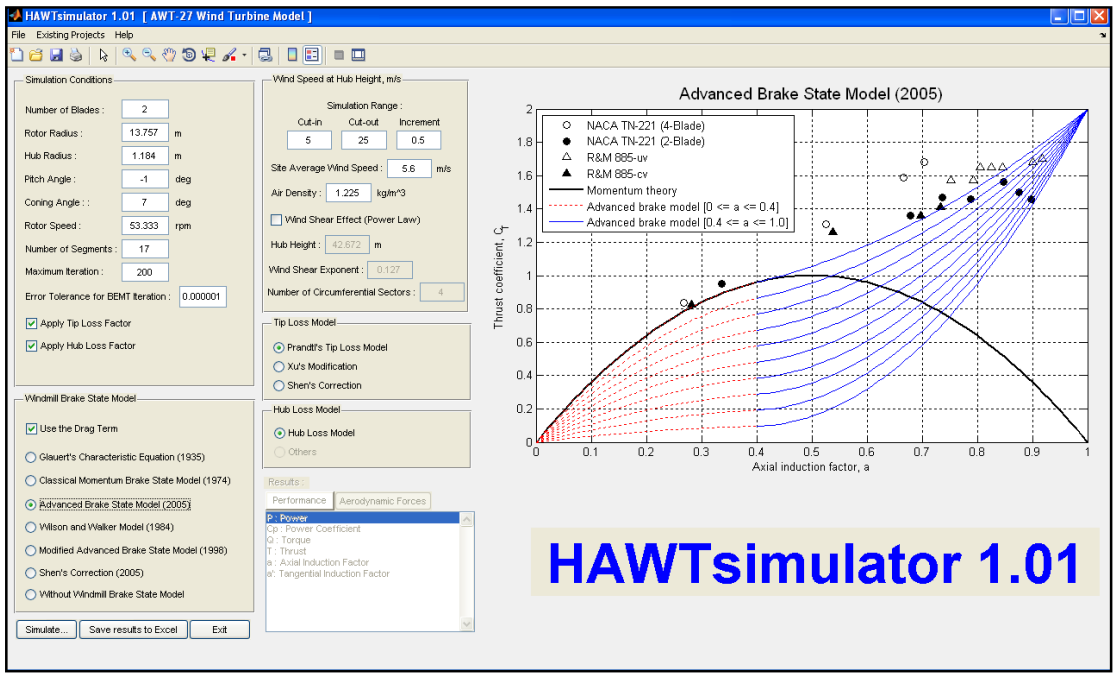

Figure 3.3-1. Wind turbine parameters and simulation conditions

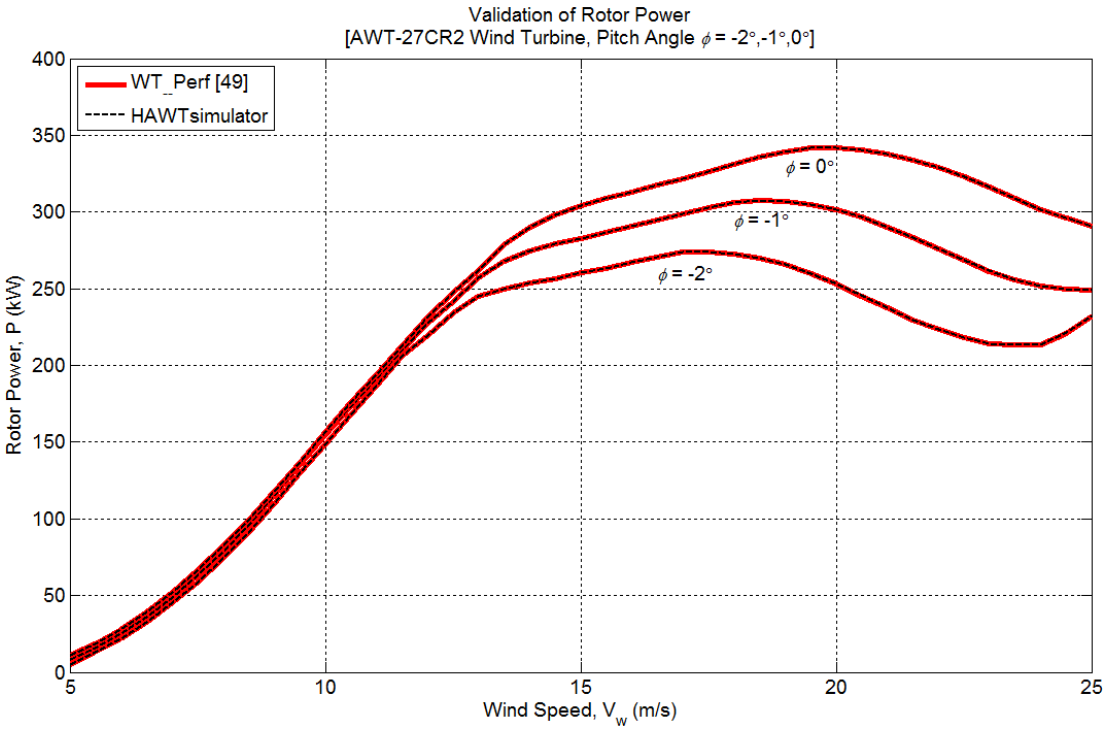

Figure 3.3-2. Validation of rotor power

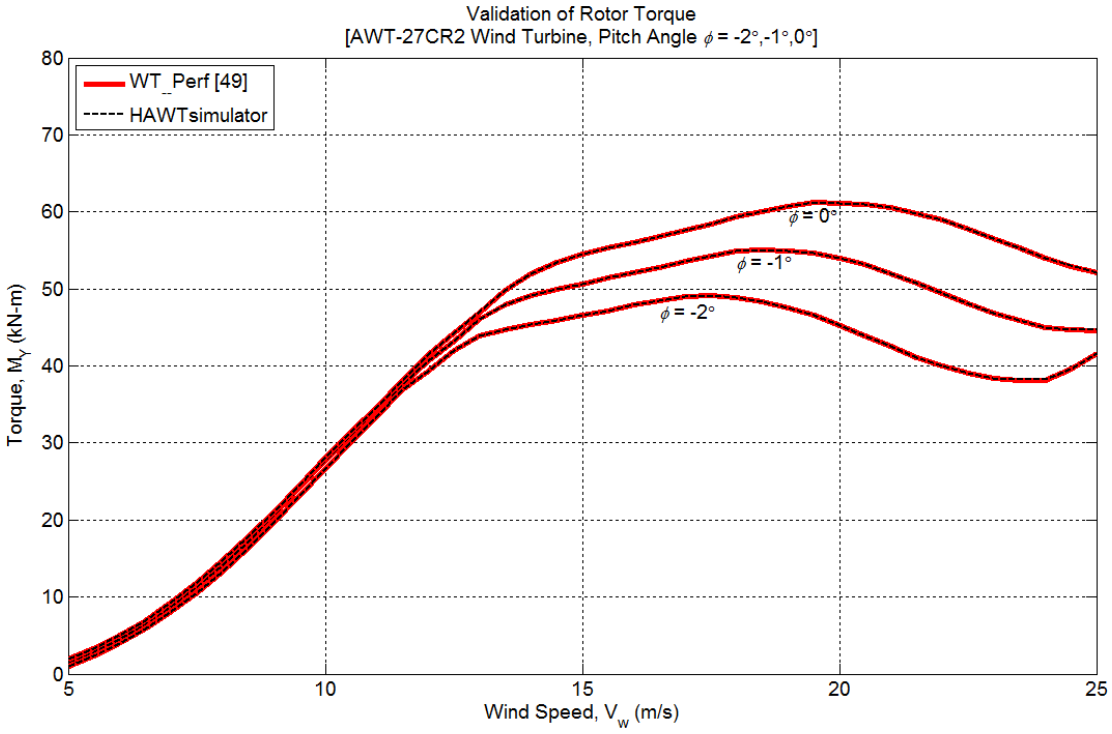

Figure 3.3-3. Validation of rotor torque

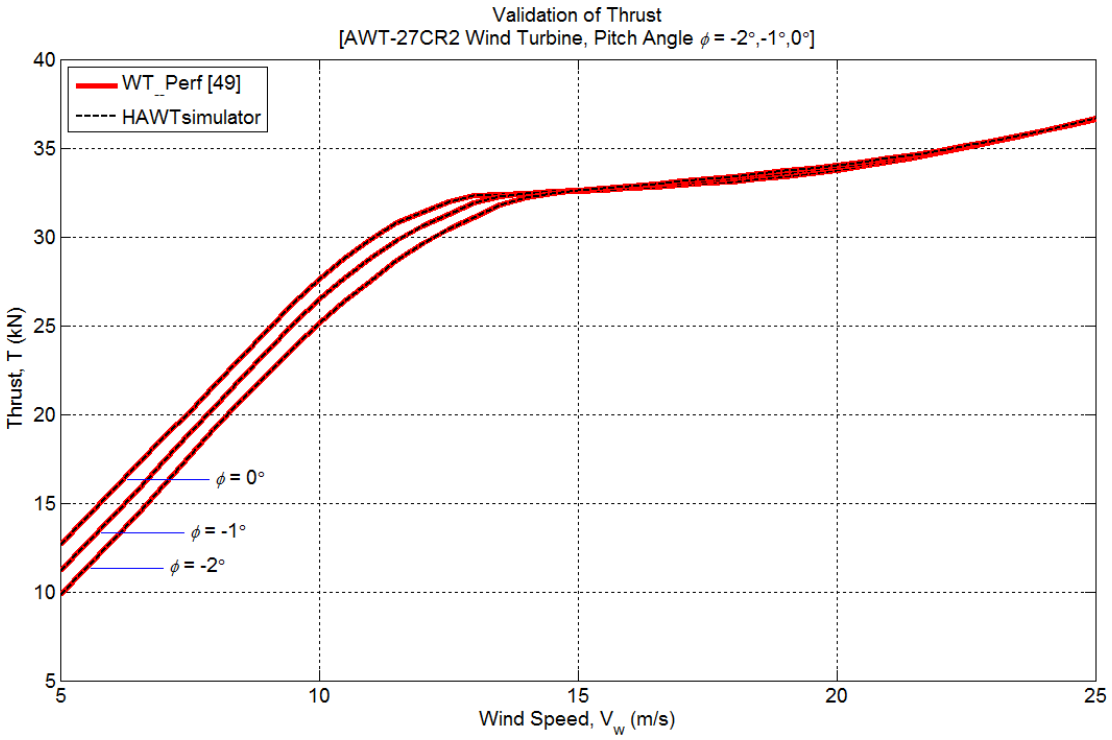

Figure 3.3-4. Validation of thrust

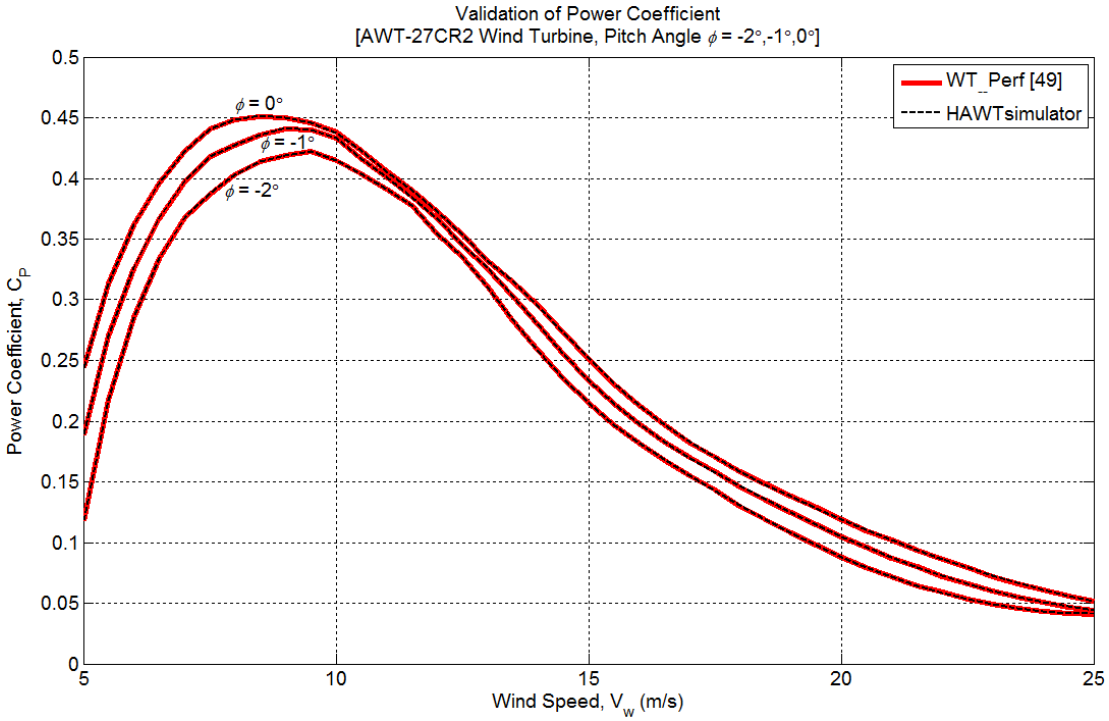

Figure 3.3-5. Validation of power coefficient

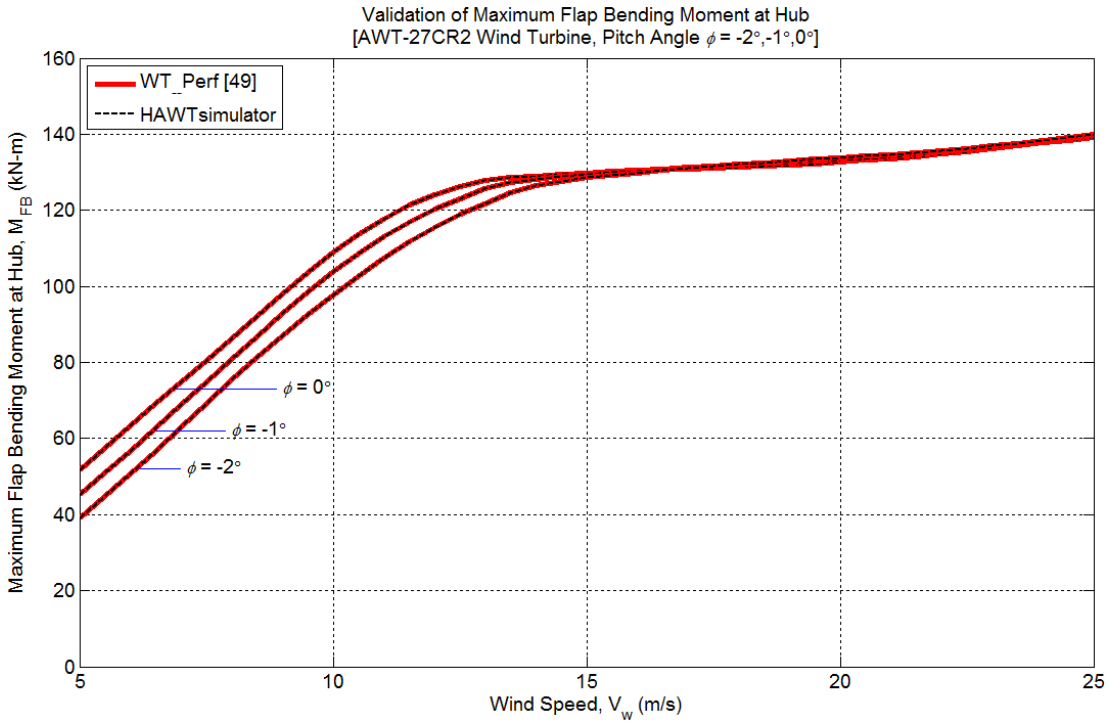

Figure 3.3-6. Validation of maximum flap bending moment at the hub

3.4 Aerodynamic Simulation of a Micon 65 Wind Turbine Model

A SERI-8 blade is installed on 65-kW three bladed, Danish up-wind turbine called Micon 65 [59-60]. The blade material is fibre-reinforced polyester resins. At the tip region, there is a pitching tip for controlling centrifugal overspeed. At the hub, the blade is connected to a ridged, fixed pitch hub. In high wind, the peak of rotor power is regulated by aerodynamic stall. Rotor power curve is designed to be flat peak near 65 kW. With clean blades, actual power is regulated closer to 80 kW. Rotor speed of 44 rpm at the input shaft is transmitted through two-stage gearbox with an output speed of 1,200 rpm. The nacelle sits on a freestanding steel tube tower and is held upwind by a yaw drive. Electric power is generated by one of two 480 VAC induction generators in the nacelle. The small generator has a 13-kW capacity and operates until wind speed exceeds about 9 m/s. Above this level the turbine switches to the large generator rated at 65 kW [61].

Firstly, the shape of the SERI-8 blade is modelled by using data reported by Ong and Tsai [62] to generate loads acting along the blade span. Secondly, specification and operating conditions of Micon 65 are loaded into HAWTsimulator to simulate rotor power. After having reasonably power curve, loads acting along the blade span are generated. They are edgewise force, F_X, flapwise force, F_Y, and a pitching moment, M_Z. These loads will be imported to ANSYS structural software to determine a critical stress value and where it occurs (see details in Section 6.4.2).

Unfortunately, the specification of Micon 65 wind turbine is not completely reported by only one research group. The data used in the simulation, listed in Tables B3 and B4, are collected from reports and research papers done by several authors who did research on Micon 65 wind turbine.

In the simulation, a pseudo SERI-8 blade is divided into 14 sections as shown in Figure A1. Simulation conditions, listed in Tables B3 and B4, are input to the HAWTsimulator via GUI as shown in Figure 3.2-1. The topology of the wind turbine, listed in Table B5, is input to the code via an input file. After finished running programme, a rotor power curve is obtained. The result is validated against rotor power curve generated by PROPPC code referenced in Tangler *et al.* [59]. As shown in Figure 3.4-1, simulated power curve is slightly different from that generated by PROPPC code [62] with a correlation value of 0.9987.

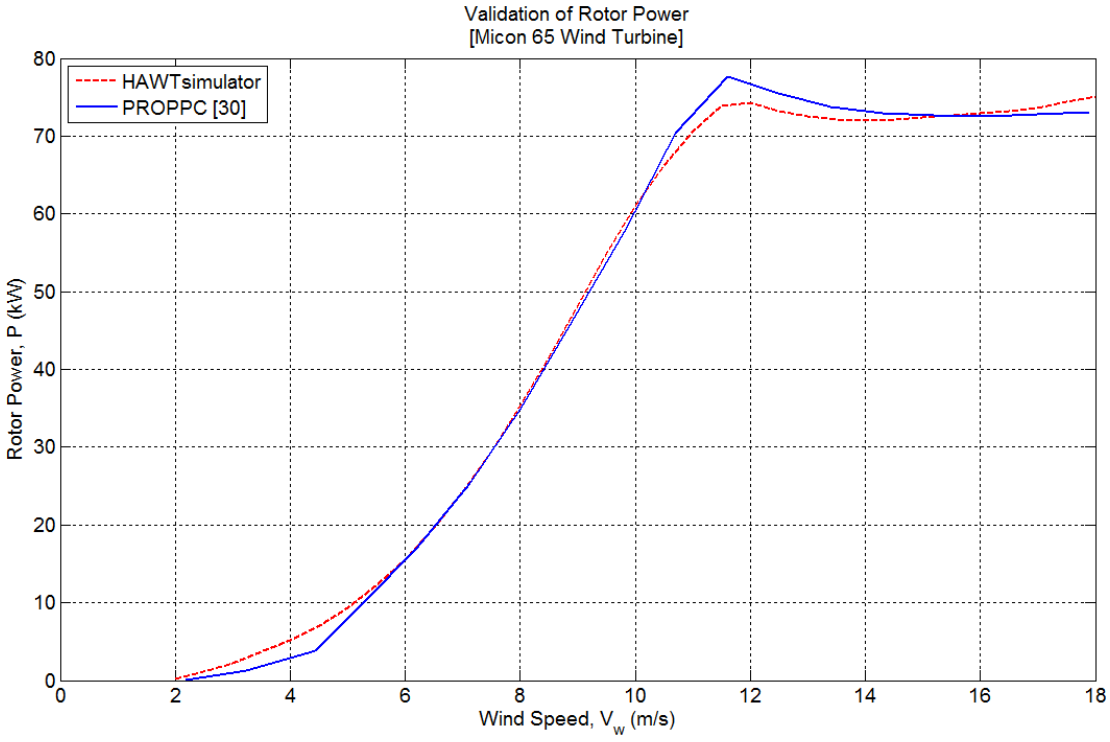

Figure 3.4-1. Validation of rotor power

The comparison in Figure 3.4-1 implies that all data used in the simulation are reasonable. Thus, loads acting along blade span at several wind speed can now be generated by varying wind speed from 0.5 m/s to 25 m/s including wind shear exponent of 0.294. At each setting wind speed, edgewise force, F_X, flapwise force, F_Y, and pitching moment, M_Z, are generated. Finally, HAWTsimulator saves these loads in *mac* format supporting to ANSYS structural software.

3.5 Summary

HAWTsimulator is an aerodynamic code used in this research project. The theory implemented in the code is based on the BEM theory derived in Chapter 2. In the code, tip and hub loss correction factors, mentioned in Section 2.4, and windmill brake state models, mentioned in Section 2.9, are added to improve the efficiency of the prediction. Basically, HAWTsimulator can be used to predict the wind turbine performance such as rotor trust, torque and power. The outstanding of the HAWTsimulator is that it can be used to generate the sets of aerodynamic loads acting along the blade span in the range of wind speed from cut-in to cut-out. These loads will be linked to ANSYS structural software to analyse stress in Section 6.4.2. Section 3.2 mentioned to the GUI showing appearance of

HAWTsimulator. GUI is designed to get simulation conditions and to display results. The flowchart shown in Figure 3.2-3 illustrates how the HAWTsimulator works.

Section 3.3 mentioned to the validation of HAWTsimulator. The results generated by HAWTsimulator are validated against those generated by WT_Perf, the existing software. The results to be validated are rotor power, torque, thrust, power coefficient and maximum flap bending moment at the hub. The comparison shows that all results are exactly the same as those predicted by the WT_Perf. This indicates that HAWTsimluator is valid and can be used with high confidence.

Section 3.4 mentioned to the Micon 65 wind turbine and the pseudo SERI-8 blade used in this research project. The specification of the wind turbine and the aerodynamic data of the SERI-8 blade are discussed in details. In the simulation, wind turbine data, blade topology and aerodynamic data are input to HAWTsimulator. Inevitably, the simulated power curve needs to be validated before generating the sets of aerodynamic loads. The validation shown in Figure 3.4-1 shows that the power curve predicted by HAWTsimulator is slightly different from the power curve reported by Tangler *et al*. [59] with a correlation value of 0.9987. Therefore, the simulated power curve is valid. Eventually, the sets of aerodynamic loads acting along the blade span in the range of wind speed from cut-in to cut-out can be generated.

Chapter 4

Fatigue Life Prediction

4.1 Introduction

The word *fatigue* is originated from Latin which means *to tire* [63]. Although this word is commonly used with physical and mental weariness in people, it has become an accepted engineering terminology for damage of materials under the action of repeating loads. In practice, fatigue is one of the observed modes of mechanical failure so it becomes an obvious design consideration for many structures. ASTM E 1823-96 [64] defined the definition of fatigue currently used as "The process of *progressive localised permanent* structural change occurring in a material subjected to conditions that produce *fluctuating* stresses and strains at some point or points and that may culminate in *cracks* or complete *fracture* after a sufficient number of fluctuations." Stephens *et al*. [26] described the meaning of this definition by emphasising to six keywords typed in italic. The word *progressive* implies that the fatigue process occurs over a period of time. The word *localised* implies that the fatigue process affects at local areas rather than throughout the component or structure. The word *permanent* implies that whenever the fatigue process causes a structural changing, the process is irreversible. The word *fluctuating* implies that the fatigue process concerns with cyclic stresses and strains. The word *cracks* implies that the fatigue process involves in nucleation and propagation of cracks. The word *fracture* implies that the final stage of the fatigue process that the specimen or component is separated into two or more parts. British Standards Institution, BS EN 1993-1-9:2005 [7], defined the definition of fatigue as "*The process of initiation and propagation of cracks through a structural part due to action of fluctuating stress*".

As mentioned, fatigue is the process of progressive localised permanent structural change occurring in a material subjected to conditions that produce fluctuating stresses and strains at some point or points and that may culminate in cracks or complete fracture after a sufficient number of fluctuations [65]. In such cases, rupture will occur at a stress much lower than static breaking strength if the number of repeated loading is sufficient. It is well known that many materials will not survive if the load is applied and then removed for several times. The underlying causes of fatigue damage are complex because of the tiny growth of the crack. With each cycle, the crack grows a little until the material fails. In

accordance with IEC 61400-23 [2], wind turbine blade is the most important part of a wind turbine. The blades are subject to a high number of loads during their targeted economical lifetime of 20 years [66] or more. Estimates of the number of load cycles are up to 10^8 or 10^9 load cycles [67]. Normally, only a limited number of samples (only one or two blades of a given design) are tested [2]. Practical and economic considerations have traditionally prevented laboratory test conditions from representing realistic load cases. In most cases, a single equivalent load case is applied during testing. The equivalent load case is calculated from experimental or design load conditions and it includes magnification factors to account for factors not accounted for during fatigue testing [2].

At present, there are three existing fatigue life models [68] which are stress-life model, strain-life model and fatigue crack growth model. Firstly, the stress life model, briefly called $S\text{-}N$ model, relates nominal stresses to the localised fatigue strengths of both notched and unnotched specimens. Secondly, the strain-life model, briefly called $\varepsilon\text{-}N$ model, relates localised strain at a notch to strain-controlled fatigue life behaviour of a smoothed specimen. The advantage of this model is that local strains can be determined by nominal stresses or strains, so it is convenient to predict crack nucleation in notch specimen. Lastly, fatigue crack growth model, briefly called $da/dN\text{-}\Delta K$ model, requires the knowledge of fracture mechanics. A crack growth rate equation is integrated to determine the number of cycles needed to extend a crack from a given crack length to a desired length. The stress-life model or strain-life model can be used to obtain a life of crack nucleation. The fatigue crack growth model is used to determine a remaining life by integrating a crack growth rate equation. The total life is a sum of crack nucleation life and crack growth life. In this research project, stress-life model is used because fibreglass composite databases for wind turbine blades [14,69-70] are reported in the forms of $S\text{-}N$ curve and Goodman's diagram. In addition, the action of fluctuating stress with equal maximum load but different in stress ratios will affect the range of fatigue life of a material. The fatigue formation at different stress ratios and all conditions of mean and alternating stresses, which can possibly be applied, are included by using a constant life diagram [68,71]. Furthermore, the principles used for analysing the total fatigue life of blade materials are only based on the constant amplitude fatigue loading. In fact, several components are subject to the irregular cyclic load in which stress amplitudes, mean stresses and loading frequencies are varied. Cycle counting methods and cumulative fatigue damage model need to be focused on.

As wind turbine blades have become longer, heavier and more expensive, the importance of fatigue testing has also been increased. The investments, which need to develop and certify the new wind turbine blades, are increasing rapidly. Moreover, fatigue testing of the full-scale blade is compulsory and it could take over half a year to completion; consequently, the time-to-market is delayed [65]. Also, the level of realism of the test can be questionable. Thus, the industry and research institutions are looking into possibilities to optimise the test procedure concerning costs, test time and test results.

In this chapter, the subject matter deals with symbols and terminologies used in fatigue analysis, stress-life approach commonly used by researchers in wind turbine community, Miner's rule (fatigue damage model) commonly used to formulate the fatigue analysis of wind turbine blades, and rainflow cycle counting used in conjunction with the stress-life approach, respectively.

4.2 General Fatigue Nomenclature

The fatigue cycle is a closed stress-strain hysteresis loop in the stress-strain time history of a solid material typically shown in Figure 4.2-1. For illustrative purpose, the cycle is usually depicted by a sinusoid shown in Figure 4.2-2. In this research project, the terminologies used in fatigue analysis are defined by referring to symbols in Figure 4.2-2. A constant amplitude sinusoidal wave represents the smallest section of periodic stress function called stress cycle.

According to British Standards Institution, BS EN 3518-1:1993 [68], the following terminologies are used throughout this thesis:

1. *Stress*, denoted by S, is the applied force divided by the original cross-sectional area. Plus sign is given for tensile stress and minus sign for compressive one.
2. *Maximum stress*, denoted by $S_{\max}$, is the highest algebraic value of stress in the cycle.
3. *Minimum stress*, denoted by $S_{\min}$, is the lowest algebraic value of stress in the cycle.

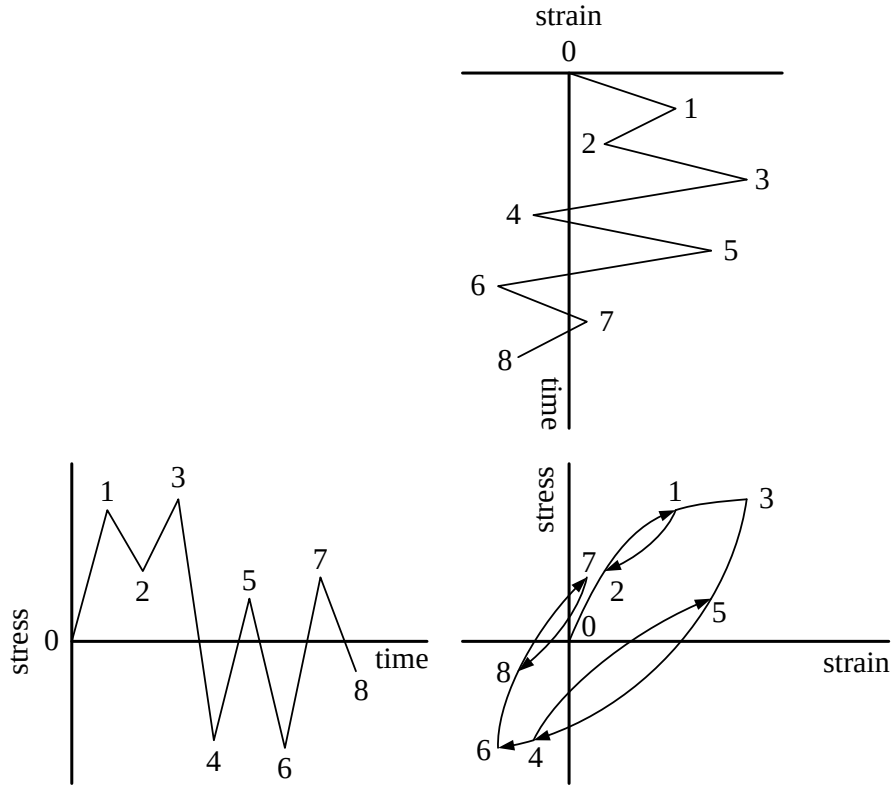

Figure 4.2-1. Stress-strain hysteresis loop for a fatigue cycle [1]

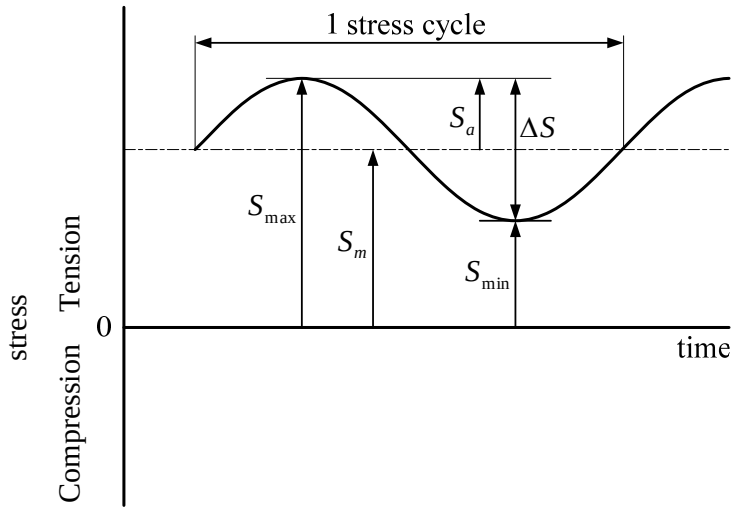

Figure 4.2-2. Typical fatigue stress cycle

4. *Mean stress*, denoted by S_m, is a half value of the sum between maximum and minimum stresses.

$$S_m = \frac{S_{\max} + S_{\min}}{2} \tag{4.2-1}$$

5. *Alternating stress*, denoted by S_a, is a half value of the difference between maximum and minimum stresses.

$$S_a = \frac{S_{\max} - S_{\min}}{2} \tag{4.2-2}$$

6. *Stress range*, denoted by ΔS, is the absolute value of the algebraic difference between maximum and minimum stresses.

$$\Delta S = \left| S_{\max} - S_{\min} \right| \tag{4.2-3}$$

From Figure 4.2-2, it is noted that:

$$S_{\max} = S_m + S_a \tag{4.2-4}$$

$$S_{\min} = S_m - S_a \tag{4.2-5}$$

$$S_a = \frac{\Delta S}{2} \tag{4.2-6}$$

7. *Number of stress cycles*, denoted by n, is the number of cycles applied.
8. *Frequency of cycle*, denoted by f, is the number of cycles applied per second.
9. *Stress ratio*, denoted by R, is the algebraic ratio of minimum stress to maximum stress in the same stress cycle.

$$R = \frac{S_{\min}}{S_{\max}} \tag{4.2-7}$$

Depending on values of stress ratio, the fatigue stress cycle may be several patterns. The fatigue stress cycle typically shown in Figure 4.2-3 could be divided into three regions according to the stress ratio.

Region 1 is the compression-compression region. Stress ratio lies in the range $1 < R < +\infty$. The fatigue stress cycle can be two patterns which are compression-compression cycle, e.g. $R = 2$ and $R = 10$, and zero-compression alternating cycle.

Region 2 is the tension-compression region. Stress ratio lies in the range $-\infty < R < 0$. The fatigue stress cycle can be three patterns which are compression-dominated alternating cycle, fully reversed cycle, i.e. $R = -1$, and tension-dominated alternating cycle.

Region 3 is the tension-tension region. Stress ratio lies in the range $0 \le R < 1$. The fatigue stress cycle can be two patterns which are zero-tension cycle and tension-tension cycle, e.g. $R = 0.1$ and $R = 0.5$.

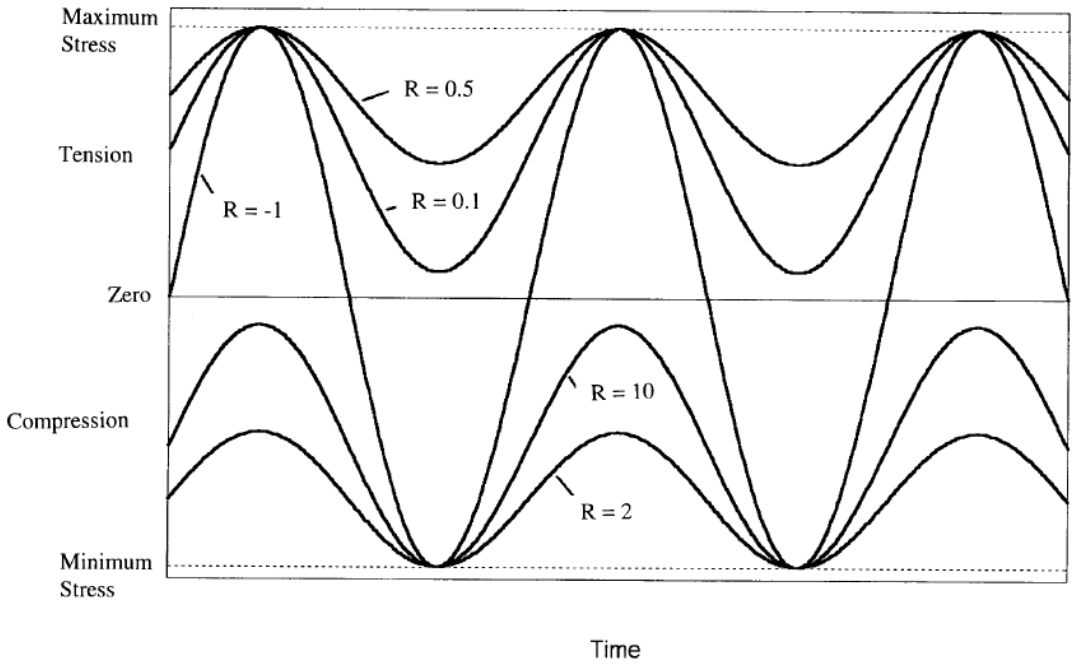

Figure 4.2-3. Constant stress amplitude sine waveform for different R-values [72]

4.3 Stress-Life Approach

In this approach, stress-life behaviour is described by an S-N curve obtained from stress-controlled fatigue testing. The S-N curve is the most widely used to present fatigue data in graphic form. This curve is established by plotting the data of the number of cycles to failure, N, against the maximum cyclic stress, S. British Standards Institution, BS EN 3518-1:1993 [68], defined the definitions related to the S-N curve as follows:

1. *Fatigue life or endurance*, N, is the number of stress cycles to failure generally stated as multiples of 10^6.
2. *Fatigue strength* is the value of stress amplitude at a stress ratio under which the specimen would have a life at least N cycles.
3. *Fatigue limit* is the value of stress amplitude below which the specimen would be expected to endure an infinite number of stress cycles.

In wind turbine application, the S-N behaviour of fibreglass wind turbine blade materials at a constant R-value has been found in three forms. The first form is a power law, one of the simplest formulations for the S-N relationship. This formulation uses a single power law to describe the entire S-N behaviour of the composite material. In the normalised form, the power law formulation is written in the form [72-73].

$$\frac{S}{S_0} = BN^{-1/n} \tag{4.3-1}$$

where n and B are a fatigue exponent and a material constant. N is the number of cycles to failure at maximum cyclic stress level S. S_0 is the static strength in the first fatigue cycle (at 10^0 cycle). In this form, B is usually taken to be one [72]. In addition, S_0 is the ultimate tensile strength for stress ratio dominated by tension; otherwise, it is the ultimate compressive strength for stress ratio dominated by compression.

The second form is a linear curve fit [72-73] forced through a point $S/S_0 = 1$.

$$\frac{S}{S_0} = 1 - b \log N \tag{4.3-2}$$

where b is the fatigue coefficient which measures fatigue resistance. It is to be noted that a higher value of b, more steeper of straight line or more fatigue sensitive $S\text{-}N$ curve. In detail analysis, Mandell *et al*. reported that most standard coupon data tend to fit better to Equation 4.3-2 whilst Equation 4.3-1 tends to give a less conservative prediction of high cycle data. Equation 4.3-1 is used to extrapolate $S\text{-}N$ results and it tends to fit the high cycle part of the dataset more accurately than Equation 4.3-2 [72].

The third form is a three-parameter equation [14,69,74]. This formulation fits the entire range of $S\text{-}N$ data including the static strength. Its mathematical implementation is not significantly more difficult than 2-parameter model. Moreover, Mandell *et al*. [75] discussed that the maximum stress value extrapolated to 10^6 cycles by the 3-parameter fit is within 10% of the extrapolated stress from a power law fit to the data for cycles above 10^3 cycles.

$$S_0 - S = aS\left[\frac{S}{S_0}\right]^b (N^c - 1) \tag{4.3-3}$$

where a, b, and c are fitting parameters.

In addition, the family of $S\text{-}N$ curves can be presented by a constant life diagram [26,71,76]. For wind turbine application, the family of $S\text{-}N$ curves is commonly formed into a Goodman diagram [77]. The dependence of the constant life curves on alternating and mean stress can also be collapsed into a single curve by means of a modified Goodman diagram. Generally, the data are collapsed to a single, zero-mean-stress $S\text{-}N$ curve (equivalent to $R = -1$). The Goodman fit defines the relationship between levels of mean and alternating stresses. This rule states that the fatigue life at a pair of alternating stress and mean stress is equal to the fatigue life at an equivalent zero-mean-stress alternating stress state of endurance limit through the relation

$$S_a = S_e\left[1 - \frac{\sigma_m}{S_{\text{ut}}}\right] \tag{4.3-4}$$

where S_{ut} is the ultimate strength of the material and S_e is the fully reversed fatigue strength or the alternating stress at $R = -1$.

Recent efforts to improve the accuracy of spectrum loading lifetime predictions have led to the development of a more complete Goodman diagram than previously available, and a more accurate fatigue model (Equation 4.3-3). Table A3 provides constant amplitude data for thirteen R-values of DD16 material. The constant load tension $(R=1)$ data is plotted by assuming a frequency of 10 cycles/second, typical of the cyclic tests. Many of the R-values produces semi-log stress versus log cycles $S-N$ trends with complex shapes, relatively flat at low cycles, steeper at medium cycles and less steep again at high cycles.

In this research project, composite material used in modelling a pseudo SERI-8 blade is a fibreglass laminate called DD16. Its $S-N$ data is described by Equation 4.3-3. DD16 material has been listed in DOE/MSU composite material fatigue database for wind turbine blades [70]. The laminate has a $[90/0/\pm 45/0]_s$ configuration with a fibre volume fraction of 0.36, typical of hand layed-up blades. The 90° and 0° plies are D155 stitched unidirectional fabric. The $\pm 45^\circ$ plies are DB120 stitched fabric. The resin is an orthopolyester. The fitting parameters for thirteen values of R-ratios are listed in Table A2. Also, an updated Goodman's diagram for DD16 fibreglass composite material is shown in Figure A2.

4.4 Fatigue Damage Model

The purpose of presenting fatigue results in the form of $S-N$ curve is to define the damage curve relating stress to the number of cycles to failure for fatigue life assessment. Most of the fatigue results in the DOE/MSU composite material fatigue database are for constant amplitude loading at particular R-values. These must be assembled into an overall Goodman diagram representation covering all values of mean stress and stress amplitude, which can then be used with an appropriate cumulative damage law to predict the lifetime of the material for a particular load spectrum. British Standards Institution: EN 3518-1:1993 [68] suggested that Miner's rule [10-12] may be used to estimate the fatigue life. A constant amplitude $S-N$ curve may be used to predict the fatigue life of similar specimens or components subjected to a random stress-time history. It is necessary first to analyse the stress-time history to extract stress cycles by rainflow cycle counting method discussed in Section 4.5. Then, the count at each level of maximum cyclic stress can be used, together with the $S-N$ curve, via a linear damage accumulation rule to predict the fatigue damage in one repetition of the stress-time history. Miner's cumulative damage rule may be written in the form

$$D = \sum_{i=1}^{i=m} \frac{n_i}{N_i} \tag{4.4-1}$$

where D is the fatigue damage per repetition sustained by a wind turbine blade that undergoes n_i stress cycles at the stress level S_i. N_i is the number of cycles to failure at the stress level S_i. n_i is the number of rainflow cycles counted for each stress cycle at the stress level S_i. m is the total number of rainflow cycles counted in one repetition.

In practice, it is assumed that failure occurs when sum of fatigue damage per repetition equals unity, i.e. $\sum D = 1$ [1,78]. Nevertheless, Miner's rule is based on three important assumptions [63]: (1) the number of stress cycles applied to a component causes the fraction of damage; (2) the order of the stress blocks does not affect the fatigue life; and (3) failure occurs when the linear sum of fatigue damage per repetition reaches unity.

In this research project, the stress-time history will be repeated M times until the sum of fatigue damage per repetition approaches unity. Thus,

$$M = \frac{1}{D} \tag{4.4-2}$$

where the unit of M in Equation 4.4-2 is repetitions.

The service lifetime can easily be calculated by multiplying duration of the stress-time history by the total number of repetitions.

$$T = t_{\text{history}} M \tag{4.4-3}$$

In this research project, the base unit of t_{history} is seconds which gives the unit of T is seconds. Then, seconds can be converted to months and years later.

4.5 Cycle Counting Method

The principles used for analysing the total fatigue life of materials are only based on the constant amplitude fatigue loading. In fact, several components are subject to the irregular cyclic load in which stress amplitudes, mean stresses and loading frequencies are

varied [63]. The service load history of an actual engineering part can be more complex. Several methods have been developed to cope with variable amplitude loading by using a data generated from constant amplitude tests as a baseline of damage summation. This method can be used in conjunction with the stress-life approach (constant amplitude fatigue analysis) and Miner's rule to estimate the fatigue life of a component subjected to the variable amplitude loading.

In practice, the several peaks in a measured signal often appear and make the number of cycles absorbed by the structure difficult to determine. There are several cycle counting methods to cope with the variable amplitude load histories. Cycle counting methods were initially developed to estimate fatigue damage generated in aeronautical structures [79]. One of the most widely used methods is rainflow cycle counting [80-84]. This counting method is used to convert irregular stress history into an equivalent set of constant amplitude block loads with different ranges. These block loads can directly be used by Miner's cumulative damage rule discussed in Section 4.4. Rainflow method is the most popular method of cycle counting [26]. It was first proposed by Matsuishi and Endo in 1968 [80]. By plotting the time axis of the stress history vertically downward, Matsuishi and Endo thought of the lines going horizontally from a reversal to a succeeding range as rain is flowing down a pagoda roof represented by peaks and valleys of the history. Thus, this method is called rainflow counting.

In this research project, the author implements a fatigue computer code called HAWTfatigue to evaluate the fatigue damage and service lifetime of HAWT blades. In the code, a simplified rainflow counting for repeating histories recommended by ASTM E 1049-85 [84] is used.

4.6 Summary

This chapter describes the word *fatigue* as an engineering terminology for damage of materials subjected to the repeated loads. Many materials will not survive if the load is applied and removed for several times. Fatigue is the process of progressive localised permanent structural change occurring in a material subjected to fluctuating stresses or strains at some point or points and that may culminate in cracks or complete fracture after a sufficient number of fluctuations. At present, there are three fatigue life models which are stress-life, strain-life and fatigue crack growth models. The stress-life model is used in this research project because the fatigue characteristics of composite materials for wind turbine

blades are documented in the $S\text{-}N$ format. Section 4.2 is relevant to the general fatigue nomenclature used in this research project. The symbols and terminologies used in fatigue analysis are defined by British Standards Institution, BS EN 3518-1:1993 [68].

As mentioned in Section 4.3, stress-life approach is commonly used in the wind turbine blade designers and researchers. In literature, especially in the wind turbine community, the formulations described the $S\text{-}N$ behaviour of fibreglass wind turbine blade materials have been found three forms: a power law; a linear curve; and a three-parameter equation. The latter formulation is up-to-date and it fits the entire range of $S\text{-}N$ data including the static strength. In this research project, DD16 composite material is used in modelling of a pseudo SERI-8 blade. This material has been listed in DOE/MSU composite material fatigue database for wind turbine blades [70]. To predict fatigue life of wind turbine blades, fatigue damage model used in this research project is mentioned in Section 4.4. Miner's cumulative damage rule, which is suggested by British Standards Institution, BS EN 3518-1:1993 [68], is used to estimate the fatigue damage and service lifetime of wind turbine blades.

Section 4.5 deals with rainflow cycle counting which is used in conjunction with the stress-life approach and Miner's rule. Rainflow cycle counting is used to convert irregular stress history into an equivalent set of constant amplitude block loads with different ranges. In this research project, rainflow algorithm is a simplified rainflow cycle counting for repeating histories. It is recommended by ASTM E 1049-85 [84].

To summarise, all background theories mentioned in this chapter are used to implement a fatigue computer code called HAWTfatigue (see Appendix C). In this research project, this computer code is used to estimate fatigue damage and service lifetime of HAWT blades.

Chapter 5

Review of Concepts and Approaches of Fatigue Signal Editing

5.1 Introduction

One major advantage of laboratory full-scale fatigue testing is the possibility of a considerable reduction in the time necessary to carry out a fatigue evaluation compared with field studies [18]. The objective of laboratory based accelerated testing is to expose the component with the equivalent test loading which its length is shorter than the length of the target loading whilst it has approximately the same damage potential. Alternative approaches used to accelerate laboratory fatigue testing are increasing the frequency of the cyclic loading, increasing the load level and removing small amplitude cycles from the time history [18]. Testing time and cost can become too expensive if the service load is not edited before testing.

Increasing the frequency of the cyclic loading is one of the alternative approaches for achieving an accelerated fatigue test. For a simple component, changes in loading frequency can be made on the basis that frequency has no or minimal effect on component fatigue strength over the normal range of frequencies encountered. However, difficulties occur in the testing of complex structures because changing the frequency content of the input may excite resonances. Resonance results in different stress distributions within the structure from those observed in service [18].

In the second approach, service load levels are scaled up by a constant value; consequently, fatigue life of the edited loading is shorter than the original life [18]. By using the edited loading, the testing time can be reduced. Fatigue life is the number of cycles to failure at a stress level that a specimen sustains before failure occurs [26,85], e.g. at approximately 10^6 cycles for steel [86].

The final approach for performing the accelerated fatigue testing is removing small amplitude cycles from the input variable amplitude (VA) fatigue loading. This approach is known as fatigue data editing [18]. The small amplitude cycles, which provide a minimal contribution to the overall fatigue damage, are omitted whilst the high amplitude cycles, which are the most damaging sections, are retained. This concept is often applied to

accelerate fatigue testing time [87-88]. By this approach, the edited loading which its length is shorter than the original length is generated [83,89]. The concept of accelerating a test by removing non-damaging events is distinctly different from the previous two approaches [88]. Using both the previous approaches, the original VA loading is not compressed so the exited loading will have the same length of time as the original loading. The last approach achieves test acceleration by considering less than the complete set of VA loadings because only a subset of the loading is required to produce the same amount of damage.

Early fatigue data editing research was conducted by Conle and Topper [89] in 1979 with the small cycle omission procedure using strain loading. The strain-life approach and the linear accumulative damage rule were used to determine the omission levels. There were three criteria of strain ranges to select the edit levels: the sequence strain ranges with the application of peak-valley (PV) and damage histogram ranges; the rainflow counted strain ranges; and the mean stress parameters. For defining the term of PV, a peak is a change in the slope from positive to negative and a valley is a change in the slope from negative to positive [84]. Evaluation of the criteria was carried out by estimating the amount of fatigue damage generated by each amplitude level of the original history, selecting several strain range levels for history editing and then comparing the amount of damage reduction predicted by each criterion with actual fatigue test results. However, it was apparent that when high overall strain levels were encountered in the total record of the VA loading, great care should be taken to eliminate smaller cycles. In 1980, a similar technique was performed by Conle and Topper [90] to edit VA loading but using lower overall strain levels in order to omit smaller cycles. The fatigue damage results from this study indicated that the presence of an overstrain effect was much larger than the previous work in 1979.

In 1986, a research conducted by Heuler and Seeger [91] using the aircraft service loading showed that the small cycles were omitted from the original loading according to the fatigue limit criteria. In this fatigue data editing, any small cycles with the stress below 50% of the materials constant amplitude (CA) fatigue limit were found to be allowable levels to be omitted. These omission levels were applicable in the fatigue tests using smooth steel and notched aluminum specimens. Using this technique, the total lives for smooth specimen (steel) and for notched specimen (aluminum) were increased by 10%-30% and 30%-70%, respectively. The omission level, 50% of the CA fatigue limit, was chosen as a fraction of the maximum load range because of simplicity and convenience.

For producing an accurate fatigue damage result; however, this fatigue data editing was not appropriate for VA fatigue damage.

Other fatigue data editing analyses involving the concept of PV reversals were conducted by Gunger and Stephens [92] in 1995 and Stephens *et al.* [93] in 1997. In these studies, the Society of Automotive Engineers Fatigue Design and Evaluation (SAEFDE) committee log skidder bending (LSB) loading was used. The combination of strain amplitude and mean obtained from the formulation of the Smith-Watson-Topper (SWT) strain-life model was used to produce an omission level in removing the small cycles. The PV domain was used to edit the PV service history where all SWT parameter cycles less than omission level were removed.

In 1999, Giacomin *et al*. [94-95] developed the Mildly Non-stationary Mission Systhesis (MNMS) algorithm for performing mission synthesis of vibration of stimuli in comfort applications. This algorithm was based on wavelet transform (WT). In 2004, Abdullah *et al*. [96] applied MNMS for the fatigue data editing. The application produced statistically accurate fatigue mission when the original signal was substantially shortened. The VA loading was compressed up to 10 times to produce the edited loading. In terms of fatigue damage potential; however, the edited VA loadings did not have similar fatigue damage as the unedited loading.

In 2001, Oh [97] introduced the application of wavelet transform to edit a VA loading measured on a light railway train component. WT is defined as the mathematical transformation in the time-scale domain and it is a significant tool for presenting local features of a signal. Oh used WT for removing spikes and de-noising contaminated signals; consequently, the light railway VA fatigue loading was compressed. By this fatigue data editing, approximately 80% of the fatigue damage was retained in the edited signal whilst 71% reduction in the record length. At moment, the application of WT is rarely found in the research field of the fatigue data editing.

In 2002, a research conducted by El-Ratal *et al*. [98] discussed the application of time correlated damage analysis for time domain fatigue data editing by using nSoft software package. The analysed VA loading measured from automobile suspension was divided into several small windows and then the fatigue damage for each window was calculated. Sections with significant fatigue damage (high amplitude cycles) were retained. On the

other hand, sections with minimal fatigue damage (small amplitude cycles) were removed. Then, high amplitude sections were assembled using the available windows joining function of the software. To validate the fatigue data editing approach, El-Ratal *et al*. performed laboratory fatigue tests using a full automobile suspension system. By applying several VA loadings to this suspension system, the test was accelerated from seven days to two days.

In 2009, Abdullah *et al*. [99] introduced the concept of using short-time Fourier transform (STFT) to remove small amplitude cycles from the original load history. STFT had been used to transform the original load history from the time domain to the time-frequency domain. The signal segments having the low power level were identified. Consequently, the small amplitude cycles having minimal or no fatigue damage potential had been removed from the original signal. On the other hand, the damage segments having high power levels were assembled to generate a new edited signal. Namely, the original fatigue damage could be retained in the edited signal produced at the end of the process. At moment, the application of STFT in fatigue data editing is found only one research.

For all the fatigue data editing techniques mentioned in this section, different VA loadings were used for different techniques. There seem to be no generally agreed rules that clarify which method is the best or what amplitude should be chosen for load omission. Practically, any fatigue data editing techniques must reduce the testing period and be technically valid [100-101].

5.2 Fatigue Signal Editing Techniques

Fatigue signal editing is a technique for removing small amplitude cycles leading to minimal fatigue damage [18]. Large amplitude events produced the majority of damage are retained and produced a shortened loading for accelerated fatigue tests [83,89]. Sections 5.2.1 to 5.2.5 deal with an overview of the currently available fatigue signal editing techniques used for summarising long records of VA fatigue loads.

5.2.1 Editing in Time Domain

Time series data is the most general format of data which contains all the information relevant to fatigue analysis. In the literature, two time domain editing techniques have been found. They are racetrack method [24] and time correlated fatigue damage (TCFD) [102].

In 1973, Fuch *et al*. proposed the ordered overall range method which is now called the racetrack method [24]. The objective of the racetrack method is to condense a long complex history of reversals to make it more useful. The condensed listing can be used as a record of the most essential features of the load history. The racetrack method is used to produce a condensed history which essential peaks and valleys are listed in their original sequence. Based on a threshold value, a stress range is retained if its absolute value is greater than the threshold value. On the other hand, a stress range is discarded if its absolute value is equal to or less than the threshold value. Unfortunately, racetrack method does not compress or shorten the length of the load history. Thus, it does not serve the purpose of accelerating testing time. A computer code for racetrack method can be found in the references [22], [23], [24] and [25]. In the field of wind turbine engineering [22-23], the racetrack method is the only one method used to edit fatigue signal.

Time correlated fatigue damage (TCFD) developed by El-Ratal *et al*. [98] is another time domain editing technique. TCFD has been developed to remove time segments. It is used by commercial software [102]. This method removes non-damage sections from the time history on the basis of time correlated fatigue damage windows of the input signal. Applying TCFD, the time history is divided into a number of short time segments. Then, fatigue damage in each time-window is calculated. Windows having minimal damage are removed whilst windows containing the majority of the fatigue damage are retained. The retained windows are assembled to produce a shortened signal for the purpose of the durability analysis. Both the percentages of retained fatigue damage and the required acceleration factors, or one of them, can be set as the editing targets [102]. TCFD is recommended because it maintains the phase and amplitude of the original time history [98].

In this research project, TCFD is used for validating the idea of using accumulative power spectral density in identifying the locations of fatigue damage events (see Section 6.2). Also, the results from STFT and WT (see Chapter 7) are validated against the results from TCFD.

5.2.2 Editing in Frequency Domain

In frequency domain, fatigue load history is often low-pass filtered to reduce small amplitudes located in the high frequency region of power spectral density (PSD) distribution [103]. The idea behind this method is that small amplitude events do not cause

much fatigue damage. Unfortunately, the low-pass filter does not reduce the length of the signal but almost certainly reduces the fatigue damage. Therefore, the frequency domain editing technique is not recommended because the time series regenerated from a frequency spectrum does not produce the same fatigue life [103].

5.2.3 Editing in Peak-Valley Domain

The peak-valley (PV) editing uses a gate level as a criterion in extracting peaks and valleys from the sampled signal. The gate level can be either the endurance of the material or a specified stress level. The PV editing procedure reduces the total number of points of the original signal. This technique can be used when the signal frequency content is not important to the fatigue damage analysis. However, the time information of the original load history is lost when this fatigue data editing technique is used [90].

5.2.4 Editing in Time-Frequency Domain

This editing method is based on STFT. Abdullah *et al*. [99] applied STFT to edit fatigue signal. In this research, STFT parameter was used as a criterion in removing the low amplitude cycles contained in the VA load history. This load was measured on automobile components. The STFT-based algorithm removed low amplitude cycles from the original signal and produced a shortened signal. The original signal was separated into two parts which were damage and non-damage parts. For the editing process, the cutoff level at a specified level of power spectral density was used as the parameter to identify the damage events contained in the original signal. The small amplitude cycles having power spectral density lower than cutoff level were removed from the original signal. The large amplitude cycles having power spectral density equal or higher than the cutoff level were retained and form the edited signal. The signal statistics of the edited signal are equivalent to those of the original signal whilst the length of the edited signal was found to be approximately 84% of the original length.

5.2.5 Editing in Time-Scale Domain

In time-scale domain, only two researches have been found in the literature. The first research was conducted by Oh [97] using a VA load history measured on light railway train component. The second research was conducted by Abdullah *et al*. [96] using a VA load history measured on automobile component.

For the first research, Oh [97] used WT as an approach for editing VA fatigue load history. The 30th order of Daubechies wavelet at the decomposition level 3 was used to edit the fatigue data by denoising, spike removal and signal compression. Based on a correlation coefficient, the order and the wavelet decomposition level were chosen. The correlation coefficient was calculated between the original signal and the de-noised signal. The VA load history measured from a light railway train component travelling over a test rail at the maximum speed at 80 km/h. This VA load history contains 103,700 data points (28,390 PV reversals). Using 30th order Daubechies wavelet function at the wavelet decomposition level 3, the background noise and spikes contained in the original load history were removed. As a result, the original signal was compressed from 28,390 PV reversals to 8,349 PV reversals. The shortened signal has its length of 71% compared to the original length. The retained fatigue damage of the shortened signal is 80% of the original fatigue damage. In this study, the fatigue damage was calculated by using Palmgren-Miner linear damage rule with the Smith-Watson-Topper (SWT) mean stress correction effect which does not account for load sequence effects.

The second research is also based on WT. Abdullah *et al*. [96] applied the MNMS algorithm, which was developed by Giacomin *et al*. [94-95], for the fatigue signal editing to produce statistically accurate fatigue missions. Consequently, the original signal was compressed up to 10 times. Unfortunately, the edited VA loadings in terms of fatigue damage potential did not have similar fatigue damage as the original loading.

5.3 Signal Analysis

A signal is a series of numbers taken from measurement by using some recording methods and it is a function of time [104]. In fatigue analysis, the signal is the cyclic force, strain or stress taken from measurement at equal time intervals [105]. In practice, the signal samplings are performed digitally. By using an analogue-to-digital converter, an experimental signal is measured and converted to the experimental signal at a series of regular time interval. Such a signal is a discrete time series. The objective of time series analysis is to determine the statistical characteristics of the original function by manipulating the series of discrete numbers [106].

5.3.1 Signal Statistics

Signal statistics are used to analyse random signals. The most commonly used statistical parameters [107] are mean, standard deviation, root-mean-square and kurtosis.

For a signal with a number n of data points in the sampled sequence n, the mean is given by

$$\bar{x} = \frac{1}{n}\sum_{i=1}^{n} x_i \tag{5.3-1}$$

By using the statistics toolbox in Matlab [108], the mean value of an array x is calculated by a command `mean(x)`.

The standard deviation is a measure of how far the signal fluctuates from the mean. In equation form, the standard deviation is given by

$$\sigma = \begin{cases} \sqrt{\frac{1}{n}\sum_{i=1}^{n} (x_i - \bar{x})^2} & n > 30 \\ \sqrt{\frac{1}{n-1}\sum_{i=1}^{n} (x_i - \bar{x})^2} & n \le 30 \end{cases} \tag{5.3-2}$$

By using the statistics toolbox in Matlab [108], a value of the standard deviation of an array x is calculated by a command `std(x)`.

The root-mean-square (rms) is the second statistical moment. It is used to quantify the overall energy content of the signal. For discrete data sets, the rms is given by

$$x_{\text{rms}} = \sqrt{\frac{1}{n}\sum_{i=1}^{n} x_i^2} \tag{5.3-3}$$

For a zero-mean signal the rms value is equal to the σ value. By using Matlab, an rms value of an array x is calculated by either a statement `sqrt(sum(x.*conj(x))/n)` or a statement `norm(x)/sqrt(n)`.

Kurtosis is the fourth statistical moment which is highly sensitive to the spikiness. It is a global signal statistics. For discrete data sets the kurtosis is defined as

$$\text{Kurt} = \frac{1}{n\sigma^4}\sum_{i=1}^{n} (x_i - \bar{x})^4 \tag{5.3-4}$$

By using statistics toolbox in Matlab [108], a kurtosis value of an array x is calculated by a command `kurtosis(x)`.

5.4 Fourier Transform

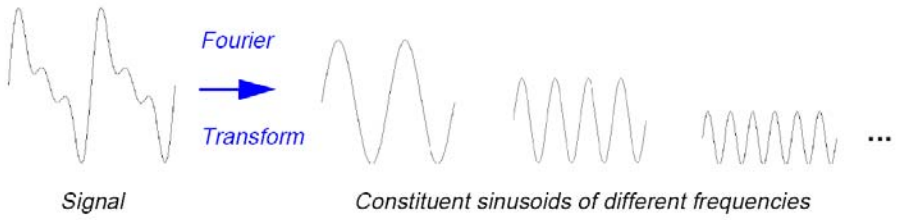

(*a*)

(*b*)

Figure 5.4-1. Fourier transform [109]

The Fourier transform breaks down a complicated signal into simple waves of different frequencies as shown in Figure 5.4-1(*a*). Another way to think of Fourier analysis is as a mathematical technique for transforming the view of the signal from time-based to frequency-based [109] as shown in Figure 5.4-1(*b*). The time it takes for a wave to oscillate once (in seconds) is called period T. The number of times a wave oscillates in 1 second is called frequency f. The relationship between the period and the frequency is given by

$$f = \frac{1}{T} \tag{5.4-1}$$

The angle rotated in 1 second (in radians per second) is called angular velocity. The relationship between the angular velocity and the frequency is given by

$$\omega = 2\pi f \tag{5.4-2}$$

Mathematically, Fourier discrete expansion is used to break down a complicated signal into three types of simple wave which are sine waves, cosine waves and a straight wave [110]. Both sine and cosine waves have frequencies that are integral multiples of a fundamental frequency.

$$x(t) = a_0 + \sum_{n=1}^{\infty} (a_n \cos n\omega t + b_n \sin n\omega t) \tag{5.4-3}$$

where

$$a_0 = \frac{1}{T} \int_{t=0}^{t=T} x(t)\, dt \tag{5.4-4}$$

$$a_n = \frac{2}{T} \int_{t=0}^{t=T} x(t) \cos n\omega t\, dt \tag{5.4-5}$$

$$b_n = \frac{2}{T} \int_{t=0}^{t=T} x(t) \sin n\omega t\, dt \tag{5.4-6}$$

Wave a_0 is a straight wave that indicates how far the entire complex periodic wave is displaced above or below zero. The periods of the sine and cosine waves are integral multiples of the period of $x(t)$. Amplitudes a_n and b_n show how much of each sine and cosine wave the complex periodic wave contains.

Complex number representation of Fourier series in Equation 5.4-3 is [110]

$$x(t) = \sum_{n=-\infty}^{\infty} C_n e^{in\omega t} = \sum_{n=-\infty}^{\infty} C_n e^{i2\pi f_n t} \tag{5.4-7}$$

where $i = \sqrt{-1}$ is the imaginary unit and C_n is complex number representation of Fourier coefficients [110].

$$C_n = \frac{1}{T} \int_{t=0}^{t=T} x(t) e^{-i2\pi f_n t}\, dt \tag{5.4-8}$$

Considering the relationship between the period and the fundamental frequency

$$\Delta f = \frac{1}{T} \tag{5.4-9}$$

If the wave takes infinite time to advance through one period, then its frequency is extremely close to zero, since the wave passes through only the tiniest function of its period in one second. When the fundamental frequency approaches zero, the interval between frequencies on the spectrum grows narrower and narrower as typically shown in Figure 5.4-2. In other words, the longer the period is, the shorter the interval is between spectrum frequencies. Eventually, when the period reaches infinity, the spectrum becomes a continuum with no gap between frequencies. Thus, all frequencies become known when the period is infinity, even those that weren't apparent through Fourier coefficients formula. Notice that the values f_n are continuous (do not jump from frequency to frequency as before) so f_n in Equations 5.4-7 and 5.4-8 can be replaced by simply f.

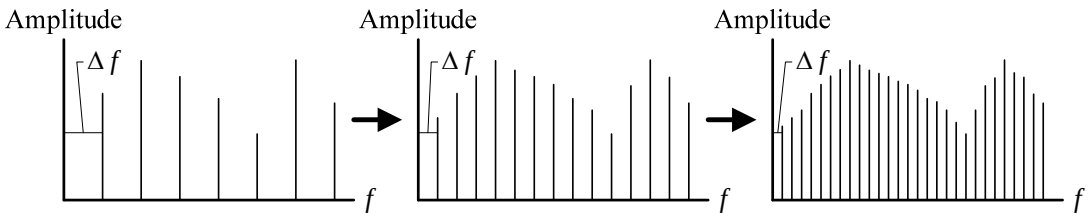

Figure 5.4-2. Spectrum of the wave [110]

Fourier transform of a signal $x(t)$ is

$$G(f) = \frac{1}{T}\int_{-\infty}^{\infty} x(t)e^{-i2\pi ft}\,dt \tag{5.4-10}$$

5.4.1 Power Spectrum and Power Spectral Density

The frequency composition of a random function can be described in terms of the spectral density of its mean square value [111]. The mean square value of a periodic time function is the sum of the mean square of the individual harmonic component present.

$$\overline{x^2} = \sum_{n=1}^{\infty} \frac{1}{2} C_n C_n^* \tag{5.4-11}$$

Thus, $\overline{x^2}$ is made up of discrete contributions in each frequency interval Δf.

First, one defines the contribution to the mean square in the frequency interval Δf as the *power spectrum* $G(f_n)$.

$$G(f_n) = \frac{1}{2} C_n C_n^* \tag{5.4-12}$$

Then, the mean square is

$$\overline{x^2} = \sum_{n=1}^{\infty} G(f_n) \tag{5.4-13}$$

Now, one defines the discrete *power spectral density* $S(f_n)$ as the power spectrum divided by the frequency interval Δf.

$$S(f_n) = \frac{G(f_n)}{\Delta f} = \frac{C_n C_n^*}{2\Delta f} \tag{5.4-14}$$

The mean square value can then be rewritten as

$$\overline{x^2} = \sum_{n=1}^{\infty} S(f_n)\Delta f \tag{5.4-15}$$

Power spectral density (PSD) is a normalised density plot describing the mean square amplitude of each sinusoidal wave with respect to its frequency. PSD shows the strength of the variations (energy) as a function of frequency. It shows at which frequency variations are strong and at which frequency variations are weak. The unit of PSD is energy per Hz (frequency width) and energy within a specific frequency range can be calculated by integrating PSD within that frequency range. Computation of PSD can be done by fast Fourier transform (FFT).

5.5 Short-Time Fourier Transform

Using the Fourier transform, the frequency components of an entire signal can be analysed but it is not possible to locate at what point in time that a frequency component occurs. This is not problematic when a stationary signal is analysed. However, Fourier analysis is not suitable for non-stationary signals. If there is a time localisation due to a particular feature in a signal such as an impulse, this will only contribute to the overall mean valued frequency distribution and feature location on the time axis is lost [106]. To

solve this deficiency, Gabor [112] adapted the Fourier transform to analyse only a small section of the signal at a time. This technique is called windowing the signal. Gabor's adaptation is called the short-time Fourier transform (STFT) which maps a signal into a two-dimensional function of time and frequency as typically shown in Figure 5.5-1.

Figure 5.5-1. Short-time Fourier transform [109]

The STFT represents a sort of compromise between the time- and frequency-based views of a signal. It provides some information about both when and at what frequencies a signal event occurs [109]. The STFT compromises between time and frequency information. However, this information can only be obtained with limited precision determined by the window length, which is chosen so as to relate the signal in time without any distortions. The STFT assumes that if a time-varying signal is divided into several segments, each segment can be assumed stationary for analysis purposes. Then, the Fourier transform is applied to each segment using Gaussian window function which is nonzero in the segment being analysed and it is set to zero outside the segment [113].

The STFT was developed from Fourier transform and it is mathematically defined as

$$\text{STFT} = X(\tau, f) = \int_{-\infty}^{+\infty} x(t)\, w(t-\tau) e^{-i2\pi ft}\, dt \qquad (5.5\text{-}1)$$

where $x(t)e^{-i\omega t}$ is the Fourier transform of the windowed signal, w is the window function and τ is the time position of the window [114]. The result of the transformation is a number of spectra localised in each windowed segment.

The time-frequency resolution depends on the selection of the window length. The time window length is defined as Δt and the frequency interval is Δf. The relationship between time window length and frequency interval is given by

$$\Delta f = \frac{1}{\Delta t} \tag{5.5-2}$$

Considering Equation 5.5-2, it is seen that time localisation is good when Δt is small. On the other hand, frequency localisation is good when Δf is small, but no both simultaneously.

Inherently, the STFT has a resolution problem. Short windows provide good time resolution but poor frequency resolution whilst long windows provide good frequency resolution but poor time resolution. The drawback of STFT is when a particular length of the time window is chosen, that window length is the same for all frequencies. Many signals require a more flexible approach which the window length can be varied to determine more accurately either time or frequency. The wavelet transform (WT) described in Section 5.6 is one of the most recent solutions to overcome the shortcomings of STFT [115].

5.5.1 Matlab Toolbox for Taking STFT

By using signal processing toolbox in Matlab [116], STFT can be taken to the input signal by a statement in the command line shown below. The result is a spectrogram typically shown in Figure 5.5-2(*b*).

```
[S,T,F,P] = spectrogram(x,window,noverlap,nfft,fs)
```

On the right hand side of the statement, there are five input parameters as follows: `x` is an input signal to be analysed; `window` is a window function; `noverlap` is the number of overlapping segments; `nfft` is the FFT length defined by the next power of 2; and `fs` is the sampling frequency.

On the left hand side of the statement, there are four output parameters as follows: `S` is the short-time Fourier transform of the input signal vector `x` and each column of `S` contains an estimate of the short-term, time-localised frequency content of `x`; `T` is a vector of times at which the spectrogram is computed (each value of `T` corresponds to the centre of each segment); `F` is a vector of frequencies corresponding to the centre of each segment; and `P`

is PSD of each segment. Matlab returns `S` and `P` as matrices with *n* rows and *m* columns given by

$$n = \begin{cases} \dfrac{\text{nfft}}{2} + 1 & \text{if nfft is even.} \\ \dfrac{\text{nfft} + 1}{2} & \text{if nfft is odd.} \end{cases} \tag{5.5-3}$$

and

$$m = \text{fix}\left(\frac{\text{n}_\text{x} - \text{n}_\text{overlap}}{\text{nfft} - \text{n}_\text{overlap}} \right) \tag{5.5-4}$$

where n_x is length of the input signal vector `x` and "fix" means *round toward zero*.

Matlab returns `T` as a row matrix with *m* columns and it returns `F` as a column matrix with *n* rows.

5.5.2 Plot of Accumulative Power Spectral Density Generated by STFT

In this research project, STFT is used to generate a plot of accumulative power spectral density (AccPSD) shown in Figure 5.5-2(*d*). The plot of AccPSD is used in the process of extracting fatigue damage parts discussed in Section 6.3. For the illustration purpose, the author uses Figure 5.5-2 to describe how to generate the plot of AccPSD. By taking STFT (with `nfft = 4`, `noverlap = 3`, `fs = 40 Hz`) to the stress-time history in Figure 5.5-2(*a*), Matlab generates the spectrogram shown in Figure 5.5-2(*b*). Changing plotting style from spectrogram to the 3D-stem plot as shown in Figure 5.5-2(*c*) shows the relationship between PSD and frequency at each time interval (or data point number). Thus, AccPSD at each time interval is easily derived by summing PSD of each frequency band at each time interval. For example, AccPSD at data point number 2 is the summation of three PSDs located at frequency bands 0, 10 and 20 Hz, and so on. By this manner, the plot of AccPSD distribution can be generated as shown in Figure 5.5-2(*d*).

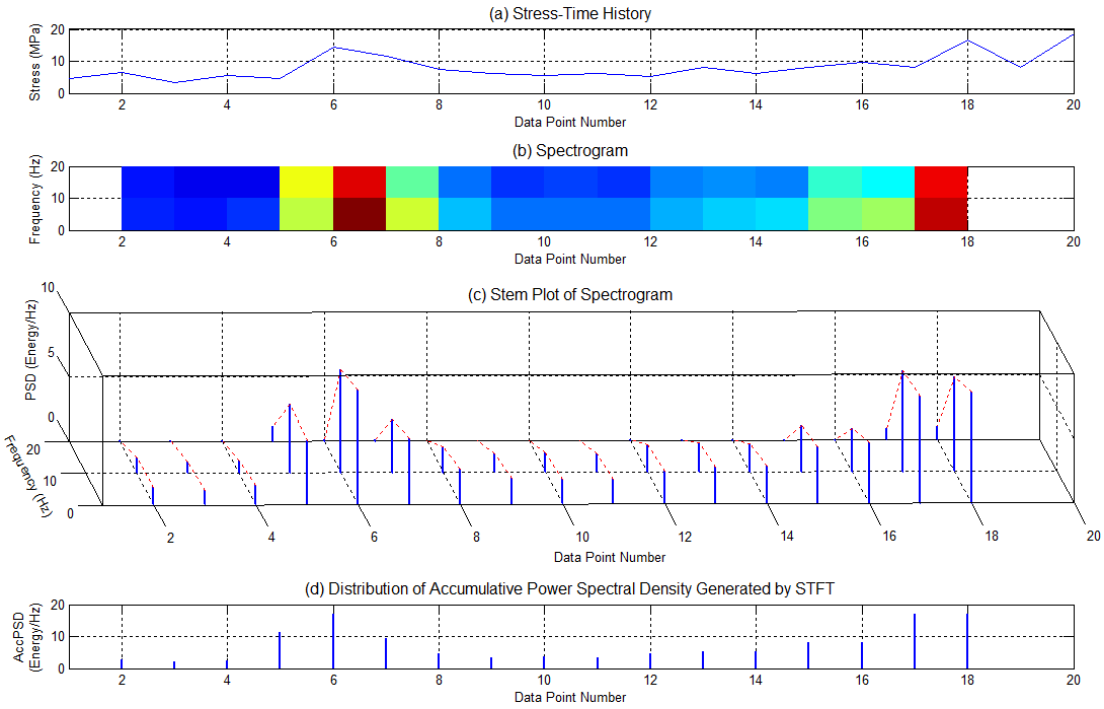

Figure 5.5-2. Stress-time history, spectrogram, 3D-stem plot and AccPSD plot generated by STFT

5.6 Wavelet Transform

For the meaning of the word "wavelet", Misiti *et al*. [109] described that "*a wavelet is a waveform of effectively limited duration that has an average value of zero.*" Burrus *et al*. [117] described that "*a wavelet is a small wave with a signal energy concentrated in time, on the condition of admissibility condition.*" Figure 5.6-1 illustrates the different between wavelets and sine waves, which are the basis of Fourier analysis. Sinusoids do not have limited duration and they extend from minus to plus infinity. Sinusoids are smooth and predictable whilst wavelets tend to be irregular and asymmetric. From Figure 5.6-1, Misiti *et al*. [109] commented that signals with sharp changes might be better analysed with an irregular wavelet than with a sinusoid. It also makes sense that local features can be described better with wavelets that have local extent. Figure 5.6-2 illustrates the different views of a signal presented by the time-based, frequency-based, STFT and wavelet analyses. It is noted that wavelet analysis does not use a time-frequency region but rather a time-scale region.

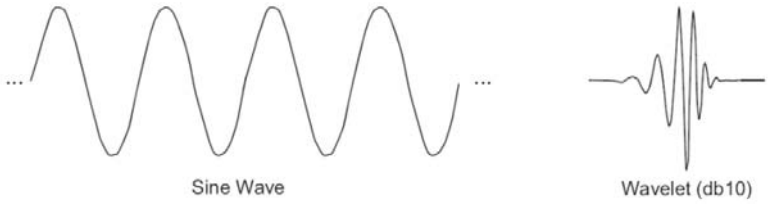

Figure 5.6-1. A sinusoidal wave and a wavelet [109]

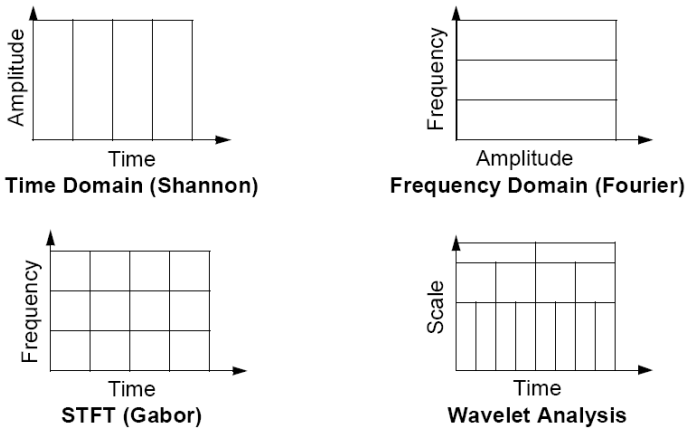

Figure 5.6-2. Views of a signal among time-based, frequency-based, STFT and WT analyses [109]

Wavelet transform (WT) represents the next logical step of a windowing technique with variable-sized regions. WT can solve the resolution problem because the window length is long for low frequencies and short for high frequencies. In other words, the frequency resolution is good for low frequencies (at high scales) and the time resolution is good at high frequencies (low scales). As illustrated in Figure 5.6-3, wavelet analysis allows the use of long time intervals where the low frequency information is wanted and shorter regions where the high frequency information is wanted.

Figure 5.6-3. Wavelet Transform [109]

WT can reveal trends, discontinuities and self-similarity of the signal. In addition, wavelet transform can compress or de-noise a signal [109]. The Fourier transform breaks down a signal into sine waves of various frequencies as typically shown in Figure 5.4-1(*a*). Similarly, WT breaks down a signal into shifted and scaled versions of a mother wavelet as typically shown in Figure 5.6-4.

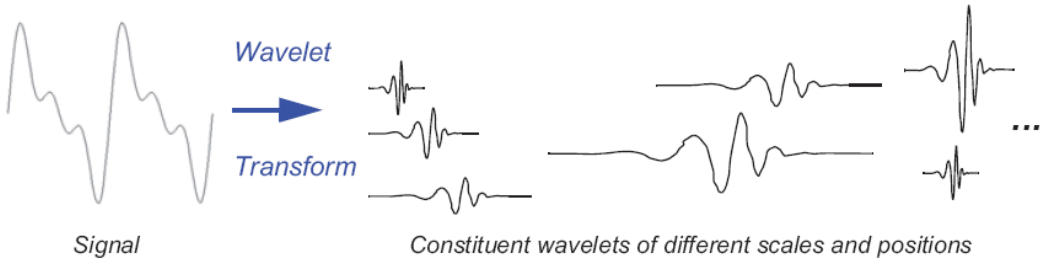

Figure 5.6-4. A typical mother wavelet and its constituent wavelets [109]

WT represents a windowing technique with variable-sized region. The harmonic form of the WT can be derived from the Fourier transform in the phase form.

$$X(\omega) = \int_{-\infty}^{+\infty} x(t) \sin(2\pi ft - \theta(f))\, dt \tag{5.6-1}$$

Let $a = 1/(2\pi f)$ be a scale parameter which controls the frequency by dilating or scaling the time t and $b' = \theta/(2\pi ft)$ be a translation parameter which translates the basic sine wave up and down the time axis. Then, Equation 5.6-1 can be rewritten as

$$X(\omega) = \int_{-\infty}^{+\infty} x(t) \sin\left(\frac{t-b'}{a}\right) dt \tag{5.6-2}$$

By replacing the sine wave with a wavelet ψ or localised oscillatory function, WT is obtained.

$$W_{\psi}(a,b') = \int_{-\infty}^{+\infty} x(t)\, \psi\left(\frac{t-b'}{a}\right) dt \tag{5.6-3}$$

The wavelet in Equation 5.6-3 is an analytical function $\psi(t)$ used to decompose a signal $x(t)$ into scaled wavelet coefficients $W_{\psi}(a,b')$.

5.6.1 Matlab Toolbox for Taking WT

By using wavelet toolbox in Matlab [109], WT can be taken to the input signal by a statement in the command line shown below.

```
COEFFS = cwt(x,a,'wname','plot')
```

This statement computes and plots the continuous wavelet coefficients, `COEFFS`, of the input signal vector `x` at real positive scales, `a`, using the wavelet whose name is `wname`. Maximum scale is defined by the next power of two of the wavelet decomposition level, i.e. $a = 2^{Level}$. `cwt` is a one-dimensional wavelet analysis function. The result is a scalogram typically shown in Figure 5.6-5(*b*). Matlab returns `COEFFS` as a matrix with *n* rows given by `Level` and *m* columns given by length of the input vector `x`.

5.6.2 Plot of Accumulative Power Spectral Density Generated by WT

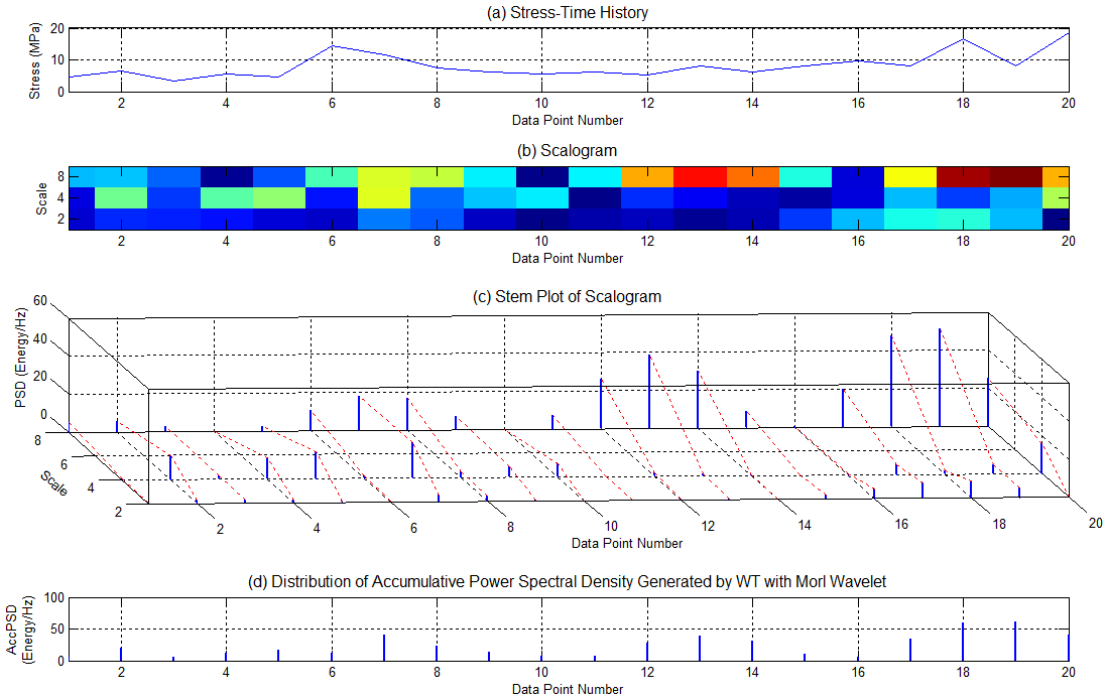

Figure 5.6-5. Stress-time history, scalogram, 3D-stem plot and AccPSD plot generated by WT with the Morl wavelet

In this research project, WT with the Morl wavelet is used to generate a plot of AccPSD shown in Figure 5.6-5(*d*). Here, Morl wavelet is chosen because it was successfully used in previous research [118]. AccPSD plot is used in the process of extracting fatigue damage parts discussed in Section 6.3. For the illustration purpose, the author uses Figure 5.6-5 to describe how to generate the plot of AccPSD. By taking WT (with `a = 2^3 = 8`, `wname = Morl`) to the stress-time history in Figure 5.6-5(*a*), Matlab generates the scalogram shown in Figure 5.6-5(*b*). Changing plotting style from scalogram to 3D-stem plot as shown in Figure 5.6-5(*c*) shows the relationship between PSD of wavelet coefficients and scale of wavelet decomposition at each time interval (or data point number). Thus, AccPSD of wavelet coefficients at each time interval is easily derived by summing PSD of each scale at each time interval. For example, AccPSD at data point number 2 is the summation of three PSDs located at scales 2, 4 and 8, and so on. By this manner, the plot of AccPSD distribution can be generated as shown in Figure 5.6-5(*d*).

5.7 Summary

This chapter reviews the concept and approach of fatigue signal editing techniques which are performed in time domain, frequency domain, peak-valley domain, time-frequency domain and time-scale domain. Relevant signal analysis, signal processing and fatigue signal editing techniques have all been mentioned. Many experimental signals exhibit non-stationary characteristics which challenge in signal analysis. By using the Fourier transform, the frequency components of an entire signal can be analysed but it is not possible to locate at what point in time that a frequency component occurred. To overcome this problem, the STFT and WT are the significant tools for analysing time-localised features of a signal.

Realising that the STFT and WT are new to the fatigue research on the field of wind turbine blades and theirs suitability to analyse non-stationary signals; therefore, they have been chosen as the methods for developing the new fatigue damage extraction discussed in Section 6.3.

Chapter 6

Extraction of Fatigue Damage Parts and Simulation Procedure

6.1 Introduction

This chapter deals with a concept of applying accumulative power spectral density (AccPSD) to identify fatigue damage events contained in the stress-time history. AccPSD has been introduced in Chapter 5. Sections 5.5.2 and 5.6.2 have illustrated how to calculate AccPSD and how to generate the plots of AccPSD versus data point number (time location) for both STFT and WT. In this chapter, AccPSD becomes the major subject matter and it is described in Section 6.2. Mathematically, each plot of AccPSD derived from STFT and WT does not have knowledge to identify where the fatigue damage events are located in the stress-time history. The author uses a plot of fatigue damage versus data point number in Figure 6.2-3(*b*) to teach AccPSD knowledge. This plot is generated by an existing method called time correlated fatigue damage (TCFD) [98,102]. TCFD is used by commercial software [102]. In addition, Section 6.2 presents the idea of using cutoff level, which is an appropriate AccPSD level, to identify the locations of fatigue damage in the stress-time history. In this research project, the cutoff level is very important because it is used as a criterion in identifying and extracting fatigue damage from the original stress-time history. The signal segments which their levels of AccPSD are equal to or higher than the cutoff level will be identified as the damage parts and vice versa for the non-damage parts. By this criterion, the damage parts will be extracted from the original stress-time history and then they are concatenated to form an edited stress-time history. Section 6.3 describes an algorithm used to extract fatigue damage parts from the stress-time history.

Section 6.4 deals with simulation procedure done in a fatigue computer code for HAWT blades, HAWTfatigue. In this research project, HAWTfatigue is implemented and designed to be run in Matlab environment (see details in Appendix C). The code is used to evaluate fatigue damage and to edit stress-time history of HAWT blades. The theories for evaluating fatigue damage are mainly based on stress-life approach and Miner's linear cumulative damage rule mentioned in Sections 4.3 and 4.4. The code consists of eight modules illustrated by a flowchart in Figure 6.4-1. The general process in evaluating the fatigue damage starts from Modules 1 to 6. Modules 7 and 8 are added to the general

process to edit the stress-time history by means of STFT- and WT-based fatigue damage part extracting methods, respectively. Both methods are the newly developed methods proposed in this research project. Flowchart in Figure 6.4-1 describes the simulation procedure step by step.

In this research project, the original stress-time history contains 68,739,939 data points with sampling rate at 40 Hz. The duration of the history is 1,718,498.475 seconds. The author cannot use Matlab toolboxes to take STFT and WT to the entire history in one analysis because of limited computer memory. Thus, the original stress-time history is separated into 688 segments as shown in Figure 6.1-1. Each segment contains 100,000 data points. For the purpose of illustration in this chapter, the segment 52 of the original stress-time history (a red signal in Figure 6.1-1 and its enlargement view in Figure 6.1-2) is intentionally selected because it clearly shows where the damage and non-damage parts are. As a typical stress-time history, the segment 52 is used to present concepts and to show examples throughout this chapter.

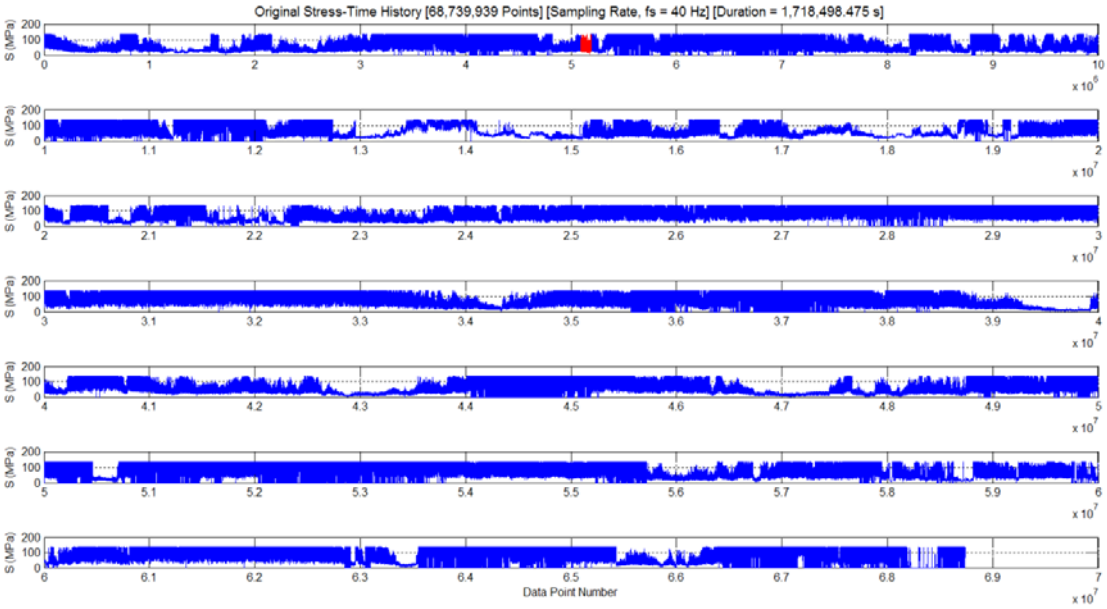

Figure 6.1-1. Original stress-time history and the segment 52 (a red signal)

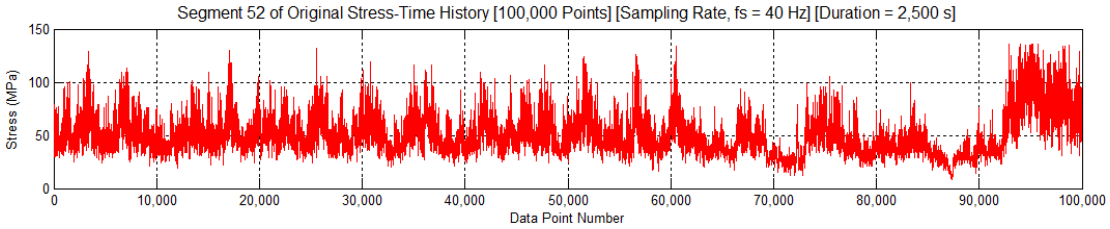

Figure 6.1-2. Enlargement view of the segment 52 in the original stress-time history

6.2 Fatigue Damage Versus Accumulative Power Spectral Density

This section mainly discusses the concept of applying accumulative power spectral density (AccPSD) to identify fatigue damage events contained in the stress-time history. How to calculate AccPSD for STFT and WT has been introduced in Sections 5.5.2 and 5.6.2, respectively. To generate the plots of AccPSD versus data point number (time location), two Matlab toolboxes are used.

By using signal processing toolbox in Matlab [116], STFT is taken to the segment 52 in Figure 6.2-1(*a*) and then a spectrogram is generated as shown in Figure 6.2-1(*b*). Spectrogram shows how the PSD of STFT coefficients distribute in time-frequency domain. The plot of AccPSD of segment 52 shown in Figure 6.2-1(*c*) is derived from spectrogram by summing the PSD of all frequency bands at each time interval.

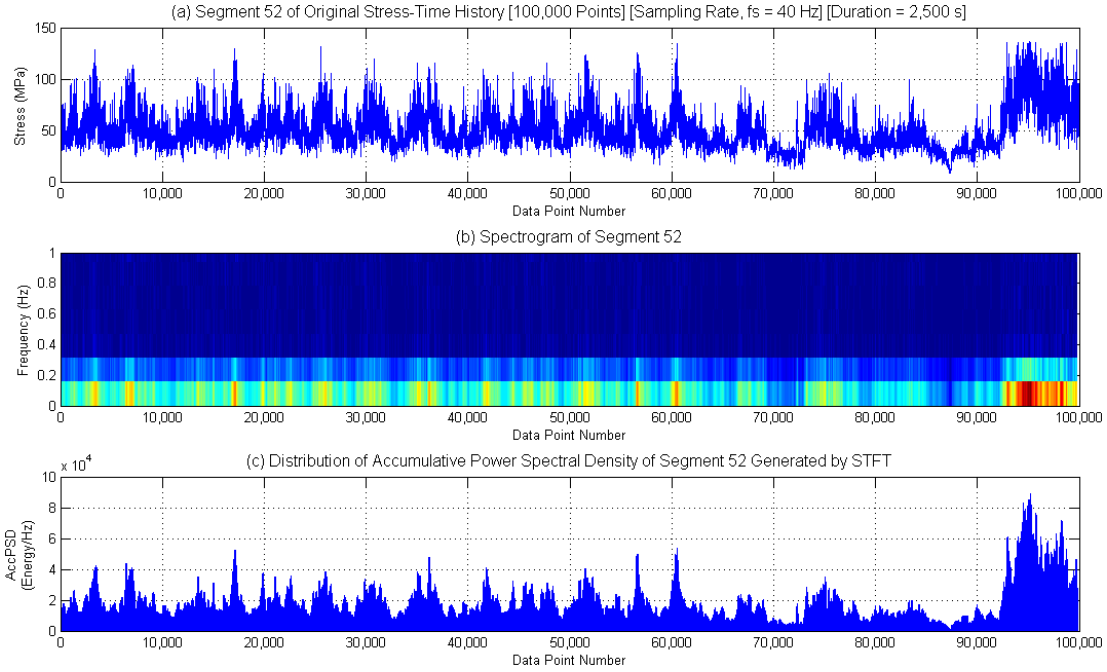

Figure 6.2-1. Results of the segment 52 generated by STFT

By using wavelet toolbox in Matlab [109], WT with the Morl wavelet is taken to the segment 52 in Figure 6.2-2(*a*) and then a scalogram is generated as shown in Figure 6.2-2(*b*). Here, the Morl wavelet is chosen because it was successfully used in previous research [118]. The scalogram shows how the PSD of wavelet coefficients distributes in time-scale domain. The plot of AccPSD of segment 52 shown in Figure 6.2-2(*c*) is derived from scalogram by summing the PSD of wavelet coefficients of all scales at each time interval.

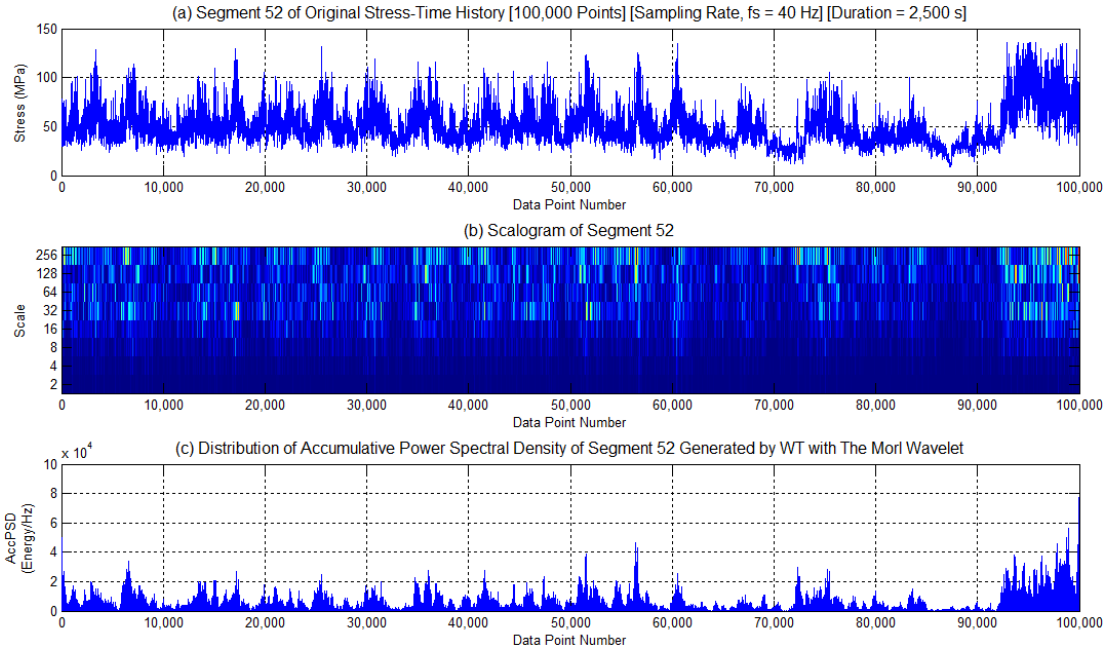

Figure 6.2-2. Results of the segment 52 generated by WT with the Morl wavelet

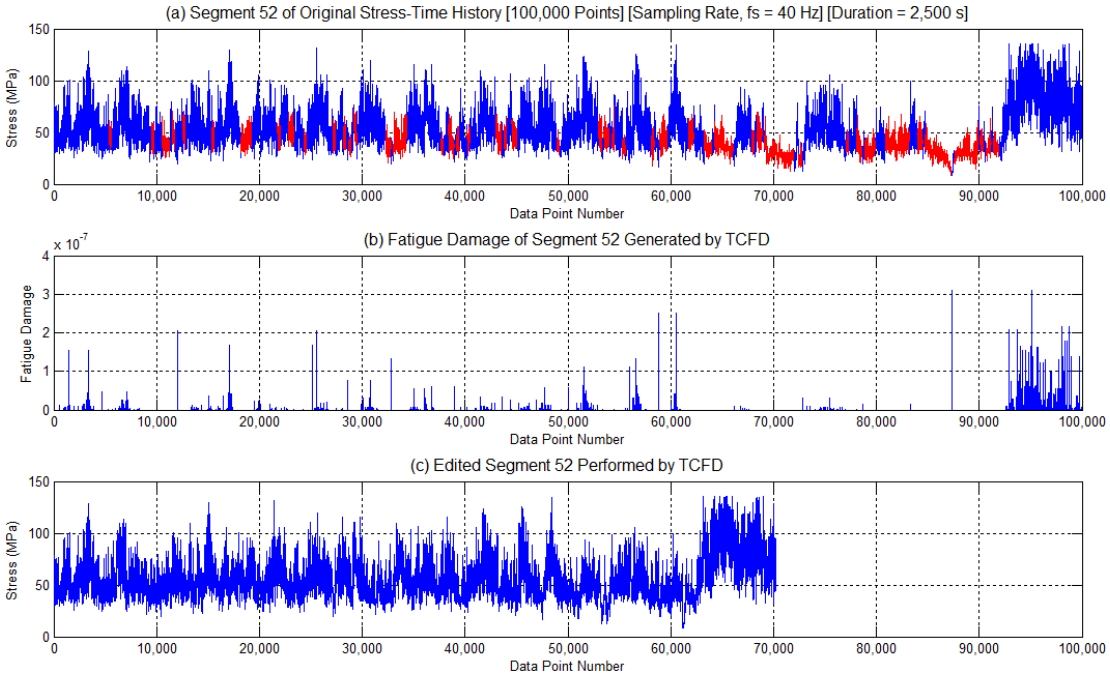

Figure 6.2-3. Results of the segment 52 generated by TCFD

At this stage, each plot of AccPSD derived from STFT and WT does not have knowledge to identify where the fatigue damage events are located in the segment 52. To teach the plot of AccPSD knowledge, the time locations that fatigue damage occurs must be known. In this research project, fatigue damage at time locations is known from an existing method called the time correlated fatigue damage (TCFD). This method is used by commercial software [102]. Based on TCFD, the author uses a plot of fatigue damage versus data point number in Figure 6.2-3(*b*) to teach AccPSD knowledge. The red signals in Figure 6.2-3(*a*) are marked by TCFD. They are non-damage parts which must be removed from the segment 52. The blue signals in Figure 6.2-3(*a*) are damage parts. They are concatenated to form an edited segment 52 shown in Figure 6.2-3(*c*).

The result in Table 6.2-1 shows that the edited segment 52 has reduction of 29.75% in length with respect to the original length. In other words, the length of the edited segment 52 is 70.25% of the original length. The retained fatigue damage per repetition of the edited segment 52 is slightly different from the original fatigue damage per repetition. The difference in fatigue damage per repetition is +0.832% whilst the differences in signal statistical parameters (mean stress, root-mean-square and kurtosis) are ±10% approximately. Here, the (+) and (-) signs mean less than and greater than, respectively.

Table 6.2-1. Statistical parameters of the segment 52 before and after editing by TCFD (See comparison among TCFD, STFT and WT in Table 6.5-1)

History	Length (Points)	Mean Stress (MPa)	rms (MPa)	Kurtosis	Fatigue Damage*
Segment 52	99,968	50.87	54.06	5.02	2.40337E-5
Edited by TCFD	70,225	56.06	59.08	4.54	2.38338E-5
% Error**	+29.75	-10.20	-9.29	+9.56	+0.832

* Fatigue damage per repetition

** (+) and (-) signs of percent error mean less than and greater than, respectively.

For example, percent error of history length is calculated from

$$\% \text{ Error of History Length} = \frac{L_{\text{Segment 52}} - L_{\text{Edited Segment 52}}}{L_{\text{Segment 52}}} \times 100$$
$$= \frac{99{,}968 - 70{,}225}{99{,}968} \times 100$$
$$= +29.75\%$$

To observe the distribution patterns among the fatigue damage obtained from TCFD and AccPSDs obtained from STFT and WT, Figures 6.2-1(*c*), 6.2-2(*c*), 6.2-3(*a*) and 6.2-3(*b*) are displayed on the same figure, i.e. Figure 6.2-4. Considering Figure 6.2-4(*a*), the fatigue damage contained in each group of the blue signals is implied by the amplitude of fatigue damage spikes shown in Figure 6.2-4(*b*). It is noticeable that each spike indicates both where and how much the fatigue damage occurs.

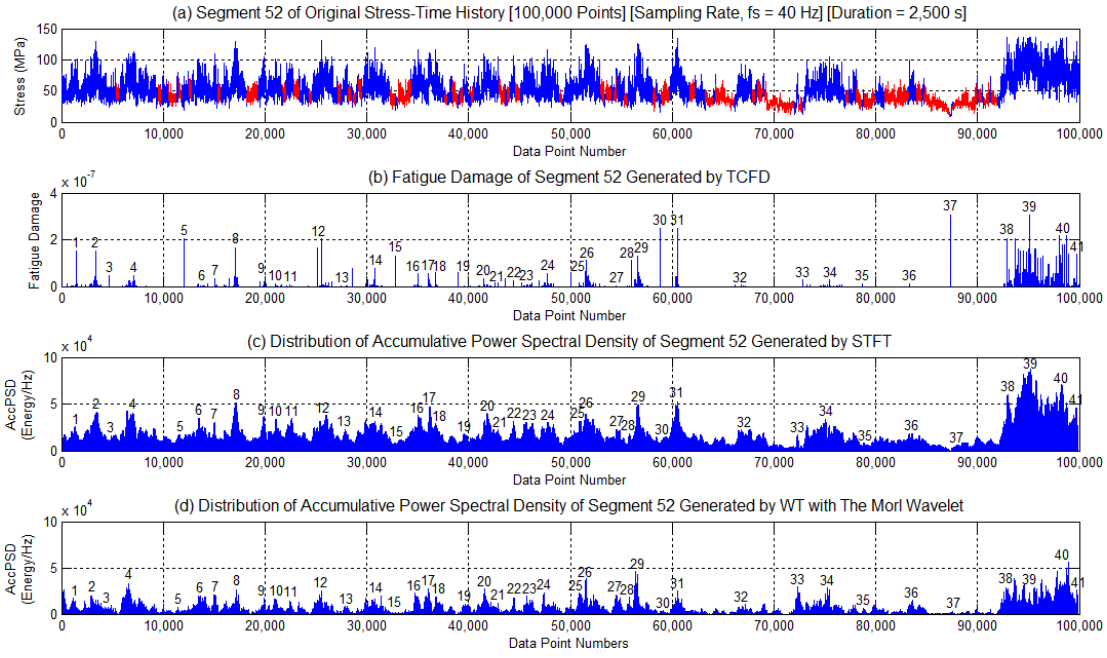

Figure 6.2-4. Damage parts, non-damage parts, fatigue damage and AccPSDs generated by STFT and WT with the Morl wavelet

By observing the distribution patterns of spikes, it has been found that almost spikes of AccPSDs in Figures 6.2-4(*c*) and 6.2-4(*d*) are located at time intervals that spikes of fatigue damage are located in Figure 6.2-4(*b*), especially at the positions 1 to 41. When comparing the amplitude of damage spikes to the amplitude of AccPSD spikes (for both

STFT and WT) at each time interval, it has been found that the amplitude of AccPSD spikes does not tell us how much fatigue damage occurs. For example, there are the same amplitude of damage spikes located at points 1 and 2 but the amplitudes of AccPSD spike at point 1, for both STFT and WT, are lower than those at point 2. The same situation occurs at points 30 and 31. Furthermore, it is outstanding that there is a high peak of damage spike at point 37 but the amplitude of AccPSD spikes at the same point are very low for both STFT and WT. Fortunately, it is clearly seen that the locations of each spike of AccPSDs tell us where the fatigue damage occurs.

Next idea is that which spikes in the plots of AccPSD should be used to identify the locations of fatigue damage. For STFT, the author tries to hide the bottom parts of AccPSD plots, generated by STFT, by using white rectangles with different heights shown in Figures 6.2-5(*b*), 6.2-5(*c*) and 6.2-5(*d*). In this research project, the upper edge of each rectangle is called cutoff level. With cutoff levels of 10,000 and 15,000 Energy/Hz, the Figures 6.2-5(*b*) and 6.2-5(*c*) show disappearing of the peaks 15, 35 and 37. By increasing cutoff level to 20,000 Energy/Hz shown in Figure 6.2-5(*d*), it has been found that the peaks 5, 15, 19, 28, 30, 33, 35, 36 and 37 are disappeared. By this manner, it is noticeable that the pattern of each group of peaks left in Figure 6.2-5(*d*) resembles the pattern of fatigue damage in Figure 6.2-5(*a*).

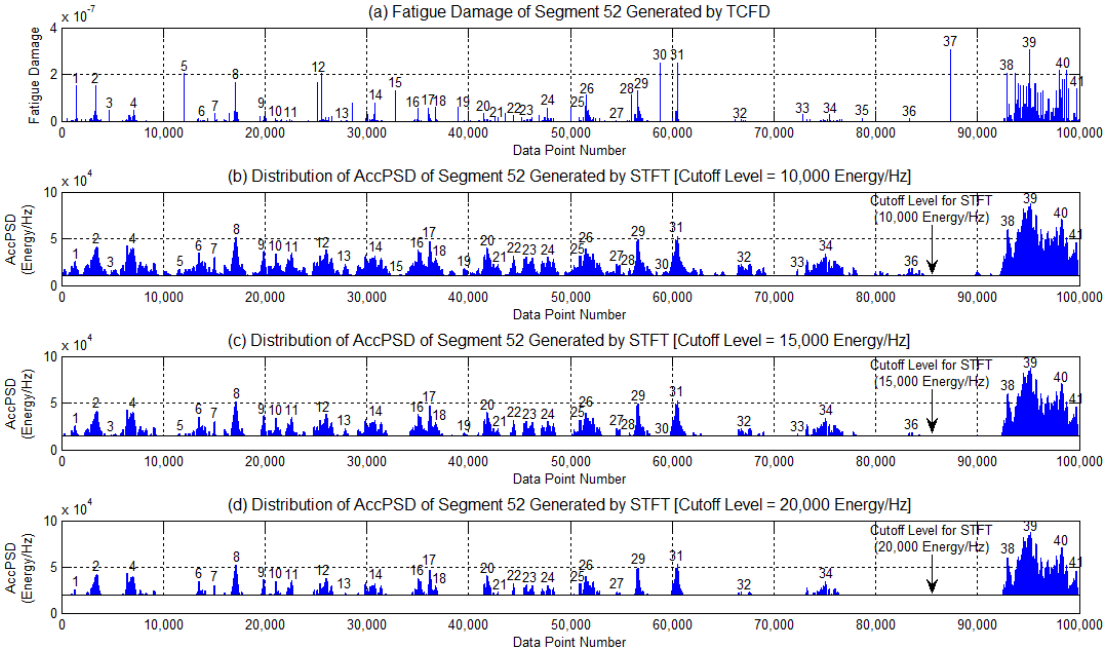

Figure 6.2-5. Comparison among fatigue damage and AccPSDs generated by STFT with three different cutoff levels

The same idea for the plot of AccPSD generated by WT, the author uses the white rectangles with different heights to hide the bottom parts of AccPSD plots as shown in Figures 6.2-6(*b*), 6.2-6(*c*) and 6.2-6(*d*). With cutoff level of 5,000 Energy/Hz, the Figure 6.2-6(*b*) shows disappearing of the peaks 15, 30 and 37. When increasing cutoff level to 10,000 Energy/Hz, Figure 6.2-6(*c*) shows disappearing of the peaks 3, 5, 13, 15, 19, 30, 32, 35 and 37. Eventually, the cutoff level is increased to 15,000 Energy/Hz and the Figure 6.2-6(*d*) shows that the peaks 3, 5, 9, 11, 13, 15, 19, 21, 30, 32, 35, 36 and 37 are disappeared.

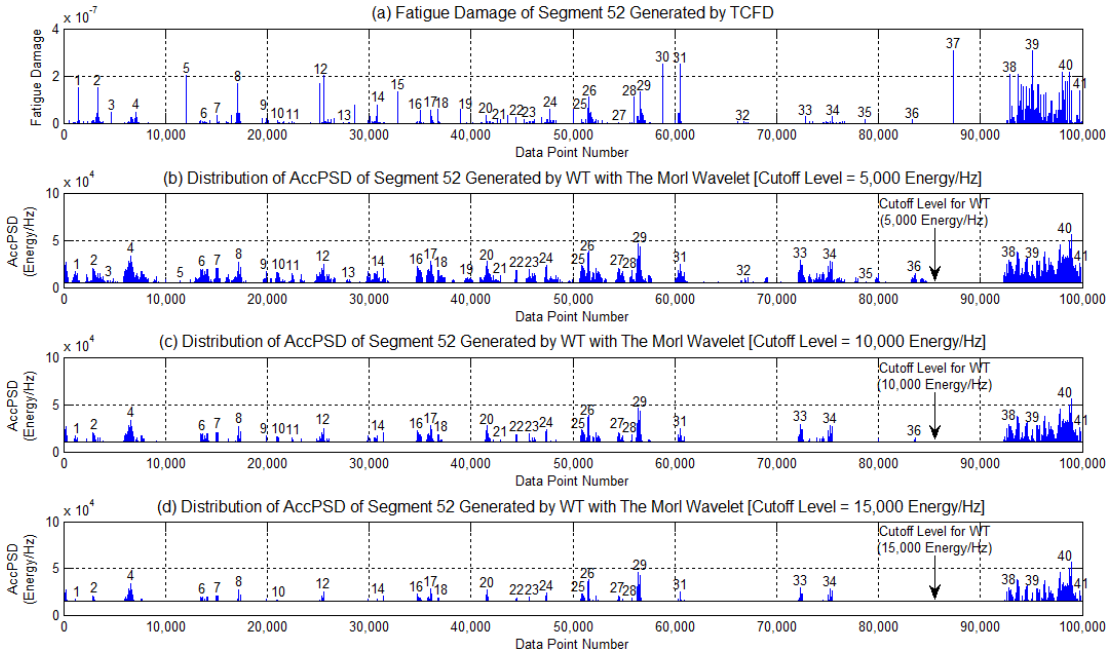

Figure 6.2-6. Comparison among fatigue damage and AccPSDs generated by WT with three different cutoff levels

For the subject matter mentioned in this section, three issues based on observation can be summarised.

1. The amplitudes of AccPSD spikes for both STFT and WT do not provide us how much fatigue damage occurs.
2. The locations of AccPSD spikes, which are observed by naked eyes, are close to the locations of fatigue damage occurred.
3. The fatigue damage events in the stress-time history could be identified by an appropriate cutoff level.

In this research project, the cutoff level is very important because it is used as a criterion in identifying and extracting fatigue damage parts from the original stress-time history. The signal segments which their levels of AccPSD are equal to or higher than cutoff level will be identified as the damage parts and vice versa for the non-damage parts. By this criterion, the damage parts will be extracted from the original stress-time history and then they are concatenated to form an edited stress-time history. Ideally, the fatigue damage contained in the edited stress-time history should be the same as the original damage. If the cutoff level is too high, the minority of fatigue damage events will be detected; consequently, the length of the edited stress-time history is very short. Also, the retained fatigue damage will dramatically deviate from the original fatigue damage. On the other hand, if the cutoff level is too low, some non-damage parts may be identified as the damage parts; consequently, the length of the edited stress-time history may be slightly reduced whilst the retained fatigue damage may not be changed or a little bit from the original fatigue damage. To determine the appropriate cutoff level, the effect of cutoff level on fatigue damage retained in the edited stress-time history has been studied in Sections 7.2 to 7.4.

To summarise, the observation done in this section implies that the plots of AccPSD, which are gained from spectrogram for STFT and scalogram for WT, enable us to identify the fatigue damage events contained in the original stress-time history.

6.3 Algorithm for Extracting Fatigue Damage Parts

This section deals with how to extract fatigue damage parts from the stress-time history. This extraction method is used in this research project. The author uses Figure 6.3-1 to demonstrate how to extract fatigue damage parts and how to generate the edited stress-time history. Considering Figure 6.3-1, the typical stress-time history consists of 20 data points. It is divided into 17 windows which their widths are given by 4 data points. AccPSD of the signal segment in each window is represented by the spike labeled by the italic number. Since each value of AccPSD is the value at the middle of each window, there is no middle data point to locate each AccPSD spike because the number of data points in each window is even. In this case, Matlab locates each AccPSD spike at the left point nearest the middle. For example, window 1 consists of data points 1, 2, 3 and 4 so there is no middle for these data points. Thus, Matlab locates AccPSD spike *1* at data point 2.

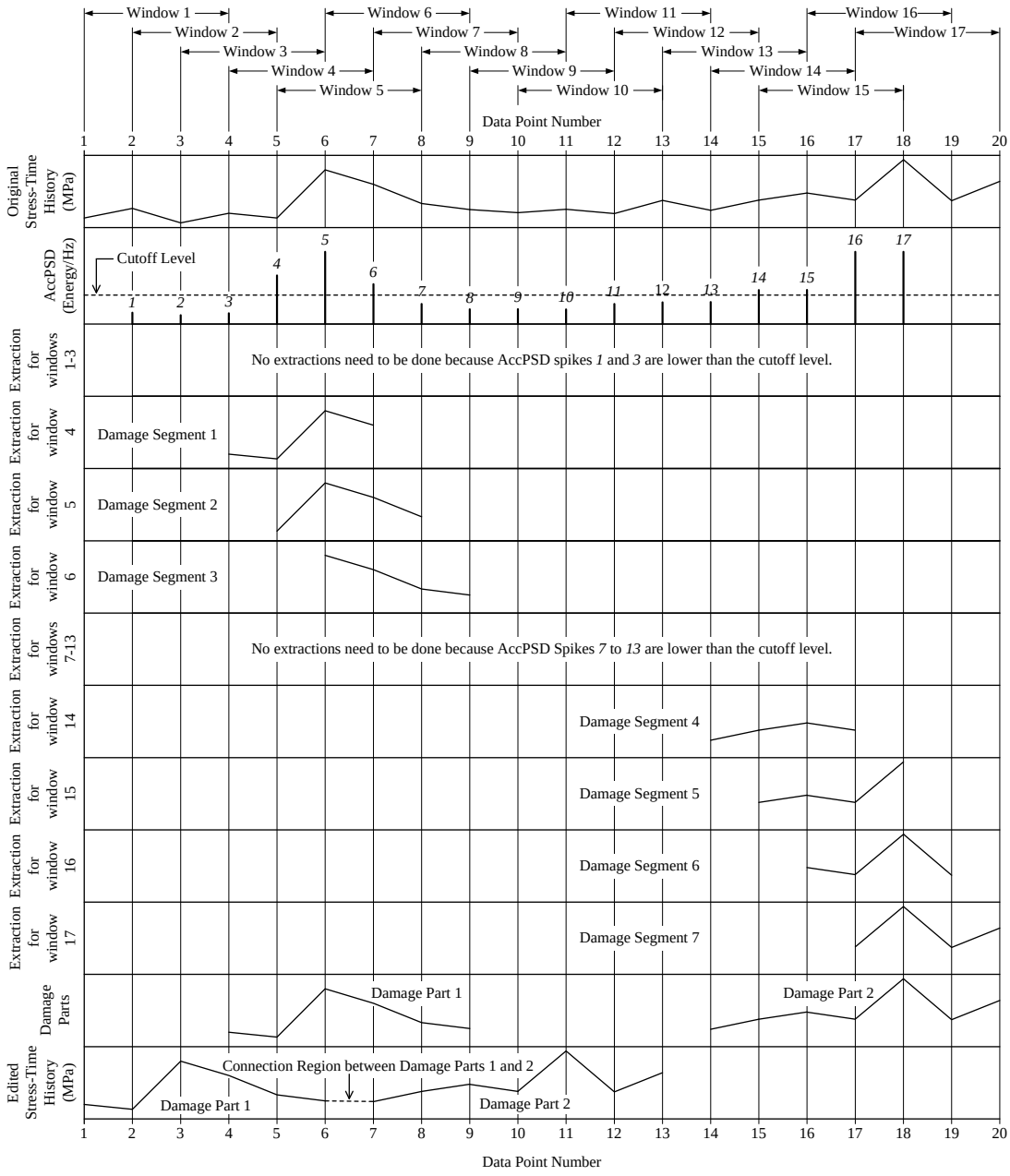

Figure 6.3-1. Algorithm for extracting fatigue damage parts

Based on a cutoff level represented by a dash line in the second plot of Figure 6.3-1, no extractions need to be done for windows 1 to 3 because the amplitudes of AccPSD spikes *1* to *3* are lower than the cutoff level. For window 4, the amplitude of AccPSD spike *4* is higher than the cutoff level so the data points 4, 5, 6 and 7 are extracted from the typical stress-time history and formed the damage segment 1. In the same manner, the amplitudes of AccPSD spikes *5* and *6* are higher than the cutoff level so data points 5, 6, 7, 8 and data

points 6, 7, 8, 9 are extracted and formed the damage segments 2 and 3, respectively. By superposing damage segments 1, 2 and 3, the damage part 1 is formed by data points 4, 5, 6, 7, 8 and 9. Similarly, the damage part 2 is formed by superposing damage segments 4, 5, 6 and 7. Eventually, damage parts 1 and 2 are concatenated to form the edited stress-time history as shown in the bottom plot of Figure 6.3-1.

6.4 Simulation Procedure

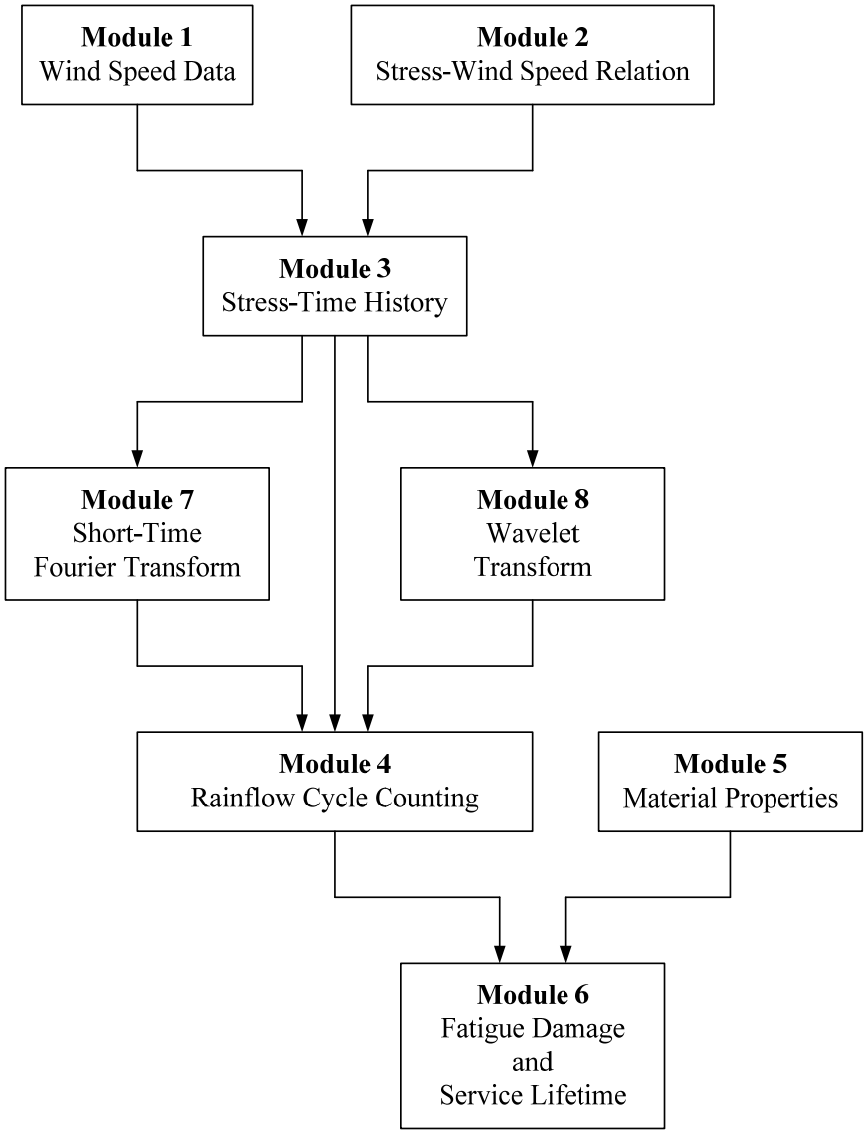

Figure 6.4-1. Modules of HAWTfatigue

HAWTfatigue is a fatigue computer code used to evaluate fatigue damage and service lifetime of HAWT blades and to edit the original stress-time history. The code is designed to be run in Matlab environment. The code consists of 8 main modules as illustrated in Figure 6.4-1. The process performed by Modules 1 to 6 is the general process. Modules 7 and 8 are added to the general process to edit the original stress-time history by newly developed methods, i.e. STFT and WT. The flowchart describes simulation procedure step by step.

6.4.1 Step 1: Load Wind Speed Data to Module 1

In this research project, the wind speed data [119] is recorded to establish the dynamic behaviour, fatigue load spectra and extreme load experienced by the wind turbine. The wind speed data was measured by using anemometers at a reference height of 61.8 m above ground level in north-east England. A wind shear exponent value of the wind speed data is 0.294 fitted by power law (see Equation 2.7-4). The wind speed data was sampled at f_s = 40 Hz for 68,739,939 data points giving the total record length of the signal of 1,718,498.475 seconds. Here, f_s is a sampling rate. Since the hub height of the Micon 65 wind turbine is at 22.86 m, the wind speed at this altitude is evaluated by power law. For the purpose of illustration, the very long wind speed data is separated into seven parts as shown in Figure 6.4-2.

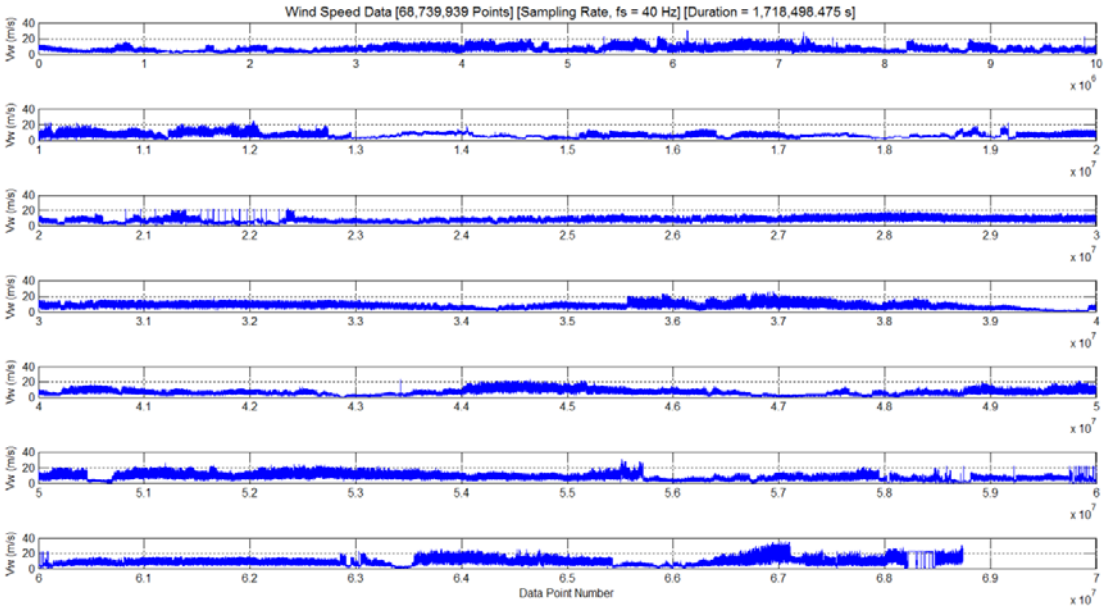

Figure 6.4-2. Wind speed at the hub height of 22.86 m with sampling rate f_s at 40 Hz [119]

The Weibull probability density function (PDF) and the cumulative distribution function (CDF) are calculated from

$$\mathrm{PDF}(V_w) = \left(\frac{k}{c}\right)\left(\frac{V_w}{c}\right)^{k-1} \exp\left[-\left(\frac{V_w}{c}\right)^{k}\right] \tag{6.4-1}$$

$$\mathrm{CDF}(V_w) = 1 - \exp\left[-\left(\frac{V_w}{c}\right)^{k}\right] \tag{6.4-2}$$

where a shape factor, k, and a scale factor, c, are given by [37]

$$k = \left(\frac{\sigma}{\bar{V}_w}\right)^{-1.086} \tag{6.4-3}$$

$$c = \frac{\bar{V}_w}{\Gamma(1+1/k)} \tag{6.4-4}$$

The gamma function in the denominator of Equation 6.4-4 can be calculated by using a Matlab command `gamma(1+1/k)`. Plotting of Equations 6.4-1 and 6.4-2 are illustrated in Figure 6.4-3. Also, the statistical parameters of the wind speed data are listed in Table 6.4-1.

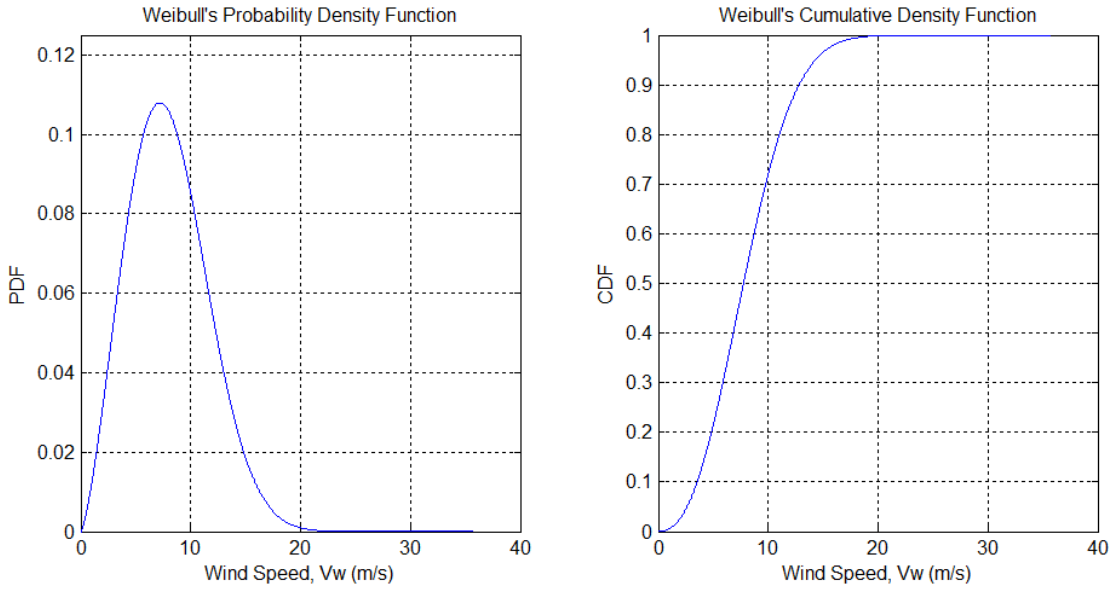

(*a*) Probability density function (*b*) Cummulative density function

Figure 6.4-3. Weibull's probability distribution

Table 6.4-1. Statistical parameters of the wind speed data

Minimum Wind Speed (m/s)	Maximum Wind Speed (m/s)	Mean Wind Speed (m/s)	Standard Deviation (m/s)	Weibull's Parameters	
				Shape Factor *k*	Scale Factor *c*
0	35.79	8.013	3.59	2.3931	9.0395

6.4.2 Step 2: Load Relationship between Stress and Wind Speed to Module 2

This relationship between stress and wind speed in Figure 6.4-4 is generated by using three computer programmes. HAWTsimulator [52] is used to generate the sets of aerodynamic loads, mentioned in Section 2.8, at different wind speeds ranging from cut-in to cut-out. NuMAD software [120] is used to generate a finite element model of the pseudo SERI-8 wind turbine blade in Figure 6.4-5. The data used by NuMAD are listed in Table A1. Both the sets of aerodynamic loads and the finite element model are imported to ANSYS structural software to determine a critical value of von Mises stress and its location on the blade as shown in Figures 6.4-6 to 6.4-8. Having finished a set of stress simulations in ANSYS, the relationship between von Mises stress and wind speed ranging from 0 m/s to 15.5 m/s is generated as shown in Figure 6.4-4. Furthermore, it is assumed that when the wind speed value be higher than 16 m/s, the yaw mechanism would turn the rotor parallel to the wind direction; consequently, von Mises stress could be assumed as zero.

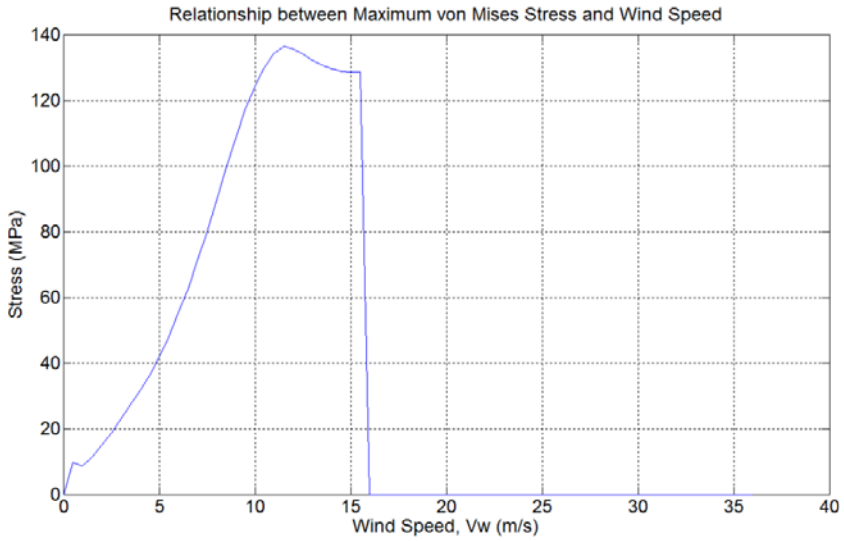

Figure 6.4-4. Relationship between maximum von Mises stress and wind speed

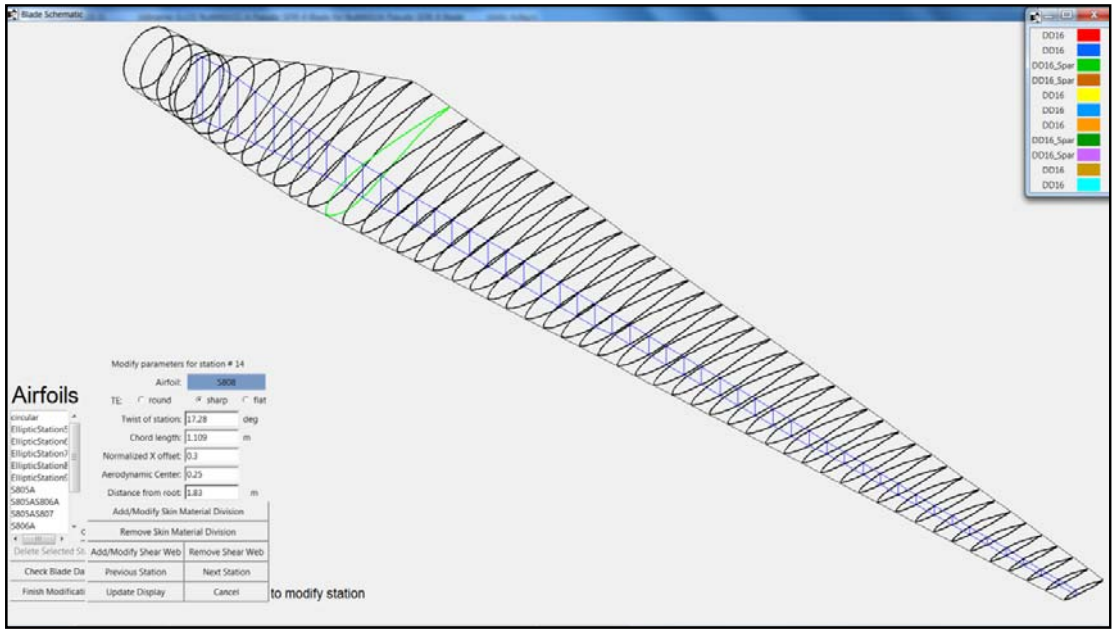

Figure 6.4-5. NuMAD software for generating the finite element model of the pseudo SERI-8 blade

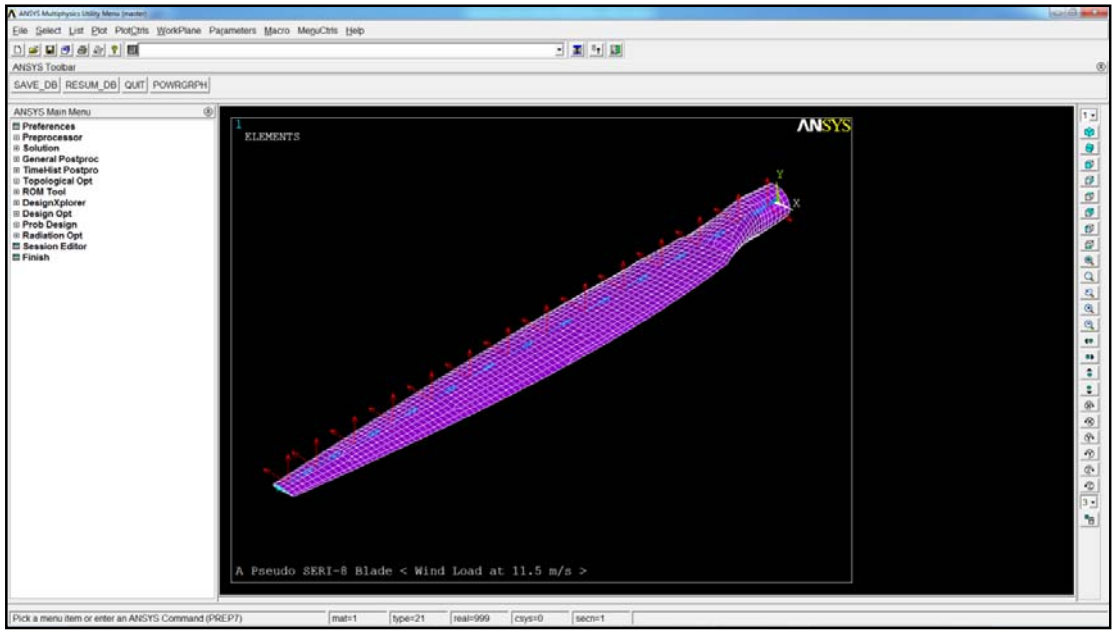

Figure 6.4-6. Finite element model of the pseudo SERI-8 blade in ANSYS with applied loads (Esize = 0.01 m, 160,602 Elements, 480,173 nodes)

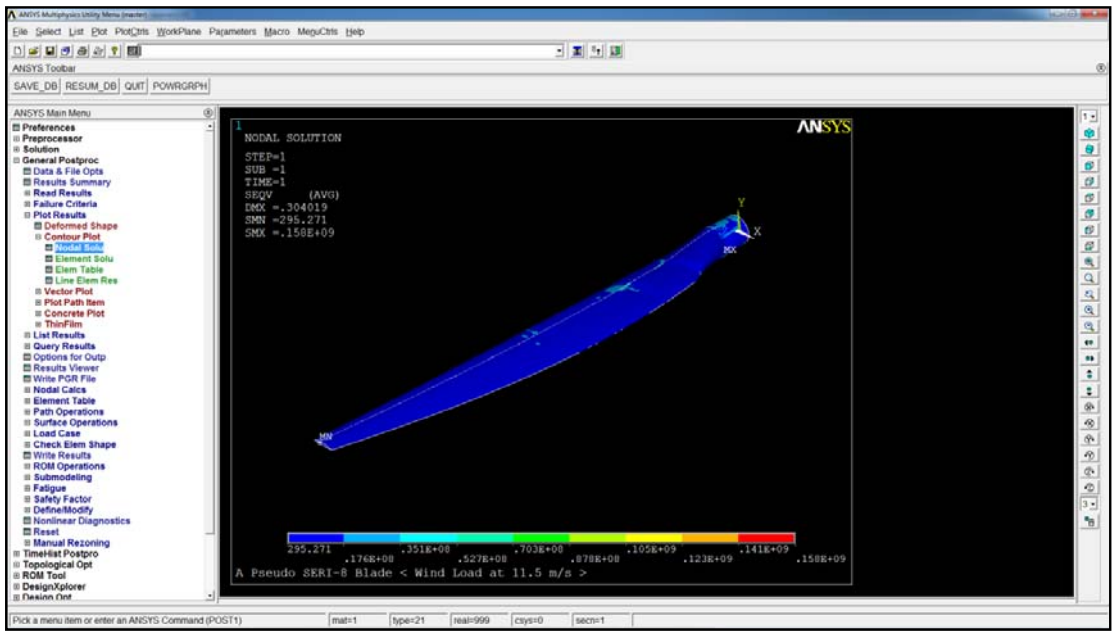

Figure 6.4-7. Typical result (maximum von Mises stress at wind speed 11.5 m/s)

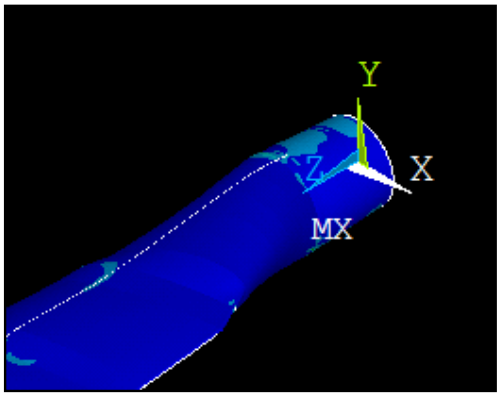

Figure 6.4-8. Enlargement view showing the critical area in Figure 6.4-7

6.4.3 Step 3: Generate Stress-Time History

Module 3 is used to generate a stress-time history in Figure 6.4-9. By relating the relationship between wind speed and time (Figure 6.4-2) with the relationship between von Mises stress and wind speed (Figure 6.4-4), the stress-time history is generated. This history is treated as an original stress-time history and it will be edited by STFT- and WT-based fatigue damage part extracting methods in Modules 7 and 8, respectively. The statistical parameters of the original stress-time history are listed in Table 6.4-2.

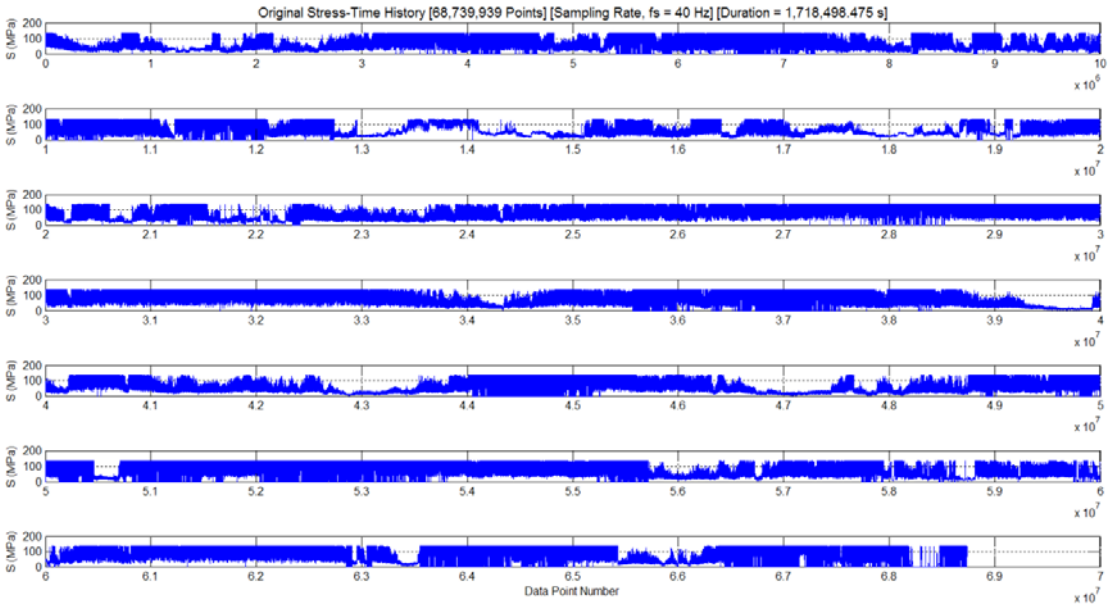

Figure 6.4-9. Original stress-time history (f_s = 40 Hz)

Table 6.4-2. Statistical parameters of the original stress-time history

Total Data (Points)	Duration (s)	Min. Stress (MPa)	Max. Stress (MPa)	Mean Stress (MPa)	Standard Deviation (MPa)	rms (MPa)	Kurtosis
68,739,939	1,718,498.475	0	136.39	81.95	40.84	90.96	1.58

6.4.4 Step 4: Count Rainflow Cycles

Module 4 is used to count rainflow cycles contained in the original stress-time history and the edited stress-time histories generated by STFT- and WT-based fatigue damage part extracting methods in Modules 7 or 8. Rainflow cycle (RFC) is a pair of stress range and mean stress. The algorithm for the rainflow cycle counting implemented in the module is a simplified rainflow counting for repeating histories recommended by ASTM E 1049-85 [84]. For the original stress-time history, the rainflow cycles counted are illustrated by a three-dimensional histogram shown in Figure 6.4-10. Also, the statistical parameters of rainflow cycles counted are listed in Table 6.4-3.

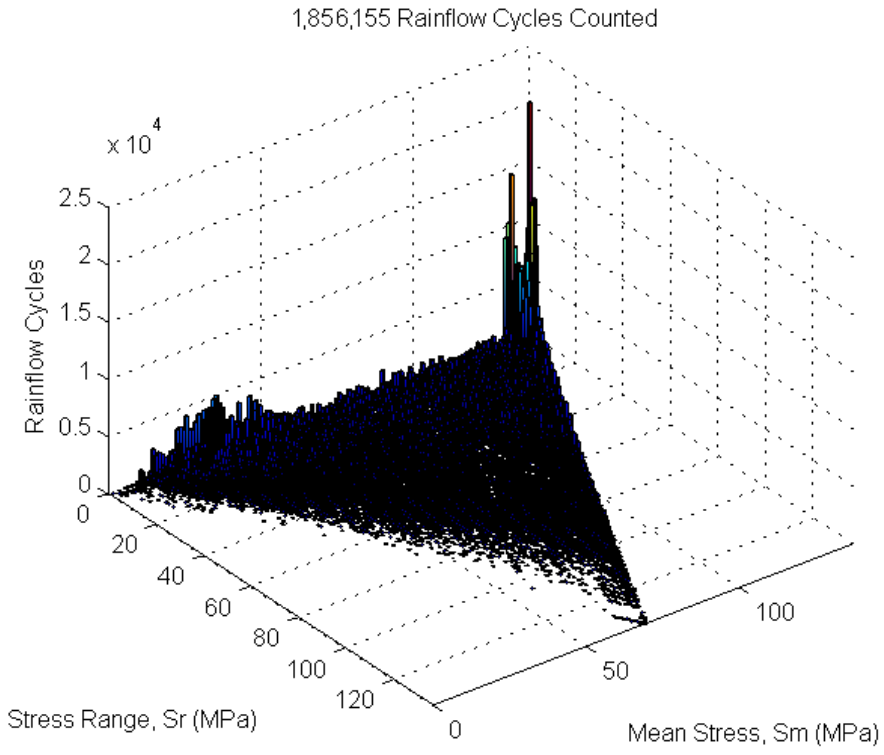

Figure 6.4-10. Histogram showing the rainflow cycles counted from the original stress-time history

Table 6.4-3. Statistical parameters of 1,856,155 rainflow cycles counted

	Maximum	Minimum	Mean	Standard Deviation
Stress Range, ΔS (MPa)	136.39	0.01	14.12	17.24
Mean Stress, S_m (MPa)	136.37	0.30	81.95	37.86

6.4.5 Step 5: Load Material Properties to Module 5

Module 5 is used to load mechanical properties listed in Table A2 and S-N curves listed in Table A3 to the code. The material properties will be used by Module 6. In this research project, the fibreglass composite material used in modelling the pseudo SERI-8 blade is a laminate called DD16. It has been listed in DOE/MSU composite material fatigue database for wind turbine blades [70]. The S-N curves of DD16 shown in Figure 6.4-11 is expressed by Equation 4.3-3 (a three-parameter equation).

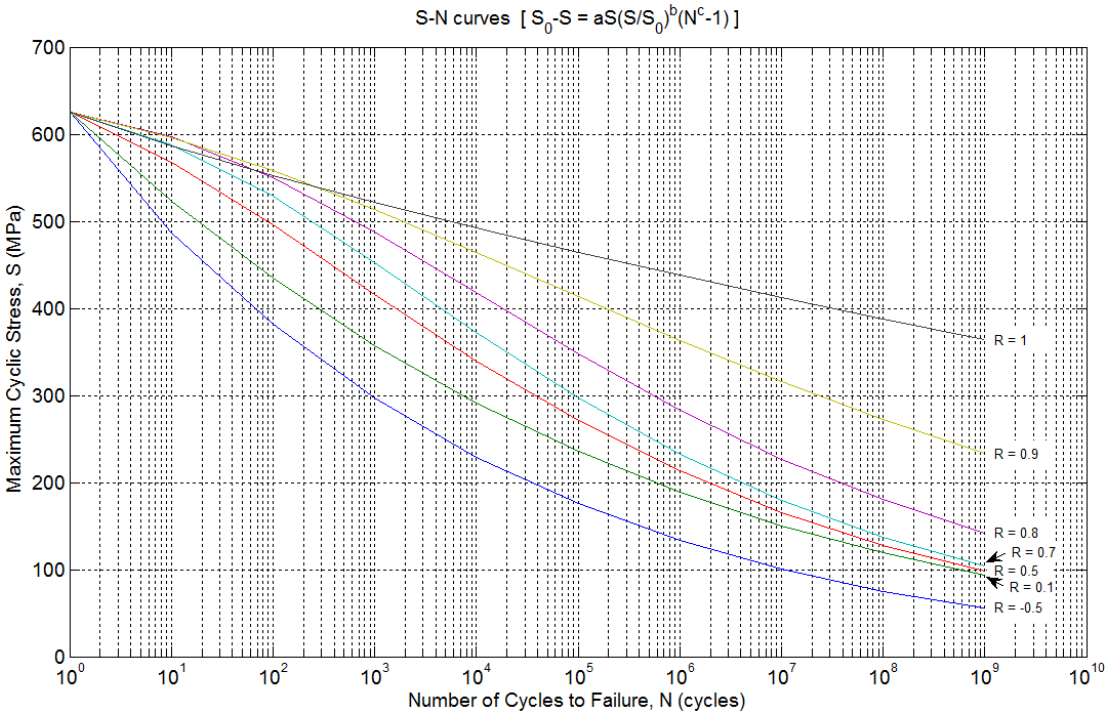

Figure 6.4-11. *S-N* curves with seven values of *R*-ratio of DD16 composite material [69]

6.4.6 Step 6: Evaluate Fatigue Damage and Service Lifetime

Module 6 is used to evaluate fatigue damage by using Miner's linear cumulative damage rule. In general, each rainflow cycle counted by Module 4 has different values of R-ratio, so the code interpolates for the number of cycles to failure of each cycle by using a family of S-N curves shown in Figure 6.4-11. Consequently, the fatigue damage per repetition can be calculated by Miner's rule (Equation 4.4-1). Having known the fatigue damage per repetition, the total number of repetitions that causes total fatigue damage equal 1.0 or closer can be calculated from Equation 4.4-2. Eventually, the service lifetime can be calculated in the unit of seconds by Equation 4.4-3. Then, seconds can be converted to months and years as listed in Table 6.4-4.

Table 6.4-4. Fatigue damage and service lifetime of the original stress-time history

Data		Value
Number of cycles per repetition		1,856,155
Damage per repetition		1.466634E-03
Total repetitions		681
Total damage		1.0
Duration of the original stress-time history (seconds)		1,718,498.475
Service lifetime:		
	seconds	1,170,297,461
	months	451.50
	years	37.63

6.4.7 Step 7: Edit Original Stress-Time History by Using STFT in Module 7

This section discusses the extraction of fatigue damage parts from the original stress-time history by STFT-based fatigue damage part extracting method. Module 7 is used to edit the original stress-time history in the time-frequency domain. The result is the shortened or edited stress-time history. In this research project, the original stress-time history, which contains 68,739,939 data points, is so long that the author cannot perform `spectrogram` command for the entire history. Thus, the original stress-time history is separated into 688 segments as shown in Figure 6.4-9. For the purpose of illustration, the segment 52 of the original stress-time history in Figure 6.4-13(*a*) is used to demonstrate how to extract the fatigue damage parts. The process is shown by a flowchart in Figure 6.4-12.

STFT truncates the original stress-time history into short data frames and then each data frame is multiplied by a Gaussian window function so that the modified signal is zero outside the data frame. The window with fixed width of 256 points is translated along the time axis by the overlapping size of 255 points. This overlapping size is chosen because it provides the high resolution in the time representation. In each translating window, the Fourier transform is applied for the calculation of PSD in the unit of Energy/Hz. For all frequency bands, PSD of each window is plotted in a time-frequency plane as shown in Figure 6.4-13(*b*). This plot is called a spectrogram.

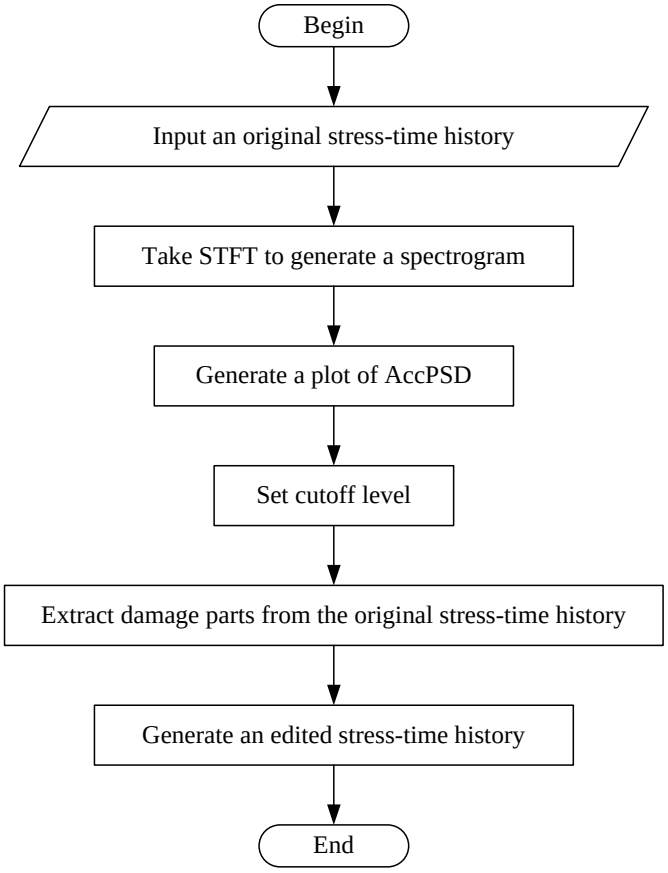

Figure 6.4-12. Flowchart for extracting fatigue damage parts by STFT in Module 7

A plot of AccPSD in Figure 6.4-13(*c*) is generated by summing the PSD of all frequency bands at each time interval (see Section 5.5.2). This plot is used to identify the locations of fatigue damage events. This concept is discussed in Section 6.2. The fatigue damage events can be determined by a cutoff level represented by a red line in Figure 6.4-13(*c*). The cutoff level is an appropriate value of AccPSD which separates the damage and non-damage events in the history. The events that have AccPSD level equal or higher than the cutoff level are classified as damage parts. On the other hand, the events that have AccPSD level lower than the cutoff level are classified as non-damage parts. In this research project, the cutoff level for STFT is 9,800 Energy/Hz. It is derived from the result presented in Section 7.2.

The damage parts extracted from the segment 52 are shown in Figure 6.4-14(*b*). Also, the non-damage parts are shown in Figure 6.4-14(*c*). The desired result of the Module 7 is the edited stress-time history shown in Figure 6.4-14(*d*). The results in Table 6.4-5 show that the edited segment 52 has reduction of 11.62% in length with respect to the original length.

In other words, the length of the edited segment 52 is 88.38% of the original length. The difference in fatigue damage per repetition is +0.288% whilst the differences in signal statistical parameters (mean stress, root-mean-square and kurtosis) are within ±10%. Here, the (+) and (-) signs mean less than and greater than, respectively.

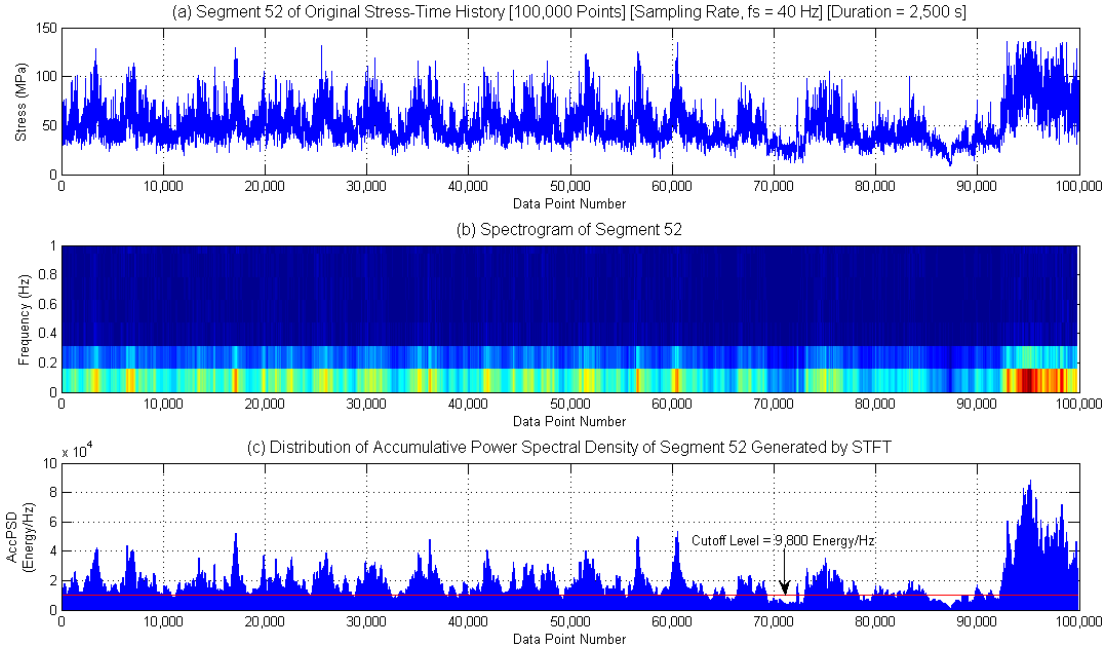

Figure 6.4-13. STFT of the segment 52

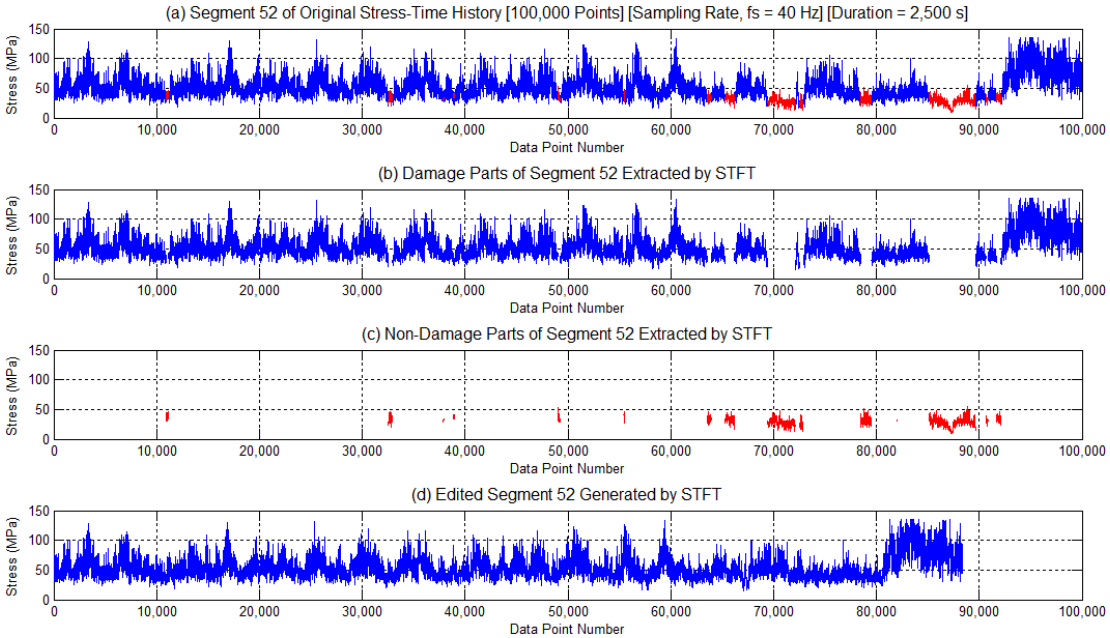

Figure 6.4-14. Results of the segment 52 generated by STFT

Table 6.4-5. Statistical parameters of the segment 52 before and after editing by STFT in Module 7 (See comparison among TCFD, STFT and WT in Table 6.5-1)

History	Length (Points)	Mean Stress (MPa)	rms (MPa)	Kurtosis	Fatigue Damage*
Segment 52	99,968	50.87	54.06	5.02	2.40337E-5
Edited by STFT	88,354	53.62	56.42	5.27	2.39645E-5
% Error**	+11.62	-5.41	-4.37	-4.98	+0.288

* Fatigue damage per repetition

** (+) and (-) signs of percent error mean less than and greater than, respectively.

6.4.8 Step 8: Edit Original Stress-Time History by Using WT in Module 8

This section discusses the extraction of damage parts from the original history by WT-based fatigue damage part extracting method. Module 8 is used to edit the original stress-time history in the time-scale domain. The result is the edited stress-time history. In this research project, the original stress-time history, which contains 68,739,939 data points, is so long that the author cannot perform `cwt` command for the entire history. Thus, the original stress-time history is separated into 688 segments as shown in Figure 6.4-9. For the purpose of illustration, the segment 52 of the original stress-time history in Figure 6.4-16(*a*) is used to demonstrate how to extract the fatigue damage parts. The process is shown by a flowchart in Figure 6.4-15.

In the process, WT is the sum over all time of the history multiplied by scaled, shifted versions of the wavelet. This process provides wavelet coefficients as a function of scale and position. In the first step of WT, a wavelet is taken and compared to a section at the start of the history. In the second step, a wavelet coefficient is calculated by comparing the energy of the history with the energy of the wavelet. The wavelet coefficient represents how closely correlated the wavelet with this section of the history. The wavelet coefficient may be interpreted as a correlation coefficient. The higher value of wavelet coefficient is, the more the similarity is. It is noted that the result depends on the shape of the selected wavelet [109]. In the third step, the wavelet is shifted to the right and then the first and the second steps are repeated, respectively. In the fourth step, the wavelet is scaled or stretched and then the process is repeated from the first step to the third step. In the last

step, the process is repeated from the first step to the fourth step for all scales. The result of this process is the wavelet coefficients produced at different scales and different sections of the history. To make sense of all coefficients, a plot on which the x-axis represents position along the history (time or data point number), the y-axis represents scale, and the colour at each x-y point represents the magnitude of the wavelet coefficient as illustrated in Figure 6.4-16(*b*). This plot is called scalogram.

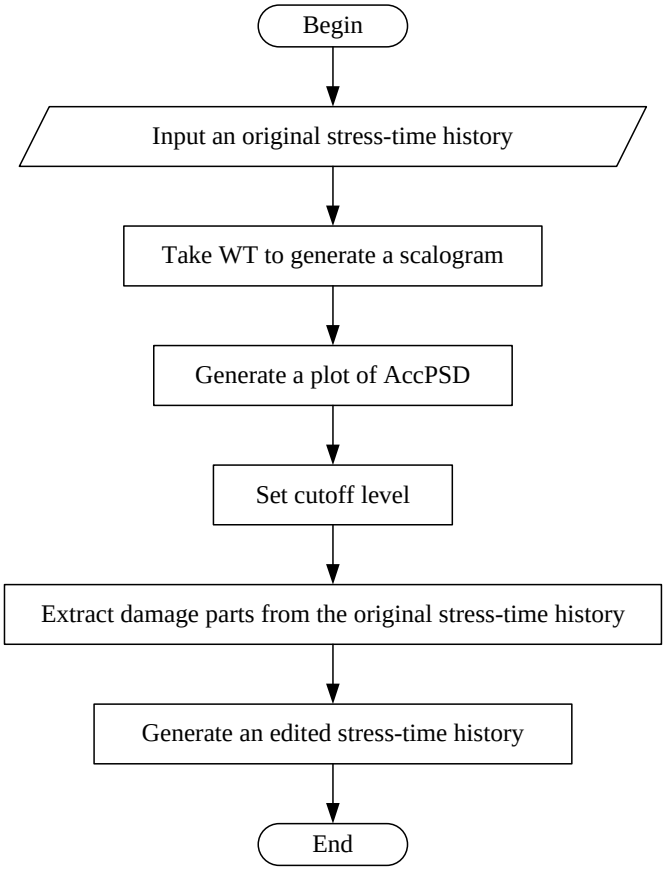

Figure 6.4-15. Flowchart for extracting fatigue damage parts by WT in Module 8

In this research project, WT is taken at the wavelet decomposition level 8 (maximum). For the purpose of illustration in this section, the Morl wavelet is applied to the segment 52 of the original stress-time history and the scalogram is generated as shown in Figure 6.4-16(*b*). A plot of AccPSD in Figure 6.4-16(*c*) is generated by summing the PSD of wavelet coefficients for all scale bands at each time interval (see Section 5.6.2). This plot is used to identify the locations of fatigue damage events. This concept is discussed in Section 6.2. The damage events can be determined by a cutoff level represented by a red line in Figure 6.4-16(*c*). The cutoff level is an appropriate value of AccPSD which separates the damage

and non-damage events in the history. The events that have AccPSD level equal or higher than the cutoff level are classified as damage parts. On the other hand, the events that have AccPSD level lower than the cutoff level are classified as non-damage parts. In this research project, the cutoff level for Morl wavelet is 2,400 Energy/Hz. It is derived from the result presented in Section 7.3.

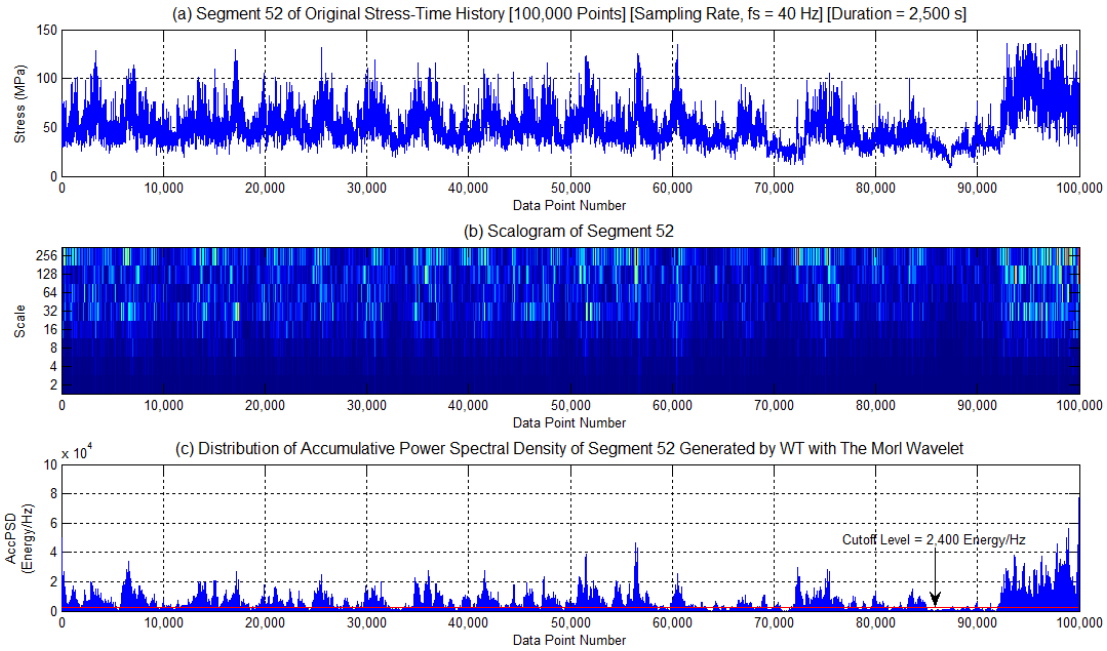

Figure 6.4-16. WT of the segment 52 by the Morl wavelet

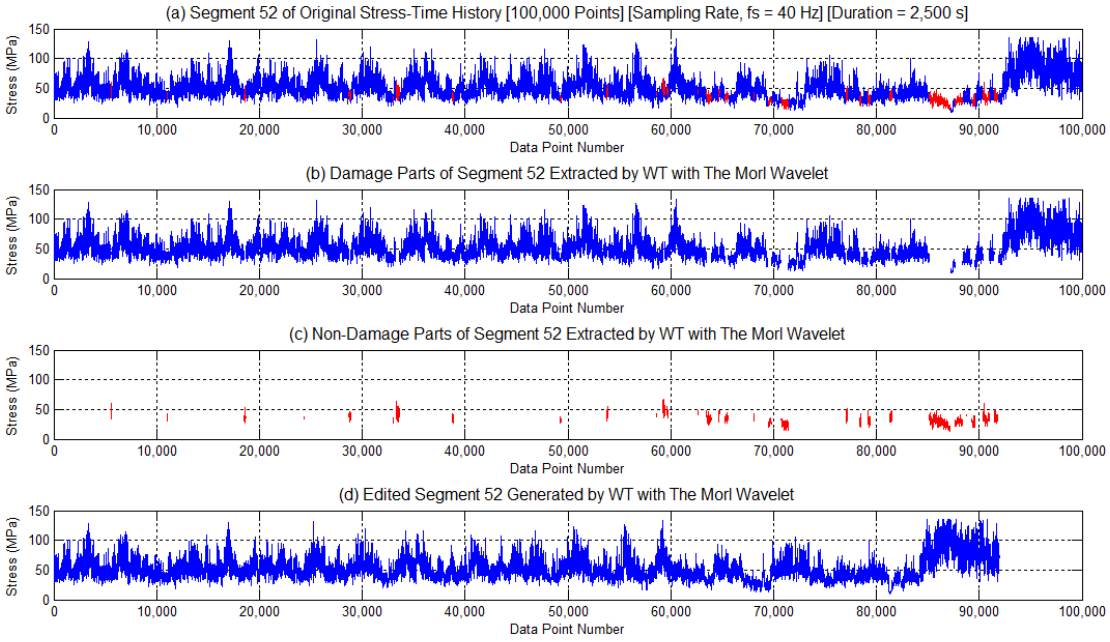

Figure 6.4-17. Results of the segment 52 generated by WT with the Morl wavelet

The damage parts extracted from the segment 52 of the original history are shown in Figure 6.4-17(*b*). Also, the non-damage parts are shown in Figure 6.4-17(*c*). The desired result of the Module 8 is the edited history shown in Figure 6.4-17(*d*). The results in Table 6.4-6 show that the edited segment 52 has reduction of 8.02% in length with respect to the original length. In other words, the length of the edited segment 52 is 91.98% of the original length. The difference in fatigue damage per repetition is +0.001% whilst the differences in signal statistical parameters (mean stress, root-mean-square and kurtosis) are within ±10%. Here, the (+) and (-) signs mean less than and greater than, respectively.

Table 6.4-6. Statistical parameters of the segment 52 before and after editing by WT with the Morl wavelet in Module 8 (See comparison among TCFD, STFT and WT in Table 6.5-1)

History	Length (Points)	Mean Stress (MPa)	rms (MPa)	Kurtosis	Fatigue Damage*
Segment 52	99,968	50.87	54.06	5.02	2.40337E-5
Edited by WT (Morl wavelet)	91,949	52.47	55.50	5.05	2.40335E-5
% Error**	+8.02	-3.15	-2.66	-0.60	+0.001

* Fatigue damage per repetition

** (+) and (-) signs of percent error mean less than and greater than, respectively.

6.5 Summary

This chapter describes the concept of applying AccPSD to identify fatigue damage events contained in the stress-time history. The observation in Section 6.2 implies that the plot of AccPSD enables us to identify the fatigue damage events contained in the original stress-time history. Based on the observation, it can be summarised that there are three issues: (1) the amplitudes of AccPSD spikes for both STFT and WT do not provide us how much fatigue damage occurs; (2) the locations of AccPSD spikes, which are observed by naked eyes, are close to the locations of fatigue damage occurred; and (3) the fatigue damage events in the stress-time history could be identified by an appropriate cutoff level. Section 6.3 described algorithm used to extract fatigue damage parts from the stress-time history.

Section 6.4 deals with step-by-step in evaluating fatigue damage contained in the stress-time history. HAWTfatigue is a software tool used in the simulation. Simulation procedure is described in this section. In Figure 6.4-1, the simulation starts from Modules 1 to 8 in sequence. Modules 1 and 2 are used to load the wind speed data and relationship between stress and wind speed to the code. Module 3 uses both data to generate the original stress-time history. This history is transferred to Module 4 to count the rainflow cycles. Based on $S\text{-}N$ data from Module 5, each rainflow cycle counted is used by Module 6 to evaluate fatigue damage and service lifetime.

By Modules 7 and 8, the original stress-time history is taken by STFT and WT to generate the plots of AccPSD shown in Figures 6.4-13 and 6.4-16. Each plot provides the time locations at where the fatigue damage occurs. Then, the damaging events are determined by a cutoff level. The events that have AccPSD level higher than or equal to the cutoff level are classified as damage parts and vice versa for non-damage parts. The damage parts are extracted from the segment 52 of the original stress-time history and they are concatenated to form the edited segment 52.

Table 6.5-1. Statistical parameters of the segment 52 before and after editing by TCFD, STFT and WT

History	Length (Points)	Mean Stress (MPa)	rms (MPa)	Kurtosis	Fatigue Damage*
Segment 52	99,968	50.87	54.06	5.02	2.40337E-5
Edited by TCFD	70,225	56.06	59.08	4.54	2.38338E-5
	(+29.75%)**	(-10.20%)	(-9.29%)	(+9.56%)	(+0.832%)
Edited by STFT	88,354	53.62	56.42	5.27	2.39645E-5
	(+11.62%)**	(-5.41%)	(-4.37%)	(-4.98%)	(+0.288%)
Edited by WT	91,949	52.47	55.50	5.05	2.40335E-5
(Morl Wavelet)	(+8.02%)**	(-3.15%)	(-2.66%)	(-0.60%)	(+0.001%)

Note: Each number in the bracket is percent error.

(+) and (-) signs of percent error mean less than and greater than, respectively.

* Fatigue damage per repetition

** Percent reduction in length of the edited stress-time histories.

The results in Table 6.5-1 show that the edited segment 52 generated by TCFD, STFT, and WT have reduction of 29.75%, 11.62%, and 8.02% in length, respectively. In other words, the lengths of the edited segment 52 are 70.25%, 88.38%, and 91.98% of the original length for TCFD, STFT, and WT, respectively. The differences in fatigue damage per repetition for TCFD, STFT, and WT are +0.832%, +0.288%, and +0.001%, respectively, whilst the differences in signal statistical parameters (mean stress, root-mean-square and kurtosis) for each method are within ±10%. Here, the (+) and (-) signs mean less than and greater than, respectively. These results suggest that AccPSDs gained from STFT and WT enable us to detect the fatigue damage events contained in the given stress-time history.

The outcome of this chapter is a conference paper [121]. This paper is relevant to the application of the Morl wavelet in editing fatigue data of horizontal axis wind turbine blades.

Chapter 7

Results and Discussion

7.1 Introduction

This chapter presents the results obtained by following the procedures of extracting fatigue damage parts discussed in Sections 6.4.7 and 6.4.8. Based on STFT procedure in Figure 6.4-12 and WT procedure in Figure 6.4-15, the fatigue damage parts are extracted from the original stress-time history in Figure 7.1-1 (see Table 6.4-4 for fatigue damage per repetition and service lifetime of this history). Then, fatigue damage parts are concatenated to form the edited stress-time histories which are the desired results. They are shown in Figures 7.4-7(*c*) to 7.4-7(*h*).

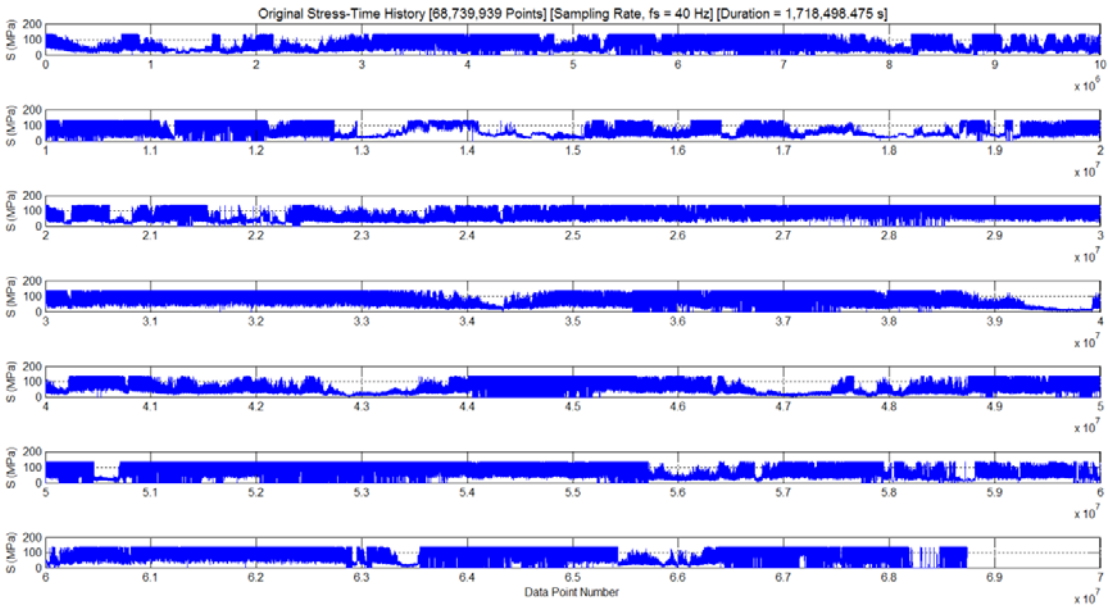

Figure 7.1-1. Original stress-time history to be edited by TCFD, STFT and WT

In this chapter, the results are presented separately into three sections as follows:

Section 7.2: Selecting a window size for STFT

Section 7.3: Selecting a wavelet decomposition level for WT

Section 7.4: Simulation results

7.2 Selecting a Window Size for STFT

The window size obtained from this section has been used by Module 7 in taking STFT. In the module, STFT is taken to the original stress-time history in Figure 7.1-1 by using Matlab's signal processing toolbox. As discussed in Section 5.5.1, `spectrogram` command is used to generate the spectrogram. One of the input arguments of this command is window size (nfft) which can be set as 2, 4, 8, 16, 32, 128 and 256 points. The question is what window size should be set in taking STFT. A comparative study is the only way to find an appropriate window size. To answer this question, it is necessary to study the window size effect on variation of fatigue damage per repetition before editing the original stress-time history by STFT.

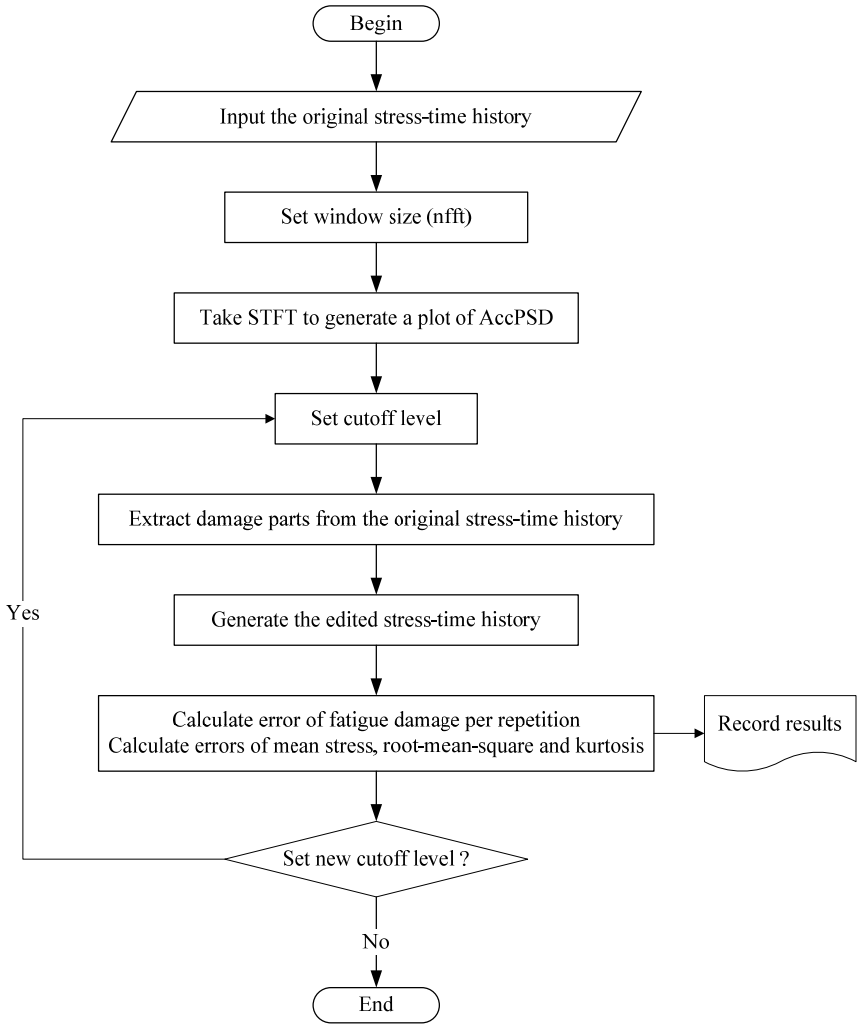

Figure 7.2-1. Procedure for studying the window size effect on variation of fatigue damage per repetition

To study the window size effect on variation of fatigue damage per repetition, the author takes STFT to the original stress-time history in Figure 7.1-1 with eight different window sizes which are 2, 4, 8, 16, 32, 64, 128, and 256 points, respectively. By working with Module 7 of HAWTfatigue and following the procedure in Figure 7.2-1, firstly, the author takes STFT with window size 2 and then a plot of AccPSD distribution for this window size is generated. The first cutoff level is set to 0 Energy/Hz (see Table D1). The fatigue damage parts are extracted and they are concatenated to form the edited stress-time history based on STFT window size 2. The fatigue damage per repetition of the edited stress-time history and signal statistical parameters are calculated and recorded in Table D1, Appendix D. Next, the author sets a new cutoff level to 5 Energy/Hz and then follows the procedure in Figure 7.2-1 again. For other cutoff levels (based on Window size 2), the results are listed in Table D1, Appendix D. In the same manner, the author changes the window size as 4, 8, 16, 32, 64, 128, and 256, respectively. The results obtained from each window size are listed in Tables D1 to D8, Appendix D. Since maximum values of AccPSD level generated by STFT with each window size are different, they cannot be compared directly. It is necessary to normalise AccPSD values listed in Tables D1 to D8, Appendix D, by theirs corresponding maximum AccPSD level existing in each table. Consequently, the relationships between normalised cutoff level and fatigue damage per repetition for each window size can be established as shown in Figure 7.2-2.

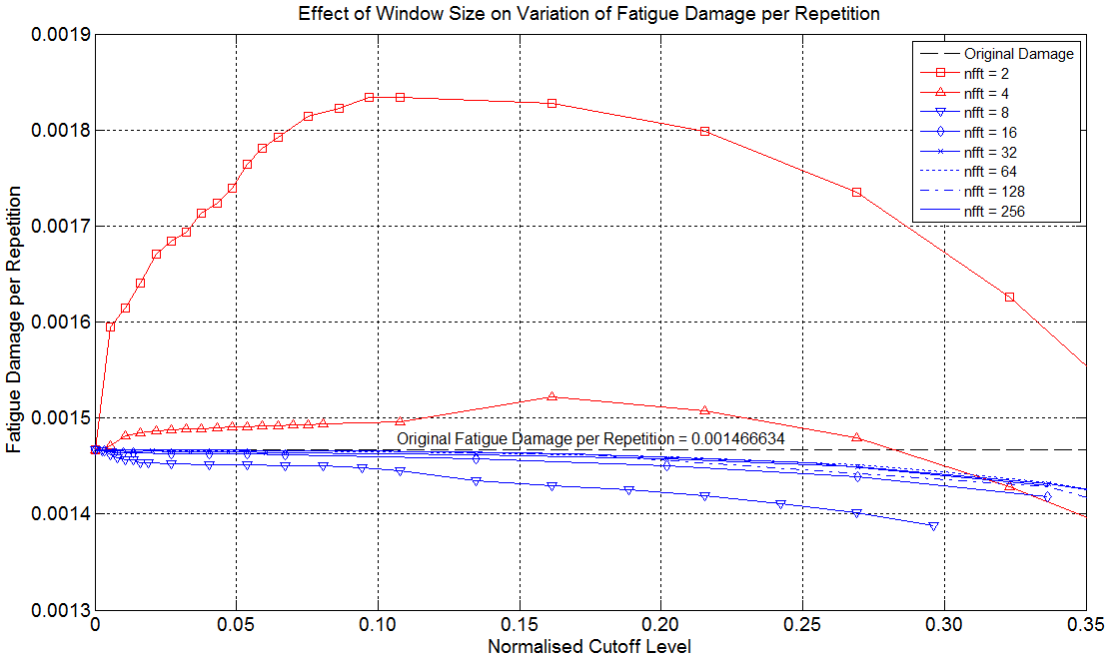

Figure 7.2-2. Effect of window size (nfft) on variation of fatigue damage per repetition

Figure 7.2-2 shows the relationships between normalised cutoff level and fatigue damage per repetition for window sizes of 2, 4, 8, 16, 32, 64, 128 and 256 points. The dash line represents a level of the original fatigue damage per repetition of the original stress-time history (see Table 6.4-4). At this stage, the author wants to know which window size should be used in taking STFT. By means of three criteria, one curve must be selected from this group. The first criterion is that the difference in fatigue damage per repetition must not be greater than ±10%. The second criterion is that the differences in mean stress, root-mean-square and kurtosis must not be greater than ±10%. The third criterion is that the length of the edited stress-time history must be the shortest one compared to each other. The first two criteria are suggested by the researchers in references [93], [99], [118] and [122].

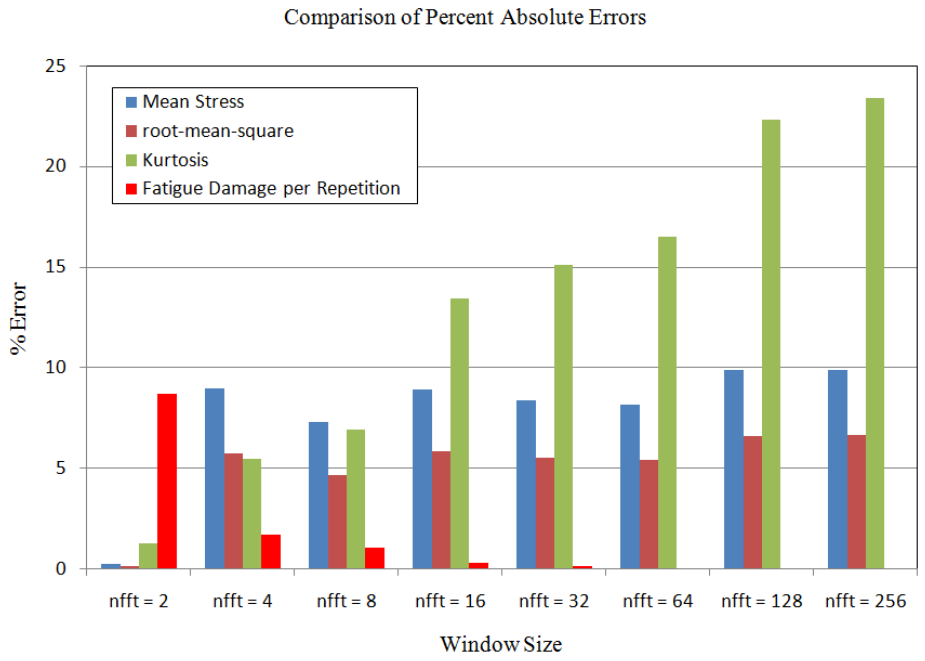

Figure 7.2-3. Percent absolute errors of mean stress, root-mean-square, kurtosis and fatigue damage per repetition

The curves in Figure 7.2-2 could be separated into two groups. The first group shows that the fatigue damage per repetition increases beyond the original level and then decreases near the end of the range being considered. The curves in this group are for window sizes 2 and 4. They should not be taken into account because their errors of fatigue damage per repetition are very high compared to others (see Figure 7.2-3). The second group shows that the fatigue damage per repetition decreases when the normalised cutoff level increases. Although all curves in this group show the desired behaviour, the curves for

window sizes of 8, 16 and 32 can be removed from the group because they show the rapid change in fatigue damage near the beginning of the range being considered. Thus, there are three curves which are still candidates as shown in Figure 7.2-4. They are for window sizes of 64, 128 and 256.

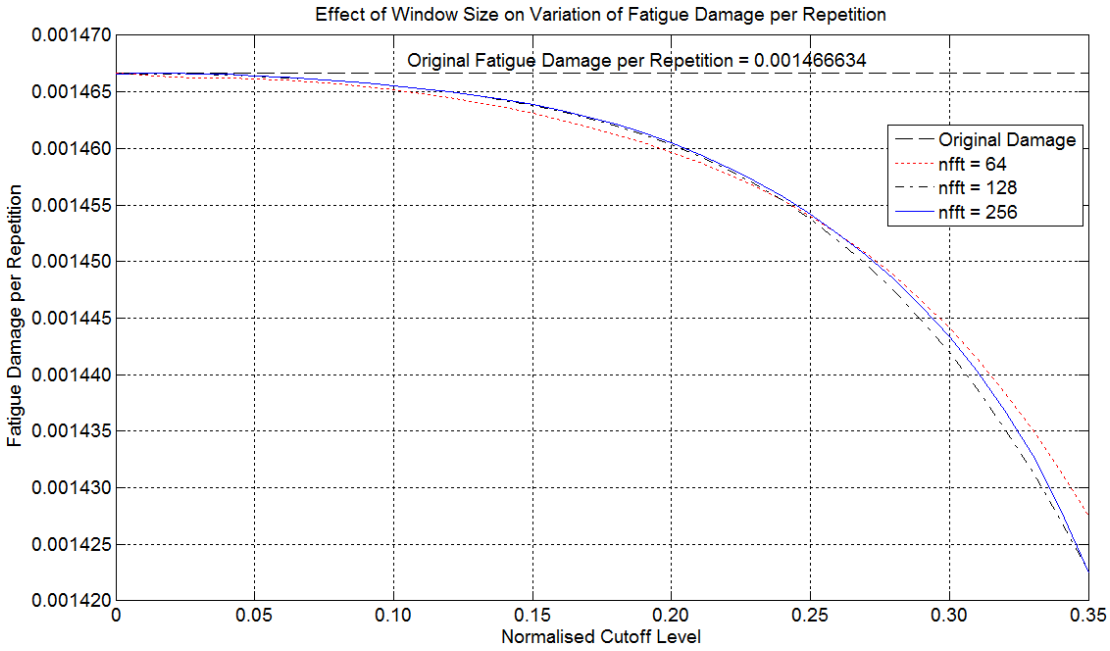

Figure 7.2-4. Comparison among three reasonable curves of fatigue damage per repetition

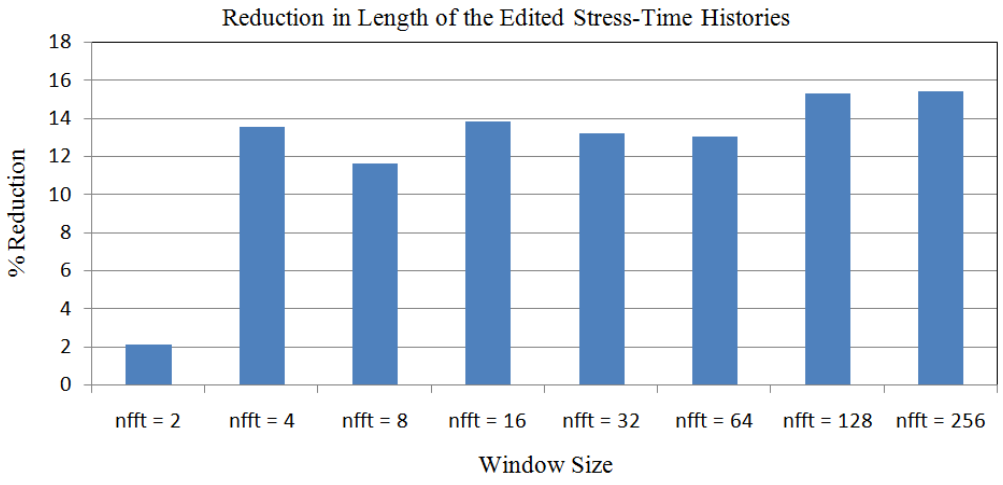

Figure 7.2-5. Comparison of reduction in length of the edited stress-time histories generated by STFT

Considering three curves in Figure 7.2-4, they show that the fatigue damage per repetition slightly decreases at the beginning and rapidly drops when the value of normalised cutoff level beyond 0.1. By naked eye, it is difficult to select one of them as a representative in taking STFT. The summarised data listed in Table 7.2-1, bar graphs in Figure 7.2-3 and bar graphs in Figure 7.2-5 are needed for selecting the best curve. It is found that all window sizes satisfy all criteria except the error of kurtosis. Also, the curves for window sizes of 2, 4, 8, 16 and 32 are not candidates now. The window sizes of 128 and 256 seem to be not different in results. But the shortest length of the edited stress history is the desired result, so the window size of 256 is selected as the representative in taking STFT. Also, the relationship between AccPSD level and fatigue damage per repetition for window size of 256 is shown in Figure 7.2-6.

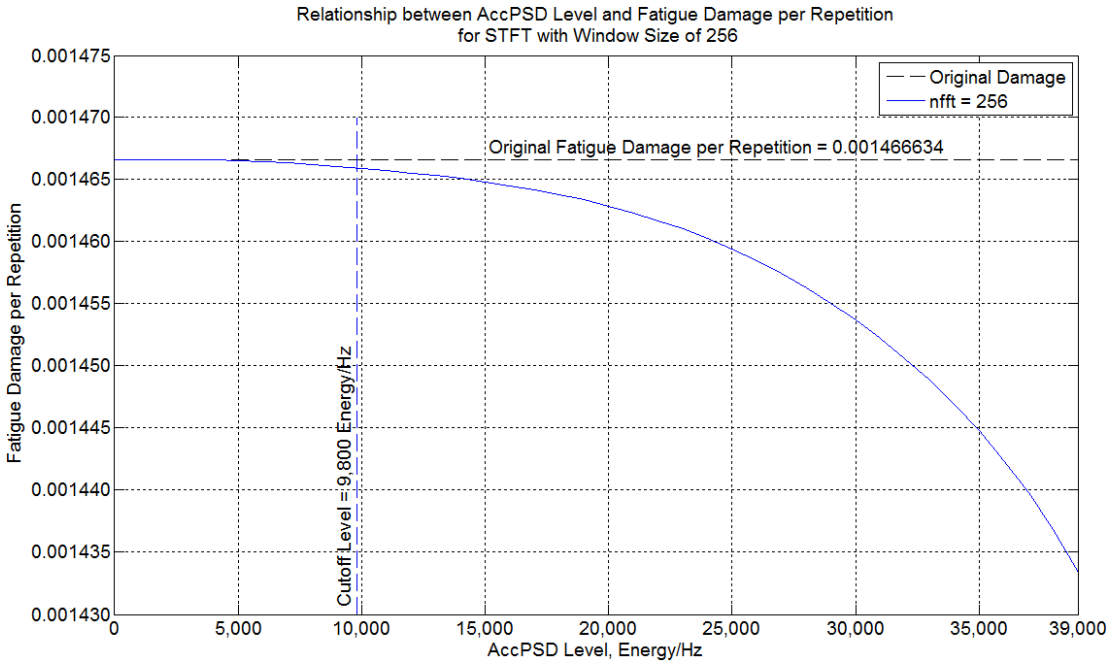

Figure 7.2-6. Curve for selecting the cutoff level of STFT

To summarise, STFT with window size of 256 and cutoff level of 9,800 Energy/Hz provides the best result. A plot of AccPSD distribution generated by STFT with window size 256 is shown in Figures 7.2-7 and 7.4-6(*a*). Also, the edited stress-time history based on cutoff level at 9,800 Energy/Hz is shown in Figures 7.2-8 and 7.4-7(*c*). The edited stress-time history has reduction of 15.38% in length with respect to the original length (see Table 7.2-1). In other words, the length of the edited stress-time history is 84.62% of the original length. The difference in fatigue damage per repetition is +0.045% whilst the

differences in mean stress and root-mean-square of the edited stress-time history are within ±10%, except for kurtosis. Here, the (+) and (-) sign mean less than and greater than, respectively.

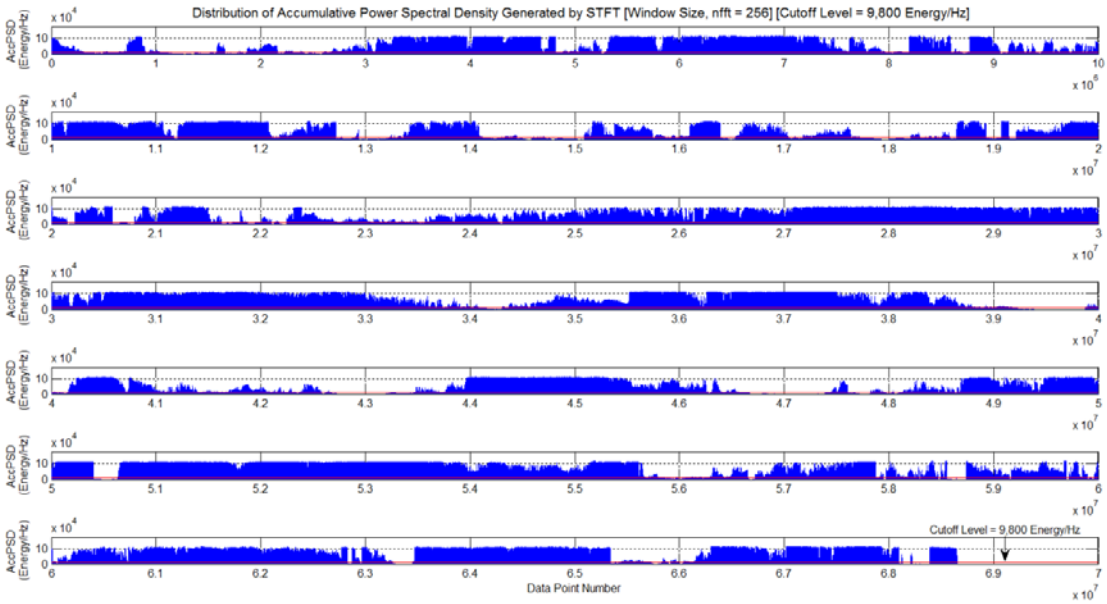

Figure 7.2-7. AccPSD distribution generated by STFT with window size 256

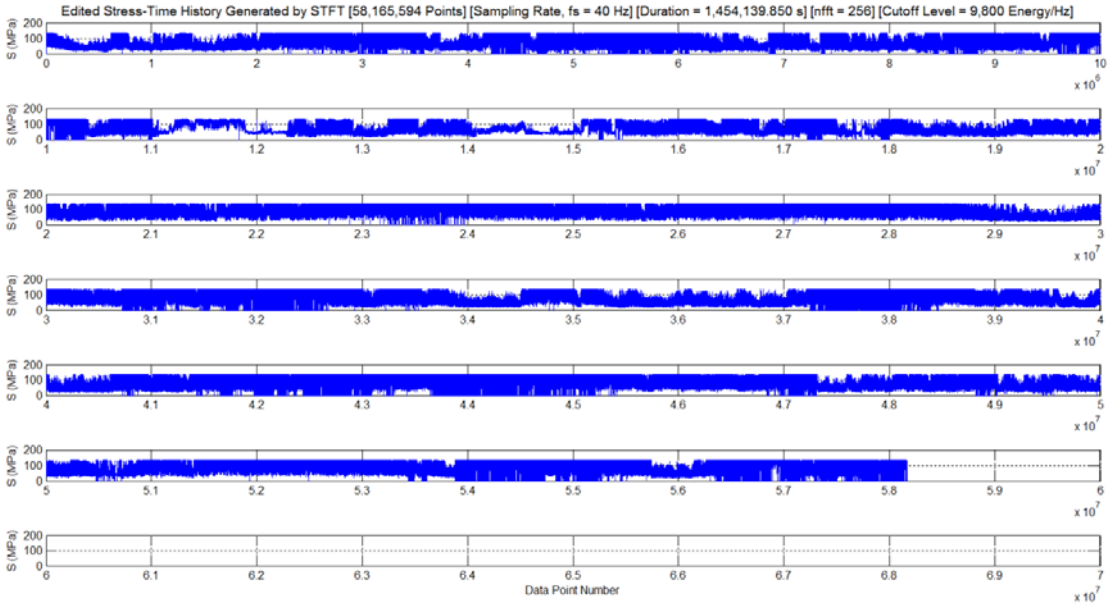

Figure 7.2-8. The edited stress-time history generated by STFT with window size 256 and cutoff level at 9,800 Energy/Hz

Table 7.2-1. Data summarised from Tables D1 to D8

Table*	nfft	Maximum AccPSD (Energy/Hz)	Cutoff Level (Energy/Hz)	Normalised Cutoff Level	Length of the Edited History** (Points)	Fatigue Damage per Repetition***	% Reduction in Length of the Edited History	% Error			
								Fatigue Damage per Repetition	Mean Stress	rms	Kurtosis
D1	2	928.7482	5	5.3836E-03	67,292,474	1.594460E-03	2.11	-8.716	+0.28	+0.17	-1.28
D2	4	1,857.5	110	5.9219E-02	59,472,482	1.491495E-03	13.48	-1.695	-9.01	-5.74	-5.49
D3	8	3,715	200	5.3836E-02	60,794,407	1.450954E-03	11.56	+1.069	-7.34	-4.69	-6.96
D4	16	7,428.7	500	6.7307E-02	59,266,807	1.461732E-03	13.78	+0.334	-8.97	-5.86	-13.45
D5	32	14,852	1,000	6.7331E-02	59,641,186	1.464056E-03	13.24	+0.176	-8.42	-5.54	-15.14
D6	64	29,694	2,000	6.7354E-02	59,774,575	1.465724E-03	13.04	+0.062	-8.19	-5.42	-16.56
D7	128	59,364	4,800	8.0857E-02	58,217,047	1.466020E-03	15.31	+0.042	-9.91	-6.63	-22.35
D8	256	118,660	9,800	8.2589E-02	58,165,594	1.465978E-03	15.38	+0.045	-9.92	-6.66	-23.45

Note: (+) and (-) signs of percent error mean less than and greater than, respectively.

* See Appendix D, Tables D1 to D8

** Length of the original stress-time history = 68,739,939 points

*** Original fatigue damage = 1.466634E-03 (see Table 6.4-4)

7.3 Selecting a Wavelet Decomposition Level for WT

The wavelet decomposition level obtained from a study in this section has been used by Module 8 in taking WT. In the module, WT is taken to the original stress-time history in Figure 7.1-1 by using Matlab's wavelet toolbox. The `cwt` command, discussed in Section 5.6.1, is used to generate the scalogram. One of the input arguments of this command is scale defined by a power of two. Here, the exponent of the power of two is the wavelet decomposition level which can be set as 1, 2, 3, 4, 5, 6, 7, 8 and 9. The question is what wavelet decomposition level should be used in taking WT. A comparative study is the only way to find an optimal level of wavelet decomposition. To answer this question, it is necessary to study the wavelet decomposition level effect on variation of fatigue damage per repetition before editing the original stress-time history by WT.

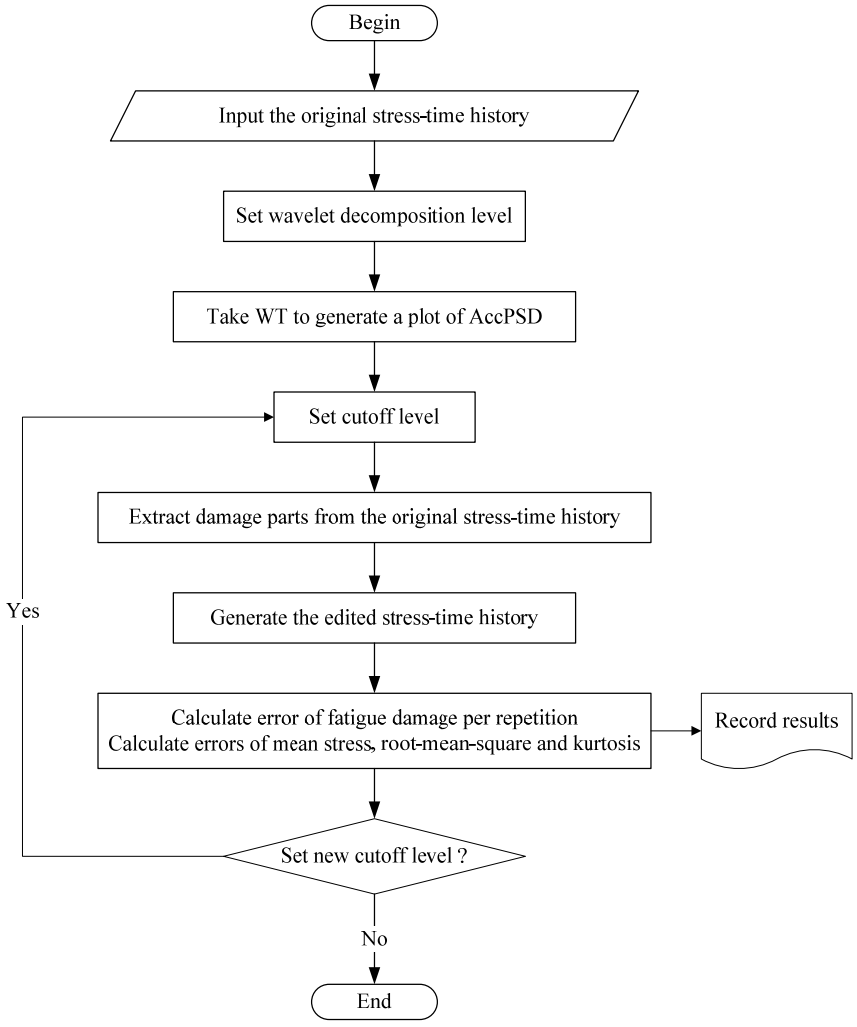

Figure 7.3-1. Procedure for studying the wavelet decomposition level effect on variation of fatigue damage per repetition

To study the wavelet decomposition level effect on variation of fatigue damage per repetition, the author takes WT with the Morl wavelet to the original stress-time history in Figure 7.1-1 with nine different wavelet decomposition levels which are 1, 2, 3, 4, 5, 6, 7, 8, and 9, respectively. Here, Morl wavelet is chosen because it was successfully used in previous research [118]. By working with Module 8 of HAWTfatigue and following the procedure in Figure 7.3-1, firstly, the author takes WT at wavelet decomposition level 1 and then a plot of AccPSD distribution for this wavelet decomposition level is generated. The first cutoff level is set to 0 Energy/Hz (see Table D9). The fatigue damage parts are extracted and they are concatenated to form the edited stress-time history based on wavelet decomposition level 1. The fatigue damage per repetition of the edited stress-time history and signal statistical parameters are calculated and recorded in Table D9, Appendix D. Next, the author sets a new cutoff level to 20,000 Energy/Hz and follows the procedure in Figure 7.3-1 again. For other cutoff levels (based on wavelet decomposition level 1), the results are listed in Table D9, Appendix D. In the same manner, the author changes the wavelet decomposition level as 2, 3, 4, 5, 6, 7, 8, and 9, respectively. The results obtained from each wavelet decomposition level are listed in Tables D9 to D17, Appendix D. Since maximum values of AccPSD level generated by WT at each wavelet decomposition level are different, they cannot be compared directly. It is necessary to normalised AccPSD values listed in Tables D9 to D17, Appendix D, by theirs corresponding maximum AccPSD level existing in each table. Consequently, the relationships between normalised cutoff level and fatigue damage per repetition for each wavelet decomposition level can be established as shown in Figure 7.3-2.

Figure 7.3-2 shows the relationships between normalised cutoff level and fatigue damage per repetition at wavelet decomposition levels 1, 2, 3, 4, 5, 6, 7, 8 and 9. The dash line represents a level of the original fatigue damage per repetition (see Table 6.4-4). At this stage, the author wants to know which wavelet decomposition level should be used in taking WT. By means of three criteria [93,99,118,122] used in Section 7.2, the only one curve must be selected from this group.

All curves in Figure 7.3-2 show that the fatigue damage per repetition decreases when the normalised cutoff level increases. Considering data listed in Table 7.3-1 and bar graphs in Figure 7.3-3, the curves for wavelet decomposition levels 2, 3, 4, 5 and 6 can be removed from the group because their errors of fatigue damage per repetition are very high compared to those of wavelet decomposition levels 7, 8 and 9. Now, there are four curves

which are still candidates as shown in Figure 7.3-4. They are for wavelet decomposition levels 1, 7, 8 and 9.

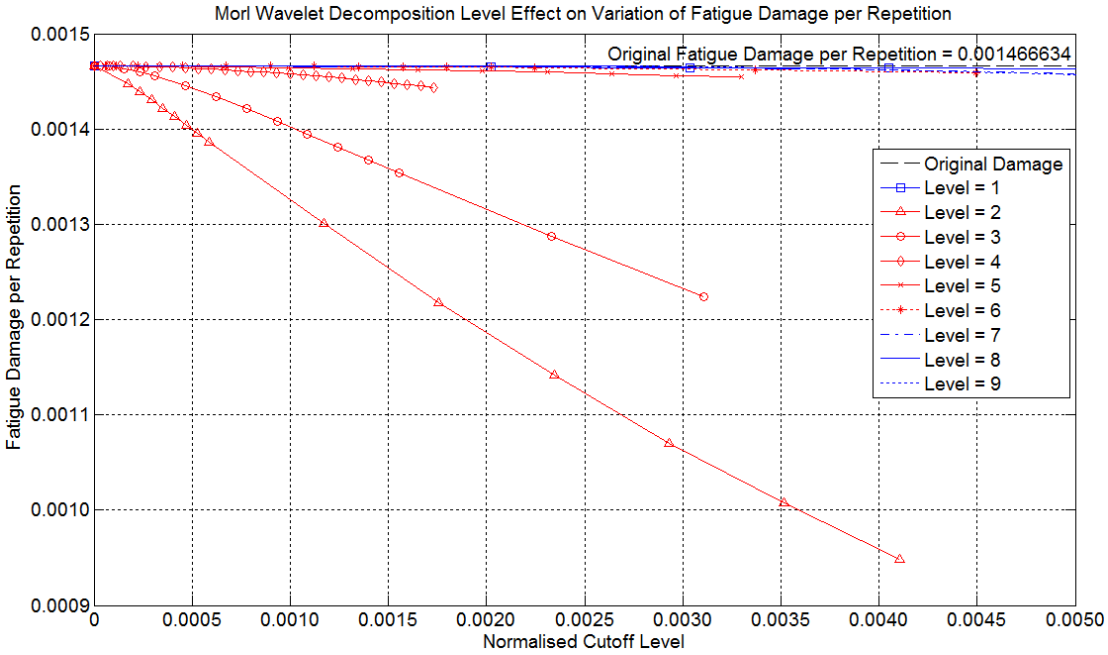

Figure 7.3-2. Effect of the Morl wavelet decomposition level on variation of fatigue damage per repetition

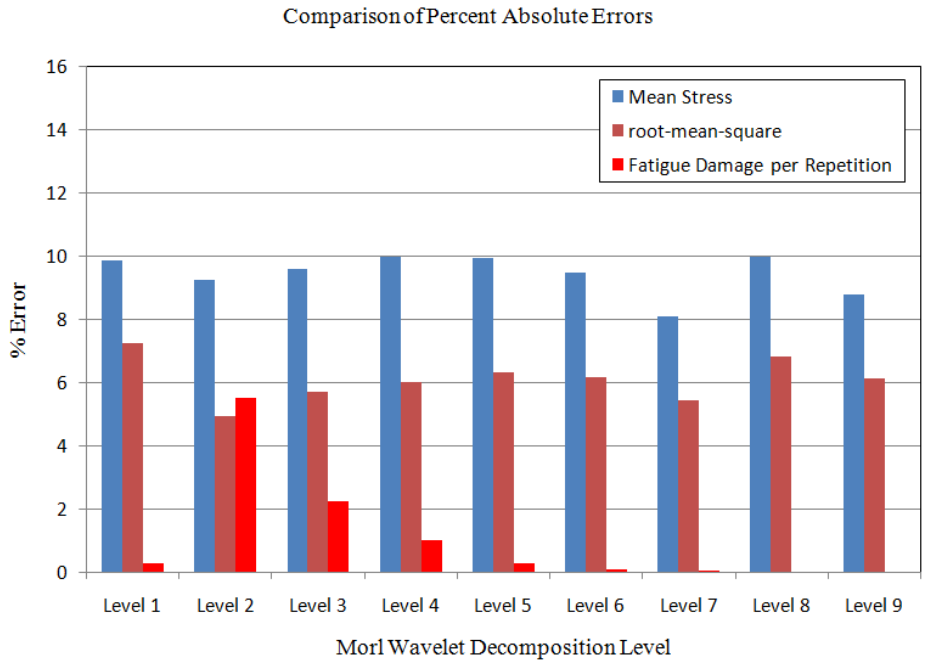

Figure 7.3-3. Percent absolute errors of mean stress, root-mean-square and fatigue damage per repetition

Considering four curves in Figure 7.3-4, they show that fatigue damage per repetition slightly decreases at the beginning and rapidly drop when the value of normalised cutoff level is beyond 0.0015, except for level 1. The curve for level 1 shows a rapid change in fatigue damage per repetition compared to others so it can also be removed. Now, there are three candidates left to be considered. They are the curves for wavelet decomposition levels 7, 8 and 9. By naked eye, it is difficult to select one of them as a representative in taking WT. The summarised data listed in Table 7.3-1, bar graphs in Figure 7.3-3 and bar graphs in Figure 7.3-5 are needed for selecting the best curve. It is found that all wavelet decomposition levels satisfy all criteria except the error of kurtosis. Now, the curves for wavelet decomposition levels 1, 2, 3, 4, 5 and 6 are not candidates. The curve for wavelet decomposition level 8 is the best curve because its error of fatigue damage per repetition is the lowest one. Thus, the curve for wavelet decomposition level 8, shown in Figure 7.3-6, is selected as the representative in taking WT. Also, the relationship between AccPSD level and fatigue damage per repetition for Morl wavelet with wavelet decomposition level 8 is shown in Figure 7.3-6.

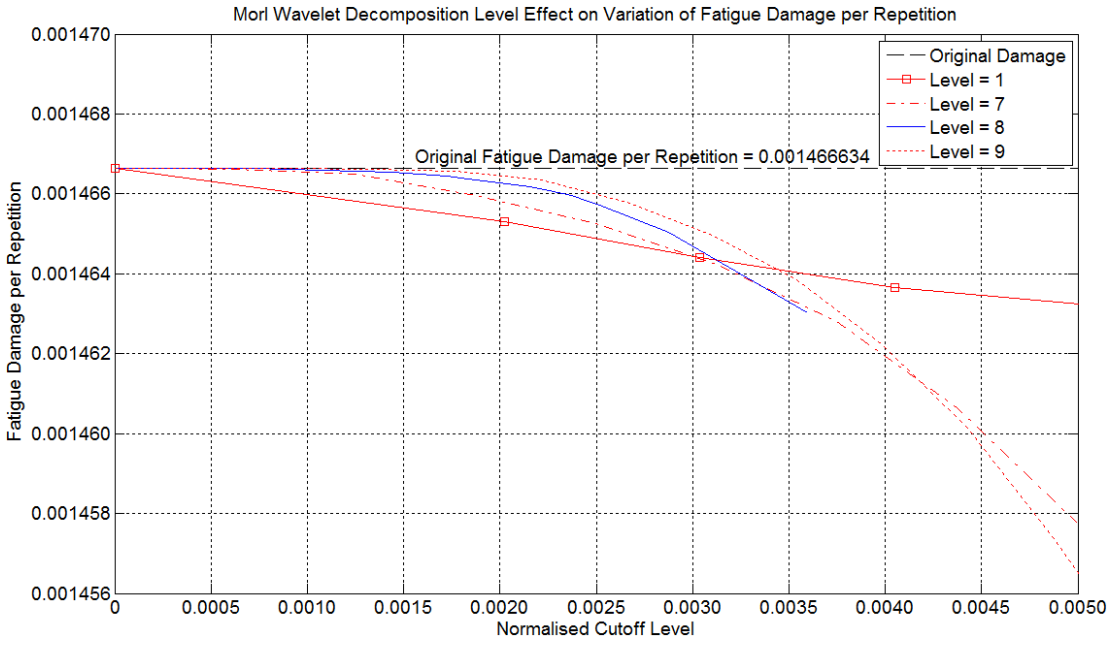

Figure 7.3-4. Comparison among four reasonable curves of damage per repetition

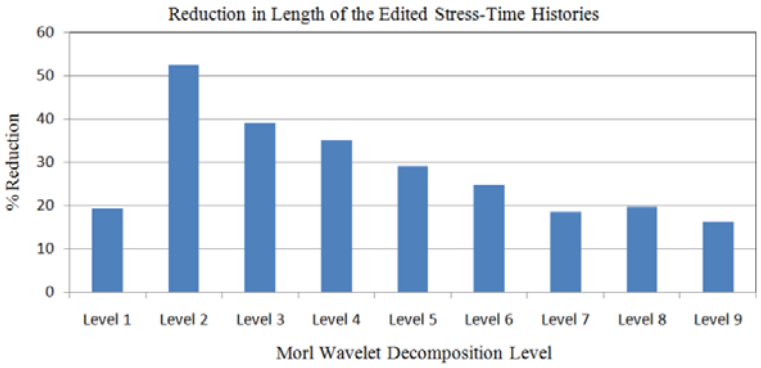

Figure 7.3-5. Comparison of reduction in length of the edited stress-time histories generated by WT with the Morl wavelet

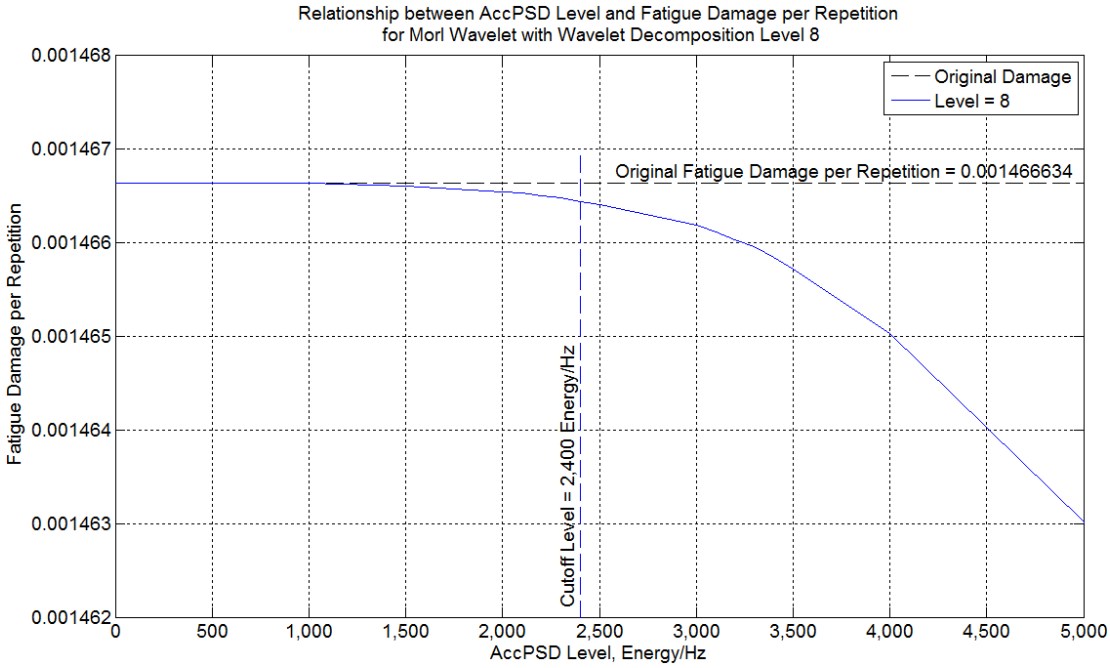

Figure 7.3-6. Curve for selecting the cutoff level of the Morl wavelet

To summarise, Morl wavelet with wavelet decomposition level 8 and cutoff level of 2,400 Energy/Hz provides the best result. The edited stress-time history in Figure 7.3-8 has reduction of 19.66% in length with respect to the original length (see Table 7.3-1). In other words, the length of the edited stress-time history is 80.34% of the original length. The difference in fatigue damage per repetition is +0.013% whilst the differences in mean stress and root-mean-square of the edited stress-time history are within ±10%, except for kurtosis. Here, the (+) and (-) sign mean less than and greater than, respectively. The AccPSD distribution generated by WT with the Morl wavelet is shown in Figures 7.3-7 and 7.4-6(*b*). Now, the author has already known that the wavelet decomposition level 8

should be used in taking WT. Thus, Meyr, Dmey, Mexh and DB30 wavelets should also be taken to the original stress-time history by setting the wavelet decomposition level at 8. The edited stress-time histories generated by WT with the Meyr, Dmey, Mexh, and DB30 are shown in Figures 7.4-7(*e*) to 7.4-7(*h*), respectively. Also, their plots of AccPSD distribution are shown in Figures 7.4-6(*c*) to 7.4-6(*f*), respectively.

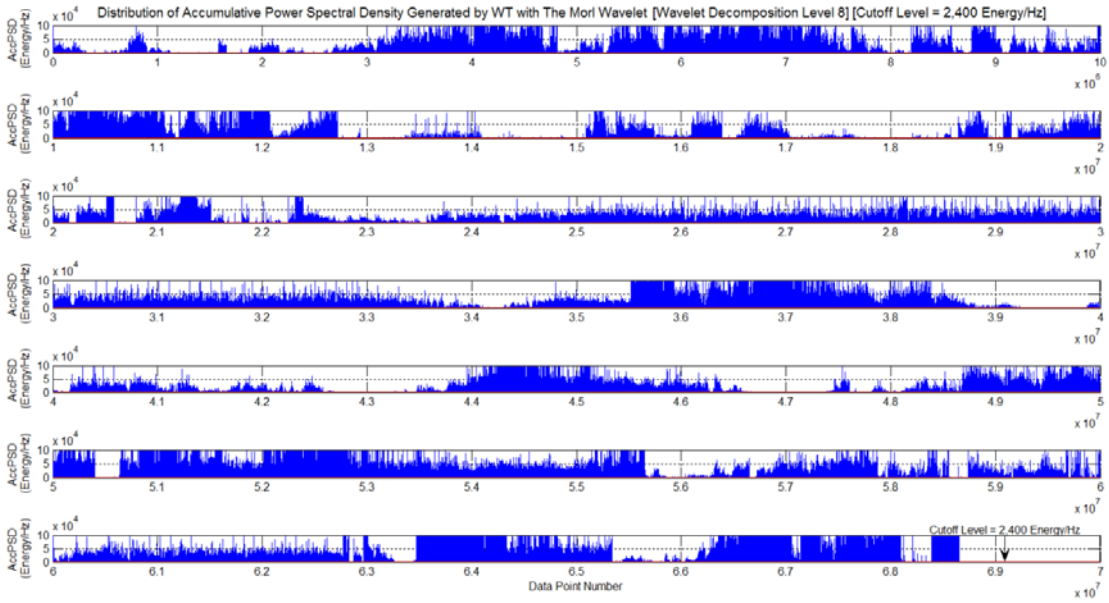

Figure 7.3-7. AccPSD distribution generated by WT with the Morl wavelet at wavelet decomposition level 8

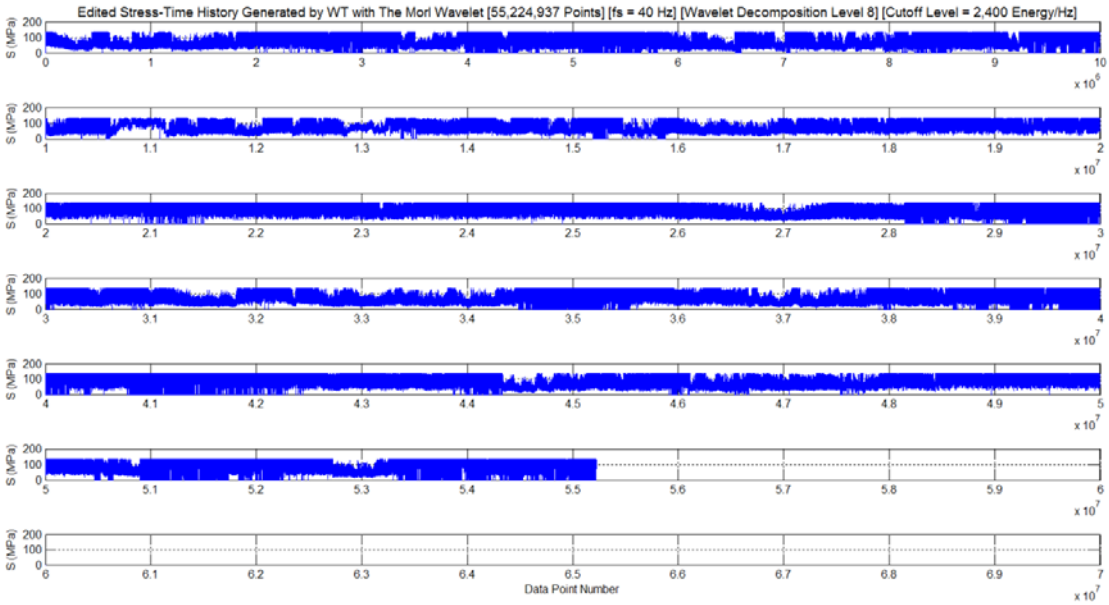

Figure 7.3-8. The edited stress-time history generated by WT with the Morl wavelet at wavelet decomposition level 8 and cutoff level at 2,400 Energy/Hz

Table 7.3-1. Data summarised from Tables D9 to D17

Table*	Level	Maximum AccPSD (Energy/Hz)	Cutoff Level (Energy/Hz)	Normalised Cutoff Level	Length of the Edited History** (Points)	Fatigue Damage per Repetition***	% Reduction in Length of the Edited History	% Error			
								Fatigue Damage per Repetition	Mean Stress	rms	Kurtosis
D9	1	9,881,800	60,000	6.0718E-03	55,539,940	1.462638E-03	19.20	+0.272	-9.86	-7.23	-32.07
D10	2	17,059	10	5.8620E-04	32,720,214	1.385630E-03	52.40	+5.523	-9.22	-4.95	-58.09
D11	3	64,322	40	6.2187E-04	41,846,758	1.433829E-03	39.12	+2.237	-9.60	-5.70	-44.92
D12	4	150,300	200	1.3307E-03	44,631,750	1.452048E-03	35.07	+0.995	-9.97	-6.01	-45.84
D13	5	303,160	500	1.6493E-03	48,783,589	1.462434E-03	29.03	+0.286	-9.94	-6.30	-37.98
D14	6	444,850	800	1.7984E-03	51,793,424	1.465167E-03	24.65	+0.100	-9.46	-6.16	-33.02
D15	7	800,040	1,000	1.2499E-03	56,107,581	1.466495E-03	18.38	+0.045	-8.10	-5.43	-25.34
D16	8	1,391,300	2,400	1.7250E-03	55,224,937	1.466437E-03	19.66	+0.013	-9.98	-6.82	-32.22
D17	9	2,258,000	4,000	1.7715E-03	57,561,061	1.466564E-03	16.26	+0.020	-8.79	-6.11	-27.42

Note: (+) and (-) signs of percent error mean less than and greater than, respectively.

* See Appendix D, Tables D9 to D17

** Length of original stress-time history = 68,739,939 points

*** Original fatigue damage = 1.466634E-03 (see Table 6.4-4)

7.4 Simulation Results

This section presents the results generated by TCFD, STFT and WT. For WT, there are five results generated by Morl, Meyr, Dmey, Mexh and DB30 wavelets. Mainly, the results are classified into four sub-sections as follows:

Section 7.4.1 Edited stress-time history generated by TCFD
Section 7.4.2 Relationship between cutoff level and damage per repetition
Section 7.4.3 Results, validation and discussion
Section 7.4.4 AccPSD, original stress-time history and edited stress-time histories

7.4.1 Edited Stress-Time History Generated by TCFD

The original stress-time history in Figure 7.1-1 is edited by TCFD. It is divided into a number of small time-window. Fatigue damage is calculated for each time-window containing a short segment of the stress-time history. All stress ranges less than a gate value are removed. Based on $S\text{-}N$ data of DD16 material, the gate value is specified at the fatigue life of 10^9 cycles (see Figure 6.4-11). Windows having no or minimal fatigue damage are removed. The retained windows are assembled to form the edited stress-time history shown in Figure 7.4-1. It has reduction of 10.18% in length with respect to the original length (see Table 7.4-2). In other words, the length of the edited stress-time history is 89.82% of the original length. The difference in fatigue damage per repetition is +0.076% whilst the differences in mean stress and root-mean-square are within ±10%, except for kurtosis. Here, the (+) and (-) sign mean less than and greater than, respectively.

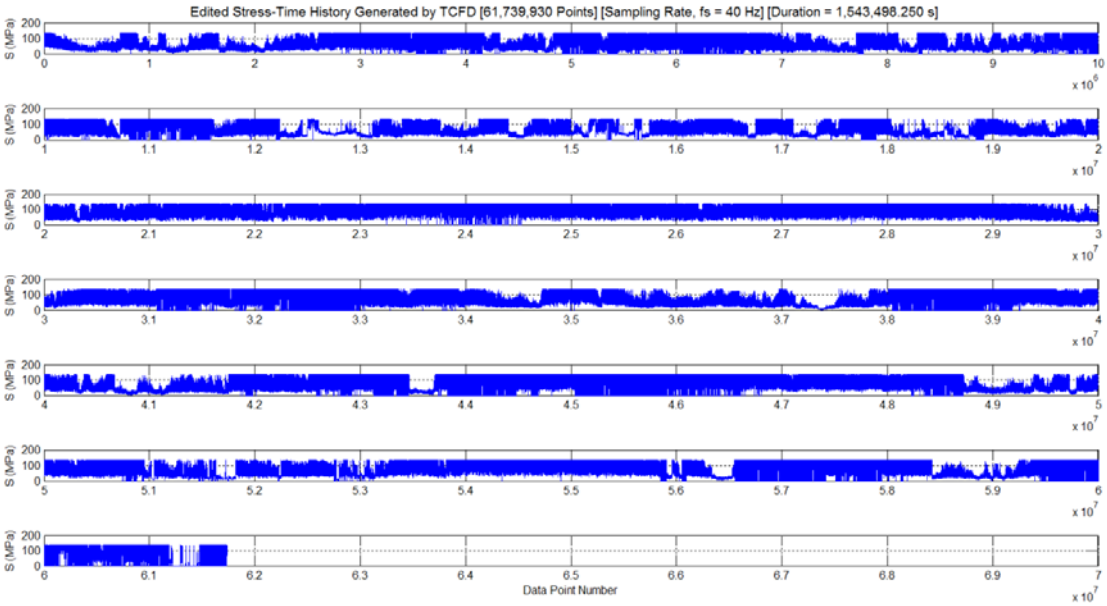

Figure 7.4-1. Edited stress-time history generated by TCFD

7.4.2 Relationship between AccPSD Level and Fatigue Damage per Repetition

This section reports the relationship between AccPSD level and fatigue damage per repetition. Figure 7.4-2 shows that the cutoff levels for STFT, Morl, and Mexh are at 9,800, 2,400, and 9,000 Energy/Hz, respectively. Also, the cutoff levels for Meyr, Dmey and DB30 are at the same level of 3,000 Energy/Hz. Table 7.4-2, Figure 7.4-3(*b*) and Figure 7.4-5(*b*) show that all cutoff levels mentioned here provides the edited stress-time histories different in length, but the errors of mean stress and root-mean-square are within ±10%, except for kurtosis. However, it is indicated that TCFD, STFT and WT have high potential in identifying fatigue damage events contained in the original stress-time history because they cause the differences in fatigue damage per repetition very much less than ±1% as shown in Figure 7.4-4(*b*) and Table 7.4-2.

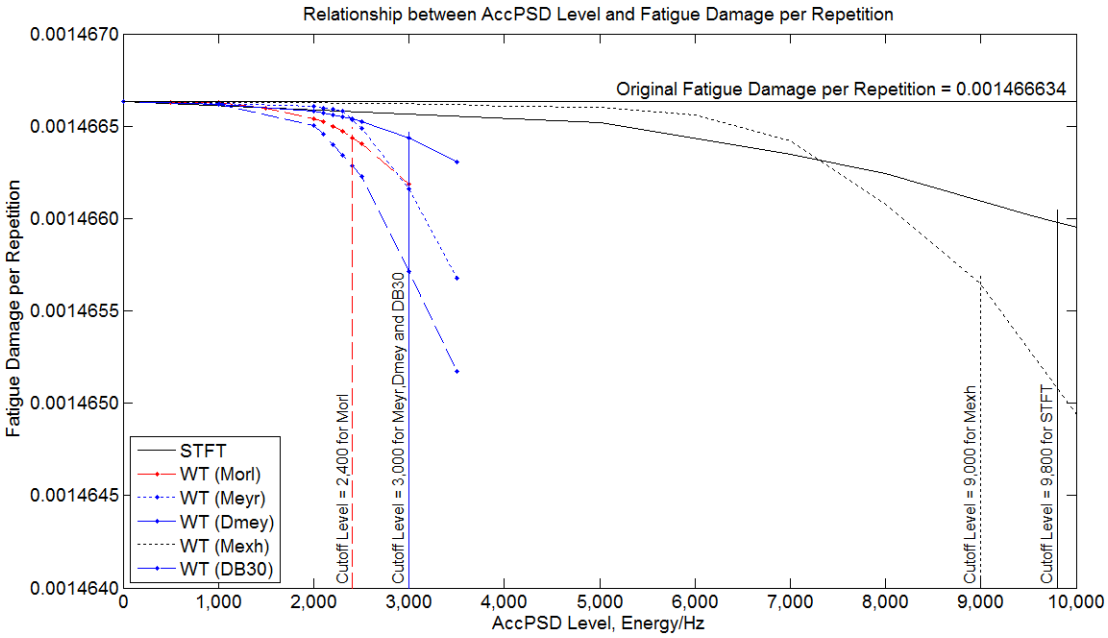

Figure 7.4-2. Relationship between AccPSD level and fatigue damage per repetition

7.4.3 Results, Validation and Discussion

Tables 7.4-1 and 7.4-2 listed data of the original stress-time history and the edited stress-time histories generated by TCFD, STFT and WT with the Morl, Meyr, Dmey, Mexh and DB30 wavelets. To make each parameter of interest easy to compare, the numerical data listed in Tables 7.4-1 and 7.4-2 have been illustrated in the graphical form as shown in Figures 7.4-3 to 7.4-5.

Table 7.4-1. Summary results of the original and edited stress-time histories

Methods	Cutoff Level (Energy/Hz)	Maximum AccPSD (Energy/Hz)	Length of History (Points)	Fatigue Damage per Repetition	Mean Stress (MPa)	rms (MPa)	Kurtosis
Original	-	-	68,739,939	1.466634E-3	81.95	90.96	1.58
TCFD	-	-	61,739,930	1.465519E-3	84.44	93.36	1.80
STFT *	9,800	1.1866E+5	58,165,594	1.465978E-3	90.07	97.01	1.95
WT (Morl) **	2,400	1.3913E+6	55,224,937	1.466437E-3	90.13	97.16	2.09
WT (Meyr) **	3,000	1.4512E+6	54,829,920	1.466158E-3	90.12	97.12	2.10
WT (Dmey) **	3,000	1.4555E+6	55,200,701	1.466435E-3	90.25	97.08	2.08
WT (Mexh) **	9,000	5.2146E+6	54,462,479	1.465643E-3	90.04	97.11	2.13
WT (DB30) **	3,000	2.0998E+6	55,546,345	1.465715E-3	90.01	97.09	2.09

* Based on window size of 256

** Based on wavelet decomposition level 8

Table 7.4-2. Normalised cutoff level, reduction in length and differences in fatigue damage per repetition and differences in signal statistical parameters

Methods	Cutoff Level (Energy/Hz)	Nomalised Cutoff Level ***	% Reduction in Length of History	% Error			
				Fatigue Damage per Repetition	Mean Stress	rms	Kurtosis
TCFD	-	-	10.18	+0.076	-3.04	-2.64	-14.05
STFT *	9,800	8.2589E-2	15.38	+0.045	-9.92	-6.66	-23.45
WT (Morl) **	2,400	1.7250E-3	19.66	+0.013	-9.98	-6.82	-32.22
WT (Meyr) **	3,000	2.0673E-3	20.24	+0.032	-9.97	-6.77	-33.10
WT (Dmey) **	3,000	2.0611E-3	19.70	+0.014	-9.88	-6.74	-32.03
WT (Mexh) **	9,000	1.7259E-3	20.77	+0.068	-9.87	-6.77	-34.92
WT (DB30) **	3,000	1.4287E-3	19.19	+0.063	-9.84	-6.74	-32.30

Note: 1. The plots of the original and edited stress time histories are shown in Figure 7.4-7.

2. (+) and (-) signs of percent error mean less than and greater than, respectively.

* Based on window size of 256

** Based on wavelet decomposition level 8

*** Each cutoff level is normalised by the maximum value of AccPSD for each method.

Table 7.4-3. Result validation

Issues	TCFD*	STFT	WT				
			Morl	Meyr	Dmey	Mexh	DB30
1. Is the edited history length less than the length of the original history?	✓	✓	✓	✓	✓	✓	✓
2. Is the reduction fatigue damage per repetition within the criterion of ±10%?	✓	✓	✓	✓	✓	✓	✓
3. Is the difference in mean stress within the criterion of ±10%? **	✓	✓	✓	✓	✓	✓	✓
4. Is the difference in root-mean-square within the criterion of ±10%? **	✓	✓	✓	✓	✓	✓	✓
5. Is the difference in kurtosis within the criterion of ±10%? **	×	×	×	×	×	×	×
6. Is the edited history length less than the length generated by TCFD?	-	✓	✓	✓	✓	✓	✓
7. Is the difference in fatigue damage per repetition of the edited history less than that of the of the edited history generated by TCFD?	-	✓	✓	✓	✓	✓	✓
8. Is this method valid?	✓	✓	✓	✓	✓	✓	✓

* TCFD (Time Correlated Fatigue Damage) is the existing method performed in commercial software.

** Criterion ±10% is suggested by previous researchers listed in references [93], [99], [118] and [122].

In this research project, the existing method, TCFD, is used to edit the original stress-time history in commercial software. Based on TCFD, the edited stress-time history has reduction of 10.18% in length compared to the length of the original stress-time history (see Table 7.4-2). Furthermore, the fatigue damage per repetition retained in the edited stress-time history is almost the same as the fatigue damage per repetition of the original stress-time history with +0.076% in difference. This difference is very much less than +1%. By this reason, it is proved that the edited stress-time history generated by TCFD is valid and it can be used as the baseline result to be compared by the edited stress-time histories generated by STFT and WT.

Considering Table 7.4-3, there are seven issues to be considered for the validation of each method. It is outstanding that there is only one issue that TCFD, STFT and WT are marked by ×. It is the difference in kurtosis which is beyond the criterion ±10% suggested by previous researchers [93,99,118,122]. This indicates that ±10% of difference in

kurtosis could not be used as the criterion in this research project. However, the overall issues listed in Table 7.5-3 indicate that all fatigue data editing methods are valid.

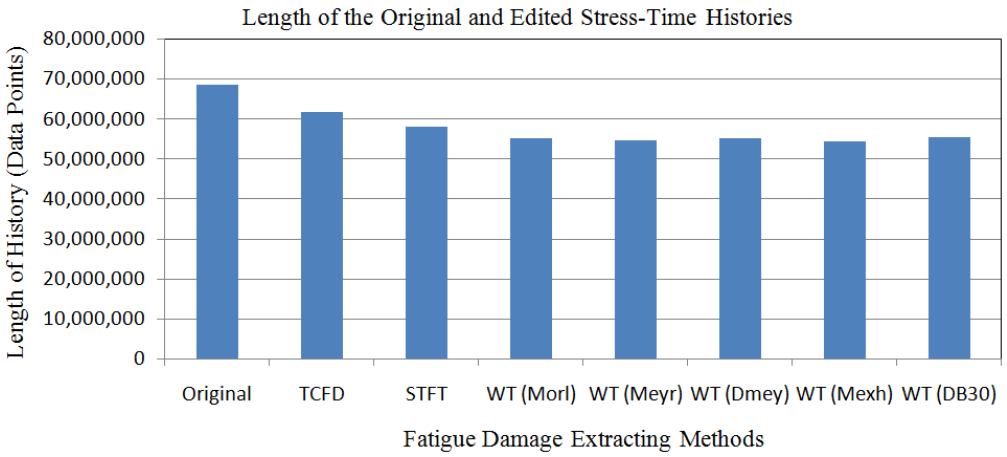

(*a*)

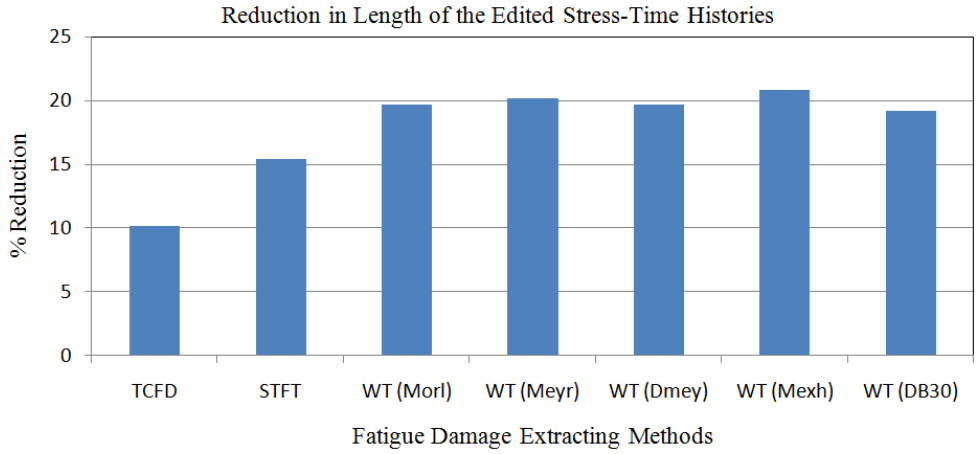

(*b*)

Figure 7.4-3. Lengths of the stress-time histories:
(*a*) length of the original and edited stress-time histories;
(*b*) reduction in length of the edited stress-time histories

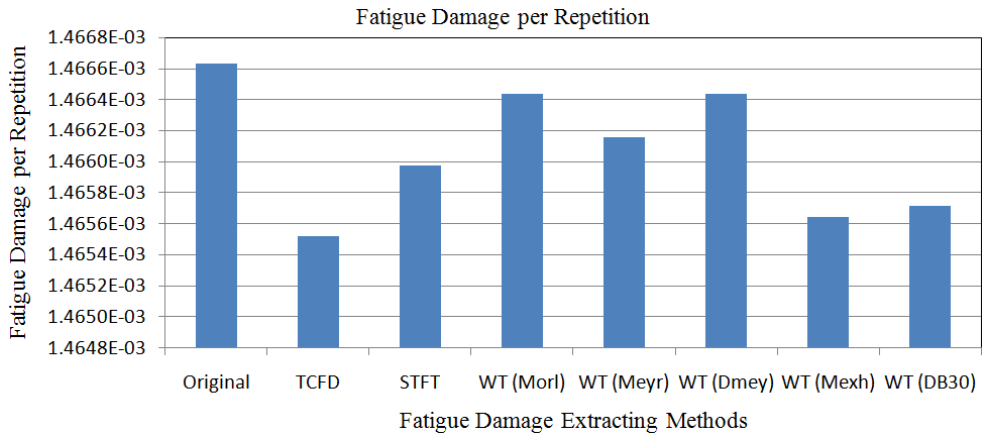

(*a*)

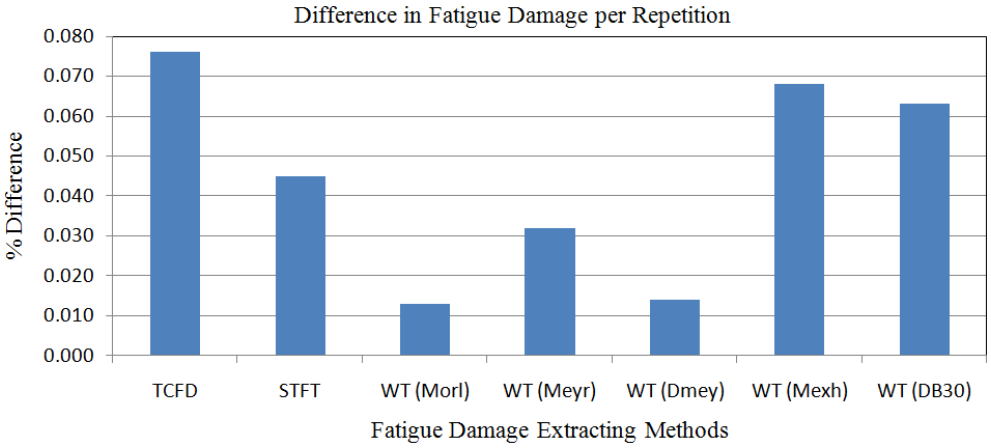

(*b*)

Figure 7.4-4. Fatigue damage per repetition:
(*a*) fatigue damage per repetition;
(*b*) difference in fatigue damage per repetition

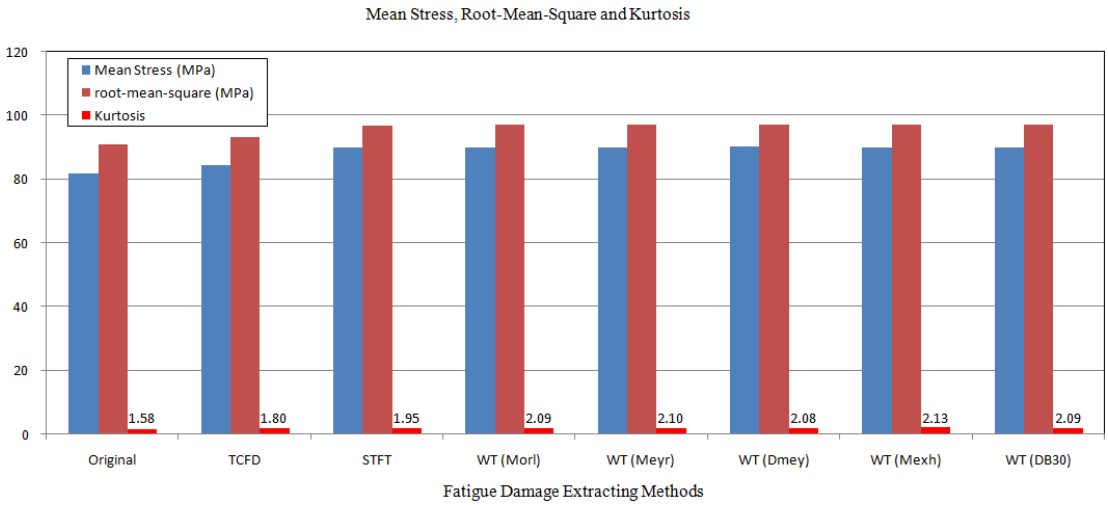

(*a*)

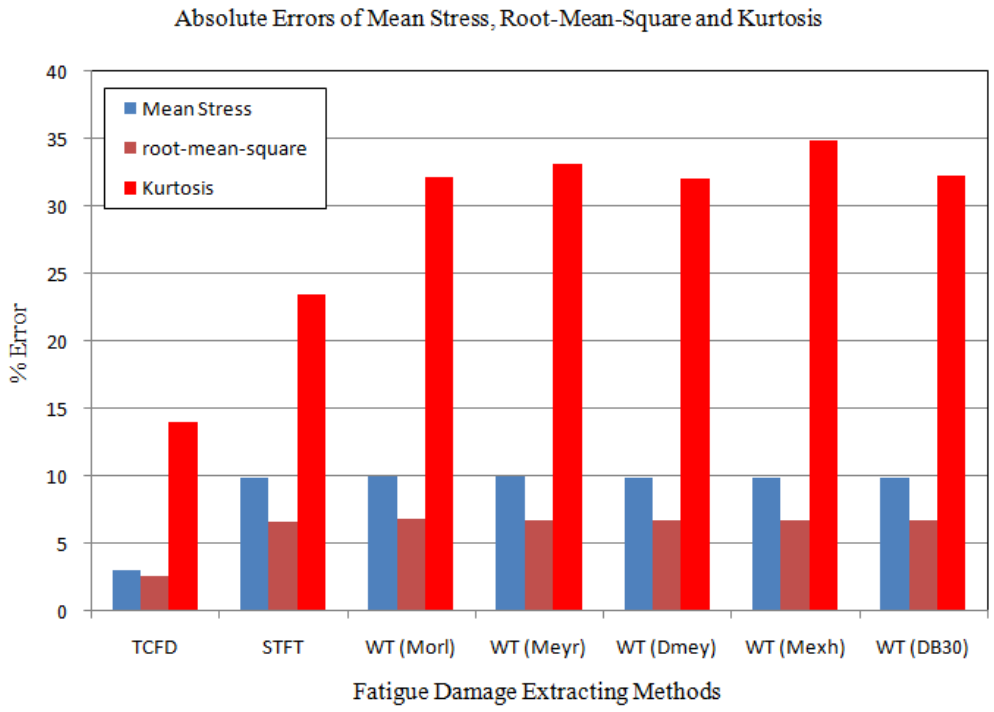

(*b*)

Figure 7.4-5. Signal statistical parameters: (*a*) mean stress, root-mean-square and kurtosis; (*b*) absolute errors of mean stress, root-mean-square and kurtosis of each method used in editing the original stress-time history

In discussion, the original stress-time history has been edited by three different methods which are TCFD, STFT and WT. The first method is done in time domain. The second method is done in time-frequency domain. The third method is done in time-scale domain. This section compares and discusses the results obtained from each method.

TCFD is the time domain editing technique used by commercial software. This technique is used to remove non-damage sections of the original stress-time history on the basis of time correlated fatigue damage windows of the input signal. The original stress-time history in Figure 7.1-1 is divided into a number of time segments. Then, fatigue damage is calculated for each time-window containing a short segment of the stress-time history. Windows having no or minimal fatigue damage are removed. On the other hand, windows having high fatigue damage are retained. The retained windows are assembled to produce the edited stress-time history as shown in Figures 7.4-1 and 7.4-7(*b*). Based on TCFD, the edited stress-time history has reduction of 10.18% in length with respect to the original length (see Table 7.4-2). In other words, the length of the edited stress-time history is 89.82% of the original length. The difference in fatigue damage per repetition is +0.076% whilst the differences in mean stress and root-mean-square of the edited stress-time history are within ±10%, except for kurtosis. Here, the (+) and (-) sign mean less than and greater than, respectively.

For STFT, Module 7 in HAWTfatigue is used to edit the original stress-time history. Before taking STFT, the window size effect on variation of fatigue damage per repetition is studied in Section 7.2. Comparison in Figure 7.2-5 shows that the window size of 256 points provides the shortest length of the edited stress-time history compared to among other window sizes. Also, the errors of mean stress and root-mean-square in Figure 7.2-3 are within ±10%, except for kurtosis. Furthermore, the results in Figure 7.4-4(*b*) and Table 7.4-2 indicate that the STFT has a high potential in identifying the fatigue damage events contained in the original stress-time history, because the difference in fatigue damage per repetition is very much less than ±1%. Here, the (+) sign means less than. By using window size of 256 points, the events having AccPSD level equal or higher than the cutoff level are classified as damage parts. On the other hand, the events having AccPSD level lower than the cutoff level are classified as non-damage parts. Here, the fatigue damage parts are extracted at the cutoff level of 9,800 Energy/Hz as shown in Figures 7.2-7 and 7.4-6(*a*) (see Table 7.4-2 for the normalised value of this cutoff level). Eventually, each damage part is concatenated to form the edited stress-time history as shown in Figures 7.2-

8 and 7.4-7(*c*). Based on STFT, the edited stress-time history has reduction of 15.38% in length with respect to the original length (see Table 7.4-2). In other words, the length of the edited stress-time history is 84.62% of the original length. The difference in fatigue damage per repetition is +0.045% whilst the differences in mean stress and root-mean-square of the edited stress-time history are within ±10%, except for kurtosis.

For WT, Module 8 in HAWTfatigue is used to edit the original stress-time history. Before taking WT, the wavelet decomposition level effect on variation of fatigue damage per repetition is studied in Section 7.3. Morl wavelet is chosen in this study because it was successfully used in previous research [118]. Comparison in Table 7.3-1 shows that the wavelet decomposition level 8 provides the minimum difference in fatigue damage per repetition compared to among other wavelet decomposition levels. Also, the errors of mean stress and root-mean-square in Figure 7.3-3 are within ±10%, except for kurtosis. Furthermore, the results in Figure 7.4-4(*b*) and Table 7.4-2 indicate that the WT with the Morl wavelet has high potential in identifying the fatigue damage events contained in the original stress-time history, because the difference in fatigue damage per repetition is very much less than ±1%. Here, the (+) sign means less than. By using wavelet decomposition level 8, the events having AccPSD level equal or higher than the cutoff level are classified as damage parts, and vice versa for the non-damage parts. Here, the fatigue damage parts are extracted at the cutoff level of 2,400 Energy/Hz as shown in Figures 7.3-7 and 7.4-6(*b*) (see Table 7.4-2 for the normalised value of this cutoff level). Then, each damage part is concatenated to form an edited stress-time history as shown in Figures 7.3-8 and 7.4-7(*d*). Based on WT with the Morl wavelet, the edited stress-time history has reduction of 19.66% in length with respect to the original length (see Table 7.4-2). In other words, the length of the edited stress-time history is 80.34% of the original length. The difference in fatigue damage per repetition is +0.013% whilst the differences in mean stress and root-mean-square of the edited stress-time history are within ±10%, except for kurtosis. Here, the (+) and (-) sign mean less than and greater than, respectively.

In this research project, five different wavelet types, which are Morl, Meyr, Dmey, Mexh and DB30 wavelets, are used to identify the fatigue damage events contained in the original stress-time history. By using wavelet decomposition level 8, each wavelet type is taken to the original stress-time history to generate the plots of AccPSD distribution shown in Figures 7.4-6(*b*) to 7.4-6(*f*). By cutoff levels listed in Table 7.4-2, WT with each wavelet types generates the edited stress-time histories shown in Figures 7.4-7(*d*) to 7.4-

7(*h*) for Morl, Meyr, Dmey, Mexh, and DB30 wavelets, respectively. The summary results in Table 7.4-2 indicate that Mexh wavelet has the maximum reduction of 20.77% in length compared to the original length, followed by Meyr (20.24%), Dmey (19.70%), Morl (19.66%), and DB30 (19.19%), respectively. The differences in fatigue damage per repetition are +0.068%, +0.032%, +0.014%, +0.013%, and +0.063% for Mexh, Meyr, Dmey, Morl, and DB30 wavelets, respectively, whilst the differences in mean stress and root-mean-square of each edited stress-time history are within ±10%, except for kurtosis. Here, the (+) and (-) sign mean less than and greater than, respectively. It is noticeable that Mexh wavelet has the maximum difference in fatigue damage per repetition, i.e. +0.068%, but this difference is very much less than +1%.

7.4.4 AccPSD, Original Stress-Time History and Edited Stress-Time Histories

This section reports the plots of AccPSD distribution generated by STFT and WT with the Morl, Meyr, Dmey, Mexh and DB30 wavelets in Figure 7.4-6. Also the plots of the the original stress-time history and the edited stress-time histories generated by TCFD, STFT, and WT with the Morl, Meyr, Dmey, Mexh and DB30 wavelets are illustrated in Figure 7.4-7. (See their statistics in Table 7.4-1)

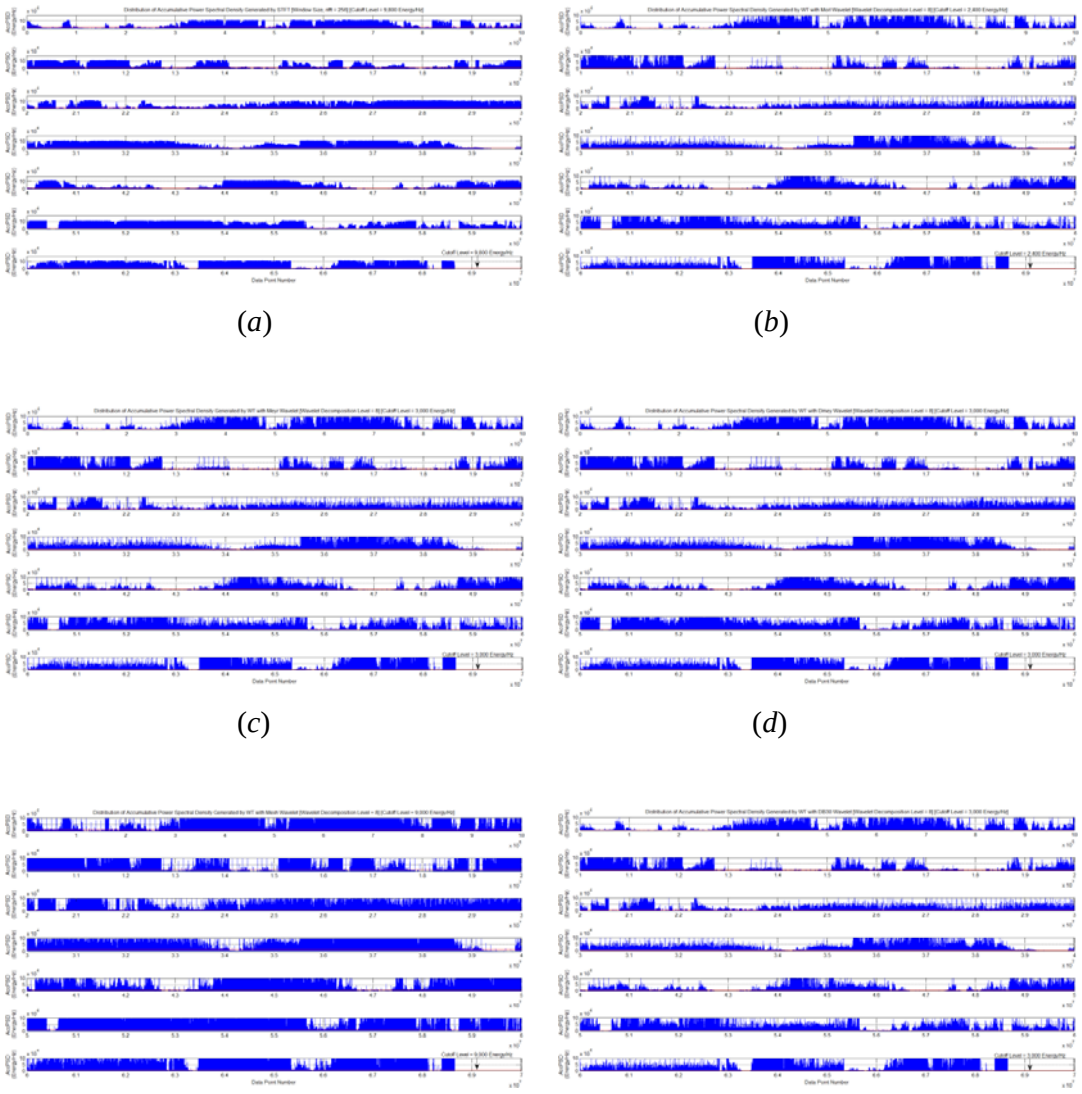

(*a*) (*b*)

(*c*) (*d*)

(*e*) (*f*)

Figure 7.4-6. Plots of AccPSD distribution generated by:
(*a*) STFT; (*b*) WT with the Morl wavelet;
(*c*) WT with the Meyr wavelet; (*d*) WT with the Dmey wavelet;
(*e*) WT with the Mexh wavelet; (*f*) WT with the DB30 wavelet

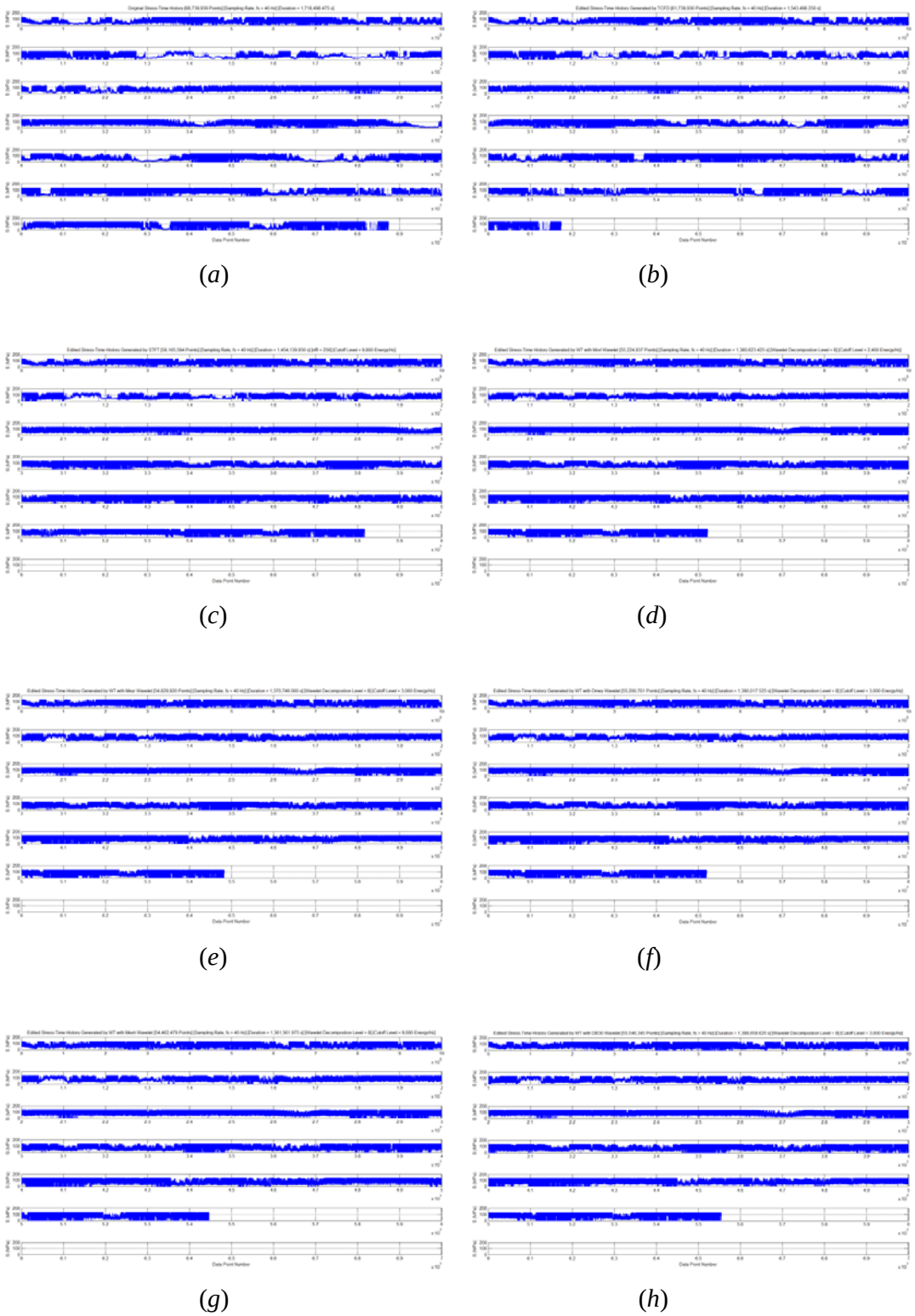

(*a*) (*b*)

(*c*) (*d*)

(*e*) (*f*)

(*g*) (*h*)

Figure 7.4-7. Stress-time histories: (*a*) Original; generated by (*b*) TCFD; (*c*) STFT; generated by WT with the (*d*) Morl wavelet; (*e*) Meyr wavelet; (*f*) Dmey wavelet; (*g*) Mexh wavelet; (*h*) DB30 wavelet

7.5 How the Novel Methods Would Be Applied to A Real Blade Test

Proportional integral derivative (PID) control can be mainly used for dynamic fatigue testing. To ensure the actual load reaches the predefined load values during testing, the loads are set as the PID control target value. Meanwhile, the test system acquires the actual load signal on the HAWT blade and the maximum value is set as the PID control feedback as illustrated by the block diagram in Figure 7.5-1.

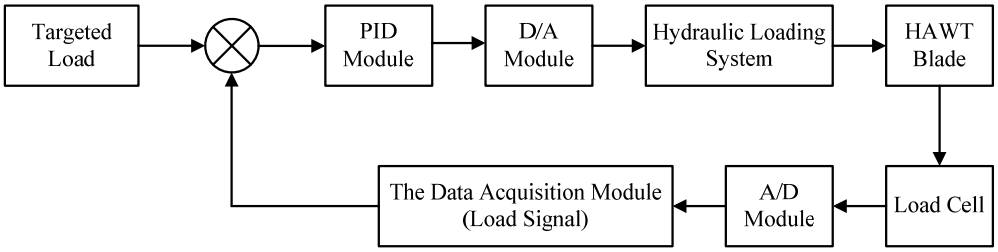

Figure 7.5-1. Load PID control block diagram

7.6 Summary

In this research project, the original stress-time history has been edited by three different methods which are TCFD, STFT and WT. The first method is done in time domain. The second method is done in time-frequency domain. The third method is done in time-scale domain.

The author compares the effectiveness of the fatigue damage extraction among TCFD, STFT and WT with the Morl, Meyr, Dmey, Mexh and DB30 wavelets. From Figure 7.4-5(*b*), it is clearly seen that errors of both mean stress and root-mean-square for each method have the same pattern and they are within ±10% whilst errors of kurtosis are beyond ±10%. It is outstanding that errors of both mean stress and root-mean-sqaure for TCFD are less than others. By this result, it is indicated that ±10% error of kurtosis could not be used as a criterion for the given stress-time history. Furthermore, the results in Figure 7.4-4(*b*) show that all methods provide their differences in fatigue damage per repetition very much less than ±1%. These differences indicate that all methods used in this study have high potential in identifying fatigue damage events contained in the given original stress-time history.

To make the analysis easier, data listed in Table 7.4-2 is rearranged by sorting the percent reduction in length of the edited stress-time histories from maximum to minimum (see

Table 7.5-1). Having considered the percent reduction in length of each edited stress-time history listed Table 7.5-1, it has been found that WT with the Mexh wavelet has the maximum reduction of 20.77% in length with respect to the original length, followed by Meyr (20.24%), Dmey (19.70%), Morl (19.66%), DB30 (19.19%), STFT (15.38%), and TCFD (10.18%), respectively. Also, it has been found from Table 7.5-1 that TCFD has the maximum difference in fatigue damage per repetition of +0.076% (compared to the original fatigue damage per repetition), followed by Mexh (+0.068%), DB30 (+0.063%), STFT (+0.045%), Meyr (+0.032%), Dmey (+0.014%), and Morl (+0.013%), respectively. Here, the (+) sign of percent error means less than.

To summarise, the summary results in Table 7.5-1 suggest that WT with the Mexh wavelet is a suitable method for extracting the fatigue damage parts from the given stress-time history despite the fact that it has the second maximum difference in fatigue damage per repetition (+0.068%). However, in this research project, WT with the Mexh wavelet provides the shortest length of the edited stress-time history (20.77%) compared to the lengths generated by TCFD, STFT and WT with the Morl, Meyr, Dmey and DB30.

Table 7.5-1. Summary results

Methods	Cutoff Level (Energy/Hz)	Nomalised Cutoff Level ***	% Reduction in Length of History	% Error			
				Fatigue Damage per Repetition	Mean Stress	rms	Kurtosis
WT (Mexh) **	9,000	1.7259E-3	20.77	+0.068	-9.87	-6.77	-34.92
WT (Meyr) **	3,000	2.0673E-3	20.24	+0.032	-9.97	-6.77	-33.10
WT (Dmey) **	3,000	2.0611E-3	19.70	+0.014	-9.88	-6.74	-32.03
WT (Morl) **	2,400	1.7250E-3	19.66	+0.013	-9.98	-6.82	-32.22
WT (DB30) **	3,000	1.4287E-3	19.19	+0.063	-9.84	-6.74	-32.30
STFT *	9,800	8.2589E-2	15.38	+0.045	-9.92	-6.66	-23.45
TCFD	-	-	10.18	+0.076	-3.04	-2.64	-14.05

Note: 1. The plots of the original and edited stress time histories are shown in Figure 7.4-7.

2. (+) and (-) signs of percent error mean less than and greater than, respectively.

* Based on window size of 256

** Based on wavelet decomposition level 8

*** Each cutoff level is normalised by the maximum value of AccPSD for each method.

Chapter 8

Summary of Research Project

This research project proposes two novel methods which are STFT- and WT-based fatigue damage part extracting methods. Each method is used to extract fatigue damage parts from the stress-time history of the horizontal axis wind turbine (HAWT) blades. A wind turbine blade used in this study is a pseudo model of a SERI-8 blade mentioned in Section 3.4. It was developed by Solar Energy Research Institute (SERI) which is now called the National Renewable Energy Laboratory (NREL). The SERI-8 blades are installed on modified Micon 65 wind turbines having a generator rating of 65 kW. The fibreglass composite material used in modelling the blade is a laminate called DD16. This material has been listed in DOE/MSU composite material fatigue database for wind turbine blades. The wind speed data was sampled at 40 Hz for 68,739,939 data points giving the total record length of 1,718,498.475 seconds (see Section 6.4.1).

In this research project, the original stress-time history to be edited by the proposed methods is generated by using four computer programmes which are HAWTsimulator, NuMAD, ANSYS and HAWTfatigue. HAWTsimulator is an aerodynamic computer code based on blade element moment (BEM) theory. It is used to generate the sets of aerodynamic loads at wind speeds ranging from cut-in to cut-out. NuMAD is used to generate a finite element model of the pseudo SERI-8 blade. Both aerodynamic loads and the finite element model are imported to ANSYS to generate a relationship between stress and wind speed. HAWTfatigue, a fatigue computer code for HAWT blades, is used to generate the original stress-time history as shown in Figure 7.1-1. This history will be edited by TCFD (time correlated fatigue damage), STFT and WT. TCFD is an existing method used by commercial software. STFT and WT are the proposed methods. The result from each method is the edited stress-time history which its length is shorter than the length of the original stress-time history whilst it can retain fatigue damage nearly the same as the original fatigue damage. Based on fatigue damage model called Miner's rule, HAWTfatigue evaluates the fatigue damage per repetition of each edited stress-time history.

In addition, the existing method, TCFD, is used to study the effectiveness of STFT- and WT-based fatigue damage part extracting methods. The results from TCFD, STFT and WT are compared. In conducting the research project, the author has gone through the steps proposed in Chapter 1, Section 1.5. The following steps have been completely accomplished.

1. The author has developed an aerodynamic computer code, HAWTsimulator, to generate a set of aerodynamic loads acting along the blade span in the range of wind speed from cut-in to cut-out. It is designed to be run in a Matlab environment. The theory implemented in the code is based on the BEM theory derived in Chapter 2. The results generated by HAWTsimulator are validated against those generated by two existing codes, WT_Perf (see Section 3.3) and PROPPC (see Section 3.4). The validation indicates that HAWTsimluator is valid and can be used with high confidence. Thus, the sets of aerodynamic loads generated by HAWTsimulator are imported to ANSYS structural software to generate a relationship between stress and wind speed. By relating this relationship to wind speed data, the original stress-time history in Figure 7.1-1 is generated. Based on wind speed data, the original stress-time history has the same sampling rate and length as the wind speed data.

During reviewing the literature relevant to the BEM theory, it is found that there are windmill brake state models proposed by several researchers in the past. Consequently, the author is interested in assessing the effect of windmill brake state models on the predicted power curve. The comparative study was done and the result was published in a journal quality.

2. The author has developed a fatigue computer code, HAWTfatigue, to evaluate the fatigue damage contained in the stress-time history of the HAWT blades. HAWTfatigue is designed to be run in a Matlab environment (see Section 6.4). The theories used in the process of fatigue calculation are based on stress-life approach and Miner's linear cumulative damage rule mentioned in Sections 4.3 and 4.4. The main results are the number of rainflow cycles counted and fatigue damage per repetition. They are validated against those calculated by commercial software. The validation shows that HAWTfatigue provides the same results as commercial software. Thus, it is indicated that HAWTfatigue is valid and can be used with high confidence.

3. The author has edited the original stress-time history in Figure 7.1-1 by TCFD. The original stress-time history, which has the same sampling rate and length as the wind speed data, is divided into a number of small time-window. Then, fatigue damage is calculated for each time-window containing a short segment of the stress-time history. All stress ranges which are less than a specified gate value are removed. Based on S-N data of DD16 composite material, the gate value is specified at the fatigue life of 10^9 cycles (see Figure 6.4-11). Windows having no or minimal fatigue damage are removed. On the other hand, windows having high fatigue damage are retained. The retained windows are assembled to produce the edited stress-time history shown in Figure 7.4-1. It has been found that the edited stress-time history generated by TCFD has reduction of 10.18% in length (see Table 7.4-2). In other words, the length of the edited stress-time history is 89.82% of the original length. The difference in fatigue damage per repetition is +0.076% (see Table 7.4-2) whilst the differences in mean stress and root-mean-square of the edited stress-time history are within ±10%, except for kurtosis. Here, the (+) and (-) sign mean less than and greater than, respectively.

4. The author has edited the original stress-time history in Figure 7.1-1 by STFT-based fatigue damage part extracting method. The signal processing toolbox in Matlab is implemented into HAWTfatigue. The window size effect of STFT on variation of fatigue damage per repetition is studied. For the given stress-time history, the results from the study in Section 7.2 suggest that the window size of 256 points should be used in taking STFT. Thus, STFT is taken to the original stress-time history to generate the plot of accumulative power spectral density (AccPSD) distribution. For STFT, AccPSD has been introduced in Section 5.5.2. It is the sum of power spectral density (PSD) of each frequency band at each time interval in the spectrogram. Also, the concept of applying AccPSD to identify fatigue damage events contained in the stress-time history has been discussed in Sections 6.2 and 6.3. It has been found from Section 6.2 that there are three issues can be summarised: (1) the amplitudes of AccPSD spikes for STFT does not provide us how much fatigue damage occurs; (2) the locations of AccPSD spikes, which are observed by naked eyes, are close to the locations of fatigue damage occurred; and (3) the fatigue damage events in the stress-time history could be identified by an appropriate cutoff level.

To determine the cutoff level, the author has studied the window size effect on variation of fatigue damage per repetition in Section 7.2. It has been found that the best cutoff level is

at 9,800 Energy/Hz (see Table 7.4-2 for the normalised value of this cutoff level). This cutoff level is used as a criterion in identifying the fatigue damage parts at time locations in the original stress-time history. Based on the cutoff level, the fatigue damage parts are identified and extracted from the original stress-time history. Then, each extracted damage part is concatenated to form a new signal called the edited stress-time history. It has been found that the edited stress-time history generated by STFT has reduction of 15.38% in length (see Table 7.4-2). In other words, the length of the edited stress-time history is 84.62% of the original length. The difference in fatigue damage per repetition is +0.045% whilst the differences in mean stress and root-mean-square of the edited stress-time history are within ±10%, except for kurtosis. Here, the (+) and (-) sign mean less than and greater than, respectively.

5. The author has edited the original stress-time history in Figure 7.1-1 by WT-based fatigue damage part extracting method. The wavelet toolbox in Matlab is implemented into HAWTfatigue. Five different wavelet types are used in this research project. They are Morl, Meyr, Dmey, Mexh and DB30 wavelets. Prior to editing the original stress-time history, Morl wavelet is used to study the effect of wavelet decomposition level on variation of fatigue damage per repetition in Section 7.3. Morl wavelet is chosen in this study because it was successfully used in previous research. For the given stress-time history, the results from the study in Section 7.3 suggest the wavelet decomposition level 8 should be used in taking WT with the Morl as a wavelet function. For, Meyr, Dmey, Mexh and DB30 wavelet functions, it is not necessary to repeat the same study to find which the wavelet decomposition level should be used in taking WT again. There are two reasons for supporting this statement. For the first reason, the results in Figure 7.4-5(*b*) and Table 7.4-2 show that each edited stress-time history generated by WT with each wavelet type has the same pattern of the absolute errors of mean stress, root-mean-square and kurtosis. The values of the errors of mean stress and root-mean-square seem to be not different whilst the values of the errors kurtosis are slightly different. For the second reason, the results in Figure 7.4-3(*b*) and Table 7.4-2 show that the reduction in length of the edited stress-time histories generated by WT with each wavelet type are slightly different. By these reasons, the author decides to use wavelet decomposition level 8 in taking WT for all wavelet types.

For each wavelet type, WT is taken to the original stress-time history in Figure 7.1-1 at wavelet decomposition level 8. Similar to STFT, the plots of accumulative power spectral density (AccPSD) distribution of each wavelet type are generated. For WT, AccPSD has

been introduced in Section 5.6.2. It is the sum of power spectral density (PSD) of wavelet coefficients of each scale at each time interval in the scalogram. Also, the concept of applying AccPSD to identify fatigue damage events contained in the stress-time history has been discussed in Sections 6.2 and 6.3. Referring to Section 5.6.1, the maximum scale used in taking WT is defined by the next power of two of the wavelet decomposition level. Here, the wavelet decomposition level is at level 8. This means that WT is taken to the original stress-time history with the maximum window size of 256 data points (2^8) for the 8^{th} scale followed by 128 data points (2^7), 64 data points (2^6), 32 data points (2^5), 16 data points (2^4), 8 data points (2^3), 4 data points (2^2), and 2 data points (2^1) for the 7^{th}, 6^{th}, 5^{th}, 4^{th}, 3^{rd}, 2^{nd}, and 1^{st} scales, respectively.

To determine the cutoff level, the author has studied the wavelet decomposition level effect on variation of fatigue damage per repetition in Section 7.3. It has been found that the best cutoff levels for Morl, Meyr, Dmey, Mexh, and DB30 wavelets are at 2,400, 3,000, 3,000, 9,000, and 3,000 Energy/Hz, respectively, (see Table 7.4-2 for the normalised value of each cutoff level). Each cutoff level is used as a criterion in identifying the fatigue damage parts at time locations in the original stress-time history. It has been found that the edited stress-time histories generated by WT with the Mexh, Meyr, Dmey, Morl, and DB30 wavelets have reductions of 20.77%, 20.24%, 19.70%, 19.66%, and 19.19% in length, respectively (see Table 7.4-2). In other words, the lengths of the edited stress-time histories generated by WT with the Morl, Meyr, Dmey, Mexh, and DB30 wavelets are 79.23%, 79.76%, 80.30%, 80.34%, and 80.81% of the original length, respectively. The differences in fatigue damage per repetition are +0.068%, +0.032%, +0.014%, +0.013%, and +0.063% for Mexh, Meyr, Dmey, Morl, and DB30 wavelets, respectively, whilst the differences in mean stress and root-mean-square of each edited stress-time history are within ±10%, except for kurtosis. Here, the (+) and (-) sign mean less than and greater than, respectively.

The results mentioned above suggest that Mexh wavelet reduces the length of the original stress-time history shorter than Meyr, Dmey, Morl and DB30 wavelets do. It can be summarised that Mexh wavelet is the best wavelet function for extracting the fatigue damage parts from the given stress-time history despite the fact that it has the maximum difference in fatigue damage per repetition (+0.068%) compared to those of Meyr, Dmey, Morl and DB30 wavelets.

6. The author compares the effectiveness of the fatigue damage extraction among TCFD, STFT and WT with the Morl, Meyr, Dmey, Mexh and DB30 wavelets. It is clearly seen from Figure 7.4-5(*b*) that errors of both mean stress and root-mean-square for each method are quite the same pattern and they are within ±10% whilst errors of kurtosis are beyond ±10%. By this result, it is indicated that ±10% error of kurtosis could not be used as a criterion for the given stress-time history. Furthermore, the results in Figure 7.4-4(*b*) show that all methods provide their differences in fatigue damage per repetition very much less than ±1%. These differences indicate that all methods used in this study have high potential in identifying fatigue damage events contained in the given original stress-time history.

Chapter 9

Conclusions and Suggestion for Future Research

9.1 Conclusions

At present, the concept of using short-time Fourier transform (STFT) and wavelet transform (WT) in extracting fatigue damage parts from the stress-time history of horizontal axis wind turbine blades is not proposed by any researchers. This research project discusses the study of fatigue damage extracting methods in time-frequency domain by using STFT and in time-scale domain by using WT. The STFT- and WT-based fatigue damage part extracting methods proposed and developed in this research project can be used to extract fatigue damage parts from the stress-time history of horizontal axis wind turbine blades.

Since STFT- and WT- based fatigue damage part extracting methods are defined here for the first time, experimental validation of the algorithms is important. Taken as a whole, the findings provide a first response to the research questions in Chapter 1, Section 1.5. Therefore, it is useful to summarise the findings in light of the research questions.

Answer for Research Question 1:

What is the best method among TCFD, STFT and WT for extracting fatigue damage parts from the given stress-time history under the purpose of accelerated fatigue test?

The comparison of the fatigue damage extracting methods among TCFD, STFT and WT suggests that WT is the best method for extracting fatigue damage parts from the given stress-time history.

Answer for Research Question 2:

Among WT with the Morl, Meyr, Dmey, Mexh and DB30 wavelets, which one is the best one for extracting fatigue damage parts from the given stress-time history under the purpose of accelerated fatigue test?

The comparison of the edited stress-time histories generated by WT with the Morl, Meyr, Dmey, Mexh and DB30 wavelets suggests that Mexh wavelet is the best wavelet for extracting fatigue damage parts from the given stress-time history.

Answer for Research Question 3:

Can STFT-based algorithm be developed to improve the accuracy of fatigue damage part extracting method with respect to TCFD, an existing method?

STFT-based algorithm generates the edited stress-time history having less the difference in fatigue damage per repetition than TCFD does. Therefore, STFT can improve the accuracy of fatigue damage part extracting part method.

Answer for Research Question 4:

Can WT-based algorithm be developed to improve the accuracy of fatigue damage part extracting method with respect to TCFD, an existing method?

WT-based algorithm generates the edited stress-time histories having less the difference in fatigue damage per repetition than TCFD does. Therefore, WT can improve the accuracy of fatigue damage part extracting part method.

Answer for Research Question 5:

What are the main factors that influence the novel fatigue damage part extracting methods?

STFT has two main factors which are window size and cutoff level. WT has three main factors which are wavelet decomposition level, cutoff level and wavelet type.

Answer for Research Question 6:

Are the edited stress-time histories generated by the novel methods suitable for accelerated fatigue testing of horizontal axis wind turbine blades?

This question cannot completely be answered unless the fatigue damage from the experiment has been known. The findings suggest that STFT- and WT-based fatigue damage part extracting methods are the useful methods for performing accelerated fatigue tests.

To conclude, in terms of the applicability of the edited stress-time history, this kind of history can be used by blade testing laboratories to accelerate fatigue testing time. STFT- and WT-based fatigue damage part extracting methods proposed in this thesis are suggested as alternative methods in accelerating fatigue testing time, especially for the field of wind turbine engineering.

9.2 Suggestion for Future Research

The STFT- and WT-based fatigue damage part extracting methods are the novel methods developed for the application in wind turbine research. Considering the limitations and problems of the STFT- and WT-based algorithms, further research works are suggested to improve the performance of these methods:

1. Choice of the wavelet function for the WT-based algorithm: Currently, five different wavelets are studied in this research project. They are Morl, Meyr, Dmey, Mexh and DB30 wavelet functions. In this research project, the finding suggests that wavelet type is the main parameter affecting fatigue damage part extraction. Mexh wavelet provides the best results for the given stress-time history. However, Mexh wavelet might not be the best for other or unfamiliar stress-time histories. There are several wavelet types left to be investigated such as Haar, Symlets, Coiflets, BiorSplines, ReverseBior and Gaussian. Further studies to determine the most suitable wavelet function and wavelet order should be performed.

2. Development of a signal segmentation algorithm for the stress-time history: In this research project, STFT- and WT-based algorithms use a cutoff level as a criterion in identifying the fatigue damage events contained in the stress-time history. Each identified fatigue damage event consists of the number of data points which are equal to the window width for both STFT and WT. These data points might form the fatigue damage parts which are contaminated by the small amplitude cycles. Currently, STFT- and WT-based algorithms used in this research project do not take this problem into account. The undesired small amplitude cycles need to be cleaned before extracting process is performed. To solve this problem in the future research, racetrack method should be applied to each fatigue damage event so as to eliminate the undesired small amplitude cycles.

3. Comparison with other signal editing techniques: In this research, the STFT- and WT-based algorithms are compared to the existing method called time correlated fatigue damage (TCFD). It is suggested to compare the STFT- and WT-based algorithms with other fatigue data editing methods (in the domain of frequency, peak-valley). Such comparison would permit a complete evaluation of the effectiveness of the STFT- and WT-based algorithms.

4. More analysis (analytically and experimentally) using other stress-time histories: In order to have the general findings, more applications using various stress-time histories obtained from various site of installed wind turbines are needed for both analytical and experimental studies.

Appendices

Appendix A

A Pseudo SERI-8 Wind Turbine Blade

In this research project, a wind turbine blade is a pseudo model of a SERI-8 blade published by Sandia National Laboratories (SNL) [62]. The SERI-8 blade is a 7.9-meter wind turbine blade developed by Solar Energy Research Institute (SERI) which is now called the National Renewable Energy Laboratory (NREL). The SERI-8 blades are installed on modified Micon 65 wind turbines having a generator rating of 65 kW [59-62]. This wind turbine is a fixed-pitch, three-bladed Danish up-wind turbine with a three-phase, 60 Hz, 480 VAC synchronous generator rated at 65 kW. The generator operates at 1,200 rpm whilst the blades rotate with a fixed speed at 44 rpm [60].

This appendix contains data and information used in generating of aerodynamic loads, analysing of stress, and predicting fatigue damage and service lifetime. The data and information are as follows:

1. A topology of the SERI-8 blade is shown in Figure A1.
2. Blade dimensions and airfoil shapes at each station of the blade are listed in Table A1.
3. Mechanical and fatigue properties of the fibreglass composite material used are listed in Tables A2 to A3.

The first two data are used for generating aerodynamic loads and generating a finite element model. A set of aerodynamic loads is generated by HAWTsimulator. The finite element model is generated by NuMAD software supported by Sandia National Laboratories [120]. NuMAD is used for converting geometry, material property and boundary condition to a set of input files to be linked to ANSYS structural software. Also, a set of aerodynamic loads generated by HAWTsimulator is linked to ANSYS structural software; consequently, a critical stress value can be determined. The third data is used by HAWTfatigue to evaluate number of cycles to failure.

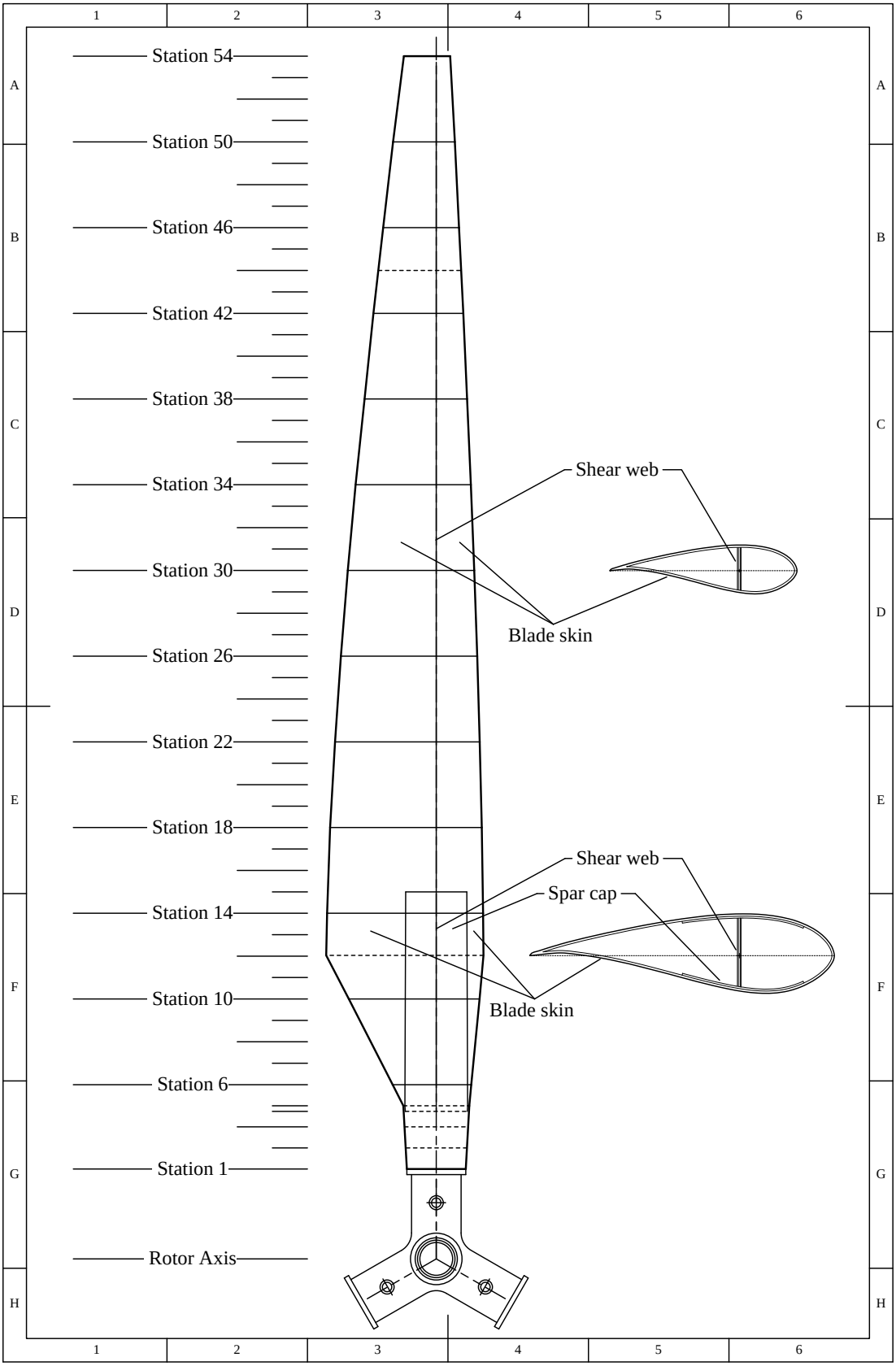

Figure A1. A topology of the pseudo SERI-8 blade

Table A1. Planform geometry data of a pseudo SERI-8 blade [62]

Station	Rotor Radius $r_{hub} + r$ (m)	Blade Radius r (m)	Chord Length c (m)	Blade Twist Angle β (deg)	Maximum Blade Thickness t_{max} (m)	Normalised x-offset of airfoil x/c (-)	Airfoil Profile
Hub	0.60	-0.04	N/A	N/A	N/A	N/A	Hub Flange
1	0.64	0.00	0.42	0	0.419	1	Root Flange
2	0.79	0.15	0.44	0	0.435	1	Circular
3	0.94	0.30	0.45	0	0.453	1	Circular
4	1.05	0.41	0.46	0	0.462	1	Circular
5	1.09	0.46	0.47	0	0.470	1	Circular
6	1.24	0.61	0.56	29.85	0.436	0.445*	Elliptic
7	1.40	0.76	0.66	28.03	0.403	0.399*	Elliptic
8	1.55	0.91	0.75	26.28	0.369	0.371*	Elliptic
9	1.70	1.07	0.84	24.60	0.336	0.349*	Elliptic
10	1.85	1.22	0.93	23.00	0.302	0.331*	Elliptic*
11	2.01	1.37	1.03	21.46	0.268	0.312*	Scaled S808*
12	2.16	1.52	1.12	20.00	0.235	0.3	S808
13	2.31	1.68	1.11	18.61	0.234	0.3	S808
14	2.46	1.83	1.11	17.28	0.233	0.3	S808
15	2.62	1.98	1.10	16.01	0.232	0.3	S808
16	2.77	2.13	1.09	14.81	0.197	0.3	S807
17	2.92	2.29	1.09	13.67	0.195	0.3	S807
18	3.07	2.44	1.08	12.59	0.194	0.3	S807
19	3.23	2.59	1.06	11.57	0.192	0.3	S807
20	3.38	2.74	1.05	10.61	0.189	0.3	S807
21	3.53	2.90	1.04	9.70	0.187	0.3	S807
22	3.68	3.05	1.03	8.85	0.185	0.3	S807
23	3.84	3.20	1.01	8.04	0.182	0.3	S807
24	3.99	3.35	1.00	7.29	0.180	0.3	S807
25	4.14	3.51	0.98	6.58	0.177	0.3	S807
26	4.29	3.66	0.97	5.93	0.174	0.3	S807
27	4.45	3.81	0.95	5.31	0.171	0.3	S807
28	4.60	3.96	0.93	4.74	0.145	0.3	S805A/S807
29	4.75	4.11	0.91	4.22	0.142	0.3	S805A/S807
30	4.90	4.27	0.90	3.73	0.139	0.3	S805A/S807
31	5.05	4.42	0.88	3.28	0.136	0.3	S805A/S807
32	5.21	4.57	0.86	2.87	0.133	0.3	S805A/S807
33	5.36	4.72	0.84	2.50	0.130	0.3	S805A/S807
34	5.51	4.88	0.82	2.16	0.127	0.3	S805A/S807
35	5.66	5.03	0.80	1.85	0.124	0.3	S805A/S807
36	5.82	5.18	0.78	1.57	0.121	0.3	S805A/S807
37	5.97	5.33	0.76	1.33	0.117	0.3	S805A/S807
38	6.12	5.49	0.73	1.11	0.114	0.3	S805A/S807
39	6.27	5.64	0.71	0.91	0.110	0.3	S805A/S807
40	6.43	5.79	0.69	0.74	0.093	0.3	S805A

Table A1. (continued)

Station	Rotor Radius $r_{hub} + r$ (m)	Blade Radius r (m)	Chord Length c (m)	Blade Twist Angle β (deg)	Maximum Blade Thickness t_{max} (m)	Normalised x-offset of airfoil x/c (-)	Airfoil Profile
41	6.58	5.94	0.67	0.59	0.090	0.3	S805A
42	6.73	6.10	0.64	0.47	0.087	0.3	S805A
43	6.88	6.25	0.62	0.36	0.083	0.3	S805A
44	7.04	6.40	0.59	0.27	0.080	0.3	S805A
45	7.19	6.55	0.57	0.20	0.077	0.3	S805A
46	7.34	6.71	0.54	0.14	0.068	0.3	S805A/S806A
47	7.49	6.86	0.52	0.09	0.065	0.3	S805A/S806A
48	7.65	7.01	0.49	0.06	0.062	0.3	S805A/S806A
49	7.80	7.16	0.47	0.03	0.058	0.3	S805A/S806A
50	7.95	7.32	0.44	0.02	0.055	0.3	S805A/S806A
51	8.10	7.47	0.41	0.01	0.047	0.3	S806A
52	8.26	7.62	0.39	0	0.044	0.3	S806A
53	8.41	7.77	0.36	0	0.041	0.3	S806A
54	8.56	7.92	0.33	0	0.038	0.3	S806A

Note:
- Rotor hub radius = 0.6 m
- Root flange thickness = 0.04 m
- Blade length = 7.92 m
- Rotor radius at tip = 8.56 m
- Blade skin thickness = 0.005 m (for all stations)
- Spar cap thickness = 0.005 m (for all stations)
- Shear web thickness = 0.005 m (for all stations)
- Fibreglass laminate = DD16 (for blade skin, spar cap and shear web) see also Table A2
- Life, drag and pitching moment coefficients of each airfoil profile are generated by XFOIL software [123]

* Defined by the author

Table A2. Fitting parameters for thirteen R-values for material DD16 and for small strands [14,69]

R-Value	Fitting Parameters		
	a	b	c
1.1	0.060	3.0	0.05
1.43	0.060	3.0	0.15
2	0.060	4.0	0.25
10	0.100	4.0	0.35
-2	0.010	4.0	0.55
-1	0.020	3.0	0.62
-0.5	0.450	0.85	0.25
0.1	0.420	0.58	0.18
0.5	0.075	2.5	0.43
0.7	0.040	2.5	0.45
0.8	0.035	2.5	0.40
0.9	0.060	2.5	0.28
1*	0.210	3.0	0.14

* Assumes a frequency of 10 Hz.

S-N Model: $\sigma_0 - \sigma = a\sigma\left[\frac{\sigma}{\sigma_0}\right]^b (N^c - 1)$

where σ = the maximum applied stress
σ_0 = the ultimate tensile (625 MPa) or compressive strength (400 MPa)
N = the number of cycles to failure
a , b , c = fitting parameters

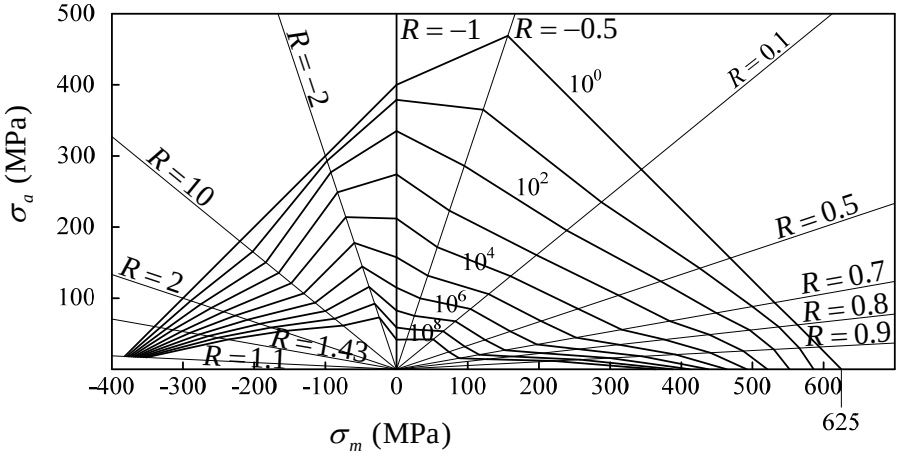

Figure A2. Goodman's diagram for thirteen R-values for material DD16 [14,69]

Table A3. *S-N* Family of the material DD16 (see all curves in Figures A3 and A4)

N	Maximum Applied Stress, MPa												
	R = 1.1	*R* = 1.43	*R* = 2	*R* = 10	*R* = -2	*R* = -1	*R* = -0.5	*R* = 0.1	*R* = 0.5	*R* = 0.7	*R* = 0.8	*R* = 0.9	*R* = 1
10^0	-400.00	-400.00	-400.00	-400.00	-400.00	-400.00	625.00	625.00	625.00	625.00	625.00	625.00	625.00
10^1	-397.15	-390.96	-384.64	-367.54	-390.91	-379.47	487.02	523.20	568.20	588.23	596.85	596.21	586.33
10^2	-394.14	-380.45	-366.49	-334.44	-369.02	-335.30	381.27	434.33	495.31	528.49	550.51	558.47	552.45
10^3	-390.96	-368.55	-346.15	-301.14	-331.60	-274.06	296.90	357.30	416.14	452.43	488.19	513.46	521.38
10^4	-387.62	-355.41	-324.32	-268.51	-284.78	-211.56	229.23	291.26	339.61	372.14	417.74	463.97	492.20
10^5	-384.12	-341.23	-301.69	-237.38	-236.79	-157.58	175.36	235.39	271.20	297.20	347.49	412.95	464.44
10^6	-380.45	-326.25	-278.90	-208.37	-192.75	-114.84	133.01	188.73	213.17	232.48	283.02	362.89	437.87
10^7	-376.63	-310.71	-256.44	-181.85	-154.73	-82.55	100.14	150.25	165.65	179.24	227.01	315.58	412.36
10^8	-372.66	-294.82	-234.71	-157.97	-123.06	-58.82	74.93	118.88	127.68	136.80	180.09	272.12	387.86
10^9	-368.55	-278.82	-214.00	-136.71	-97.24	-41.67	55.78	93.56	97.83	103.67	141.71	233.05	364.34

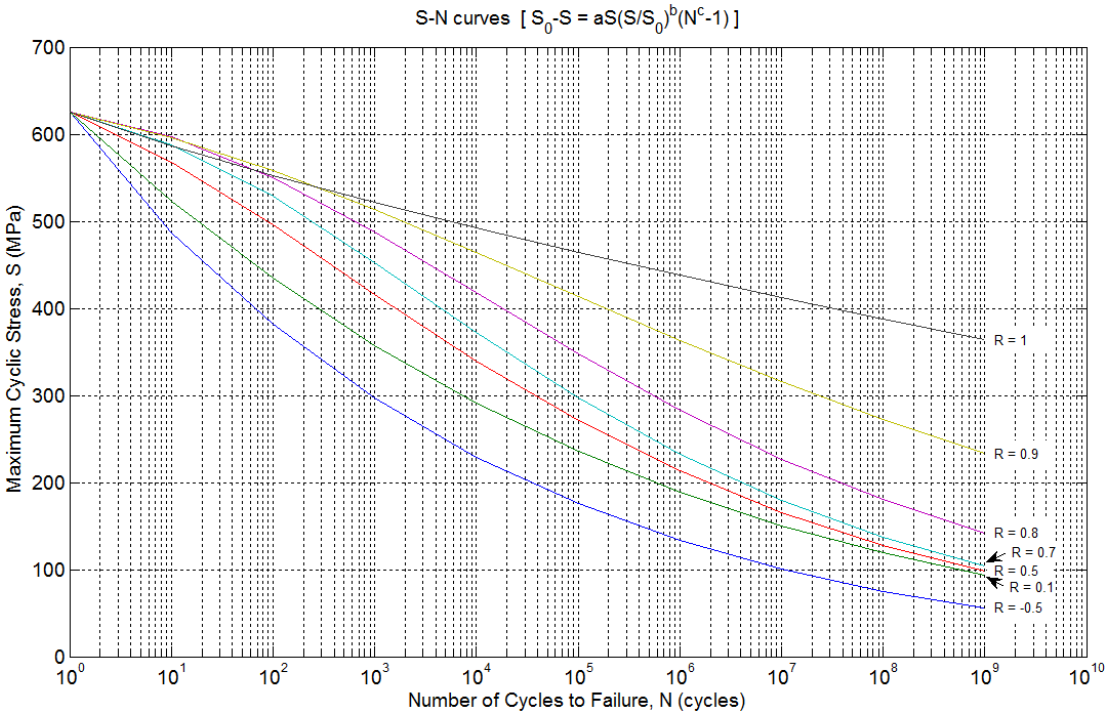

Figure A3. *S-N* curves of DD16 composite material with *R*-ratio of 1, 0.9, 0.8, 0.7, 0.5, 0.1 and -0.5

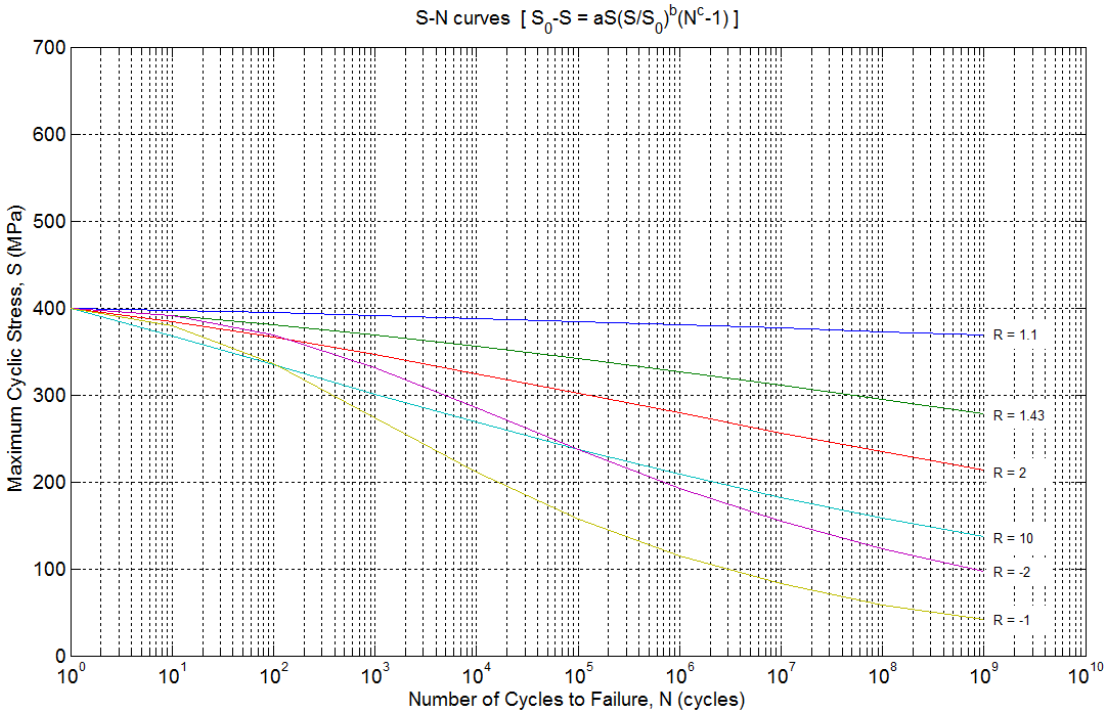

Figure A4. *S-N* curves of DD16 composite material with *R*-ratio of -1, -2, 10, 2, 1.43 and 1.1

Appendix B

Data for Validation

This appendix contains data used for validating HAWTsimulator and aerodynamic simulation of Micon 65 wind turbine.

B1. Data for Validation of HAWTsimulator

HAWTsimulator is validated by comparing simulated results with those generated by WT_Perf (v3.00, 21st June 2004) [49].

Table B1. Data of AWT-27CR2 wind turbine [49]

Issues	Descriptions
Turbine model	AWT-27CR2
Orientation	Downwind
Rated power, P	300 kW
Number of blades, B	2
Rotor radius, R	13.757 m
Hub radius, r_{hub}	1.184 m
Coning angle, δ	7°
Pitch angle, ϕ	$-2^\circ, -1^\circ, 0^\circ$
Rotor speed, Ω	53.333 rpm
Number of blade elements, n_{segment}	17
Air density, ρ	$1.225\ \text{kg}/\text{m}^3$
Hub height, H_0	42.672 m
Range of wind speed at hub height	Cut-in: $5\ \text{m/s}$ Cut-out: $22\ \text{m/s}$ Step of increment: $0.5\ \text{m/s}$
Annual average wind speed at site	$5.6\ \text{m/s}$
Windmill brake state model	Advanced brake state model
Tip loss model	Prandtl
Hub loss model	Prandtl
Use drag term in the axial induction calculation	Yes
Use drag term in the tangential induction factor	Yes
Error tolerance for induction iterations	1×10^{-6}
Error tolerance for tangential induction iteration	1×10^{-6}

Table B2. Data loaded to HAWTsimulator in simulating AWT-27CR2 wind turbine

Section	r/R	c/R	Pretwist Angle β (deg)	Airfoil No.	Twist Axis x/c	t_{max}/c
1	0.1089	0.0563	6.100	1	0.3	0.24
2	0.1546	0.0632	5.764	1	0.3	0.24
3	0.2232	0.0699	5.470	1	0.3	0.24
4	0.3145	0.0805	4.996	2	0.3	0.24
5	0.4060	0.0834	4.208	3	0.3	0.24
6	0.4973	0.0792	3.172	4	0.3	0.24
7	0.5887	0.0738	2.086	5	0.3	0.21
8	0.6801	0.0677	1.117	6	0.3	0.21
9	0.7715	0.0603	0.424	7	0.3	0.21
10	0.8401	0.0517	0.122	8	0.3	0.21
11	0.8857	0.0470	0.076	9	0.3	0.21
12	0.9177	0.0419	0.048	9	0.3	0.21
13	0.9360	0.0391	0.041	9	0.3	0.21
14	0.9543	0.0364	0.033	9	0.3	0.21
15	0.9726	0.0334	0.023	10	0.3	0.21
16	0.9863	0.0301	0.012	10	0.3	0.21
17	0.9954	0.0285	0.006	10	0.3	0.21

Note:

1. Data in Table B2 is extracted from subfolders of WT_Perf [49], which can be downloaded from http://wind.nrel.gov/designcodes/simulators/wtperf/.

2. Data in the columns r/R, c/R, β, x/c, and t_{max}/c are extracted from x:\WTP_v310b-mlb_all\Source\CertTest\Test02_AWT27.wtp

3. Aerodynamic tables of each airfoil can be found from:

Airfoil No.1: x:\WTP_v310b-mlb_all\Source\CertTest\Airfoils\AWT-27\AWT27_05.dat
Airfoil No.2: x:\WTP_v310b-mlb_all\Source\CertTest\Airfoils\AWT-27\AWT27_15.dat
Airfoil No.3: x:\WTP_v310b-mlb_all\Source\CertTest\Airfoils\AWT-27\AWT27_25.dat
Airfoil No.4: x:\WTP_v310b-mlb_all\Source\CertTest\Airfoils\AWT-27\AWT27_35.dat
Airfoil No.5: x:\WTP_v310b-mlb_all\Source\CertTest\Airfoils\AWT-27\AWT27_45.dat
Airfoil No.6: x:\WTP_v310b-mlb_all\Source\CertTest\Airfoils\AWT-27\AWT27_55.dat
Airfoil No.7: x:\WTP_v310b-mlb_all\Source\CertTest\Airfoils\AWT-27\AWT27_65.dat
Airfoil No.8: x:\WTP_v310b-mlb_all\Source\CertTest\Airfoils\AWT-27\AWT27_75.dat
Airfoil No.9: x:\WTP_v310b-mlb_all\Source\CertTest\Airfoils\AWT-27\AWT27_85.dat
Airfoil No.10: x:\WTP_v310b-mlb_all\Source\CertTest\Airfoils\AWT-27\AWT27_95.dat

B2. Data for Validation of Micon 65 Wind Turbine

Specification of Micon 65 wind turbine is not completely reported by only one research group. The data listed in Table B3 are collected from reports and research papers done by several researchers who did research on SERI-8 blade and Micon 65.

Table B3. Data of Micon 65 wind turbine

Issues	Descriptions	Reference	Remarks
Turbine model	Micon 65	[59-61]	
Rated power	65 kW	[59-61]	
Orientation	Upwind	[61]	
Number of blades	3	[61]	
Rotor radius	8.56 m	[62]	
Hub radius	0.64 m	[62]	
Blade length	7.92 m	[62]	
Coning angle	0°		Assumed
Pitch angle	3.46°	[59]	
Rotor speed	44 rpm		
Air density	$1.225\,\mathrm{kg/m^3}$		Assumed
Hub height	22.86 m		
Wind shear exponent	0.127	[124]	
Annual average wind speed at site	5.81 m/s	[125]	

Table B4. Aerodynamic simulation conditions of Micon 65 wind turbine

Issues	Descriptions
Number of blade elements	14
Range of wind speed at hub height	Start: 0.5 m/s End: 25 m/s Step of increment: 0.5 m/s
Windmill brake state model	Shen's correction
Tip loss model	Shen
Hub loss model	Prandtl
Use drag term in the axial induction calculation	Yes
Use drag term in the tangential induction factor	Yes
Error tolerance for induction iterations	1×10^{-6}
Error tolerance for tangential induction iteration	1×10^{-6}

Table B5. Data to be loaded to HAWTsimulator in simulating Micon 65 wind turbine

Section	r/R	c/R	Pretwist Angle β (deg)	Airfoil No.	Twist Axis x/c	$t_{\max}/c$
1	0.0920	0.0508	0	1	0.3	1
2	0.1454	0.0657	29.85	2	0.3	0.21
3	0.2166	0.1090	23.00	2	0.3	0.21
4	0.2878	0.1296	17.28	2	0.3	0.21
5	0.3590	0.1256	12.59	3	0.3	0.18
6	0.4303	0.1199	8.85	3	0.3	0.18
7	0.5015	0.1128	5.93	3	0.3	0.18
8	0.5727	0.1047	3.73	4	0.3	0.16
9	0.6439	0.0957	2.16	4	0.3	0.16
10	0.7151	0.0858	1.11	4	0.3	0.16
11	0.7863	0.0750	0.47	5	0.3	0.14
12	0.8575	0.0636	0.14	6	0.3	0.12
13	0.9288	0.0514	0.02	6	0.3	0.12
14	0.9822	0.0418	0	7	0.3	0.11

Note:

1. Airfoil shapes for each airfoil No. are as follows:
   Airfoil No.1: Circular
   Airfoil No.2: S808
   Airfoil No.3: S807
   Airfoil No.4: S805A/S807
   Airfoil No.5: S805A
   Airfoil No.6: S805A/S806A
   Airfoil No.7: S806A
2. Airfoil characteristics (α, C_L, C_D and $C_{M_{1/4}}$) of each airfoil are generated by XFOIL software [123,126].

Appendix C

Description of HAWTfatigue

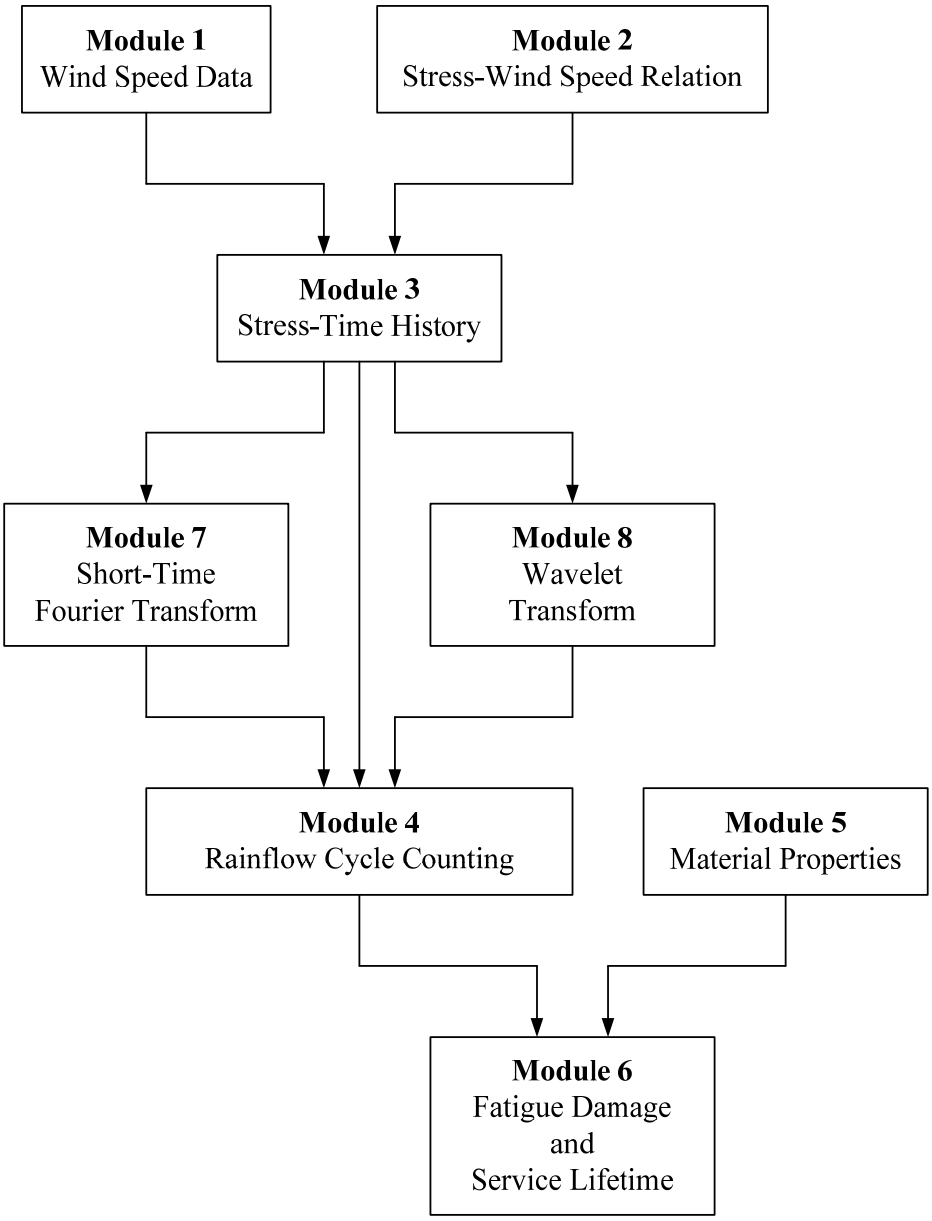

Figure C1. Modules of HAWTfatigue

In this research project, it is necessary to develop a fatigue computer code, HAWTfatigue. The objectives of the code are to edit the stress-time history and to predict fatigue damage and service lifetime of HAWT blades. The code is designed to be run in Matlab environment. In predicting service lifetime, the code is mainly based on stress-life approach and Miner's linear cumulative damage rule. In the code, there are eight modules illustrated by flowchart in Figure C1. The flowchart shows a big picture of how HAWTfatigue works. Basically, the code contains a general process in evaluating the fatigue damage and service lifetime starting at Module 1 and finishing at Module 6. Modules 7 and 8 are added to the general process to edit the stress-time history. Next sections, how HAWTfatigue works has been briefly explained module-by-module.

Module 1: Wind Speed Data

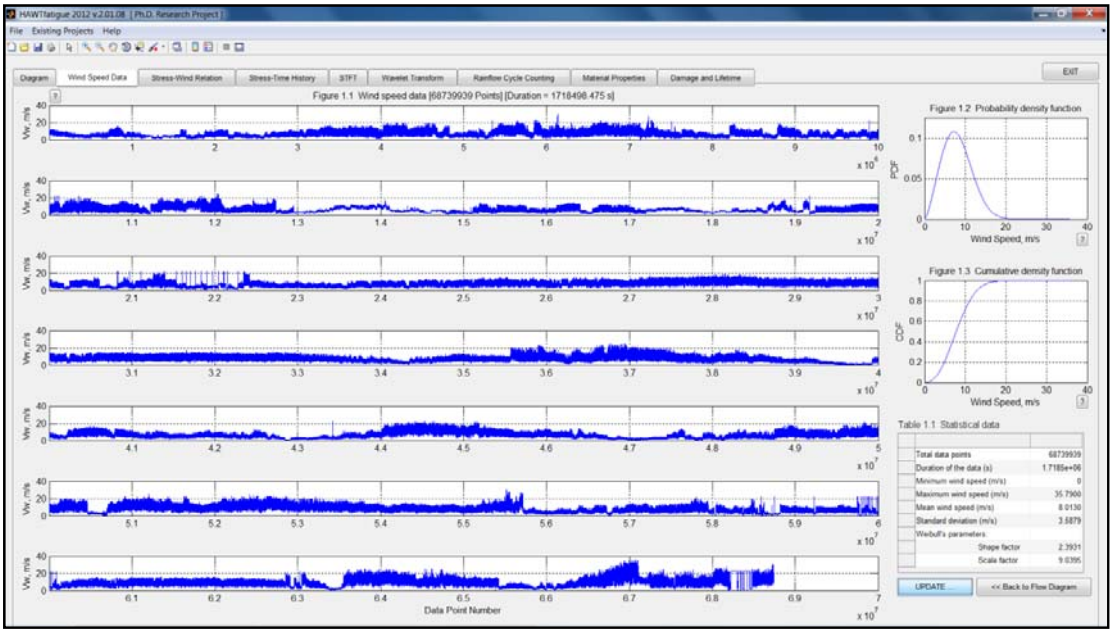

Figure C2. Module 1: Wind speed data

Module 1 is used to load the wind speed data into the code. The pattern of the wind speed data is displayed. The statistical parameters which are minimum, maximum, mean, standard deviation, Weibull's probability density function (PDF) and Weibull's cumulative distribution function (CDF) of the wind speed are also displayed. The Weibull probability density function (PDF) and the cumulative distribution function (CDF) are calculated from

$$\mathrm{PDF}(V_w) = \left(\frac{k}{c}\right)\left(\frac{V_w}{c}\right)^{k-1} \exp\left[-\left(\frac{V_w}{c}\right)^{k}\right] \tag{C1}$$

$$\mathrm{CDF}(V_w) = 1 - \exp\left[-\left(\frac{V_w}{c}\right)^{k}\right] \tag{C2}$$

where a shape factor is given by [37]

$$k = \left(\frac{\sigma}{\overline{V}_w}\right)^{-1.086} \tag{C3}$$

and a scale factor is given by [37]

$$c = \frac{\overline{V}_w}{\Gamma(1+1/k)} \tag{C4}$$

Gamma function in the denominator of Equation C4 is calculated by using a Matlab command `gamma(1+1/k)`.

Module 2: Relationship between Wind Speed and Stress

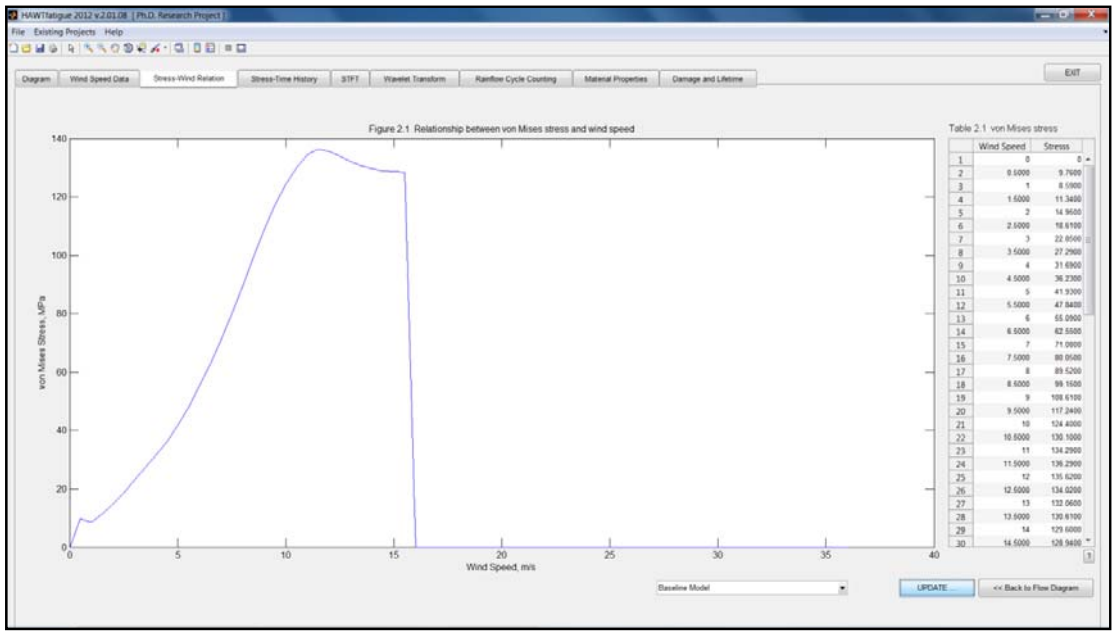

Figure C3. Module 2: Wind speed-stress relationship

The module is used to generate a relationship between wind speed data and von-Mises stress in the range of wind speed value from minimum to maximum. There are three codes

directly relevant to this module. HAWTsimulator is used to generate the sets of aerodynamic loads at different wind speeds ranging from cut-in to cut-out. NuMAD is used to generate a finite element model of the pseudo SERI-8 blade. Both the sets of aerodynamic loads and the finite element model are imported to ANSYS structural software to determine a critical value of von-Mises stress and its location on the blade. Having finished a set of stress simulations in ANSYS, a curve of von-Mises stress versus wind speed is generated.

Module 3: Original Stress-Time History

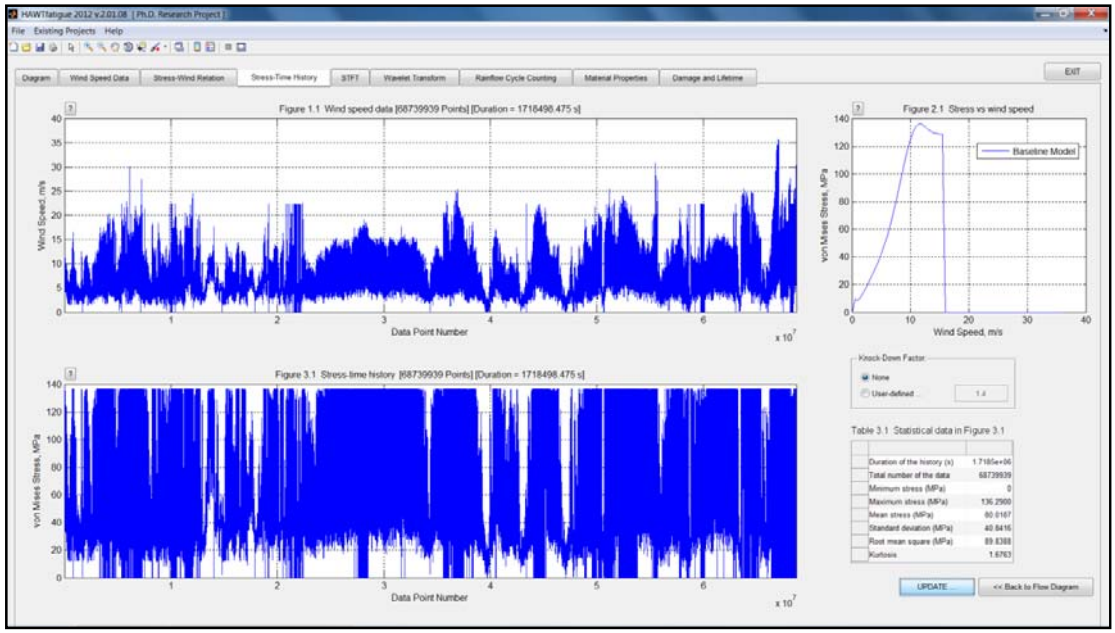

Figure C4. Module 3: Original stress-time history

The module is used to generate a stress-time history which is one of the important parts of this research project. By relating the relationship between wind speed and time from Module 2 with the relationship between wind speed and von-Mises stress, the stress-time history is generated. This history is treated as an original stress-time history.

Module 4: Rainflow Cycle Counting

The module is used to count rainflow cycles contained in the stress-time history generated by Module 3 or edited stress-time history generated by Modules 7, 8 or 9. Rainflow algorithm implemented in the module is a simplified rainflow counting for repeating histories recommended by ASTM E 1049-85 [84]. Rainflow cycles counted are

plotted in a three-dimensional histogram to illustrate the pairs of stress range and mean stress, and a number of cycles counted. Also, the statistical parameters of rainfall cycles are displayed on the GUI.

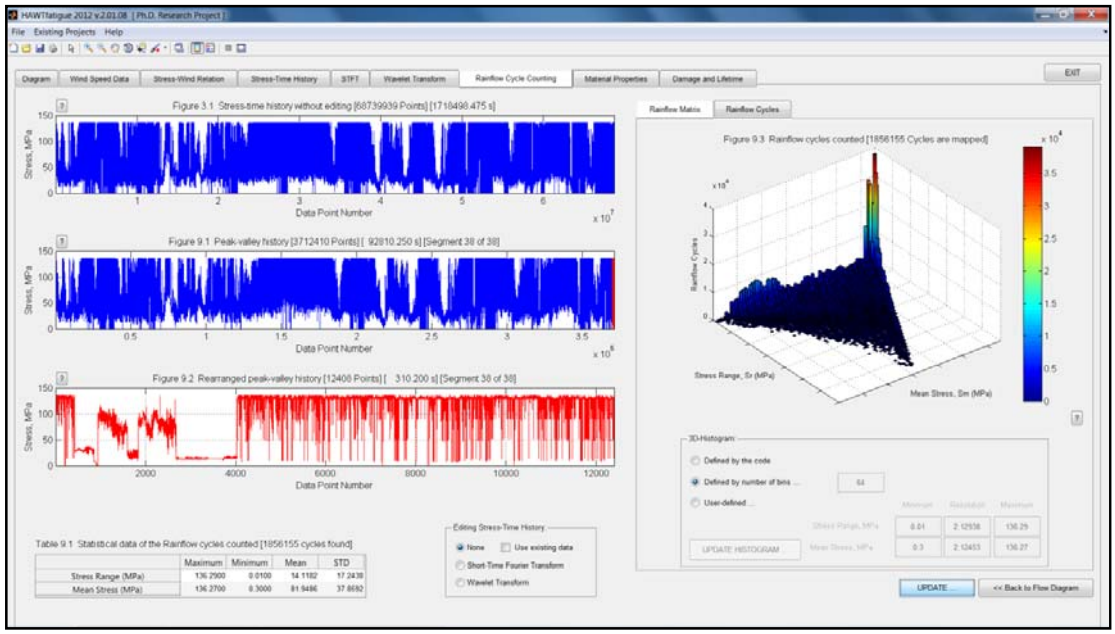

Figure C5. Module 4: Rainfall cycle counting

Module 5: Material Properties

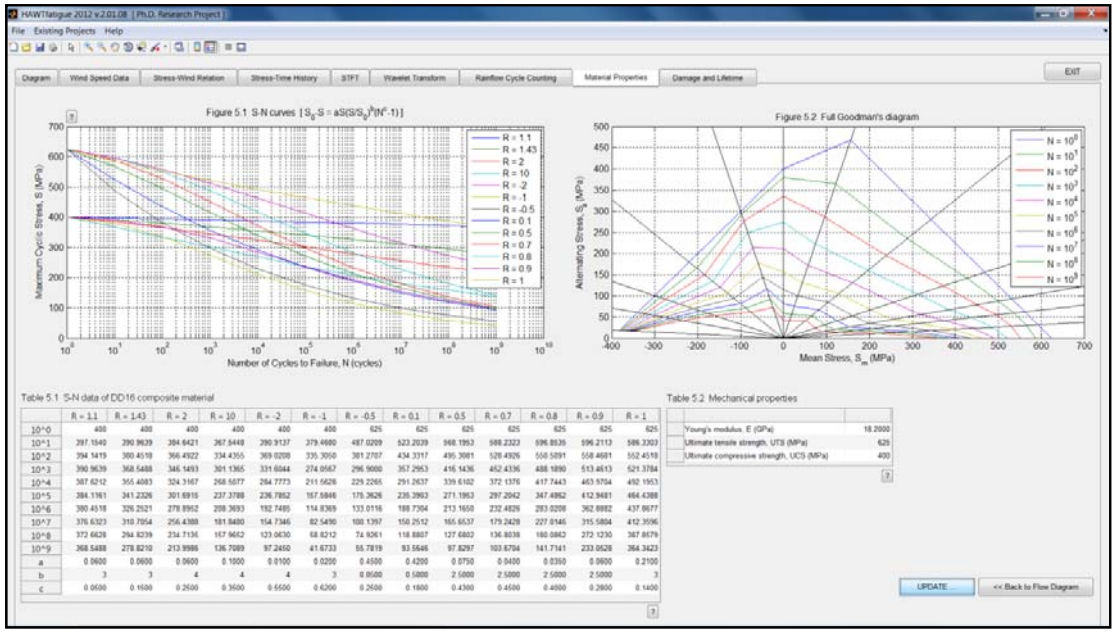

Figure C6. Module 5: Module of material properties

The module is mainly used to load mechanical properties and a set of $S-N$ curves from data files and store them in the memory. Then the code plots the $S-N$ curves, generates the Goodman's diagram, and displays $S-N$ data in the tabular form as shown in Figure C6. Material properties will be used by Module 6.

Module 6: Fatigue Damage and Service Lifetime

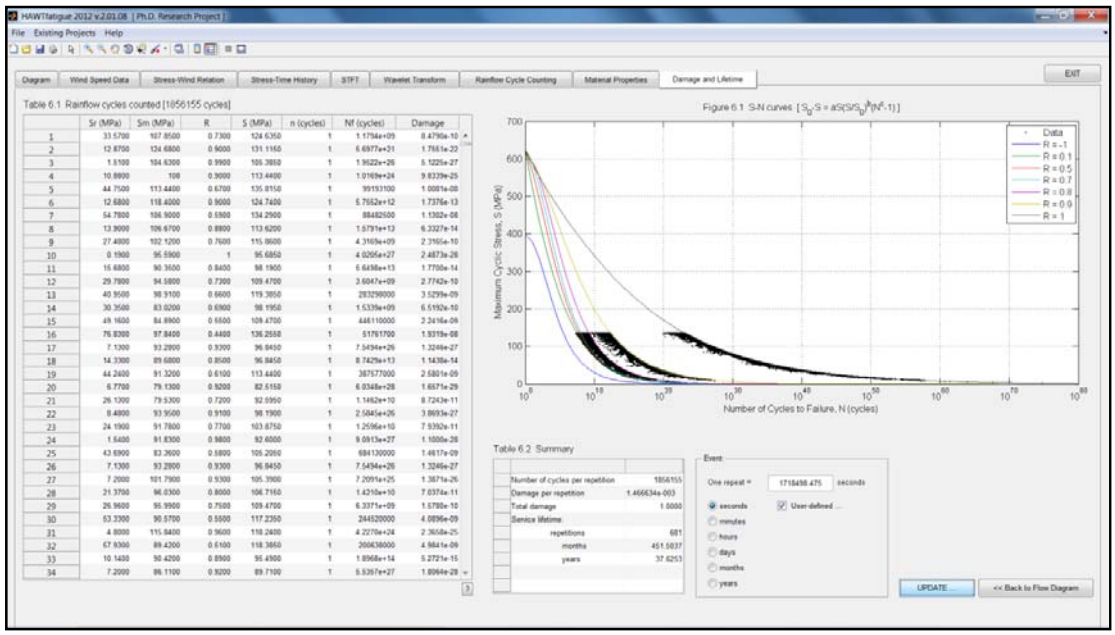

Figure C7. Module 6: Fatigue damage and service lifetime

The module is used to evaluate fatigue damage by using Miner's linear cumulative damage rule. In general, each rainflow cycle counted by Module 5 has different values of R-ratio, so the code interpolates for the number of cycles to failure of each cycle from a family of $S-N$ curves prepared in Module 1. By using Miner's rule, fatigue damage is calculated and converted to service lifetime in the unit of repetitions, months and years. In addition, the code displays each rainflow cycle counted on a plot of $S-N$ as shown in Figure C7.

Module 7: Short-Time Fourier Transform

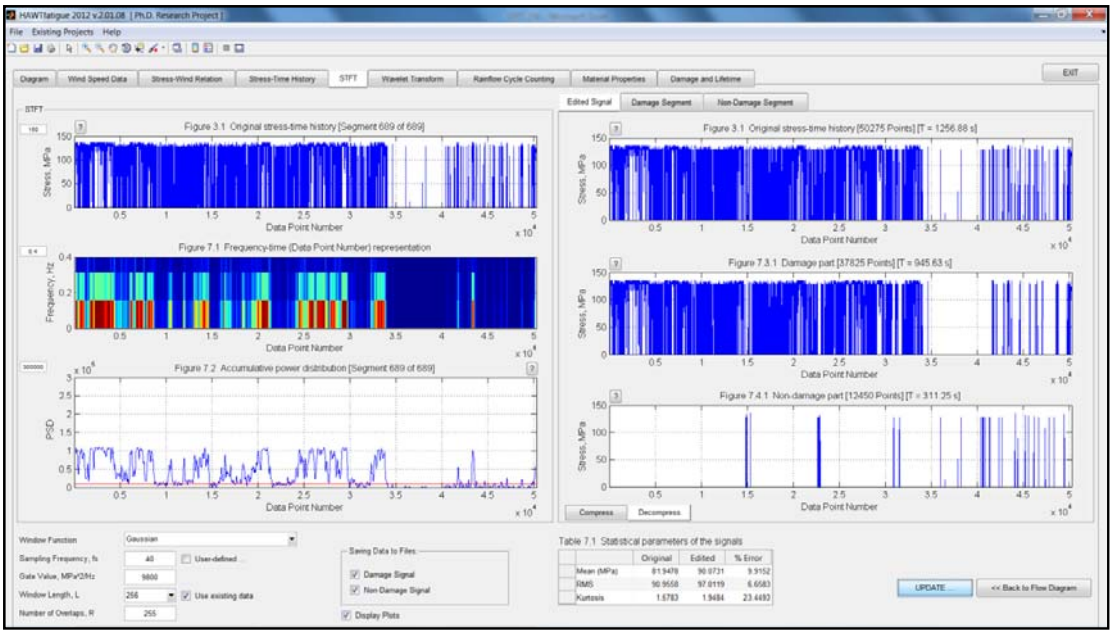

Figure C8. Module 7: Short-time Fourier transform

The module is used to edit the stress-time history in the time-frequency domain by means of STFT-based fatigue damage part extracting method (see Sections 6.2 and 6.3). In the STFT process, stress-time history is divided into small windows. FFT is taken to the signal in each window. The result of STFT is a spectrogram which provides information of time, frequency and power spectral density (PSD). A plot of accumulative power spectral density (AccPSD) distribution is generated by summing PSD of all frequency bands at each time interval. AccPSD for STFT has been introduced in Section 5.5.2. The plot of AccPSD distribution provides the time locations of fatigue damage events in the stress-time history. The fatigue damage events can be determined by a cutoff level. The cutoff level is an appropriate value of AccPSD which is used to separate the damage and non-damage parts contained in the original stress-time history. The events having AccPSD level equal or higher than the cutoff level are classified as damage parts. On the other hand, the events having AccPSD level lower than the cutoff level are classified as non-damage parts. The damage parts are concatenated to form an edited stress-time history.

Module 8: Wavelet Transform

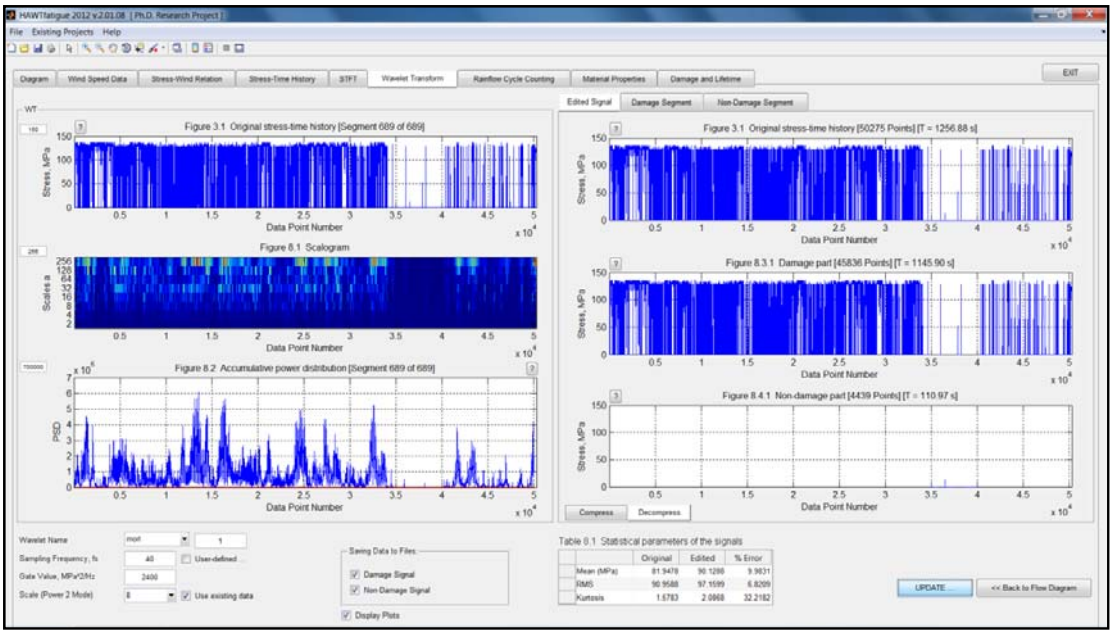

Figure C9. Module 8: Wavelet transform

The module is used to edit the stress-time history in the time-scale domain by means of WT-based fatigue damage part extracting method (see Sections 6.2 and 6.3). In the process, WT is the sum over all time of the history multiplied by scaled, shifted versions of the wavelet. This process produces wavelet coefficients as a function of scale and position. In the first step of WT algorithm, a wavelet is taken and compared to a section at the start of the history. In the second step, a wavelet coefficient is calculated by comparing the energy of the history and the energy of the wavelet. The wavelet coefficient represents how closely correlated the wavelet with this section of the history. The wavelet coefficient may be interpreted as a correlation coefficient. The higher value of wavelet coefficient is, the more the similarity is. It is noted that the results will depend on the shape of the selected wavelet [109]. In the third step, the wavelet is shifted to the right and then the first and the second steps are repeated, respectively. In the fourth step, the wavelet is scaled or stretched and then the process is repeated from the first step to the third step. In the last step, the process is repeated from the first step to the fourth step for all scales. The result of this process is the wavelet coefficients produced at different scales and different sections of the history. To make sense of all coefficients, a plot on which the x-axis represents position along the history (time or data point number), the y-axis represents

scale, and the colour at each x - y point represents the magnitude of the wavelet coefficient. This plot is called scalogram. A plot of accumulative power spectral density (AccPSD) distribution is generated by summing the power spectral density (PSD) of wavelet coefficients for all scale bands at each time interval (see Section 5.6.2). This plot provides the locations of the fatigue damage events in the original stress-time history. The damage events can be determined by a cutoff level. The cutoff level is an appropriate value of AccPSD level which is used to separate the damage and non-damage events in the original stress-time history. The events having AccPSD level equal or higher than the cutoff level are classified as damage parts. On the other hand, the events having AccPSD level lower than the cutoff level are classified as non-damage parts. The damage parts are concatenated to form an edited stress-time history.

Appendix D

Results from Stress-Time History Editing

This appendix contains raw data obtained from each simulation mentioned in Chapter 7. Data are separated into three groups as follows:

Group 1: Raw data for selecting window size used in taking STFT (Tables D1 to D8)

Group 2: Raw data for selecting wavelet decomposition level in taking WT (Tables D9 to D17)

Group 3: Raw data for selecting cutoff level of each wavelet type (Tables D18 to D21)

Table D1. Data from the edited stress-time histories generated by STFT with window size of 2 points (Max. AccPSD = 928.7 Engery/Hz)

Cutoff Level (Energy/Hz)	Normalised Cutoff Level	Length of the Edited History (Points)	Fatigue Damage per Repetition	% Reduction in Length of the Edited History	% Error [(+) and (-) signs mean less than and greater than, respectively.]			
					Fatigue Damage per Repetition	Mean Stress	rms	Kurtosis
0	0	68,739,939	1.466634E-03	0	0	0	0	0
5	5.3836E-03	67,292,474	1.594460E-03	2.11	-8.716	0.28	0.17	-1.28
10	1.0767E-02	66,671,071	1.614337E-03	3.01	-10.071	-0.50	-0.28	-0.77
15	1.6151E-02	65,875,215	1.640265E-03	4.17	-11.839	-1.49	-0.87	-0.32
20	2.1534E-02	65,162,095	1.670902E-03	5.20	-13.928	-2.35	-1.40	-0.18
25	2.6918E-02	64,253,748	1.684498E-03	6.53	-14.855	-3.44	-2.07	-0.20
30	3.2302E-02	63,314,734	1.693167E-03	7.89	-15.446	-4.56	-2.78	-0.38
35	3.7685E-02	62,573,725	1.713774E-03	8.97	-16.851	-5.44	-3.35	-0.62
40	4.3069E-02	61,635,891	1.723712E-03	10.33	-17.528	-6.54	-4.07	-1.13
45	4.8452E-02	60,716,512	1.739346E-03	11.67	-18.594	-7.63	-4.78	-1.78
50	5.3836E-02	59,826,961	1.763941E-03	12.97	-20.271	-8.68	-5.48	-2.54
55	5.9219E-02	59,006,069	1.780594E-03	14.16	-21.407	-9.65	-6.13	-3.37
60	6.4603E-02	57,988,175	1.792670E-03	15.64	-22.230	-10.87	-6.95	-4.59
70	7.5370E-02	56,468,531	1.813862E-03	17.85	-23.675	-12.70	-8.19	-6.79
80	8.6137E-02	55,012,126	1.822711E-03	19.97	-24.279	-14.46	-9.40	-9.59
90	9.6905E-02	53,626,238	1.833947E-03	21.99	-25.045	-16.15	-10.58	-12.92
100	1.0767E-01	51,851,373	1.833804E-03	24.57	-25.035	-18.33	-12.11	-18.53
150	1.6151E-01	46,203,522	1.827236E-03	32.79	-24.587	-25.64	-17.32	-48.57
200	2.1534E-01	42,500,816	1.798237E-03	38.17	-22.610	-30.56	-20.92	-89.45
250	2.6918E-01	39,643,841	1.735324E-03	42.33	-18.320	-34.31	-23.74	-144.14
300	3.2302E-01	36,965,643	1.626389E-03	46.22	-10.893	-37.74	-26.38	-228.46
350	3.7685E-01	34,468,487	1.481580E-03	49.86	-1.019	-40.89	-28.85	-355.42

Table D2. Data from the edited stress-time histories generated by STFT with window size of 4 points (Max. AccPSD = 1,857.5 Engery/Hz)

Cutoff Level (Energy/Hz)	Normalised Cutoff Level	Length of the Edited History (Points)	Fatigue Damage per Repetition	% Reduction in Length of the Edited History	% Error [(+) and (-) signs mean less than and greater than, respectively.]			
					Fatigue Damage per Repetition	Mean Stress	rms	Kurtosis
0	0	68,739,939	1.466634E-03	0	0	0	0	0
10	5.3836E-03	67,413,179	1.470579E-03	1.93	-0.269	0.46	0.26	-1.87
20	1.0767E-02	66,821,498	1.481382E-03	2.79	-1.006	-0.29	-0.17	-1.46
30	1.6151E-02	66,056,021	1.484301E-03	3.90	-1.205	-1.23	-0.73	-1.14
40	2.1534E-02	65,380,821	1.486186E-03	4.89	-1.333	-2.05	-1.23	-1.11
50	2.6918E-02	64,499,199	1.487860E-03	6.17	-1.447	-3.10	-1.89	-1.27
60	3.2301E-02	63,584,474	1.488701E-03	7.50	-1.505	-4.18	-2.57	-1.61
70	3.7685E-02	62,880,363	1.489174E-03	8.52	-1.537	-5.01	-3.10	-1.99
80	4.3069E-02	61,968,677	1.490104E-03	9.85	-1.600	-6.08	-3.80	-2.68
90	4.8452E-02	61,087,033	1.490557E-03	11.13	-1.631	-7.11	-4.48	-3.52
100	5.3836E-02	60,244,263	1.490806E-03	12.36	-1.648	-8.10	-5.13	-4.48
110	5.9219E-02	59,472,482	1.491495E-03	13.48	-1.695	-9.01	-5.74	-5.49
120	6.4603E-02	58,494,886	1.492235E-03	14.90	-1.746	-10.16	-6.52	-7.01
130	6.9987E-02	57,712,384	1.492664E-03	16.04	-1.775	-11.09	-7.15	-8.40
140	7.5370E-02	57,040,983	1.493067E-03	17.02	-1.802	-11.90	-7.70	-9.70
150	8.0754E-02	56,327,412	1.493422E-03	18.06	-1.826	-12.75	-8.28	-11.29
200	1.0767E-01	52,555,596	1.496417E-03	23.54	-2.031	-17.30	-11.46	-23.50
300	1.6151E-01	47,104,657	1.522323E-03	31.47	-3.797	-24.22	-16.39	-57.88
400	2.1534E-01	43,522,163	1.507500E-03	36.69	-2.786	-28.87	-19.81	-103.35
500	2.6918E-01	40,746,497	1.479604E-03	40.72	-0.884	-32.45	-22.49	-160.95
600	3.2301E-01	38,159,956	1.428753E-03	44.49	+2.583	-35.69	-24.99	-241.65
700	3.7685E-01	35,741,992	1.365187E-03	48.00	+6.917	-38.66	-27.32	-351.35

Table D3. Data from the edited stress-time histories generated by STFT with window size of 8 points (Max. AccPSD = 3,715 Engery/Hz)

Cutoff Level (Energy/Hz)	Normalised Cutoff Level	Length of the Edited History (Points)	Fatigue Damage per Repetition	% Reduction in Length of the Edited History	% Error [(+) and (-) signs mean less than and greater than, respectively.]			
					Fatigue Damage per Repetition	Mean Stress	rms	Kurtosis
0	0	68,739,939	1.466634E-03	0	0	0	0	0
10	2.6918E-03	67,793,368	1.465527E-03	1.38	+0.075	0.99	0.54	-3.07
20	5.3836E-03	67,638,540	1.461978E-03	1.60	+0.317	0.79	0.43	-2.88
30	8.0754E-03	67,546,741	1.458979E-03	1.74	+0.522	0.67	0.36	-2.79
40	1.0767E-02	67,083,437	1.456895E-03	2.41	+0.664	0.09	0.02	-2.62
50	1.3459E-02	66,669,410	1.456119E-03	3.01	+0.717	-0.42	-0.28	-2.53
60	1.6151E-02	66,344,473	1.453244E-03	3.48	+0.913	-0.82	-0.52	-2.37
70	1.8843E-02	66,093,357	1.452924E-03	3.85	+0.935	-1.13	-0.70	-2.36
100	2.6918E-02	64,847,686	1.452428E-03	5.66	+0.969	-2.61	-1.62	-2.78
150	4.0377E-02	62,797,135	1.451629E-03	8.65	+1.023	-5.01	-3.15	-4.37
200	5.3836E-02	60,794,407	1.450954E-03	11.56	+1.069	-7.34	-4.69	-6.96
250	6.7295E-02	58,652,741	1.450323E-03	14.67	+1.112	-9.83	-6.37	-10.97
300	8.0754E-02	57,106,702	1.449766E-03	16.92	+1.150	-11.65	-7.61	-14.79
350	9.4213E-02	55,506,927	1.448362E-03	19.25	+1.246	-13.54	-8.92	-19.79
400	1.0767E-01	53,556,342	1.445301E-03	22.09	+1.455	-15.86	-10.55	-27.73
500	1.3459E-01	50,358,430	1.434510E-03	26.74	+2.190	-19.80	-13.34	-44.92
600	1.6151E-01	48,123,038	1.429529E-03	29.99	+2.530	-22.62	-15.36	-63.57
700	1.8843E-01	46,288,876	1.425168E-03	32.66	+2.827	-24.95	-17.06	-84.43
800	2.1534E-01	44,768,099	1.419057E-03	34.87	+3.244	-26.88	-18.49	-106.43
900	2.4226E-01	43,389,964	1.410916E-03	36.88	+3.799	-28.62	-19.79	-130.90
1,000	2.6918E-01	42,165,557	1.401001E-03	38.66	+4.475	-30.16	-20.95	-156.78
1,100	2.9610E-01	40,902,849	1.387765E-03	40.50	+5.378	-31.72	-22.14	-188.08

Table D4. Data from the edited stress-time histories generated by STFT with window size of 16 points (Max. AccPSD = 7,428.7 Engery/Hz)

Cutoff Level (Energy/Hz)	Normalised Cutoff Level	Length of the Edited History (Points)	Fatigue Damage per Repetition	% Reduction in Length of the Edited History	% Error [(+) and (-) signs mean less than and greater than, respectively.]			
					Fatigue Damage per Repetition	Mean Stress	rms	Kurtosis
0	0	68,739,939	1.466634E-03	0	0	0	0	0
25	3.3653E-03	67,972,322	1.465384E-03	1.12	+0.085	1.25	0.67	-3.80
50	6.7307E-03	67,797,137	1.464233E-03	1.37	+0.164	1.03	0.55	-3.65
75	1.0096E-02	67,447,511	1.463691E-03	1.88	+0.201	0.59	0.29	-3.52
100	1.3461E-02	66,922,109	1.463544E-03	2.64	+0.211	-0.06	-0.09	-3.50
200	2.6923E-02	65,149,248	1.463108E-03	5.22	+0.240	-2.17	-1.39	-4.22
300	4.0384E-02	63,188,013	1.462739E-03	8.08	+0.266	-4.46	-2.85	-6.18
400	5.3845E-02	61,252,826	1.462535E-03	10.89	+0.279	-6.68	-4.31	-9.20
500	6.7307E-02	59,266,807	1.461732E-03	13.78	+0.334	-8.97	-5.86	-13.45
1,000	1.3461E-01	51,301,460	1.457169E-03	25.37	+0.645	-18.34	-12.43	-49.74
1,500	2.0192E-01	46,481,857	1.450545E-03	32.38	+1.097	-24.31	-16.76	-99.06
2,000	2.6923E-01	43,256,924	1.438653E-03	37.07	+1.908	-28.30	-19.74	-153.89

Table D5. Data from the edited stress-time histories generated by STFT with window size of 32 points (Max. AccPSD = 14,852 Engery/Hz)

Cutoff Level (Energy/Hz)	Normalised Cutoff Level	Length of the Edited History (Points)	Fatigue Damage per Repetition	% Reduction in Length of the Edited History	% Error [(+) and (-) signs mean less than and greater than, respectively.]			
					Fatigue Damage per Repetition	Mean Stress	rms	Kurtosis
0	0	68,739,939	1.466634E-03	0	0	0	0	0
100	6.7331E-03	67,944,851	1.465645E-03	1.16	+0.067	1.24	0.65	-4.19
200	1.3466E-02	67,092,526	1.465274E-03	2.40	+0.093	0.23	0.06	-4.19
300	2.0199E-02	66,357,290	1.465483E-03	3.47	+0.078	-0.69	-0.50	-4.47
400	2.6932E-02	65,355,079	1.465317E-03	4.92	+0.090	-1.87	-1.23	-5.21
500	3.3665E-02	64,347,648	1.464915E-03	6.39	+0.117	-3.04	-1.97	-6.22
600	4.0399E-02	63,424,475	1.464540E-03	7.73	+0.143	-4.11	-2.66	-7.41
700	4.7132E-02	62,472,002	1.464521E-03	9.12	+0.144	-5.20	-3.37	-8.91
800	5.3865E-02	61,521,751	1.464330E-03	10.50	+0.157	-6.28	-4.09	-10.70
900	6.0598E-02	60,528,278	1.464208E-03	11.95	+0.165	-7.41	-4.85	-12.90
1,000	6.7331E-02	59,641,186	1.464056E-03	13.24	+0.176	-8.42	-5.54	-15.14
2,000	1.3466E-01	51,842,610	1.461657E-03	24.58	+0.339	-17.48	-11.91	-51.79
3,000	2.0199E-01	47,011,638	1.457642E-03	31.61	+0.613	-23.34	-16.18	-101.65
4,000	2.6932E-01	43,641,101	1.448856E-03	36.51	+1.212	-27.50	-19.26	-153.21
5,000	3.3665E-01	40,499,149	1.431155E-03	41.08	+2.419	-30.89	-22.13	-214.16
6,000	4.0399E-01	37,572,142	1.400920E-03	45.34	+4.481	-34.75	-24.78	-294.90
7,000	4.7132E-01	34,758,893	1.352098E-03	49.43	+7.809	-37.93	-27.29	-395.00

Table D6. Data from the edited stress-time histories generated by STFT with window size of 64 points (Max. AccPSD = 29,694 Engery/Hz)

Cutoff Level (Energy/Hz)	Normalised Cutoff Level	Length of the Edited History (Points)	Fatigue Damage per Repetition	% Reduction in Length of the Edited History	% Error [(+) and (-) signs mean less than and greater than, respectively.]			
					Fatigue Damage per Repetition	Mean Stress	rms	Kurtosis
0	0	68,739,939	1.466634E-03	0	0	0	0	0
1,000	3.3677E-02	64,471,091	1.466287E-03	6.21	+0.024	-2.85	-1.87	-6.19
2,000	6.7354E-02	59,774,575	1.465724E-03	13.04	+0.062	-8.19	-5.42	-16.56
3,000	1.0103E-01	55,858,296	1.465192E-03	18.74	+0.098	-12.66	-8.53	-31.03
4,000	1.3471E-01	51,874,637	1.463812E-03	24.53	+0.192	-17.32	-11.85	-54.21
5,000	1.6838E-01	49,036,881	1.462044E-03	28.66	+0.313	-20.78	-14.33	-77.69
6,000	2.0206E-01	46,886,017	1.459265E-03	31.79	+0.502	-23.42	-16.25	-102.00
7,000	2.3574E-01	45,071,181	1.455868E-03	34.43	+0.734	-25.65	-17.90	-127.51
8,000	2.6941E-01	43,415,525	1.450952E-03	36.84	+1.069	-27.65	-19.40	-155.32
9,000	3.0309E-01	41,794,129	1.443307E-03	39.20	+1.591	-29.61	-20.87	-185.34
10,000	3.3677E-01	40,198,857	1.432485E-03	41.52	+2.328	-29.61	-20.87	-185.34
11,000	3.7045E-01	38,657,389	1.418445E-03	43.76	+3.286	-33.31	-23.69	-257.24
12,000	4.0412E-01	37,170,211	1.400496E-03	45.93	+4.510	-35.01	-25.02	-299.94
13,000	4.3780E-01	35,689,546	1.376983E-03	48.08	+6.113	-36.69	-26.33	-347.27
14,000	4.7148E-01	34,223,562	1.346610E-03	50.21	+8.184	-38.34	-27.62	-399.99
15,000	5.0515E-01	32,815,225	1.310351E-03	52.26	+10.656	-39.89	-28.85	-458.19
20,000	6.7354E-01	26,216,821	1.003503E-03	61.86	+31.578	-46.81	-34.37	-847.82
25,000	8.4192E-01	18,758,956	4.893348E-04	72.71	+66.636	-53.47	-39.64	-1656.88

Table D7. Data from the edited stress-time histories generated by STFT with window size of 128 points (Max. AccPSD = 59,364 Engery/Hz)

Cutoff Level (Energy/Hz)	Normalised Cutoff Level	Length of the Edited History (Points)	Fatigue Damage per Repetition	% Reduction in Length of the Edited History	% Error [(+) and (-) signs mean less than and greater than, respectively.]			
					Fatigue Damage per Repetition	Mean Stress	rms	Kurtosis
0	0	68,739,939	1.466634E-03	0	0	0	0	0
2,000	3.3690E-02	64,567,654	1.466445E-03	6.07	+0.013	-2.69	-1.80	-7.70
4,000	6.7381E-02	59,840,205	1.466120E-03	12.95	+0.035	-8.06	-5.36	-17.45
4,300	7.2434E-02	59,227,884	1.466098E-03	13.84	+0.037	-8.76	-5.84	-19.24
4,400	7.4119E-02	59,025,614	1.466008E-03	14.13	+0.043	-8.99	-6.00	-19.86
4,500	7.5804E-02	58,823,704	1.466025E-03	14.43	+0.042	-9.22	-6.15	-20.52
4,600	7.7488E-02	58,621,527	1.466080E-03	14.72	+0.038	-9.45	-6.31	-21.19
4,700	7.9173E-02	58,425,560	1.466002E-03	15.00	+0.043	-9.67	-6.47	-21.80
4,800	8.0857E-02	58,217,047	1.466020E-03	15.31	+0.042	-9.91	-6.63	-22.35
4,900	8.2542E-02	58,014,332	1.465993E-03	15.60	+0.044	-10.15	-6.79	-23.00
5,000	8.4226E-02	57,816,141	1.465944E-03	15.89	+0.047	-10.37	-6.95	-23.66
6,000	1.0107E-01	55,750,887	1.465437E-03	18.90	+0.082	-12.73	-8.60	-32.12
8,000	1.3476E-01	51,770,276	1.464256E-03	24.69	+0.162	-17.38	-11.91	-56.10
10,000	1.6845E-01	48,906,255	1.462917E-03	28.85	+0.253	-20.84	-14.41	-80.83
20,000	3.3690E-01	39,959,110	1.428510E-03	41.87	+2.599	-31.60	-22.42	-223.72
30,000	5.0536E-01	32,354,602	1.284739E-03	52.93	+12.402	-40.04	-29.05	-469.23
40,000	6.7381E-01	22,523,759	9.457514E-04	67.23	+35.516	-46.96	-34.59	-854.01
50,000	8.4226E-01	17,724,305	4.424820E-04	74.22	+69.830	-53.61	-39.82	-1633.34

Table D8. Data from the edited stress-time histories generated by STFT with window size of 256 points (Max. AccPSD = 118,660 Engery/Hz)

Cutoff Level (Energy/Hz)	Normalised Cutoff Level	Length of the Edited History (Points)	Fatigue Damage per Repetition	% Reduction in Length of the Edited History	% Error [(+) and (-) signs mean less than and greater than, respectively.]			
					Fatigue Damage per Repetition	Mean Stress	rms	Kurtosis
0	0	68,739,939	1.466634E-03	0	0	0	0	0
5,000	4.2137E-02	63,496,340	1.466521E-03	7.63	+0.008	-3.89	-2.58	-9.78
6,000	5.0565E-02	62,305,264	1.466549E-03	9.36	+0.006	-5.23	-3.47	-12.04
7,000	5.8992E-02	61,107,240	1.466347E-03	11.10	+0.020	-6.59	-4.38	-14.78
8,000	6.7420E-02	59,974,862	1.466241E-03	12.75	+0.027	-7.86	-5.25	-17.81
9,000	7.5847E-02	58,953,485	1.466051E-03	14.24	+0.040	-9.02	-6.04	-20.85
9,300	7.8375E-02	58,655,254	1.466074E-03	14.67	+0.038	-9.36	-6.27	-21.79
9,400	7.9218E-02	58,545,483	1.465973E-03	14.83	+0.045	-9.47	-6.35	-22.11
9,500	8.0061E-02	58,459,248	1.466021E-03	14.96	+0.042	-9.58	-6.43	-22.43
9,600	8.0903E-02	58,362,183	1.466061E-03	15.10	+0.039	-9.69	-6.50	-22.75
9,700	8.1746E-02	58,261,693	1.465994E-03	15.24	+0.044	-9.81	-6.58	-23.11
9,800	8.2589E-02	58,165,594	1.465978E-03	15.38	+0.045	-9.92	-6.66	-23.45
9,900	8.3432E-02	58,066,509	1.466004E-03	15.53	+0.043	-10.03	-6.74	-23.80
10,000	8.4274E-02	57,970,413	1.465952E-03	15.67	+0.047	-10.14	-6.81	-24.14
15,000	1.2641E-01	52,737,941	1.464840E-03	23.28	+0.122	-16.14	-11.06	-50.57
20,000	1.6855E-01	48,980,305	1.462911E-03	28.75	+0.254	-20.63	-14.30	-82.16
30,000	2.5282E-01	44,171,765	1.453736E-03	35.74	+0.879	-26.42	-18.58	-145.42
40,000	3.3710E-01	40,130,708	1.429608E-03	41.62	+2.525	-31.11	-22.15	-222.74
50,000	4.2137E-01	36,200,324	1.373980E-03	47.34	+6.317	-35.46	-25.55	-324.57
60,000	5.0565E-01	32,438,795	1.276558E-03	52.81	+12.960	-39.48	-28.74	-454.44
70,000	5.8992E-01	28,963,769	1.129810E-03	57.86	+22.966	-43.02	-31.58	-608.27
80,000	6.7420E-01	25,485,562	9.347771E-04	62.92	+36.264	-46.34	-34.24	-799.99

Table D9. Data from the edited stress-time histories generated by WT with the Morl wavelet at wavelet decomposition level 1 (Max. AccPSD = 9,881,880 Engery/Hz)

Cutoff Level (Energy/Hz)	Normalised Cutoff Level	Length of the Edited History (Points)	Fatigue Damage per Repetition	% Reduction in Length of the Edited History	% Error [(+) and (-) signs mean less than and greater than, respectively.]			
					Fatigue Damage per Repetition	Mean Stress	rms	Kurtosis
0	0	68,739,939	1.466634E-03	0	0	0	0	0
20,000	2.0239E-03	60,739,940	1.465295E-03	11.64	+0.091	-4.83	-3.65	-18.26
30,000	3.0359E-03	59,339,940	1.464398E-03	13.67	+0.152	-6.00	-4.47	-20.02
40,000	4.0478E-03	57,839,940	1.463644E-03	15.86	+0.204	-7.65	-5.60	-23.97
50,000	5.0598E-03	56,739,940	1.463213E-03	17.46	+0.233	-8.63	-6.32	-27.30
60,000	6.0718E-03	55,539,940	1.462638E-03	19.20	+0.272	-9.86	-7.23	-32.07
70,000	7.0837E-03	53,755,190	1.456863E-03	21.80	+0.666	-11.62	-8.48	-39.62
80,000	8.0957E-03	52,539,940	1.457292E-03	23.57	+0.637	-12.95	-9.49	-46.23
90,000	9.1077E-03	51,639,940	1.455540E-03	24.88	+0.756	-13.91	-10.19	-51.23
100,000	1.0120E-02	50,739,940	1.454220E-03	26.19	+0.846	-14.86	-10.91	-57.03
150,000	1.5179E-02	47,439,940	1.440035E-03	30.99	+1.814	-18.39	-13.55	-81.44
200,000	2.0239E-02	44,639,940	1.417267E-03	35.06	+3.366	-21.06	-15.57	-104.75
250,000	2.5299E-02	40,339,940	1.359048E-03	41.32	+7.336	-24.99	-18.65	-145.35
300,000	3.0359E-02	37,339,940	1.307623E-03	45.68	+10.842	-26.35	-19.78	-169.28
350,000	3.5419E-02	31,739,940	1.138791E-03	53.83	+22.353	-28.46	-21.70	-198.05

Table D10. Data from the edited stress-time histories generated by WT with the Morl wavelet at wavelet decomposition level 2 (Max. AccPSD = 17,059 Engery/Hz)

Cutoff Level (Energy/Hz)	Normalised Cutoff Level	Length of the Edited History (Points)	Fatigue Damage per Repetition	% Reduction in Length of the Edited History	% Error [(+) and (-) signs mean less than and greater than, respectively.]			
					Fatigue Damage per Repetition	Mean Stress	rms	Kurtosis
0	0	68,739,939	1.466634E-03	0	0	0	0	0
3	1.7586E-04	44,453,377	1.447653E-03	35.33	+1.294	-6.97	-3.69	-33.00
4	2.3448E-04	41,800,826	1.439270E-03	39.19	+1.866	-7.48	-3.94	-37.91
5	2.9310E-04	39,664,075	1.430562E-03	42.30	+2.460	-7.88	-4.14	-42.17
6	3.5172E-04	37,871,592	1.421808E-03	44.91	+3.056	-8.21	-4.32	-45.95
7	4.1034E-04	36,334,325	1.413300E-03	47.14	+3.636	-8.50	-4.49	-49.38
8	4.6896E-04	34,989,647	1.404322E-03	49.10	+4.249	-8.77	-4.65	-52.52
9	5.2758E-04	33,796,341	1.395059E-03	50.83	+4.880	-9.00	-4.80	-55.39
10	5.8620E-04	32,720,214	1.385630E-03	52.40	+5.523	-9.22	-4.95	-58.09
20	1.1724E-03	25,554,986	1.300772E-03	62.82	+11.309	-10.78	-6.08	-77.77
30	1.7586E-03	21,462,400	1.218040E-03	68.78	+16.950	-11.54	-6.76	-91.12
40	2.3448E-03	18,651,263	1.141310E-03	72.87	+22.182	-11.97	-7.23	-99.96
50	2.9310E-03	16,541,223	1.069760E-03	75.94	+27.060	-12.21	-7.58	-105.64
60	3.5172E-03	14,874,179	1.007331E-03	78.36	+31.317	-12.34	-7.87	-109.14
70	4.1034E-03	13,511,105	9.487506E-04	80.34	+35.311	-12.37	-8.08	-110.85

Table D11. Data from the edited stress-time histories generated by WT with the Morl wavelet at wavelet decomposition level 3 (Max. AccPSD = 64,322 Engery/Hz)

Cutoff Level (Energy/Hz)	Normalised Cutoff Level	Length of the Edited History (Points)	Fatigue Damage per Repetition	% Reduction in Length of the Edited History	% Error [(+) and (-) signs mean less than and greater than, respectively.]			
					Fatigue Damage per Repetition	Mean Stress	rms	Kurtosis
0	0	68,739,939	1.466634E-03	0	0	0	0	0
5	7.7734E-05	57,909,668	1.465763E-03	15.76	+0.059	-4.52	-2.85	-15.55
10	1.5547E-04	53,565,492	1.463139E-03	22.08	+0.238	-6.16	-3.76	-21.90
15	2.3320E-04	50,546,021	1.459880E-03	26.47	+0.461	-7.14	-4.30	-26.98
20	3.1094E-04	48,194,163	1.455690E-03	29.89	+0.746	-7.83	-4.68	-31.36
30	4.6640E-04	44,580,559	1.445686E-03	35.15	+1.428	-8.84	-5.25	-38.69
40	6.2187E-04	41,846,758	1.433829E-03	39.12	+2.237	-9.60	-5.70	-44.92
50	7.7734E-04	39,644,909	1.421754E-03	42.33	+3.060	-10.19	-6.08	-50.50
60	9.3281E-04	37,797,160	1.408362E-03	45.01	+3.973	-10.69	-6.40	-55.57
70	1.0883E-03	36,201,511	1.394750E-03	47.34	+4.901	-11.12	-6.70	-60.19
80	1.2437E-03	34,797,287	1.380944E-03	49.38	+5.843	-11.51	-6.98	-64.43
90	1.3992E-03	33,539,730	1.367466E-03	51.21	+6.762	-11.84	-7.22	-68.37
100	1.5547E-03	32,407,185	1.353745E-03	52.86	+7.697	-12.14	-7.44	-72.03
150	2.3320E-03	27,940,725	1.287075E-03	59.35	+12.243	-13.20	-8.29	-87.11
200	3.1094E-03	24,716,356	1.224106E-03	64.04	+16.536	-13.84	-8.86	-98.16

Table D12. Data from the edited stress-time histories generated by WT with the Morl wavelet at wavelet decomposition level 4 (Max. AccPSD = 150,300 Engery/Hz)

Cutoff Level (Energy/Hz)	Normalised Cutoff Level	Length of the Edited History (Points)	Fatigue Damage per Repetition	% Reduction in Length of the Edited History	% Error [(+) and (-) signs mean less than and greater than, respectively.]			
					Fatigue Damage per Repition	Mean Stress	rms	Kurtosis
0	0	68,739,939	1.466634E-03	0	0	0	0	0
5	3.3267E-05	65,006,440	1.466574E-03	5.43	+0.004	-0.92	-0.74	-7.80
10	6.6534E-05	63,142,161	1.466565E-03	8.14	+0.005	-2.11	-1.47	-9.77
15	9.9800E-05	61,720,262	1.466471E-03	10.21	+0.011	-2.89	-1.93	-11.32
20	1.3307E-04	60,498,611	1.466354E-03	11.99	+0.019	-3.47	-2.26	-12.71
30	1.9960E-04	58,449,685	1.466030E-03	14.97	+0.041	-4.31	-2.71	-15.20
40	2.6613E-04	56,737,510	1.465657E-03	17.46	+0.067	-4.94	-3.03	-17.51
50	3.3267E-04	55,302,173	1.465276E-03	19.55	+0.093	-5.45	-3.29	-19.68
60	3.9920E-04	54,053,960	1.464712E-03	21.36	+0.131	-5.89	-3.52	-21.76
70	4.6574E-04	52,957,592	1.463953E-03	22.96	+0.183	-6.30	-3.74	-23.74
80	5.3227E-04	51,989,911	1.463469E-03	24.37	+0.216	-6.67	-3.95	-25.64
90	5.9880E-04	51,114,793	1.462644E-03	25.64	+0.272	-7.03	-4.16	-27.50
100	6.6534E-04	50,322,085	1.461930E-03	26.79	+0.321	-7.37	-4.36	-29.33
110	7.3187E-04	49,593,621	1.461172E-03	27.85	+0.372	-7.70	-4.56	-31.12
120	7.9840E-04	48,919,654	1.460407E-03	28.83	+0.425	-8.00	-4.75	-32.86
130	8.6494E-04	48,283,340	1.459480E-03	29.76	+0.488	-8.30	-4.94	-34.57
140	9.3147E-04	47,683,606	1.458586E-03	30.63	+0.549	-8.58	-5.11	-36.26
150	9.9800E-04	47,118,385	1.457645E-03	31.45	+0.613	-8.84	-5.28	-37.93
160	1.0645E-03	46,580,758	1.456419E-03	32.24	+0.696	-9.09	-5.44	-39.55
170	1.1311E-03	46,061,737	1.455391E-03	32.99	+0.767	-9.33	-5.60	-41.18

Table D12. (continued)

Cutoff Level (Energy/Hz)	Normalised Cutoff Level	Length of the Edited History (Points)	Fatigue Damage per Repetition	% Reduction in Length of the Edited History	% Error [(+) and (-) signs mean less than and greater than, respectively.]			
					Fatigue Damage per Repetition	Mean Stress	rms	Kurtosis
180	1.1976E-03	45,569,736	1.454369E-03	33.71	+0.836	-9.55	-5.74	-42.74
190	1.2641E-03	45,091,615	1.453318E-03	34.40	+0.908	-9.76	-5.87	-44.29
200	1.3307E-03	44,631,750	1.452048E-03	35.07	+0.995	-9.97	-6.01	-45.84
210	1.3972E-03	44,187,327	1.450656E-03	35.72	+1.089	-10.16	-6.13	-47.35
220	1.4637E-03	43,762,953	1.449358E-03	36.34	+1.178	-10.34	-6.25	-48.82
230	1.5303E-03	43,347,642	1.447993E-03	36.94	+1.271	-10.52	-6.36	-50.28
240	1.5968E-03	42,944,743	1.446531E-03	37.53	+1.371	-10.69	-6.47	-51.71
250	1.6633E-03	42,550,253	1.444997E-03	38.10	+1.475	-10.84	-6.58	-53.13
260	1.7299E-03	42,169,824	1.443507E-03	38.65	+1.577	-11.00	-6.68	-54.55

Table D13. Data from the edited stress-time histories generated by WT with the Morl wavelet at wavelet decomposition level 5 (Max. AccPSD = 303,160 Engery/Hz)

Cutoff Level (Energy/Hz)	Normalised Cutoff Level	Length of the Edited History (Points)	Fatigue Damage per Repetition	% Reduction in Length of the Edited History	% Error [(+) and (-) signs mean less than and greater than, respectively.]			
					Fatigue Damage per Repetition	Mean Stress	rms	Kurtosis
0	0	68,739,939	1.466634E-03	0	0	0	0	0
20	6.5972E-05	64,890,964	1.466616E-03	5.60	+0.001	-1.05	-0.87	-8.45
40	1.3194E-04	63,089,938	1.466620E-03	8.22	+0.001	-2.33	-1.67	-10.40
60	1.9792E-04	61,676,097	1.466624E-03	10.28	+0.001	-3.28	-2.25	-12.04
80	2.6389E-04	60,465,038	1.466416E-03	12.04	+0.015	-4.00	-2.69	-13.53
100	3.2986E-04	59,392,167	1.466372E-03	13.60	+0.018	-4.57	-3.03	-14.95
200	6.5972E-04	55,363,617	1.465468E-03	19.46	+0.080	-6.48	-4.13	-21.24
300	9.8958E-04	52,596,930	1.464416E-03	23.48	+0.151	-7.87	-4.97	-27.07
400	1.3194E-03	50,506,359	1.463454E-03	26.53	+0.217	-8.99	-5.69	-32.61
500	1.6493E-03	48,783,589	1.462434E-03	29.03	+0.286	-9.94	-6.30	-37.98
600	1.9792E-03	47,301,717	1.461083E-03	31.19	+0.378	-10.77	-6.84	-43.29
700	2.3090E-03	46,000,012	1.459626E-03	33.08	+0.478	-11.46	-7.30	-48.31
800	2.6389E-03	44,834,000	1.458009E-03	34.78	+0.588	-12.07	-7.69	-53.20
900	2.9687E-03	43,798,804	1.456204E-03	36.28	+0.711	-12.58	-8.03	-57.74
1,000	3.2986E-03	42,835,241	1.454302E-03	37.69	+0.841	-13.05	-8.34	-62.19

Table D14. Data from the edited stress-time histories generated by WT with the Morl wavelet at wavelet decomposition level 6 (Max. AccPSD = 444,850 Engery/Hz)

Cutoff Level (Energy/Hz)	Normalised Cutoff Level	Length of the Edited History (Points)	Fatigue Damage per Repetition	% Reduction in Length of the Edited History	% Error [(+) and (-) signs mean less than and greater than, respectively.]			
					Fatigue Damage per Repetition	Mean Stress	rms	Kurtosis
0	0	68,739,939	1.466634E-03	0	0	0	0	0
25	5.6199E-05	66,487,060	1.466630E-03	3.28	0	0.15	-0.13	-7.18
50	1.1240E-04	65,275,568	1.466628E-03	5.04	0	-0.84	-0.78	-8.53
100	2.2479E-04	63,450,709	1.466616E-03	7.69	+0.001	-2.27	-1.68	-10.66
200	4.4959E-04	60,587,199	1.466545E-03	11.86	+0.006	-4.20	-2.85	-14.38
300	6.7438E-04	58,411,710	1.466397E-03	15.03	+0.016	-5.44	-3.59	-17.68
400	8.9918E-04	56,703,010	1.466159E-03	17.51	+0.032	-6.46	-4.22	-20.80
500	1.1240E-03	55,268,521	1.465926E-03	19.60	+0.048	-7.33	-4.77	-23.84
600	1.3488E-03	53,990,082	1.465682E-03	21.46	+0.065	-8.12	-5.28	-26.87
700	1.5736E-03	52,848,995	1.465431E-03	23.12	+0.082	-8.82	-5.74	-29.94
800	1.7984E-03	51,793,424	1.465167E-03	24.65	+0.100	-9.46	-6.16	-33.02
900	2.0232E-03	50,825,459	1.464810E-03	26.06	+0.124	-10.06	-6.55	-36.13
1,000	2.2479E-03	49,944,173	1.464450E-03	27.34	+0.149	-10.59	-6.91	-39.15
1,500	3.3719E-03	46,340,717	1.462205E-03	32.59	+0.302	-12.72	-8.33	-53.89
2,000	4.4959E-03	43,602,835	1.459005E-03	36.57	+0.520	-14.15	-9.29	-67.21

Table D15. Data from the edited stress-time histories generated by WT with the Morl wavelet at wavelet decomposition level 7 (Max. AccPSD = 800,040 Engery/Hz)

Cutoff Level (Energy/Hz)	Normalised Cutoff Level	Length of the Edited History (Points)	Fatigue Damage per Repetition	% Reduction in Length of the Edited History	% Error [(+) and (-) signs mean less than and greater than, respectively.]			
					Fatigue Damage per Repetition	Mean Stress	rms	Kurtosis
0	0	68,739,939	1.466634E-03	0	0	0	0	0
50	6.2497E-05	66,960,446	1.466633E-03	2.59	0	0.53	0.09	-6.95
100	1.2499E-04	65,906,211	1.466632E-03	4.12	0	-0.42	-0.53	-8.16
150	1.8749E-04	64,971,971	1.466631E-03	5.48	0	-1.25	-1.07	-9.29
200	2.4999E-04	64,107,671	1.466630E-03	6.74	0	-2.03	-1.56	-10.40
250	3.1248E-04	63,304,004	1.466629E-03	7.91	0	-2.71	-1.99	-11.49
300	3.7498E-04	62,561,403	1.466628E-03	8.99	0	-3.30	-2.36	-12.52
350	4.3748E-04	61,876,447	1.466625E-03	9.98	+0.001	-3.84	-2.69	-13.55
400	4.9998E-04	61,252,309	1.466618E-03	10.89	+0.001	-4.33	-2.99	-14.55
450	5.6247E-04	60,686,958	1.466614E-03	11.72	+0.001	-4.76	-3.27	-15.49
500	6.2497E-04	60,161,597	1.466610E-03	12.48	+0.002	-5.17	-3.52	-16.41
750	9.3745E-04	58,134,589	1.466495E-03	15.43	+0.009	-6.64	-4.47	-20.87
1,000	1.2499E-03	56,107,581	1.465968E-03	18.38	+0.045	-8.10	-5.43	-25.34
1,500	1.8749E-03	53,074,528	1.465263E-03	22.79	+0.093	-10.23	-6.85	-34.42
2,000	2.4999E-03	50,615,176	1.464230E-03	26.37	+0.164	-11.87	-7.97	-43.46
2,500	3.1248E-03	48,563,507	1.462815E-03	29.35	+0.260	-13.12	-8.81	-52.09
3,000	3.7498E-03	46,805,748	1.460657E-03	31.91	+0.408	-14.09	-9.48	-60.22
3,500	4.3748E-03	45,261,619	1.457755E-03	34.16	+0.605	-14.87	-10.00	-67.86
4,000	4.9998E-03	43,846,422	1.457755E-03	36.21	+0.605	-15.56	-10.47	-75.37

Table D16. Data from the edited stress-time histories generated by WT with the Morl wavelet at wavelet decomposition level 8 (Max. AccPSD = 1,391,300 Engery/Hz)

Cutoff Level (Energy/Hz)	Normalised Cutoff Level	Length of the Edited History (Points)	Fatigue Damage per Repetition	% Reduction in Length of the Edited History	% Error [(+) and (-) signs mean less than and greater than, respectively.]			
					Fatigue Damage per Repetition	Mean Stress	rms	Kurtosis
0	0	68,739,939	1.466634E-03	0	0	0	0	0
500	3.5938E-04	63,674,684	1.466630E-03	7.37	0	-2.73	-2.01	-11.53
1,000	7.1875E-04	60,651,073	1.466628E-03	11.77	0	-5.53	-3.83	-17.11
1,500	1.0781E-03	58,446,098	1.466595E-03	14.98	+0.003	-7.41	-5.07	-22.42
2,000	1.4375E-03	56,575,709	1.466539E-03	17.70	+0.006	-8.94	-6.11	-27.83
2,100	1.5094E-03	56,221,904	1.466522E-03	18.21	+0.008	-9.21	-6.29	-28.93
2,200	1.5813E-03	55,882,810	1.466499E-03	18.70	+0.009	-9.48	-6.47	-30.03
2,300	1.6531E-03	55,551,970	1.466470E-03	19.19	+0.011	-9.73	-6.64	-31.11
2,400	1.7250E-03	55,224,937	1.466437E-03	19.66	+0.013	-9.98	-6.82	-32.22
2,500	1.7969E-03	54,913,460	1.466405E-03	20.11	+0.016	-10.22	-6.99	-33.31
3,000	2.1563E-03	53,433,222	1.466185E-03	22.27	+0.031	-11.33	-7.75	-38.80
3,100	2.2281E-03	53,159,630	1.466109E-03	22.67	+0.036	-11.53	-7.88	-39.88
3,200	2.3000E-03	52,882,775	1.466023E-03	23.07	+0.042	-11.73	-8.02	-40.99
3,300	2.3719E-03	52,617,246	1.465950E-03	23.45	+0.047	-11.92	-8.15	-42.07
3,400	2.4438E-03	52,348,145	1.465840E-03	23.85	+0.054	-12.10	-8.28	-43.15
3,500	2.5156E-03	52,092,914	1.465714E-03	24.22	+0.063	-12.28	-8.40	-44.21
4,000	2.8750E-03	50,901,427	1.465031E-03	25.95	+0.109	-13.09	-8.96	-49.42
5,000	3.5938E-03	48,774,308	1.463019E-03	29.05	+0.246	-14.46	-9.91	-59.55
10,000	7.1875E-03	40,529,907	1.431662E-03	41.04	+2.385	-18.13	-12.48	-103.17
15,000	1.0781E-02	32,849,055	1.325244E-03	52.21	+9.640	-19.87	-13.94	-136.19
20,000	1.4375E-02	25,504,999	1.135411E-03	62.90	+22.584	-20.74	-15.08	-152.54

Table D17. Data from the edited stress-time histories generated by WT with the Morl wavelet at wavelet decomposition level 9 (Max. AccPSD = 2,258,000 Engery/Hz)

Cutoff Level (Energy/Hz)	Normalised Cutoff Level	Length of the Edited History (Points)	Fatigue Damage per Repetition	% Reduction in Length of the Edited History	% Error [(+) and (-) signs mean less than and greater than, respectively.]			
					Fatigue Damage per Repetition	Mean Stress	rms	Kurtosis
0	0	68,739,939	1.466634E-03	0	0	0	0	0
1,000	4.4287E-04	64,192,333	1.466633E-03	6.62	0	-2.47	-1.86	-11.10
2,000	8.8574E-04	61,452,703	1.466630E-03	10.60	0	-5.23	-3.68	-16.50
3,000	1.3286E-03	59,383,167	1.466626E-03	13.61	+0.001	-7.17	-4.99	-21.81
3,500	1.5500E-03	58,472,114	1.466564E-03	14.94	+0.005	-7.98	-5.55	-24.62
4,000	1.7715E-03	57,561,061	1.466343E-03	16.26	+0.020	-8.79	-6.11	-27.42
5,000	2.2143E-03	55,957,493	1.465795E-03	18.60	+0.057	-10.16	-7.05	-33.02
6,000	2.6572E-03	54,528,319	1.464966E-03	20.67	+0.114	-11.32	-7.86	-38.58
7,000	3.1001E-03	53,200,690	1.463843E-03	22.61	+0.190	-12.31	-8.54	-44.04
8,000	3.5430E-03	51,961,710	1.462212E-03	24.41	+0.302	-13.15	-9.13	-49.38
9,000	3.9858E-03	50,838,318	1.460136E-03	26.04	+0.443	-13.91	-9.66	-54.66
10,000	4.4287E-03	49,782,383	1.457407E-03	27.58	+0.629	-14.53	-10.10	-59.58
11,000	4.8716E-03	48,726,243	1.454310E-03	29.12	+0.840	-15.10	-10.49	-64.59
12,000	5.3144E-03	47,764,735	1.450032E-03	30.51	+1.132	-15.58	-10.83	-69.25
13,000	5.7573E-03	46,817,640	1.445305E-03	31.89	+1.454	-16.03	-11.14	-73.81
14,000	6.2002E-03	45,866,711	1.439054E-03	33.28	+1.880	-16.44	-11.43	-78.37
15,000	6.6430E-03	44,939,041	1.387203E-03	34.62	+5.416	-16.79	-11.69	-82.65
20,000	8.8574E-03	40,302,021	1.173073E-03	41.37	+20.016	-18.19	-12.75	-101.55
30,000	1.3286E-02	32,942,314	7.616980E-04	52.08	+48.065	-19.69	-14.27	-124.82
50,000	2.2143E-02	18,668,564	7.616980E-04	72.84	+48.065	-20.23	-15.95	-130.54

Table D18. Data from the edited stress-time histories generated by WT with the Meyr wavelet at wavelet decomposition level 8 (Max. AccPSD = 1,451,200 Engery/Hz)

Cutoff Level (Energy/Hz)	Normalised Cutoff Level	Length of the Edited History (Points)	Fatigue Damage per Repetition	% Reduction in Length of the Edited History	% Error [(+) and (-) signs mean less than and greater than, respectively.]			
					Fatigue Damage per Repetition	Mean Stress	rms	Kurtosis
0	0	68,739,939	1.466634E-03	0	0	0	0	0
1,000	6.8908E-04	61,604,981	1.466622E-03	10.38	+0.001	-4.63	-3.23	-15.14
2,000	1.3782E-03	57,830,164	1.466606E-03	15.87	+0.002	-7.74	-5.27	-23.89
2,100	1.4471E-03	57,501,510	1.466598E-03	16.35	+0.002	-7.98	-5.43	-24.79
2,200	1.5160E-03	57,172,808	1.466590E-03	16.83	+0.003	-8.23	-5.60	-25.71
2,300	1.5849E-03	56,862,116	1.466579E-03	17.28	+0.004	-8.47	-5.76	-26.60
2,400	1.6538E-03	56,557,343	1.466537E-03	17.72	+0.007	-8.69	-5.91	-27.52
2,500	1.7227E-03	56,249,667	1.466486E-03	18.17	+0.010	-8.93	-6.07	-28.48
3,000	2.0673E-03	54,829,920	1.466158E-03	20.24	+0.032	-9.97	-6.77	-33.10
3,100	2.1362E-03	54,558,521	1.466108E-03	20.63	+0.036	-10.15	-6.90	-34.00
3,200	2.2051E-03	54,296,836	1.466051E-03	21.01	+0.040	-10.34	-7.03	-34.90
3,300	2.2740E-03	54,034,261	1.465874E-03	21.39	+0.052	-10.52	-7.15	-35.83
3,400	2.3429E-03	53,776,671	1.465791E-03	21.77	+0.057	-10.71	-7.28	-36.75
3,500	2.4118E-03	53,515,176	1.465676E-03	22.15	+0.065	-10.89	-7.40	-37.72

Table D19. Data from the edited stress-time histories generated by WT with the Dmey wavelet at wavelet decomposition level 8 (Max. AccPSD = 1,455,500 Engery/Hz)

Cutoff Level (Energy/Hz)	Normalised Cutoff Level	Length of the Edited History (Points)	Fatigue Damage per Repetition	% Reduction in Length of the Edited History	% Error [(+) and (-) signs mean less than and greater than, respectively.]			
					Fatigue Damage per Repetition	Mean Stress	rms	Kurtosis
0	0	68,739,939	1.466634E-03	0	0	0	0	0
1,000	6.8705E-04	61,753,696	1.466620E-03	10.16	+0.001	-4.47	-3.12	-14.79
2,000	1.3741E-03	58,086,296	1.466580E-03	15.50	+0.004	-7.61	-5.19	-23.22
2,100	1.4428E-03	57,768,395	1.466572E-03	15.96	+0.004	-7.87	-5.36	-24.10
2,200	1.5115E-03	57,459,600	1.466563E-03	16.41	+0.005	-8.11	-5.53	-24.97
2,300	1.5802E-03	57,159,882	1.466552E-03	16.85	+0.006	-8.35	-5.69	-25.84
2,400	1.6489E-03	56,863,685	1.466540E-03	17.28	+0.006	-8.59	-5.85	-26.72
2,500	1.7176E-03	56,581,511	1.466525E-03	17.69	+0.007	-8.81	-6.00	-27.57
3,000	2.0611E-03	55,200,701	1.466435E-03	19.70	+0.014	-9.88	-6.74	-32.03
3,100	2.1299E-03	54,942,137	1.466411E-03	20.07	+0.015	-10.08	-6.87	-32.90
3,200	2.1986E-03	54,695,729	1.466387E-03	20.43	+0.017	-10.27	-7.00	-33.78
3,300	2.2673E-03	54,451,500	1.466363E-03	20.79	+0.018	-10.45	-7.12	-34.64
3,400	2.3360E-03	54,198,439	1.466340E-03	21.15	+0.020	-10.64	-7.25	-35.56
3,500	2.4047E-03	53,960,861	1.466307E-03	21.50	+0.022	-10.81	-7.37	-36.44

Table D20. Data from the edited stress-time histories generated by WT with the Mexh wavelet at wavelet decomposition level 8 (Max. AccPSD = 5,214,600 Engery/Hz)

Cutoff Level (Energy/Hz)	Normalised Cutoff Level	Length of the Edited History (Points)	Fatigue Damage per Repetition	% Reduction in Length of the Edited History	% Error [(+) and (-) signs mean less than and greater than, respectively.]			
					Fatigue Damage per Repetition	Mean Stress	rms	Kurtosis
0	0	68,739,939	1.466634E-03	0	0	0	0	0
1,000	1.9177E-04	65,618,194	1.466628E-03	4.54	+0.0004	-0.87	-0.80	-8.83
2,000	3.8354E-04	63,323,477	1.466627E-03	7.88	+0.0005	-3.01	-2.18	-12.33
2,100	4.0272E-04	63,126,830	1.466626E-03	8.17	+0.0005	-3.19	-2.29	-12.67
2,200	4.2189E-04	62,940,684	1.466625E-03	8.44	+0.0006	-3.36	-2.40	-13.01
2,300	4.4107E-04	62,758,131	1.466624E-03	8.70	+0.0007	-3.52	-2.51	-13.34
2,400	4.6025E-04	62,576,874	1.466623E-03	8.97	+0.0008	-3.68	-2.61	-13.69
2,500	4.7942E-04	62,401,872	1.466622E-03	9.22	+0.0008	-3.83	-2.71	-14.02
3,000	5.7531E-04	61,592,653	1.466621E-03	10.40	+0.0009	-4.52	-3.17	-15.62
3,100	5.9448E-04	61,437,674	1.466620E-03	10.62	+0.0010	-4.77	-3.25	-15.93
3,200	6.1366E-04	62,189,014	1.466619E-03	9.53	+0.0010	-4.77	-3.33	-16.24
3,300	6.3284E-04	61,151,937	1.466618E-03	11.04	+0.0011	-4.88	-3.40	-16.53
3,400	6.5202E-04	60,999,174	1.466617E-03	11.26	+0.0012	-5.00	-3.48	-16.85
3,500	6.7119E-04	60,853,423	1.466616E-03	11.47	+0.0012	-5.12	-3.56	-17.17
4,000	7.6708E-04	60,151,693	1.466610E-03	12.49	+0.0016	-5.70	-3.95	-18.75
5,000	9.5885E-04	58,801,054	1.466603E-03	14.46	+0.0021	-6.76	-4.66	-22.17
6,000	1.1506E-03	57,585,973	1.466560E-03	16.23	+0.0050	-7.67	-5.28	-25.28
7,000	1.3424E-03	56,448,922	1.466421E-03	17.88	+0.0145	-8.50	-5.84	-28.59
8,000	1.5342E-03	55,404,728	1.466076E-03	19.40	+0.0380	-9.24	-6.34	-31.86
9,000	1.7259E-03	54,462,479	1.465643E-03	20.77	+0.0676	-9.87	-6.77	-34.92

Table D20. (continued)

Cutoff Level (Energy/Hz)	Normalised Cutoff Level	Length of the Edited History (Points)	Fatigue Damage per Repetition	% Reduction in Length of the Edited History	% Error [(+) and (-) signs mean less than and greater than, respectively.]			
					Fatigue Damage per Repetition	Mean Stress	rms	Kurtosis
10,000	1.9177E-03	53,546,191	1.464939E-03	22.10	+0.1156	-10.47	-7.18	-38.07
15,000	2.8765E-03	49,546,976	1.457297E-03	27.92	+0.6366	-12.68	-8.68	-52.63
20,000	3.8354E-03	45,958,547	1.435481E-03	33.14	+2.1241	-14.06	-9.63	-65.15
25,000	4.7942E-03	42,458,887	1.397939E-03	38.23	+4.6839	-15.05	-10.36	-76.17
30,000	5.7531E-03	39,105,560	1.341550E-03	43.11	+8.5286	-15.69	-10.88	-84.65

Table D21. Data from the edited stress-time histories generated by WT with the DB30 wavelet at wavelet decomposition level 8 (Max. AccPSD = 2,099,800 Engery/Hz)

Cutoff Level (Energy/Hz)	Normalised Cutoff Level	Length of the Edited History (Points)	Fatigue Damage per Repetition	% Reduction in Length of the Edited History	% Error [(+) and (-) signs mean less than and greater than, respectively.]			
					Fatigue Damage per Repetition	Mean Stress	rms	Kurtosis
0	0	68,739,939	1.466634E-03	0	0	0	0	0
1,000	4.7624E-04	62,033,503	1.466620E-03	9.76	+0.001	-4.55	-3.22	-14.90
2,000	9.5247E-04	58,426,836	1.466501E-03	15.00	+0.009	-7.67	-5.27	-23.49
2,100	1.0001E-03	58,117,424	1.466456E-03	15.45	+0.012	-7.91	-5.44	-24.35
2,200	1.0477E-03	57,809,234	1.466400E-03	15.90	+0.016	-8.14	-5.59	-25.22
2,300	1.0953E-03	57,514,917	1.466340E-03	16.33	+0.020	-8.38	-5.75	-26.08
2,400	1.1430E-03	57,221,358	1.466285E-03	16.76	+0.024	-8.60	-5.90	-26.96
2,500	1.1906E-03	56,929,075	1.466226E-03	17.18	+0.028	-8.82	-6.05	-27.83
3,000	1.4287E-03	55,546,345	1.465715E-03	19.19	+0.063	-9.84	-6.74	-32.30
3,100	1.4763E-03	55,273,089	1.465670E-03	19.59	+0.066	-10.05	-6.89	-33.26
3,200	1.5240E-03	55,020,207	1.465592E-03	19.96	+0.071	-10.24	-7.02	-34.16
3,300	1.5716E-03	54,749,136	1.465485E-03	20.35	+0.078	-10.43	-7.15	-35.12
3,400	1.6192E-03	54,487,824	1.465354E-03	20.73	+0.087	-10.62	-7.28	-36.07
3,500	1.6668E-03	52,425,932	1.465175E-03	23.73	+0.099	-10.78	-7.39	-36.94

Appendix E

Paper Publications

The author has published the outcomes of this study to two publishers as follows:

[1] Pratumnopharat, P. & Leung, P. S. (2011) 'Validation of various windmill brake state models used by blade element momentum calculation', *Renewable Energy*, 36(11), pp. 3222-3227 [Online]. Available at: www.sciencedirect.com (Accessed: 6th June 2011).

[2] Pratumnopharat, P., Leung, P. S. & Court, R. S. (2012) 'Application of Morlet wavelet in the stress-time history editing of horizontal axis wind turbine blades', *2nd International Symposium on Environment-Friendly Energies and Applications (EFEA 2012)*, Newcastle upon Tyne, United Kingdom 25-27 June 2012, pp. 396-401.

Publication 1

Renewable Energy 36 (2011) 3222–3227

Contents lists available at ScienceDirect

Renewable Energy

journal homepage: www.elsevier.com/locate/renene

Validation of various windmill brake state models used by blade element momentum calculation

P. Pratumnopharat*, P.S. Leung

Mechanical Engineering Division, School of Computing, Engineering and Information Sciences, Northumbria University, Ellison Place, Newcastle upon Tyne, NE1 8ST, UK

ARTICLE INFO

Article history:
Received 18 October 2010
Accepted 23 March 2011
Available online 5 May 2011

Keywords:
Blade element momentum theory
Windmill brake state model
Tip loss model
Wind turbine performance
Axial induction factor

ABSTRACT

The concept of windmill brake state model is considered in this paper. Blade Element Momentum (BEM) calculation often calculates the value of thrust coefficient in windmill brake state. Unfortunately, thrust coefficient predicted by momentum theory deviated dramatically from the experimental data when the value of axial induction factor is greater than 0.5. To solve this problem and to increase the accuracy of the prediction, windmill break state model including tip loss effect must be applied to equations of thrust coefficient. The problem of interest is that which windmill break state model is suitable for the wind turbine model being simulated. The purpose of this paper is to compare the rotor power predicted by six different windmill brake state models. The aerodynamic code based on BEM theory has been implemented in Matlab and validated with the simulated result of AWT-27 wind turbine model reported by National Renewable Energy Laboratory (NREL). Six windmill brake state models to be compared are Glauert's characteristic equation, classical brake state model, advanced brake state model, Wilson and Walker model, modified advanced brake state model, and Shen's correction. The predicted power curves obtained from each windmill brake state model are compared to the measured power curve of AWT-27/P4. It has been shown that Shen's correction gives the highest correlation to the measured data with r-square of 0.970 and the predicted annual energy production (AEP) is different from measured data by only 6.3%.

1. Introduction

In predicting performance of wind turbines, the Blade Element Momentum (BEM) theory is still commonly used by wind turbine designers and researchers. The BEM theory has significant advantages in computational speed [1,2] and ease of implementation. Historically, Glauert [3] originated the basic concepts of aerodynamic analysis of airscrew propellers and windmills. In 1974, Wilson et al. [4,5] extended Glauert's work for application to wind turbines and presented a step-by-step procedure for calculating performance characteristics of wind turbines. The accuracy of the BEM codes is dependent on two-dimensional wind tunnel test which is normally known to over-predict thrust and under-predict peak torque [6,7]. In addition, the BEM theory does not include the effects of three-dimensional flow velocities due to the rotation of the blade [7,8].

In recent years, researchers have optimized and modified the BEM calculation to provide more accurate results. Several strategies in solving the non-linear equations, e.g. iterative techniques of the induction factors and convergence rate accelerator of the induction loop [9], are proposed. There are many corrections proposed to increase the precision of prediction. Windmill brake state model is the one to be considered because the BEM calculation often calculates the value of thrust coefficient in this state of operation. Referring to Stoddard's work in 1977 [10], the behaviour of wind turbine rotors were correlated with known experimental data for helicopters reported by Glauert in 1926 [11]. Stoddard's work showed that thrust coefficient predicted by momentum theory deviated dramatically from the Glauert's experimental data (without tip loss effect) when the value of axial induction factor is greater than 0.5. To solve this problem and to increase the accuracy of the prediction, several researchers applied tip loss effect to the thrust coefficient equation and then proposed windmill break state models. The problem of interest is that which windmill break state model is suitable for the wind turbine model being simulated.

The objective of this article is to compare the wind turbine power curves predicted by BEM theory with six different windmill brake state models listed in Table 1. Also, the predicted results are compared with the existing measured power curve of AWT-27/P4 wind turbine [12]. To achieve this objective, the authors implement the aerodynamic code based on BEM theory in Matlab and validate the code with the existing WT_Perf code [13].

* Corresponding author.
E-mail address: panu.pratumnopharat@northumbria.ac.uk (P. Pratumnopharat).

0960-1481/$ – see front matter © 2011 Elsevier Ltd. All rights reserved.
doi:10.1016/j.renene.2011.03.027

Nomenclature

a	Axial induction factor
a'	Tangential induction factor
a_{new}	New value of axial induction factor
a'_{new}	New value of tangential induction factor
a_c	Critical value of axial induction factor
B	Number of blades
c	Chord length
C_D	Drag coefficient
C_L	Lift coefficient
C_T	Thrust coefficient
dQ	Torque at a blade element
dr	Blade element length
dT	Thrust at a blade element
F	Total loss factor
P	Rotor power
P_{avg}	Average power of the wind turbine
$R(V)$	Rayleigh probability distribution function
R	Rotor radius
r	Radius at any blade element
S_w	Algebraic group defined in text
V_i	Cut-in speed
V_o	Cut-out speed
V_{rel}	Relative flow velocity
V_w	Upstream wind speed
$\overline{V}$	Average wind speed at site
α	Angle of attack
β	Pre-twist angle of the blade
ϕ	Pitch angle
δ	Conning angle
$\Delta\alpha_c$	Cascade correction of angle of attack
φ	Inflow angle
λ_r	Local speed ratio
ρ	Air density
σ	Solidity ratio
Ω	Rotational velocity of the rotor

2. Blade element momentum theory

The basic concept of aerodynamic analysis is based on Glauert's airscrew theory [3]. The development of the airscrew theory followed two independent lines of thought, which may conveniently be called the *momentum* theory and the *blade element* theory. Wilson et al. [4,5] extended Glauert's airscrew theory for application to wind turbines and presented a step by step in calculating performance characteristics of wind turbines. Momentum theory refers to an analysis of thrust and torque by applying the conservation of the linear and angular momentum to an annulus control volume [14]. Blade element theory refers to an analysis of aerodynamic forces at a section of the blade as a function of blade geometry. The results of these theories are combined into what is known as *blade element momentum* (BEM) theory.

The accuracy of the BEM calculation can be improved by including the total loss factor, which is a combination of tip and hub loss factors, into the momentum analysis. The most straightforward one is Prandtl's tip and hub loss correction models [3]. Later, Prandtl's tip loss correction model was improved by [8]. The up-to-date tip loss correction model is proposed by [15].

Thrust and torque equations [5] derived from momentum theory are:

$$dT_{MT} = F4\pi r\rho V_w^2 a(1-a)dr\ \cos^2\delta \tag{1}$$

$$dQ_{MT} = F4\pi r^3\rho V_w(1-a)a'\Omega dr\ \cos^4\delta \tag{2}$$

Thrust and torque equations [5] derived from blade element theory are:

$$dT_{BET} = \frac{1}{2}\rho BcV_{rel}^2(C_L\cos\varphi + C_D\sin\varphi)dr\ \cos\delta \tag{3}$$

$$dQ_{BET} = \frac{1}{2}\rho BcV_{rel}^2(C_L\sin\varphi - C_D\cos\varphi)r\ \cos\delta\ dr \tag{4}$$

where $V_{rel} = V_w(1-a)\cos\delta/\sin\varphi$. It is to be noted that lift and drag coefficients are the function of the angle of attack (see Fig. 1).

$$\alpha = \varphi - \beta - \phi + \Delta\alpha_c \tag{5}$$

where α and φ are measured positive towards stall. β and φ are measured positive towards feather. $\Delta\alpha_c$ can be found in [5,16].

In addition, the lift and drag coefficients of an airfoil are not often available over the entire range of ±180° and the BEM codes frequently simulate conditions in which the angle of attack goes beyond the normal operating range of an airfoil. In order to generate aerodynamic coefficients in the post stall region, *a set of Viterna's empirical equations* [17–19] can be used.

When the thrust equations from momentum theory, Eq. (1), and blade element theory, Eq. (3), are equated and performed some algebraic manipulation, an expression of the axial induction factor is obtained [5].

$$a = \frac{1}{\dfrac{4F\sin^2\varphi}{\sigma\cos^2\delta(C_L\cos\varphi + C_D\sin\varphi)} + 1} \tag{6}$$

Similarly, an expression of the tangential induction factor is [5]

$$a' = \frac{1}{\dfrac{4F\sin\varphi\cos\varphi}{\sigma(C_L\sin\varphi - C_D\cos\varphi)} - 1} \tag{7}$$

where $\sigma = Bc/(2\pi r\cos\delta)$ is a solidity ratio.

By iterative method, six unknowns (φ, F, α, C_T, a, and a') can be solved and then total thrust and torque (T and Q) can be calculated. Consequently, rotor power can be easily calculated by

$$P = \int \Omega\, dQ = \Omega Q \tag{8}$$

The average power of the wind turbine is defined as

$$P_{avg} = \int_{V_i}^{V_o} PR(V)dV \tag{9}$$

where

$$R(V) = \frac{\pi}{2}\left(\frac{V}{\overline{V}^2}\right)\exp\left(-\frac{\pi}{4}\left(\frac{V}{\overline{V}}\right)^2\right) \tag{10}$$

Table 1
Windmill brake state models.

Parameters	Glauert's characteristic equation [21–23]	Classical momentum brake state model [43,13,28]	Advanced brake state model [13,22,24,25]	Wilson and Walker model [16,21]	Modified advanced brake state model [13,20,25]	Shen's correction [19]
Thrust coefficient	$C_T = \begin{cases} 4a^2(1-a), & a \le 1/3 \\ 4a(1-\frac{3}{4}a-\frac{3}{16}a), & a > 1/3 \end{cases}$	$C_T = a^2(1-a^2) = 4a_c(1-a)^2$	$C_T = \begin{cases} \frac{4a^2(1-a)}{B^2+\left(4F-\frac{40}{9}\right)a+\left(\frac{50}{9}-4F\right)a^2}, & a > 0.4 \end{cases}$	$C_T = \begin{cases} 4a^2(1-a), & a \le a_c \\ 4a^2[4-(1-2a_c)a], & a > a_c \end{cases}$	$C_T = \begin{cases} 4a^2(1-a), & a < 0.4 \\ F(0.889) = 0.4464a + 1.556a^2, & a \ge 0.4 \end{cases}$	$C_T = \begin{cases} 4a^2(1-a), & a \le a_c \\ 4[a^2F + (1-2a_c)F]a, & a > a_c \end{cases}$
Axial induction factor	$a = \begin{cases} \frac{1-\sqrt{1-C_T/F}}{2}, & C_T \le 0.889F \\ \frac{1}{3}+\frac{5}{36}+\sqrt{\left(\frac{1}{3}-\frac{5}{36}\right)^2+\frac{C_T}{9F}}, & C_T > 0.889F \end{cases}$	$a = \frac{2k_c+F-\sqrt{(F-4k_c)(1-F)}}{2(k_c+F)}$	$a = \frac{18F-20-3\sqrt{C_T(50-36F)+12F(3F-4)}}{36F-50}$	$a = \begin{cases} \frac{1-\sqrt{1-C_T/F}}{2}, & C_T \le 0.64F \\ \frac{C_T-4F}{4(1-2a_c)}, & C_T > 0.64F \end{cases}$	$a = \begin{cases} \frac{1-\sqrt{1-C_T/F}}{2}, & C_T < 0.96F \\ 0.1432+\sqrt{-0.05108+0.6427\frac{C_T}{F}}, & C_T \ge 0.96F \end{cases}$	$a = \begin{cases} \frac{1-\sqrt{1-C_T}}{2}, & C_T \le 0.888 \\ \frac{2+Y(1-F)-\sqrt{Y(1-F)+Y^2}}{2(1+Y)}, & C_T > 0.888 \end{cases}$
Tangential induction factor	$a' = \frac{1}{\frac{4F\sin\varphi\cos\varphi}{\sigma'(C_L\sin\varphi-C_D\cos\varphi)}-1}$	$a' = \frac{1}{\frac{4F\sin\varphi\cos\varphi}{\sigma'(C_L\sin\varphi-C_D\cos\varphi)}+1}$	$a' = \frac{1}{\frac{4F\sin\varphi\cos\varphi}{\sigma'(C_L\sin\varphi-C_D\cos\varphi)}-1}$	$a' = \frac{1}{\frac{4F\sin\varphi\cos\varphi}{\sigma'(C_L\sin\varphi-C_D\cos\varphi)}-1}$	$a' = \begin{cases} \frac{0}{\sqrt{1+\frac{4F}{\pi\lambda_r^2}}-1}, & 1+\frac{4F}{\pi\lambda_r^2} < 0 \\ \frac{1}{2}, & 1+\frac{4F}{\pi\lambda_r^2} \ge 0 \end{cases}$	$a' = \frac{1}{\frac{(1-3F)^2}{1-a}-1}$
Constants	$Y = \begin{cases} \frac{1}{\frac{3}{16}\left(\frac{C_T}{F}\right)^2+\frac{3}{4}}, & C_T \le \frac{8}{9}F \\ \frac{145}{169}\frac{C_T}{F}+\frac{32}{2197}+\left(\frac{C_T}{F}-\frac{145}{169}\right)^{1/3}, & C_T > \frac{8}{9}F \end{cases}$	$S_m = \frac{\sigma'\cos^2\varphi}{8\sin^2\varphi}(C_L\cos\varphi+C_D\sin\varphi)$ $\sigma' = \frac{Bc}{2\pi r\cos\varphi}$	–	$a_c = 0.2$	$a^* = \frac{4aF(1-a)}{\lambda_r^2}$	$a_c = 1/3$ $Y_1 = \frac{4F\sin^2\varphi}{\sigma'(C_L\cos\varphi+C_D\sin\varphi)}$ $Y_2 = \frac{4F\sin\varphi\cos\varphi}{\sigma'(C_L\cos\varphi-C_D\cos\varphi)}$ $F_1 = \frac{2}{\pi}\cos^{-1}\left[\exp\left(-\frac{B(R-r)}{2r\sin\varphi}\right)\right]$ $g = \exp(-0.125(\lambda_r-21))+0.1$ $F = \frac{F_1}{gF_2}$

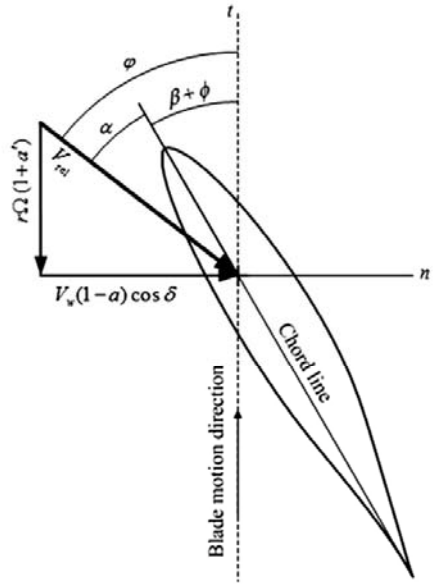

Fig. 1. Parameters relevant to the angle of attack.

3. Windmill brake state models

In 1926, Glauert [11] reported the experimental results showing thrust coefficient equation, $C_T = 4a(1-a)$, is not valid if the axial induction factor exceeds 0.4 approximately (see Fig. 2). *Glauert's empirical formula* was reported in a quadratic form [20].

$$C_T = 0.889 - 0.444a + 1.556a^2 \tag{11}$$

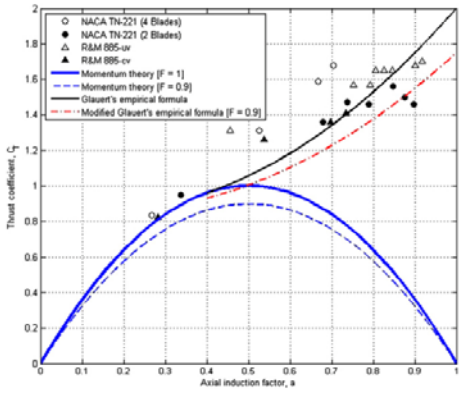

Fig. 2. Discontinuity problem (experimental data are digitised from [5]).

Eq. (11) gives the same value as momentum theory when a is 0.4, as well as the same slope of the curve, and yields $C_T = 2$ at $a = 1$ (see Fig. 2). However, the total loss factor is not taken into account. In the BEM calculation, a numerical problem (gap) occurs when the total loss correction factor is applied to the thrust equation obtained from the classical momentum theory, i.e. $C_T = 4aF(1-a)$. Plotting Eq. (11) shows a gap between the momentum theory curve and Glauert's empirical curve as shown in Fig. 2. This gap causes a discontinuity when a computer is used to iterate for the new value of axial induction factor.

In 1981, Hibbs and Radkey [20] modified Glauert's empirical formula, Eq. (11), by replacing a with aF, i.e.

$$C_T = 0.889 - 0.444aF + 1.556a^2F^2 \tag{12}$$

This modification just lowers the entire parabolic curve and cannot completely eliminate the gap problem as shown in Fig. 2. To solve discontinuity, six different windmill brake state models (listed in Table 1) have been included in BEM calculation.

3.1. Glauert's characteristic equation

Glauert's characteristic equation found in [21–23] is a cubic equation (see Fig. 3(a)).

$$C_T = 4aF\left(1 - \frac{1}{4}(5-3a)a\right), \quad a > 1/3 \tag{13}$$

3.2. Classical momentum brake state model

In 1974, Wilson and Lissaman [4] developed a wind turbine analysis computer code named PROP and used *Wilson model* as a windmill brake state model. Later, in 1976, Wilson, Lissaman and Walker [5] reported the state of the art of performance prediction

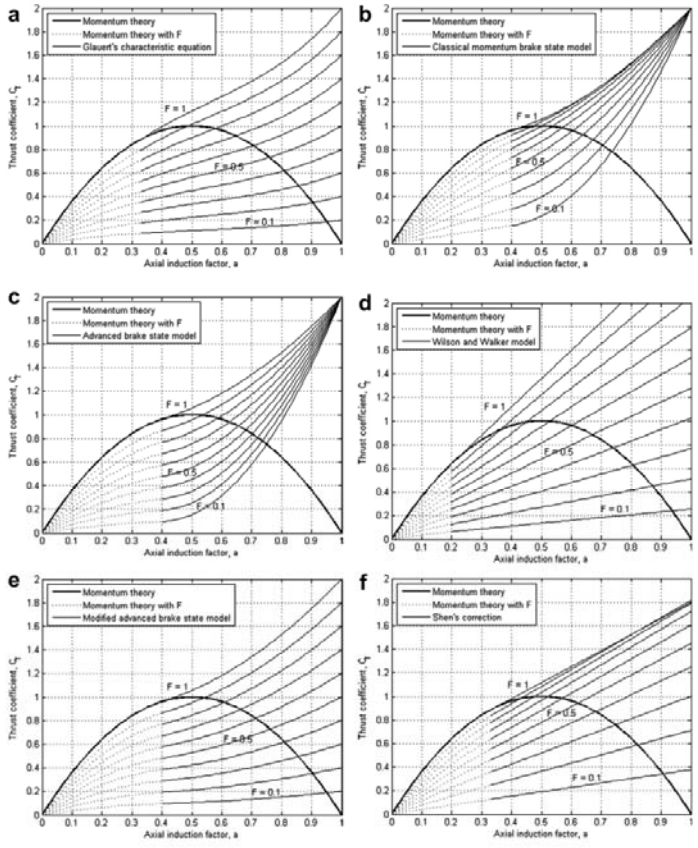

Fig. 3. Windmill brake state models: (a) Glauert's characteristic equation; (b) classical momentum brake state model; (c) advanced brake state model; (d) Wilson and Walker model; (e) modified advanced brake state model; (f) Shen's correction.

methods for both horizontal and vertical wind turbines and suggested using Wilson model (see Fig. 3(b)) to predict the wind turbine performance. From 1981 to 1983, Hibbs and Radkey [20] updated version of the PROP code and renamed Wilson model as *classical momentum brake state model*. At present, this model has been using by WT_Perf [13] under the name *classical brake model*.

$$C_T = (1-aF)aF = \frac{\sigma\cos^2\delta}{4\sin^2\varphi}(C_L\cos\varphi + C_D\sin\varphi)(1-a)^2 \qquad (14)$$

3.3. Advanced brake state model

Referring to Eq. (11), this equation was called advanced brake state model by Hibbs and Radkey [20]. Unfortunately, it cannot completely eliminate gab problem. In 1997, Buhl [13] simplified the calculation of advanced brake state model implemented in WT_Perf by replacing original advanced brake state model with a simple parabola (see Fig. 3(c)).

$$C_T = B_2a^2 + B_1a + B_0 \qquad (15)$$

where

$$\begin{aligned} B_2 &= 1/0.18 - 4F \\ B_1 &= 0.8(F - B_2) \\ B_0 &= 2 - B_1 - B_2 \end{aligned} \qquad (16)$$

In 2005, Buhl [24] published this simplification, Eq. (15), in another form.

$$C_T = \frac{8}{9} + \left(4F - \frac{40}{9}\right)a + \left(\frac{50}{9} - 4F\right)a^2, \quad a > 0.4 \qquad (17)$$

Eq. (17) has also been found in AeroDyn [25].

3.4. Wilson and Walker model

Wilson [16] reported Wilson and Walker model which is published in 1984. This model is a straight line (see Fig. 3(d)) derived by the first order of Taylor series. Wilson quoted that this model well agrees with vortex theory calculations and produces good results between the calculated and measured performance and loads. At present, this model is also reported in [21].

$$C_T = 4F\left[a_c^2 + (1-2a_c)a\right], \quad a > (a_c \approx 0.2) \qquad (18)$$

3.5. Modified advanced brake state model

In 1998, Buhl [13] modified the use of Glauert's empirical formula [20] implemented in WT_Perf so that the coefficients of the quadratic (see Fig. 3(e)) are a function of the losses.

$$C_T = 0.889F - 0.444aF + 1.556a^2F^2, \quad a > 0.4 \qquad (19)$$

Table 2
Annual energy production (AEP) at 8.5 m/s annual average wind speed at site.

Windmill brake state models	AEP [kWh]
AWT-27/P4 measured data [12]	792,780
Glauert's characteristic equation	821,722
Classical momentum brake state model	793,399
Advanced brake state model	812,563
Wilson and Walker model	859,510
Modified advanced brake state model	811,306
Shen's correction	842,475
Without brake state model	776,908

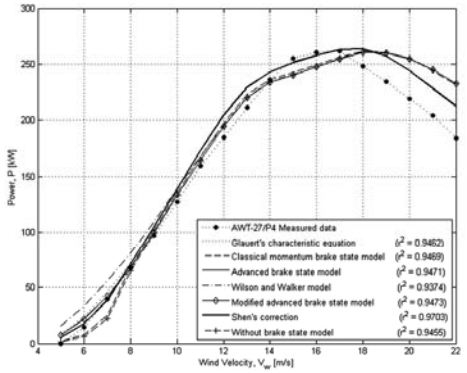

Fig. 4. Rotor power curve.

Buhl did not name this relation, so, in this paper, it might be called *modified advanced brake state model*. Also, Buhl changed equation of thrust coefficient for $a \le 0.4$ from $C_T = 4aF(1-aF)$ to $C_T = 4aF(1-a)$. In the same year, Pierce and Buhl changed the induction factor calculations in AeroDyn to mimic that of WT_Perf.

3.6. Shen's correction

In 2005. Shen et al. [15] proposed a new tip loss correction model to predict the physical behaviour in the proximity of the tip. The local thrust coefficient is replaced by a linear relation (see Fig. 3(f)) when the value of axial induction factor becomes greater than a critical value.

$$C_T = 4\left[a_c^2F^2 + (1-2a_cF)aF\right], \quad a > (a_c = 1/3) \qquad (20)$$

where

$$a = \frac{2 + Y_1 - \sqrt{4Y_1(1-F) + Y_1^2}}{2(1+FY_1)} \qquad (21)$$

$$Y_1 = \frac{4F\sin^2\varphi}{\sigma F_1(C_L\cos\varphi + C_D\sin\varphi)} \qquad (22)$$

$$F_1 = \frac{2}{\pi}\cos^{-1}\left[\exp\left(-g\frac{B(R-r)}{2r\sin\varphi}\right)\right] \qquad (23)$$

$$g = \exp[-0.125(B\lambda_r - 21)] + 0.1 \qquad (24)$$

4. Comparison of windmill brake state models

In this section, power curve of AWT-27/P4 wind turbine model [12] is used as a base line. Each windmill brake state model listed in Table 1 is implemented in aerodynamic code. The predicted and measured power curves are compared and shown in Table 2 and Fig. 4.

5. Conclusions

Based on BEM theory, this paper compares the rotor power curves predicted by using six different windmill brake state models

to the measured rotor power curve of AWT-27/P4 wind turbine. Firstly, it is convenient to compare a rotor power curve predicted by the BEM theory without windmill brake state model to the measured rotor power curve. Considering the first range of wind speed (5–8 m/s) in Fig. 4, the predicted curve deviated from the measured one. In the second range (8–14 m/s), the predicted curve agrees with the measured one but slightly over-predict. In the third range (14 to 17 m/s), the predicted power level is less than the measured data and vice versa for the fourth range (17–22 m/s).

Secondly, all predicted power curves with windmill brake state model are compared to the curve predicted by without using windmill brake state model. The power curves predicted by using each model show the same pattern as the one without windmill brake state model in the range of wind speed from 8 to 22 m/s. In this range, the power curve predicted by using Shen's correction is closer to the measured curve. In the normal operating range (8–17 m/s), each windmill brake state model has little effect on power curve or energy production. However, it is important to consider the predicted power curves in a startup or shutdown operation (5–8 m/s). In this range, the predicted power curves can be classified into three groups. The first group, which consists of the classical momentum brake state model and without brake state model, predicts lower power level than the measured one. The second group, which is Wilson and Walker model, predicts higher power level than the measured one. The last group, which consists of Glauert's characteristic equation, advanced brake state model, modified advanced brake state model and Shen's correction, predicts the power level close to the measured one. In addition, the power curve predicted by using the advanced brake state model and Glauert's characteristic equation are nearly coincided. Finally, the variation between all of the predicted results and the measured AEP values listed in Table 2 are less than 9%.

It is clear from the present study that Shen's correction gives the highest correlation to the measured data with r-square of 0.970 and its predicted AEP compared to measured data is 6.3%.

Acknowledgements

The authors would like to thank the Royal Thai Government Scholarship for financial support.

References

[1] Clifton-Smith MJ. Wind turbine blade optimization with tip loss corrections. Wind Engineering 2009;33:477–96.
[2] Lanzafame R, Messina M. Power curve control in micro wind turbine design. Energy 2010;35:556–61. doi:10.1016/j.energy.2009.10.025.
[3] Glauert H. In: Durand WF, editor. Airplane propellers Aerodynamic Theory, vol. IV; Division L. 1935. p. 169–360.
[4] Wilson RE, Lissaman PBS. Applied aerodynamics of wind power machines. The National Science Foundation; 1974. 1–109.
[5] Wilson RE, Lissaman PBS, Walker SN. Aerodynamic performance of wind turbines; 1976. p. 1–164.
[6] Tangler JL, Michael SS. An evaluation of an empirical model for stall delay due to rotation for HAWTs. Report NREL/CP-440-23258. National Renewable Energy Laboratory; July 1997. p. 1–13.
[7] Benini E. Significant of blade element momentum theory in performance prediction of marine propellers. Ocean Engineering 2004;31:957–74.
[8] Xu G, Sankar LN. Development of engineering aerodynamics models using a viscous flow methodology on the NREL phase VI rotor. Wind Energy 2002;5:171–83. doi:10.1002/we.73.
[9] Maheri A, Noroozi S, Toomer C, Vinney J. Damping the fluctuating behaviour and improving the convergence rate of the axial induction factor in the BEMT based rotor aerodynamic codes. European Wind Energy Conference & Exhibition, Athens, Greece; 27 February–2 March 2006. p. 1–4.
[10] Stoddard FS. Momentum theory and flow states for windmill. Wind Technology Journal 1977;1:3–9.
[11] Glauert H. The analysis of experimental results in the windmill brake and vortex ring states of an airscrew. Reports and memoranda, no. 1026 His Majesty's Stationery Office; 1926. p. 1–8.
[12] Poore R. NWTC AWT-26 research and retrofit project summary of AWT-26/27 turbine research and development. National Renewable Energy Laboratory; January 2000. Subcontract Report NREL/SR-500-269261–51.
[13] Buhl ML, Jr., NWTC Design Codes (WT_Perf by Marshall Buhl), National Wind Technology Center, Last modified 21st June 2004 [Online]. Available from: http://wind.nrel.gov/designcodes/simulators/wtperf/ [accessed 20 October 2009].
[14] Manwell JF, McGowan JG, Rogers AL. Wind energy explained: theory, design and application. John Wiley & Sons Inc.; 2002.
[15] Shen WZ, Mikkelsen R, Sorensen JN, Bak C. Tip loss corrections for wind turbine computations. Wind Energy 2005;8:457–75. doi:10.1002/we.153.
[16] Wilson RE. Aerodynamic behavior of wind turbines. In: Spera DA, editor. Wind turbine technology: fundamental concepts of wind turbine engineering. ASME Press; 1998. p. 215–82.
[17] Viterna LA, Corrigan RD. Fixed pitch rotor performance of large horizontal axis wind turbines. NASA Lewis Research Center; 1982. 69–85.
[18] Laino DJ. NWTC Design Codes (FoilCheck by Dr. David J. Laino), (Version 2.03). Last modified 10 May 2005, National Wind Technology Center. Available from: http://wind.nrel.gov/designcodes/preprocessors/foilchk/ [accessed 20 October 2009].
[19] Hansen C. NWTC Design Codes (AirfoilPrep by Dr. Craig Hansen), (version v2p2), Last modified 15 January 2007, National Wind Technology Center. Available from: http://wind.nrel.gov/designcodes/preprocessors/airfoilprep/ [accessed 20 October 2009].
[20] Hibbs B, Radkey RL. Calculating rotor performance with the revised 'PROP' computer code. Report No. PFN-13470W. AeroVironment, Inc.; 1983. pp. 1-813.
[21] Hansen MOL. In: Aerodynamics of wind turbines. 2nd ed. London: Earthscan; 2008.
[22] Bak C, Fuglsang P, Sørensen NN, Madsen HA, Shen WZ, Sørensen JN. Airfoil characteristics for wind turbines. Risø National Laboratory, Report No. Risø R-1065(EN); March 1999. p. 1–51.
[23] Mejia JM, Chejne F, Smith R, Rodriguez LF, Fernandez O, Dyner I. Simulation of wind energy output at Guajira, Colombia. Renewable Energy 2006;31:383–99. doi:10.1016/j.renene.2005.03.014.
[24] Buhl, ML. Jr., A new empirical relationship between thrust coefficient and induction factor for the turbulent windmill state. National Renewable Energy Laboratory, technical report NREL/TP-500-36834; August 2005. p. 1–7.
[25] Laino DJ. NWTC design codes (AeroDyn by Dr. David J. Laino) (version 12.58). Last modified: 5 July 2005. Available from: http://wind.nrel.gov/designcodes/simulators/aerodyn/ [accessed 20 October 2009].

Publication 2

2nd International Symposium on Environment-Friendly Energies and Applications (EFEA 2012) Northumbria University

Application of Morlet Wavelet in The Stress-Time History Editing of Horizontal Axis Wind Turbine Blades

Panu Pratumnopharat[1], Pak Sing Leung[1] and Richard S. Court[2]
1: Mechanical Engineering Division
School of Computing, Engineering and Information Sciences, Northumbria University
Newcastle, UK
panu.pratumnopharat@northumbria.ac.uk
ps.leung@northumbria.ac.uk
2: National Renewable Energy Centre, NaREC
Newcastle, UK
richard.court@narec.co.uk

***Abstract*—This article presents a novel method in extracting fatigue damage from the stress-time history of the horizontal axis wind turbine blades. A novel method based on wavelet transform (WT) is proposed to shorten the length of the stress-time history. Based on Morlet wavelet (Morl), WT is taken to the stress-time history to generate a plot of accumulative power spectral density (PSD) distribution with time. The variation of fatigue damage with the accumulative PSD levels is studied to determine the cutoff level which is controlled by the differences in the global signal statistics (mean stress, root-mean-square and kurtosis).**

WT method uses the cutoff level as a criterion in identifying fatigue damage parts at time locations of the stress-time history. Then, the fatigue damage parts are extracted from the original stress-time history and concatenated to form the edited stress-time history. In addition, Time Correlated Fatigue Damage (TCFD) method, which is an existing used by commercial software, is used to study the effectiveness of WT method. The comparison of the differences in fatigue damage and stress-time history length produced by TCFD and WT methods is performed. It is found that the differences in fatigue damage of TCFD and Morl are +0.076% and +0.013%. The lengths of the edited stress-time history provided by TCFD and Morl are 89.8% and 82.3% of the original length, respectively. The results suggest that not only does WT method improve accuracy of fatigue damage retained in the edited stress-time history, but also it provides the length of the edited stress-time history shorter than TCFD method does. Also, the results suggest that WT method is a useful method for performing accelerated fatigue tests.

Finally, WT method is suggested as an alternative technique in fatigue durability study, especially for the field of wind turbine engineering.

Keywords- Wavelet transform; Power spectral density; Fatigue data editing; Horizontal axis wind turbine blades

I. INTRODUCTION

Modern wind turbines are fatigue critical machines [1] used to generate electricity from the wind. These rotating machines are subject to combination of several loadings that are highly irregular in nature. Also, the blades of a wind turbine rotor are generally regarded as the most critical components of the wind turbine system [2]. The problem of interest is that wind turbine blades failed at unexpectedly high rates. The major cause of this failure is fatigue due to cyclic nature of the loading [3-6].

The unexpectedly high rate of the blade failure led the designers and researchers to develop fatigue analysis capabilities to prevent breakage of the blade. After finalising the aerodynamic design of any new blade, the fatigue life of the blades in their structural design must be carefully considered and the full scale testing needs to be done to ensure the blade can withstand all likely loading during service. Structural design requirements, such as strain limit along the fibre direction, surface stress limit, and fatigue life time over 20 years, are specified by the design requirements of the IEC 61400-1 international specification [7]. Thus, the wind turbine blades must have long operation life of 20-30 years.

Fatigue test must be carried out at some at some stage in a development of a blade to gain confidence in its ultimate service performance and on legal requirement. Full-scale testing is evaluated where the desire to reduce production costs must be balanced with the necessity to avoid expensive service failures. A full-scale fatigue test of a wind turbine blade is considered as an essential part of verifying the design of any new wind turbine blades. Wind turbine blades experience a range of complex forces throughout their working life, and it is not possible to simulate exactly these conditions in any accelerated laboratory experiments [4]. Also, durability requires knowledge of service loads because these loads are used for the laboratory testing of the component [8-9]. The objective of laboratory based accelerated testing is to expose the component to a test loading which is much shorter than the target loading, but which has approximately the same damage potential. These techniques are used to accelerate laboratory fatigue testing [10], to increase the frequency of the cyclic loading, to increase the load level, and to remove small amplitude cycles from the time history. Without editing the service load before performing the tests, test time and cost can become prohibitive.

II. Importance of Fatigue Data Editing

At present, it is found in the wind turbine community that racetrack method is the only one method found to be existing used in editing fatigue loading. Racetrack method [11] is used to produce a condensed history in which essential peaks and valleys are listed in their original sequence. By removing small amplitude cycles from the time history, this method is useful for condensing histories to those few events, perhaps the 10 percent of events that do most of the damage, which usually account for more than 90 percent of all calculated damage [11-13]. Unfortunately, racetrack method does not compress or shorten the length of the fatigue loading; say, the edited loading will have the same time length as the original loading. So, it cannot serve the purpose of accelerating testing time and reducing energy cost in testing. The need to reduce testing time and energy cost whilst simultaneously retaining the high amplitude cycles that produce the majority of fatigue damage is of interest to investigate the issue of fatigue loading compression.

The authors review the techniques of fatigue data editing. For all the fatigue data editing techniques, different variable loadings were used for different techniques. It seems to be no generally agreed rules that clarify which method is the best, or what amplitude should be chosen for load omission. In practice, any fatigue data editing technique must reduce the testing period and be technically valid.

As mentioned earlier, racetrack method cannot compress the time history. This is the problem that motivated the authors to interest in fatigue data editing by removing small amplitude cycles. Such a method is defined as a method for omitting the small amplitude cycles which provide a minimal contribution to the overall fatigue damage, whilst retaining the high amplitude cycles which are the most damaging sections [10]. In the wind turbine applications, this concept is still not proposed for the purpose of achieving accelerated fatigue tests which shorten the total test time required. Such a method to summarise variable loadings measured on the wind turbine blade whilst preserving the local load-time cycle sequences is the subject of this article.

The objectives of this article are to present a novel method in extracting fatigue damage parts from the stress-time history of horizontal axis wind turbine (HAWT) blades and to study the efficiency of the novel method proposed. A novel method is based on wavelet transform (WT). The Morl wavelet function is used to identify and extract fatigue damaging parts from a stress-time history of HAWT blades. Then, the extracted segments are combined to produce a shortened signal called an edited stress-time history. Furthermore, it has equivalent global signal statistics and fatigue damage as the original stress-time history.

The research described in this article was motivated by the authors' belief that WT is a suitable method for use in fatigue data editing. Since the stress-time history normally exhibit nonstationary signal behaviour, WT (time-scale analysis) would be expected to be a natural choice of analysis method. With this method, the fatigue loading sections that produce the majority of fatigue damage can be identified based on the concept of accumulative power spectral density (PSD) level. Furthermore, literature review suggests that there is no fatigue data editing technique used WT for identifying and extracting fatigue damage parts from the stress-time history of HAWT blades.

III. Material and Methods

A. Wind Turbine Blade Model

The HAWT blade used in this study is a pseudo model of a SERI-8 blade [14] developed by Solar Energy Research Institute (SERI) which is now called the National Renewable Energy Laboratory (NREL). The SERI-8 blades were installed on modified Micon 65 wind turbines having a generator rating of 65 kW.

B. Material Properties

The fibreglass composite material used in modelling the pseudo SERI-8 blade is a laminate called DD16. This material has been listed in DOE/MSU composite material fatigue database for wind turbine blades [15]. The fatigue and mechanical properties of material DD16 are listed in [16].

C. Wind Speed Data

The wind speed data is obtained from the OWTES project [17]. It was recorded to establish the dynamic behaviour, fatigue load spectra, and extreme load experienced by the wind turbine. It was measured by using anemometers at a reference height of 61.8 m above ground level in north-east England. A wind shear exponent value of the wind speed data was 0.294 fitted by power law. The wind speed data was sampled at 40 Hz for 68,739,939 data points which gave the total record length of the signal of 1,718,498.475 seconds. Since the hub height of the Micon 65 wind turbine is at 22.86 m, the wind speed at this altitude is evaluated by power law.

D. Stress-Time History

The relationship between stress and wind speed is generated by using three computer programmes. HAWTsimulator [18], in-house software, is used to generate the sets of aerodynamic loads at wind speeds ranging from cut-in to cut-out. This software is an aerodynamic computer code based on blade element momentum theory. It is designed to be run in Matlab environment. NuMAD software [19] is used to generate a finite element model of the pseudo SERI-8 blade. Both the sets of aerodynamic loads and the finite element model (Esize = 0.01 m, 160,602 Elements, 480,173 nodes) are imported to ANSYS structural software to determine a critical value of von-Mises stress and its location on the blade. Having finished stress analysis in ANSYS, the relationship between stress and wind speed is generated.

HAWTfatigue, in-house software, is used to generate a stress-time history. This software is a fatigue computer code for HAWT blades. It is designed to be run in Matlab environment. By relating the relationship between wind speed and time with the relationship between stress and

wind speed, the stress-time history is generated. For the purpose of illustration, the very long stress-time history is separated into seven parts as shown in Figure 5. This history is treated as an original stress-time history and it will be edited by Time Correlated Fatigue Damage (TCFD) method in commercial software and WT method in HAWTfatigue.

The rainflow cycles contained in the stress-time history are counted by rainflow cycle counting method [20]. In general, each rainflow cycle counted has different values of *R*-ratio, so HAWTfatigue interpolates for the number of cycles to failure of each cycle by using a family of *S-N* curves. Consequently, the fatigue damage can be evaluated by a fatigue damage model commonly known as Miner's rule [21-22]. The iterative calculation is performed until the total damage value is 1.0 or closer. Then, the total damage is converted to service lifetime in the unit of months and years.

E. WT-Based Stress-Time History Editing

This section introduces to the application of WT in extracting the fatigue damage parts from the original stress-time history. Based on WT, HAWTfatigue edits the original stress-time history in the time-scale domain. The result is the shortened or edited stress-time history. The process of fatigue damage extraction is shown in Figure 1.

The result of WT process is the wavelet coefficients produced at different scales by different sections of the history. The wavelet coefficients constitute the results of a regression of the original stress-time history performed on the wavelets. To make sense of all coefficients, a plot on which the *x*-axis represents position along the history (time or data point number), the *y*-axis represents scale, and the colour at each *x*-*y* point represents the magnitude of the wavelet coefficient. This plot is called scalogram.

In this study, WT is performed for 8 decomposition levels (maximum). Morl wavelet function is applied to the original stress-time history shown in Figure 5 and the scalogram is generated. A plot of accumulative PSD distribution with time is generated by summing the PSD of wavelet coefficients for all scale bands at each time interval. Also, the plot provides the accumulative PSD level information at time location and it has a significant relation to the fatigue damage potential distribution (see Section V). The damaging events can be determined by a cutoff level. The cutoff level is an appropriate value of the accumulative PSD which separates the damage and non-damage events in the history. The events that have accumulative PSD level higher than or equal to the cutoff level are classified as damage parts. On the other hand, the events that have accumulative PSD level lower than the cutoff level are classified as non-damage parts. Eventually, all damage parts are concatenated to form the edited stress-time histories shown in Figure 7. Its length is shorter than the original length whilst the majority of the fatigue damage can be retained.

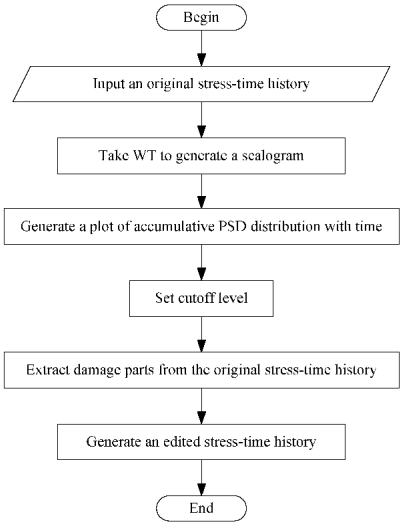

Figure 1. Flowchart for extracting fatigue damage.

IV. THEORY

A wavelet is a waveform of effectively limited duration that has an average value of zero [23]. On the condition of admissibility condition, a wavelet is a small wave with a signal energy concentrated in time [24]. Wavelets are different from sine waves, which are the basis of Fourier analysis. Sinusoids do not have limited duration and they extend from minus to plus infinity. Sinusoids are smooth and predictable whilst wavelets tend to be irregular and asymmetric. Wavelet transform represents the next logical step of a windowing technique with variable-sized regions. Wavelet analysis allows the use of long time intervals where the low frequency information is wanted, and shorter regions where the high frequency information is wanted. In the literature, there are four different views of a signal presented by the time-based, frequency-based, short-time Fourier transform, and wavelet analyses [23]. It is noticed that wavelet analysis does not use a time-frequency region but rather a time-scale region.

Wavelet is capable of revealing aspects of data that other signal analysis techniques miss, aspect like trends, breakdown points, discontinuities in higher derivatives, and self-similarity. Furthermore, wavelet analysis can often compare or de-noise a signal without appreciable degradation [23] because it affords a different view of data than those presented by traditional techniques. Fourier transform breakes up a signal into sine waves of various frequencies. Similarly, wavelet transform breaks up a signal into shifted and scaled versions of the original or mother

wavelet. Signals with sharp changes might be better analysed with an irregular wavelet than with a sinusoid [23]. It also makes sense that local features can be described better with wavelets that have local extent.

The wavelet transform is defined in the time-scale domain and is a significant tool for analysing time-localised features of a signal. It represents a windowing technique with variable-sized region. The harmonic form of the wavelet transform can be derived from the Fourier transform in the phase form.

A wavelet transform can be classified as either a continuous wavelet transform (CWT) or a discrete wavelet transform (DWT) depending on the discretisation of the scale parameter of the analysing wavelet. The wavelet method can solve the resolution problem because the window length is long for low frequencies and short for high frequencies. Therefore, the frequency resolution is good for low frequencies (at high scales) and the time resolution is good at high frequencies (low scales). One of the earliest practical applications of wavelet analysis has been used in many applications in science and engineering.

V. Validation of Wt-Based History Editing

The validation process of WT-based stress-time history editing is presented in Figure 2. The segment 52 of the original stress-time history in Figure 5 is particularly selected for evaluating the newly developed fatigue damage extracting technique associated with the WT. The plots of accumulative PSD for damage and non-damage parts extracted by WT method in HAWTfatigue are compared to those extracted by TCFD method [25] in commercial software.

Comparing the segment 52 in Figure 3(*a*) to its plot of accumulative PSD distribution with time in Figure 3(*b*) shows an analogy between magnitudes of accumulated PSD and stress magnitudes, especially at positions 1 to 26 where both of them posses high magnitudes. The accumulative PSD of each part is investigated to study the efficiency of WT method based on fatigue damage event. Figures 3(*c*) and 3(*d*) show that the damage part contained accumulative PSD value higher than the cutoff level represented by a dash line. Here, the cutoff level is 2400 Energy/Hz. On the other hand, Figures 4(*c*) and 4(*d*) show that the non-damage part contained accumulative PSD value lower than the cutoff level. Based on cutoff level as a criterion, there are some disagreement between TCFD and WT methods in the regions *A*, *B*, *C* and *D* shown in Figure 3(*c*). Especially in region *A*, peaks 7 and 8 appear but TCFD does not detect them as the damage parts whilst WT does. In the region *B*, almost peaks are higher than the cutoff level but TCFD does not detect them as the damage parts. The same situation occurs in the regions *C* and *D*. Nevertheless, it is clearly seen that the damage parts provide information of higher accumulative PSD at time location. Furthermore, the accumulative PSD has a significant relation to the fatigue damage potential distribution.

The validation result suggests that the accumulative PSD gained from WT method is enable us to detect the damage events contained in the given stress-time history.

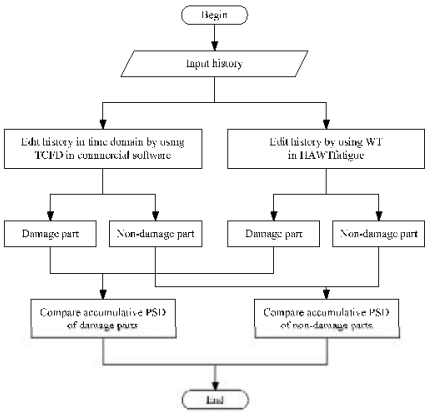

Figure 2. Flowchart for the validation of WT effectiveness.

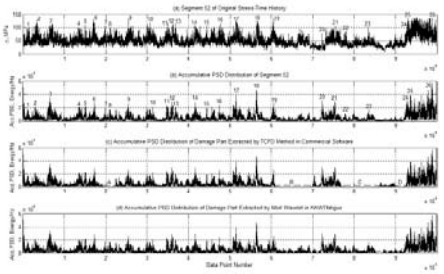

Figure 3. Accumulative PSD distribution of damage part.

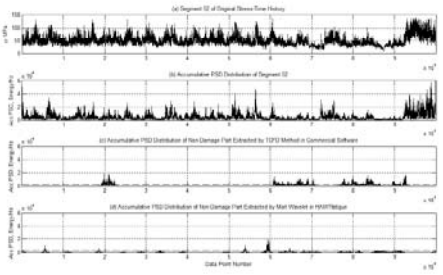

Figure 4. Accumulative PSD distribution of non-damage part.

VI. Results and Discussion

In this article, the original stress-time history shown in Figure 5 is edited by TCFD and WT methods. The first method is done in time domain whilst the second method is done in time-scale domain. This section discusses the results obtained from each method.

TCFD method is the time domain editing technique used by commercial software. This technique is used to remove non-damaging sections of the original stress-time history on the basis of time correlated fatigue damage windows of the input signal. Based on TCFD method, the damage signal is divided into a number of time segments. Then, fatigue damage is calculated for each time-window containing a short segment of stress-time history. Windows having minimal damage are removed to retain the windows containing the majority of the fatigue damage. These windows are assembled together to produce the edited stress-time history as shown in Figure 6. Its length is 89.8% of the original length with fatigue damage error of +0.076% as listed in Table I.

TABLE I: SUMMARY RESULTS

Method	% Compression	% Error			
		Fatigue Damage	Mean Stress	rms	Kurtosis
TCFD	10.2	+0.076	-3.04	-2.64	-14.05
Morl	17.7	+0.013	-9.98	-6.82	-32.22

For WT method, HAWTfatigue is used to edit the original stress-time history. By using decomposition level 8, the events that have accumulative PSD level higher than or equal to the cutoff level are classified as damage parts. On the other hand, the events that have accumulative PSD level lower than the cutoff level are classified as non-damage parts. Here, the fatigue damage parts contained in the original stress-time history are extracted by each wavelet type at the cutoff levels listed in Table I. Eventually, each damage part is concatenated to form the edited stress-time history as shown in Figure 7.

In this article, the authors compare the efficiency of fatigue damage extraction between TCFD and WT methods. From Table I, it is clearly seen that the differences in both mean stress and rms for each method are within $\pm 10\%$, whilst the differences in kurtosis are beyond $\pm 10\%$. Furthermore, the results in Table I indicate that $\pm 10\%$ error of kurtosis cannot be used as a criterion for the given stress-time history. However, each method provides the difference in fatigue damage very much less than $\pm 1\%$. Thus, it is indicated that each method has high potential in identifying fatigue damage events contained in the given original stress-time history, especially WT method. Having considered the length of the edited stress-time histories, results in Table I shows that Morl provides the length of the edited stress-time history as 82.3% of the original length, whilst TCFD method provides 89.8%.

Finally, the findings suggest that WT method can be used for extracting the damage parts from the stress-time history of HAWT blades. Not only does WT method provide shorter length of the edited stress-time history than TCFD does but also it improves the accuracy of the edited stress-time history. Furthermore, the findings suggest that WT is a suitable method.

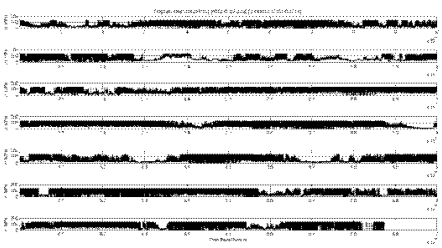

Figure 5. Original stress-time history.

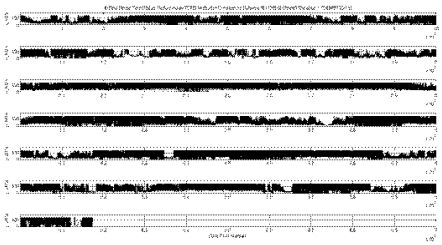

Figure 6. Edited stress-time history performed by TCFD method.

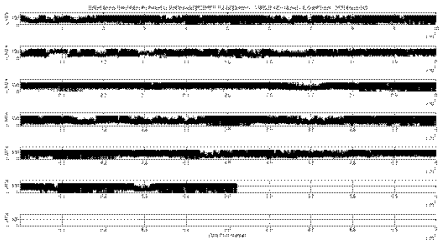

Figure 7. Edited stress-time history performed by Morl wavelet.

VII. CONCLUSIONS

At present, the concept of using WT in editing stress-time history of HAWT blades is not proposed by any researchers. This article discusses the study of a fatigue damage extracting technique in time-scale domain by using WT method. Wavelet function used in this study is Morl. The WT method proposed and developed in this research can be used to edit stress-time history of HAWT blades.

WT method is able to solve the problem of retaining sequence information when summarising stress-time history of HAWT blades. WT algorithm is developed to identify and extract fatigue damaging parts from the original stress-time history. The edited stress-time history which preserves the load cycle sequence is generated from the combination of the main fatigue damaging parts. It should have equivalent global signal statistics and fatigue damage to the original stress-time history. Since WT method is defined here for the first time, experimental validation of the algorithm is important.

The comparison of the fatigue damage extracted by TCFD and WT methods suggests that WT is a better method for editing the given stress-time history under the purpose of accelerated fatigue test.

To conclude, in terms of the applicability of the edited stress-time history, this kind of history can be normally used in the durability laboratory scale fatigue test. Such test is very important in the fatigue design criteria, especially for the task of accelerated fatigue testing. Finally, WT method is suggested as the alternative technique in fatigue durability study, especially for the field of wind turbine engineering.

ACKNOWLEDGMENT

The authors would like to thank the Royal Thai Government Scholarship for financial support.

REFERENCES

[1] H. J. Sutherland. "On the fatigue analysis of wind turbines", Sandia National Laboratories, (SAND99-0089), 1999.

[2] British Standards Institution. "Wind turbine generator systems – Part 23: Full-scaled structural testing of rotor blades", DD IEC TS 61400-23:2002, 2002.

[3] Z. L. Mahri and M. S. Rouabah. "Fatigue estimation for a rotating blade of a wind turbine", *Rev. Energ. Ren. Energy*, vol. 5, pp. 39-47, 2002.

[4] J. A. Epaarachchi and P. D. Clausen. "The development of a fatigue loading spectrum for small wind turbine blades", *Journal of Wind Engineering and Industrial Aerodynamics*, 94(4), pp. 207-223, 2006.

[5] J. C. Marin, A. Barroso, F. Paris and J. Canas. "Study of damage and repair of blades of a 300 kW wind turbine", *Energy*, 33(7), pp. 1068-1083, 2008.

[6] J. C. Marin, A. Barroso, F. Paris and J. Canas. "Study of fatigue damage in wind turbine blades", *Engineering Failure Analysis*, 16(2), pp. 656-668, 2009.

[7] British Standards Institution. "Wind turbines – Part 1: Design requirements", BS EN 61400-1:2005, 2005.

[8] R. L. Ridder, R. W. Landgraf and S. Thangjitham. "Reliability analysis of an automotive wheel assembly", *Society of Automotive Engineers (930406)*, pp. 1-11, 1993.

[9] T. Goswani. "Low cycle fatigue life prediction – a new model", *International Journal of Fatigue*, 19(2), pp. 109-115, 1997.

[10] N. E. Frost, K. J. Marsh and L. P. Pook. *Metal fatigue*. Oxford University Press, 1974.

[11] H. O. Fuchs, D. V. Nelson, M. A. Burke and T. L. Toomay. "Shortcuts in cumulative damage analysis", *Fatigue under complex loading: Analyses and experiments, The Society of Automotive Engineers*, Advances in Engineering Vol. 6, Wetzel, R. M. ed., pp. 145-162, 1997.

[12] D. V. Nelson and H. O. Fuchs. "Predictions of cumulative fatigue damage using condensed load histories", *Fatigue under complex loading: Analyses and experiments, The Society of Automotive Engineers*, Advances in Engineering Vol. 6, Wetzel, R. M. ed., pp. 163-187, 1997.

[13] R. I. Stephens, A. Fatemi, R. R. Stephens and H. O. Fuchs. *Metal fatigue in engineering*. 2nd edn. New York: John Wiley & Sons, 2001.

[14] C. H. Ong and S. W. Tsai. "The use of carbon fibers in wind turbine blade design: A SERI-8 blade example", Sandia National Laboratories, (Report No. SAND2000-0478), pp. 1-69, 2000.

[15] J. F. Mandell and D. D. Samborsky. "DOE/MSU composite material fatigue database March 31, 2010 version 19.0", Sandia National Laboratories, 2010.

[16] H. J. Sutherland and J. F. Mandell. "Updated Goodman diagrams for fiberglass composite materials using the DOE/MSU fatigue database", *Global Windpower 2004*, pp. 1-12, 2004.

[17] T. R. Camp, M. J. Morris, R. van Rooij, J. van der Tempel, M. Zaaijer, A. Henderson, K. Argyriadis, S. Schwartz, H. Just, W. Grainger and D. Pearce. "Design methods for offshore wind turbines at exposed sites", Garrad Hassan and Partners, Ltd. (Report No. 2317/BR/22D), pp. 1-65, 2003.

[18] P. Pratumnopharat and P. S. Leung. "Validation of various windmill brake state models used by blade element momentum calculation", *Renewable Energy*, 36(11), pp. 3222-3227, 2011.

[19] D. L. Laird and B. R. Resor. *NuMAD User's Manual*. Draft edn. Sandia National Laboratories, 2009.

[20] ASTM E 1049-85. "Standard practices for cycle counting in fatigue analysis", *1988 Annual Book of ASTM Standards: Metals Test Methods and Analytical Procedures*, 03.01, pp. 5-9, 1997.

[21] A. Palmgren. "Die Lebensdauer von Kugellagern", *Zeitschrift-Vereines Deutscher Ingenieure*, 68(14), pp. 339-341, 1924.

[22] M. A. Miner. "Cumulative damage in fatigue", *Journal of Applied Mechanics*, 12(3), pp. A159-A164, 1945.

[23] M. Misiti, Y. Misiti, G. Oppenheim and J. M. Poggi. *Wavelet toolbox for use with matlab*. User's Guide version 1, 1997.

[24] C. S. Burrus, R. A. Gopinath and H. Guo. *Introduction to wavelets and wavelet transforms: a premier*. New Jersey, California: Prentice-Hall, Inc, 1998.

[25] ANSYS 13.0 nCode DesignLife. *DesignLife theory guide*. HBM-nCode, pp. 1-210, 2012.

Certificate of Presentation of Paper

northumbria UNIVERSITY
School of Computing, Engineering and Information Sciences

2nd International Symposium on Environment Friendly Energies and Applications

(EFEA 2012)

25th – 27th June 2012, Newcastle-upon-Tyne, UK

The paper

Application of Morlet Wavelet in The Stress-Time History Editing of Horizontal Axis Wind Turbine Blades

by

Panu Pratumnopharat, Pak Sing Leung, Richard S. Court

was presented at EFEA 2012 on 26th June 2012

Dr. K. Busawon
Conference Chair

List of References

[1] Sutherland, H. J. (1999) *On the fatigue analysis of wind turbines*. Sandia National Laboratories, (SAND99-0089) [Online]. Available at: www.sandia.gov (Accessed: 16th December 2008).

[2] British Standards Institution (2002) 'Wind turbine generator systems – Part 23: Full-scaled structural testing of rotor blades', DD IEC TS 61400-23:2002 [Online]. Available at: www.bsigroup.com (Accessed: 2nd October 2008).

[3] Mahri, Z. L. & Rouabah, M. S. (2002) 'Fatigue estimation for a rotating blade of a wind turbine', *Rev. Energ. Ren.*, 5, pp. 39-47 [Online]. Available at: www.cder.dz (Accessed: 12th November 2008).

[4] Epaarachchi, J. A. & Clausen, P. D. (2006) 'The development of a fatigue loading spectrum for small wind turbine blades', *Journal of Wind Engineering and Industrial Aerodynamics*, 94(4), pp. 207-223 [Online]. Available at: www.sciencedirect.com (Accessed: 19th November 2008).

[5] Marin, J. C., Barroso, A., Paris, F. & Canas, J. (2008) 'Study of damage and repair of blades of a 300 kW wind turbine', *Energy*, 33(7), pp. 1068-1083 [Online]. Available at: www.sciencedirect.com (Accessed: 9th September 2008).

[6] Marin, J. C., Barroso, A., Paris, F. & Canas, J. (2009) 'Study of fatigue damage in wind turbine blades', *Engineering Failure Analysis*, 16(2), pp. 656-668 [Online]. Available at: www.sciencedirect.com (Accessed: 24th January 2009).

[7] British Standards Institution (2005) 'Eurocode 3: Design of steel structures – Part 1-9: Fatigue', BS EN 1993-1-9:2005 [Online]. Available at: www.bsigroup.com (Accessed: 27th October 2008).

[8] British Standards Institution (2005) 'Wind turbines – Part 1: Design requirements', BS EN 61400-1:2005 [Online]. Available at: www.bsigroup.com (Accessed: 21st February 2009).

[9] Shokrieh, M. M. & Rafiee, R. (2006) 'Simulation of fatigue failure in a full composite wind turbine blade', *Composite Structures*, 74(3), pp. 332-342 [Online]. Available at: www.sciencedirect.com (Accessed: 6th January 2009).

[10] Palmgren, A. (1924) 'Die Lebensdauer von Kugellagern', *Zeitschrift-Vereines Deutscher Ingenieure*, 68 No. 14, pp. 339-341.

[11] Miner, M. A. (1945) 'Cumulative damage in fatigue', *Journal of Applied Mechanics*, 12(3), pp. A159-A164.

[12] Miner, M. A. (1946) 'Cumulative damage in fatigue', *Journal of Applied Mechanics*, 13(2), pp. A169-A171.

[13] Nijssen, R. P. L., van Wingerde, A. M. & van Delft, D. R. V. (2007) 'Wind turbine rotor blade materials: Estimating service lives', *Society for the Advancement of Material and Process Engineering (SAMPE)*, 43(2), pp. 7-15.

[14] Sutherland, H. J. & Mandell, J. F. (2004) 'Effect of mean stress on the damage of wind turbine blades', *Journal of Solar Energy Engineering*, 126(4), pp. 1041-1049 [Online]. Available at: http://onlinelibrary.wiley.com (Accessed: 6th February 2009).

[15] Ronold, K. O., Wedel-Heinen, J. & Christensen, C. J. (1999) 'Reliability-based fatigue design of wind-turbine rotor blades', *Engineering Structures*, 21(12), pp. 1101-1114 [Online]. Available at: www.sciencedirect.com (Accessed: 24th January 2009).

[16] Ridder, R. L., Landgraf, R. W. & Thangjitham, S. (1993) 'Reliability analysis of an automotive wheel assembly', *Society of Automotive Engineers (930406)*, pp. 1-11.

[17] Goswani, T. (1997) 'Low cycle fatigue life prediction – a new model', *International Journal of Fatigue*, 19(2), pp. 109-115.

[18] Frost, N. E., Marsh, K. J. & Pook, L. P. (1974) Metal fatigue. Oxford University Press.

[19] White, D. (2004) *New method for dual-axis fatigue testing of large wind turbine blades using resonance excitation and spectral loading*. National Renewable Energy Laboratory, (Technical Report No. NREL/TP-500-35268, April 2004), pp. 1-185 [Online]. Available at: www.nrel.gov (Accessed: 14th September 2008).

[20] Court, R. S., Ridley, S., Jones, H., Bonnet, P. A. & Dutton, A. G. (2009) 'Fatigue testing of wind turbine blades with computational verification', *ICCM-17 17th International Conference on Composite Materials*. Edinburgh International Convention Centre (EICC), Edinburgh, UK, 27-31 July 2009, pp. 1-10 [Online]. Available at: www.supergen-wind.org.uk (Accessed: 18th February 2010).

[21] Greaves, P. R., Dominy, R. G., Ingram, G. L., Long, H. & Court, R. S. (2012) 'Evaluation of dual-axis fatigue testing of large wind turbine blades', *Proceedings of the Institution of Mechanical Engineers, Part C: Journal of Mechanical Engineering Science*, 226(7), pp. 1693–1704 [Online]. Available at: http://pic.sagepub.com/ (Accessed: 30th June 2012).

[22] Schluter, L. L. & Sutherland, H. J. (1991) *User's guide for life2's rainflow counting algorithm*. Sandia National Laboratories, (SAND90-2259), pp. 1-37 [Online]. Available at: www.sandia.gov (Accessed: 22nd December 2008).

[23] Buhl, Jr. M. L. (2010) *NWTC Design Codes (MCrunch by Marshall Buhl)* (alpha v1.00.00y-mlb, 8.4 MB, 21st May 2010, file: CompFatigue.m, 60 kB) [Computer Program] Matlab, Command line: 981-1089, Last modified 25th October 2010, Distributor: National Wind Technology Center [Online]. Available at: http://wind.nrel.gov (Accessed: 5th March 2011).

[24] Fuchs, H. O., Nelson, D. V., Burke, M. A. & Toomay, T. L. (1977) 'Shortcuts in cumulative damage analysis', *Fatigue under complex loading: Analyses and experiments, The Society of Automotive Engineers*, Advances in Engineering Vol. 6, Wetzel, R. M. ed., pp. 145-162.

[25] Nelson, D. V. & Fuchs, H. O. (1977) 'Predictions of cumulative fatigue damage using condensed load histories', *Fatigue under complex loading: Analyses and experiments,The Society of Automotive Engineers*, Advances in Engineering Vol. 6, Wetzel, R. M. ed., pp. 163-187.

[26] Stephens, R. I., Fatemi, A., Stephens, R. R. & Fuchs, H. O. (2001) *Metal fatigue in engineering*. 2nd edn. New York: John Wiley & Sons.

[27] Clifton-Smith, M. J. (2009) 'Wind turbine blade optimization with tip loss corrections', *Wind Engineering*, 33(5), pp. 477-496.

[28] Lanzafame, R. & Messina, M. (2010) 'Power curve control in micro wind turbine design', *Energy*, 35(2), pp. 556-561 [Online]. Available at: www.sciencedirect.com (Accessed: 8th January 2010).

[29] Glauert, H. (1935) 'Airplane propellers', in Durand, W. F. (ed.) *Aerodynamic theory*. Vol. IV Division L, pp. 169-360.

[30] Wilson, R. E. & Lissaman, P. B. S. (1974) *Applied aerodynamics of wind power machines*, the National Science Foundation, pp. 1-109 [Online]. Available at: http://ir.library.oregonstate.edu (Accessed: 10th January 2010).

[31] Wilson, R. E., Lissaman, P. B. S. & Walker, S. N. (1976) *Aerodynamic performance of wind turbines*. pp. 1-164 [Online]. Available at: http://wind.nrel.gov (Accessed: 19th December 2009).

[32] Tangler, J. L. & Selig, M. S. (1997) *An evaluation of an empirical model for stall delay due to rotation for HAWTs*. National Renewable Energy Laboratory, (Report NREL/CP-440-23258, July 1997), pp. 1-13 [Online]. Available at: www.osti.gov (Accessed: 25th October 2009).

[33] Benini, E. (2004) 'Significance of blade element theory in performance prediction of marine propellers', *Ocean Engineering*, 31(8-9), pp. 957-974 [Online]. Available at: www.sciencedirect.com (Accessed: 8th January 2010).

[34] Xu, G. & Sankar, L. N. (2002) 'Development of engineering aerodynamics models using a viscous flow methodology on the NREL phase VI rotor', *Wind Energy*, 5(2-3), pp. 171-183 [Online]. Available at: http://www3.interscience.wiley.com (Accessed: 25th December 2009).

[35] Stoddard, F. S. (1977) 'Momentum theory and flow states for windmill' *Wind Technology Journal*, 1(1), pp. 3-9.

[36] Glauert, H. (1926) *The analysis of experimental results in the windmill brake and vortex ring states of an airscrew*. (Reports and Memoranda, No. 1026 His Majesty's Stationery Office February 1926) pp. 1-10.

[37] Manwell, J. F., McGowan, J. G. & Rogers, A. L. (2002) *Wind energy explained: Theory, design and application*. John Wiley & Sons Inc.

[38] Hibbs, B. & Radkey, R. L. (1983) *Calculating rotor performance with the revised 'PROP' computer code*. AeroVironment, Inc., (Report No. PFN-13470W), pp. 12-14.

[39] Burton, T., Sharpe, D., Jenkins, N. & Bossanyi, E. (2001) *Wind energy handbook*. John Wiley & Sons Inc.

[40] Moriarty, P. J. & Hansen, A. C. (2005) *AeroDyn theory manual*. National Renewable Energy Laboratory, (Technical report NREL/TP-500-36881, December 2005) pp. 1-36 [Online]. Available at: www.nrel.gov (Accessed: 6th October 2009).

[41] Shen, W. Z., Mikkelsen, R., Srensen, J. N. & Bak, C. (2005) 'Tip loss corrections for wind turbine computations', *Wind Energy*, 8(4), pp. 457-475 [Online]. Available at: http://www3.interscience.wiley.com (Accessed: 17th December 2009).

[42] Maalawi, K. Y. & Badawy, T. S. (2001) 'A direct method for evaluating performance of horizontal axis wind turbines'. *Renewable & Sustainable Energy Reviews*, 5(22), pp. 175-190 [Online]. Available at: www.elesvier.com (Accessed: 6th October 2009).

[43] Ahlund, K. (2004) *Investigation of the NREL NASA/Ames wind turbine aerodynamics database*. Swedish Defence Research Agency, (Scientific Report FOI-R-1243-SE, June 2004), pp. 1-57 [Online]. Available at: http://www2.foi.se (Accessed: 30th October 2009).

[44] Ingram, G. L. (2005) *Wind turbine blade analysis using the blade element momentum method version 1.0*. School of Engineering, Durham University, (13th December 2005), pp. 1-21 [Online]. Available at: www.dur.ac.uk (Accessed: 7th September 2009).

[45] Bak, C., Fuglsang, P., Sørensen, N. N., Madsen, H. A., Shen, W. Z. & Sørensen, J. N. (1999) *Airfoil characteristics for wind turbines*. Risø National Laboratory, (Report No. Risø-R-1065(EN), March 1999), pp. 1-51 [Online]. Available at: www.cd3wd.com (Accessed: 11th April 2010).

[46] Mejia, J. M., Chejne, F. Smith, R., Rodriguez, L. F., Fernandez, O. & Dyner, I. (2006) 'Simulation of wind energy output at Guajira, Colombia', *Renewable Energy*, 31(3), pp. 383-399 [Online]. Available at: www.sciencedirect.com (Accessed: 1st December 2009).

[47] Hansen, M. O. L. (2008) *Aerodynamics of wind turbines*. 2nd edn. London: Earthscan.

[48] Akins, R. E. (1989) 'Rainflow counting based on predicted stress spectra' *Eighth ASME Wind Energy Symposium*, The Twelfth Annual Energy-Sources Technology Conference and Exhibition, Houston, Texas, January 22-28, 1989, SED-Vol. 7, p. 131.

[49] Buhl, Jr. M. L. (2004) *NWTC Design Codes (WT_Perf by Marshall Buhl)* (version 3.10, WTP_Subs.f90, 1.5 MB, 17th December 2004) [Computer Program] Fortran 90, Command line: 1076-1083 and 1306, Last modified 17th December 2004, Distributor: National Wind Technology Center [Online]. Available at: http://wind.nrel.gov (Accessed: 20th October 2009).

[50] Laino, D. J. (2005) *NWTC Design Codes (AeroDyn by Dr. David J. Laino)* (version 12.58, AeroSubs.f90, 672 KB, 28th June 2005) [Computer Program] Fortran 90, Command line: 3335-3455, Last modified 5th July 2005, Distributor: National Wind Technology Center [Online]. Available at: http://wind.nrel.gov (Accessed: 20th October 2009).

[51] Wilson, R. E. (1998) 'Aerodynamic behavior of wind turbines', in Spera, D. A. (ed.) *Wind turbine technology: Fundamental concepts of wind turbine engineering*. ASME Press, pp. 215-282.

[52] Pratumnopharat, P. & Leung, P. S. (2011) 'Validation of various windmill brake state models used by blade element momentum calculation', *Renewable Energy*, 36(11), pp. 3222-3227 [Online]. Available at: www.sciencedirect.com (Accessed: 6th June 2011).

[53] Buhl, Jr., M. L. (2005) *A new empirical relationship between thrust coefficient and induction factor for the turbulent windmill state*. National Renewable Energy Laboratory, (Technical report NREL/TP-500-36834, August 2005) pp. 1-8 [Online]. Available at: http://wind.nrel.gov (Accessed: 6th October 2009).

[54] Viterna, L. A. & Corrigan, R. D. (1982) *Fixed pitch rotor performance of large horizontal axis wind turbines*. NASA Lewis Research Center, pp. 69-85 [Online]. Available at: http://adsabs.harvard.edu (Accessed: 6th October 2009).

[55] Viterna, L. A. & Janetzke, D. C. (1982) *Theoretical and experimental power from large horizontal-axis wind turbines*. National Aeronautics and Space Administration, Lewis Research Center, (DOE/NASA/20320-41 NASA TM-82944), pp. 1-17 [Online]. Available at: http://ntrs.nasa.gov (Accessed: 6th January 2010).

[56] Laino, D. J. (2005) *NWTC Design Codes (FoilCheck by Dr. David J. Laino)* (version 2.03, Foilchk.f90, 254 KB, 30th May 2002) [Computer Program] Fortran 90, Command line: 1654-1829, Last modified 10th May 2005, Distributor: National Wind Technology Center [Online]. Available at: http://wind.nrel.gov (Accessed: 20th October 2009).

[57] Hansen, C. (2007) *NWTC Design Codes (AirfoilPrep by Dr. Craig Hansen)* (version v2p2, AirfoilPrep_v2p2.xls, 350 KB, 13th December 2005) [Computer Program] Excel, Macro name: *cmdButtonFoilcheck_Click*, Command line: 189-240, Last modified 15th January 2007, Distributor: National Wind Technology Center [Online]. Available at: http://wind.nrel.gov (Accessed: 20th October 2009).

[58] Buhl, M. L., Jr., Wright, A. D. & Tangler, J. L. (1997) *Wind turbine design codes: a preliminary comparison of the aerodynamics*. National Renewable Energy Laboratory, (Report NREL/CP-500-23975, December 1997), pp. 1-9 [Online]. Available at: www.osti.gov (Accessed: 25th October 2009).

[59] Tangler, J., Smith, B., Kelley, N. & Jager, D. (1992) *Measured and predicted rotor performance for the SERI advanced wind turbine blades*. National Renewable Energy Laboratory, (Report No. NREL/TP-257-4594), pp. 1-7 [Online]. Available at: www.osti.gov (Accessed: 7th October 2010).

[60] Sutherland, H. J. (2001) 'Preliminary analysis of the structural and inflow data from the list turbine', *Wind Energy*, American Institute of Aeronautics and Astronautics, AIAA-2001-0041, pp. 1-11 [Online]. Available at: www.osti.gov (Accessed: 18th October 2010).

[61] McNiff, B. P., Musial, W. D. & Errichello, R. (1991) *Variations in gear fatigue life for different wind turbine braking strategies*. Solar Energy Research Institute, (Report No. SERI/TP-257-3984), pp. 1-8 [Online]. Available at: www.osti.gov (Accessed: 7th October 2010).

[62] Ong, C. H. & Tsai, S. W. (2000) *The use of carbon fibers in wind turbine blade design: A SERI-8 blade example*. Sandia National Laboratories, (Report No. SAND2000-0478), pp. 1-69 [Online]. Available at: http://windpower.sandia.gov (Accessed: 15th December 2009).

[63] Suresh, S. (1998) 'Cumulative damage', *Fatigue of Materials*. 2nd edn. Cambridge University Press.

[64] ASTM E 1823-96 (1997) 'Standard terminology relating to fatigue and fracture testing', *1997 Annual Book of ASTM Standards: Metals Test Methods and Analytical Procedures*, 03.01, pp. 1-21.

[65] Burkner, F., van Wingerde, A. M. & Busmann, H. G. (2008) 'Testing of rotor blades of wind turbines', *DEWEK 2008 Ninth German Wind Energy Conference – Book of Abstracts*, Bremen, Germany 26-27 November 2008, pp. 75 [Online]. Available at: www.dewek.de (Accessed: 19th December 2008).

[66] Kong, C., Kim, T., Han, D. & Sugiyama, Y. (2006) 'Investigation of fatigue life for a medium scale composite wind turbine blade', *International Journal of Fatigue*, 28(10), pp. 1382-1388 [Online]. Available at: www.sciencedirect.com (Accessed: 9th September 2008).

[67] Nijssen, R. P. L. (2006) 'Fatigue life prediction and strength degradation of wind turbine rotor blade composites' *Knowledge Centre Wind Turbine Materials and Constructions (KC-WMC)*, Netherland [Online]. Available at: www.sandia.gov (Accessed: 16th December 2008).

[68] British Standards Institution (1993) 'Methods of fatigue testing – Part 1: Guide to general principles', BS EN 3518-1:1993 [Online]. Available at: www.bsigroup.com (Accessed: 7th October 2008).

[69] Sutherland, H. J. & Mandell, J. F. (2004) 'Updated Goodman diagrams for fiberglass composite materials using the DOE/MSU fatigue database', *Global Windpower 2004*, pp. 1-12 [Online]. Available at: www.sandia.gov (Accessed: 12th March 2009).

[70] Mandell, J. F. & Samborsky, D. D. (2010) 'DOE/MSU composite material fatigue database March 31, 2010 version 19.0', *Sandia National Laboratories* [Online]. Available at: www.sandia.gov (Accessed: 20th May 2010).

[71] Sendeckyj, G. P. (2001) 'Constant life diagrams - a historical review', *International Journal of Fatigue*, pp. 347-353 [Online]. Available at: www.sciencedirect.com (Accessed: 16th February 2009).

[72] Mandell, J. F. & Samborsky, D. D. (1997) 'DOE/MSU composite material fatigue database: test methods, materials, and analysis', *Sandia National Laboratories*, (SAND97-3002) [Online]. Available at: www.sandia.gov (Accessed: 22nd December 2008).

[73] Mandell, J. F., Reed, R. M. & Samborsky, D. D. (1992) 'Fatigue of fiberglass wind turbine blade materials', *Sandia National Laboratories*, (SAND92-7005) [Online]. Available at: www.sandia.gov (Accessed: 22nd December 2008).

[74] Spera, D. A. (2009) 'Fatigue design of wind turbines', in Spera, D. A. (ed.) Wind turbine technology: Fundamental concepts of wind turbine engineering. ASME Press, pp. 663-720.

[75] Mandell, J. F., Samborsky, D. D., Wahl, N. K. & Sutherland, H. J. (2003) 'Testing and analysis of low cost composite materials under spectrum loading and high cycle fatigue conditions', *In Proceedings of The 14th International Conference on Composite Materials (ICCM-14), Society of Manufacturing Engineers.* San Diego, California, pp. 1-10 [Online]. Available at: http://energy.sandia.gov (Accessed: 22nd December 2009).

[76] Goodman, J. (1899) *Mechanics applied to engineering*. London: Longmans, Green, and Co.

[77] Ansell, M. P. (1987) 'Layman's guide to fatigue: The Geoff Pontin Memorial Lecture, sponsored by British Tradewinds', *Wind Energy Conversion 1987: proceedings of the 9th British Wind Energy Association Conference*. Edinburge 1-3 April 1987, Edinburge, Scotland: Mechanical Engineering, pp. 39-54.

[78] Sutherland, H. J. (1989) *Analytical framework for the LIFE2 computer code*. Sandia National Laboratories, (SAND89-1397), pp. 5-6 [Online]. Available at www.sandia.gov (Accessed: 15th October 2010).

[79] Lalanne, C. (2002) 'Counting methods for analyzing random time history', *Mechanical vibration and shock – fatigue damage*. Hermes Penton Science, London, 4, pp. 135-191.

[80] Matsuishi, M. & Endo, T. (1968) 'Fatigue of metals subjected to varying stress – fatigue lives under random loadings' Murakami, in Murakami, Y. (ed.) *The rainflow method in fatigue: The Tatsuo Endo Memorial Volume*. Butterworth-Heinemann Ltd., 1991, pp. XXI-XXIV.

[81] Downing, S. D. & Socie, D. F. (1982) 'Simple rainflow counting algorithms', *International Journal of Fatigue*, 4(1), pp. 31-40.

[82] Rychlik, I. (1987) 'A new definition of the rainflow cycle counting method', *International Journal of Fatigue*, 9(2), pp. 119-121.

[83] Conle, A., Grenier, G., Johnson, H., Kemp, S., Kopp, G. & Morton, M. (1997) 'Service history determination', in Rice, R. C. (ed.) *SAE fatigue design handbook.* 3rd edn. AE-22. Warrendale, pp. 115-158.

[84] ASTM E 1049-85 (1988) 'Standard practices for cycle counting in fatigue analysis', *1988 Annual Book of ASTM Standards: Metals Test Methods and Analytical Procedures*, 03.01, pp. 764-772.

[85] Fuchs, H. O. & Stephens, R. I. (1980) *Metal fatigue in engineering.* New York: John Wiley & Sons.

[86] Dowling, E. (1999) *Mechanical behavior of materials: engineering methods for deformation, fracture and fatigue.* 2nd edn. Prentice-Hall.

[87] Rotem, A. (1981) 'Accelerated fatigue testing method', *International Journal of Fatigue*, 3(4) pp. 211-215.

[88] Leese, G. E. & Mullin, R. L. (1991) 'The role of fatigue analysis in vehicle test simulation laboratory', *Society of Automotive Engineers (910166)*, pp. 1-12.

[89] Conle, A. & Topper, T. H. (1979) 'Evaluation of small cycle omission criteria for shortening of fatigue service histories', *International Journal of Fatigue*, 1(1), pp. 23-28.

[90] Conle, A. & Topper, T. H. (1980) 'Overstrain effects during variable amplitude service history testing', *International Journal of Fatigue*, 2(3), pp. 130-136.

[91] Heuler, P. & Seeger, T. (1986) 'A criterion for omission of variable amplitude loading histories', *International Journal of Fatigue*, 8(4), pp. 225-230.

[92] Gunger, J. E. & Stephens, R. I. (1995) 'Variable amplitude history editing and accelerated testing of SAE 1045 steel', *SAE Technical Papers (950704)*, pp. 1-13.

[93] Stephens, R. I., Dindinger, P. M. & Gunger, J. E. (1997) 'Fatigue damage editing for accelerated durability testing using strain range and SWT parameter criteria', *International Journal of Fatigue*, 19(8-9), pp. 599-606.

[94] Giacomin, J. A., Steinwolf, A. & Abdullah, S. (1999) 'A vibration mission synthesis algorithm for mildly nonstationary road data', *ATA 6th International Conference on the New Role of Experimentation in Modern Automotive Product Development Process*, Florence, Italy, 17-19 November.

[95] Giacomin, J., Steinwolf, A. & Staszewski, W. J. (2000) 'An algorithm for mildly nonstationary mission synthesis (MNMS)', *Engineering Integrity*, Vol. 7, pp. 44-56.

[96] Abdullah, S, Giacomin, J. A. & Yates, J. R. (2004) 'A mission synthesis algorithm for fatigue damage analysis', *Proceedings of the Institution of Mechanical Engineers. Part D, Journal of automobile engineering.* 218(3), pp. 243-258 [Online]. Available at: http://pid.sagepub.com (Accessed: 22nd December 2011).

[97] Oh, C. S. (2001) 'Application of wavelet transform in fatigue history editing', *International Journal of Fatigue*, 23(3), pp. 241-250 [Online]. Available at: www.sciencedirect.com (Accessed: 9th September 2011).

[98] El-Ratal, W., Bennebach, M., Lin, X. & Plaskitt, R. (2002) 'Fatigue life modelling and accelerated tests for components under variable amplitude loads', *In Symposium on Fatigue Testing and Analysis under Variable Amplitude Loading Conditions, Tenth International Spring Meeting of SF2M*. Tours, France, 29-31 May 10(3), pp. 349-366.

[99] Abdullah, S., Nizwan, C. K. E. & Nuawi, M. Z. (2009) 'A study of fatigue data editing using the Short-Time Fourier Transform (STFT)', *American Journal of Applied Sciences*, 6(4), pp. 565-575 [Online]. Available at: www.scipub.org (Accessed: 26th June 2010).

[100] Wang, Z. & Chen, Z. W. (1999) 'Influence of small load cycle omission on fatigue damage accumulation', *Fatigue'99, Proceedings of the Seventh International Fatigue Congress, edited by Wu., X. R. & Wang, Z. G.* Beijing, P.R., China, pp. 1113-1118.

[101] Yan, J. H., Zheng, X. L. & Zhao, K. (2001) 'Experimental investigation on the small-load-omitting criterion', *International Journal of Fatigue*, 23(5), pp. 403-425 [Online]. Available at: www.sciencedirect.com (Accessed: 9th September 2011).

[102] ANSYS 13.0 nCode DesignLife (2012) *DesignLife theory guide.* HBM-nCode, pp. 1-210.

[103] Vold, H. & Morrow, D. (1993) 'Compression of time histories used for component fatigue evaluation', *The Engineering Society for Advancing Mobility Land Sea Air and Space (930403)*, International Congress and Exposition, Detroit, Michigan, March 1-5, pp. 1-8.

[104] Meyer, Y. (1993) *Wavelet: algorithm and applications*. Philadelphia, USA: SIAM.

[105] Harvey, C. (1993) *Time series model*. 2nd edn. Cambridge: MIT Press.

[106] Newland, N. E. (1993) *An introduction to random vibrations, spectral and wavelet analysis*. 3rd edn. Mineola, New York: Dover Publications Inc.

[107] Hinton, P. R. (2004) *Statistics explained*. 2nd edn. New York: Routledge.

[108] Matlab User's Guide (1999) *Statistics toolbox for use with Matlab*. User's Guide Version 2, The Mathworks Inc. [Online]. Available at: www.mathworks.com (Accessed: 6th June 2010).

[109] Misiti, M., Misiti, Y., Oppenheim, G. & Poggi, J. M. (1997) *Wavelet toolbox for use with matlab*. User's Guide version 1 [Online]. Available at: www.mathworks.com (Accessed: 6th June 2010).

[110] Gleason, A. (2006) *Who is Fourier? A mathematical advanture*. Boston, Language Research Foundation.

[111] Thomas, W. T. & Dahleh, M. D. (1998) *Theory of vibration with applications*. 5th edn. New Jersey: Prentice Hall, Inc.

[112] Gabor, D. (1944) 'Theory of communication'.

[113] Park, T. H. (2010) *Introduction to digital signal processing – computer musically speaking*. New Jersey: World Scientific.

[114] Chui, C. K. (1992) *An introduction to wavelets.* San Diego: Academic Press.

[115] Grossmann, A. & Morlet, J. (1984) 'Decomposition of hardy functions into square integrable wavelets of constant shape', *Siam Journal on Mathematical Analysis*, 15(4), pp. 723-736.

[116] Matlab User's Guide (1999) *Signal processing toolbox for use with Matlab*. User's Guide Version 4.2, The Mathworks Inc. [Online]. Available at: www.mathworks.com (Accessed: 6th June 2010).

[117] Burrus, C. S., Gopinath, R. A. & Guo, H. (1998) *Introduction to wavelets and wavelet transforms: a premier*. New Jersey, California: Prentice-Hall, Inc.

[118] Abdullah, S., Putra, T. E., Nuawi, M. Z., Nopiah, Z. M., Arifin, A. & Abdullah, L. (2010) 'Time-frequency localization analysis for extracting fatigue damaging events', *ISPRA'10 Proceedings of the 9th WSEAS international conference on Signal processing, robotics and automation.* pp. 31-35 [Online]. Available at: www.wseas.us (Accessed: 26th June 2010).

[119] Camp, T. R., Morris, M. J., van Rooij, R., van der Tempel, J., Zaaijer, M., Henderson, A., Argyriadis, K., Schwartz, S., Just, H., Grainger, W. & Pearce, D. (2003) Design methods for offshore wind turbines at exposed sites. Garrad Hassan and Partners, Ltd. (Report No. 2317/BR/22D), pp. 1-65 [Online]. Available at: www.offshorewindenergy.org (Accessed: 23rd September 2011).

[120] Laird, D. L. & Resor, B. R. (2009) *NuMAD User's Manual*. Draft edn. Sandia National Laboratories.

[121] Pratumnopharat, P., Leung, P. S. & Court, R. S. (2012) 'Application of Morlet wavelet in the stress-time history editing of horizontal axis wind turbine blades', *2nd International Symposium on Environment-Friendly Energies and Applications (EFEA 2012)*, Newcastle upon Tyne, United Kingdom 25-27 June 2012, pp. 396-401.

[122] Nopiah, Z. M., Abdullah, S., Baharin, M. N., Putra, T. E., Sahadan, S. N. & Willis, K. O. (2011) 'Comparative study on data editing techniques for fatigue time series signals', *Advanced Materials Research*, 146-147(2), pp. 1681-1684 [Online]. Available at: www.scientific.net (Accessed: 28th February 2012).

[123] Drela, M. & Youngren, H. (2001) *Xfoil 6.94 user's guide*. pp. 1-33 [Online]. Available at: http://clubmodelisme.free.fr (Accessed: 17th August 2010).

[124] Kelley, N. D., Wright, A. D., Buhl, Jr., M. L. & Tangler, J. L. (1996) *Long-term simulation of turbulence-induced loads using the SNLWIND-3D, FAST, YawDyn, and ADAMS numerical codes*. National Renewable Energy Laboratory, (Report No. NREL/CP-440-21673), pp. 1-12 [Online]. Available at: www.osti.gov (Accessed: 8th October 2010).

[125] Tangler, J., Smith, B. & Jager, D. (1992) *SERI advanced wind turbine blades*. National Renewable Energy Laboratory, (Report No. NREL/TP-257-4492), pp. 1-6 [Online]. Available at: www.osti.gov (Accessed: 10th October 2010).

[126] Mauclère, X. (2009) *Automatic 2D airfoil generation, evaluation and optimisation using MATLAB and XFOIL*. Master Thesis, Technical University of Denmark, pp. 1-45 [Online]. Available at: www.studenterpraest.dtu.dk (Accessed: 17th August 2010).